Spring 1-1-2015

Separation challenges and optimizations of sustainable algae and lignocellulose based biofuels

Birendra Adhikari
University of Colorado at Boulder, birendra.adhikari@colorado.edu

SEPARATION CHALLENGES AND OPTIMIZATIONS OF SUSTAINABLE ALGAE AND LIGNOCELLULOSE BASED BIOFUELS

by

BIRENDRA ADHIKARI

B.S., Texas A&M University, 2009

M.S., University of Colorado Boulder, 2013

A thesis submitted to the

Faculty of the Graduate School of the

University of Colorado in partial fulfillment

of the requirement for the degree of

Doctor of Philosophy

Department of Mechanical Engineering

2015

This dissertation entitled:

Separation challenges and optimizations of sustainable algae and lignocellulose based biofuels

written by Birendra Adhikari

has been approved for the Department Mechanical Engineering

_____

John Pellegrino, Ph.D.

_____

Jonathan Stickel, Ph.D.

Date_____

The final copy of this thesis has been examined by the signatories, and we
Find that both the content and the form meet acceptable presentation standards
Of scholarly work in the above mentioned discipline.

Abstract

Birendra Adhikari (Ph.D., Mechanical Engineering)

Separation challenges and optimizations of sustainable algal and lignocellulose based biofuels

Dissertation directed by Professor John Pellegrino

Algae and lignocellulosic biomass are viewed as viable renewable energy sources. However, higher cost of production is a major hurdle to make them competitive with fossil fuel sources. In case of algae fuel, the larger material and energy input required for the growth and processing is making algal biofuel both environmentally and economically unsustainable. In case of lignocellulosic biomass, the cost of unit operation steps, including that of enzymatic hydrolysis, to produce monomer sugars is very high. These problems gave us key engineering opportunities to investigate better extraction methods of lipids from algae and continuous enzymatic hydrolysis of lignocellulosic biomass.

We performed techno-economic and life-cycle analysis of five probable 'algae to fuel' processes and came up with the conclusion that the extraction and dewatering of algae are the major bottlenecks. We hypothesized and tested an extraction method of lipids from wet algae with a 'novel' solvent mixture of diesel and isopropanol so that the lipids can be extracted directly from wet algae with a cheaper overall cost without actually killing the algae. We found out that algal lipids can be extracted using this 'novel' extraction method and the algae can also regrow in certain extraction conditions.

The batch enzymatic hydrolysis is very inefficient method of hydrolysis of lignocellulosic biomass. We hypothesized and tested a membrane based reactor system for

continuous hydrolysis of lignocellulosic biomass so that the monomer sugars, inhibitors during the hydrolysis, can remain low in concentration in the reactor and because of that, the reaction rate and overall conversion can go up. Our techno-economic study suggested that the continuous system can be cheaper than the batch mode of production. We learned that the complex nature of the lignocellulosic slurry makes the system difficult to design due to clogging and settling of biomass in the reactor and adjoining tubes. To understand this aspect, a fundamental study of the fluid dynamics of the biomass in a membrane module with the goal of designing a better header that can 'mitigate' clogging of the membrane structure (tubes and/or module) was done using *OpenFOAM*. We found out that certain geometries of membrane arrangement in a membrane module are preferable to some other ones.

For My Family.

Acknowledgements

This dissertation is the ultimate product of the support I am getting from my family throughout my life.

Special thanks to my dad and mom. They always encourage me to be the best person that I can possibly be. Thanks to my uncle Yedu Prasad, aunt Tap Kumari, my wife Shanti, brother Keshab, sister Anjula, my son Bigyan and niece Aagrima.

I am extremely thankful to Prof. John Pellegrino for everything. John, you are have been really a great, very encouraging and patient mentor for me.

I am also very thankful to Dr. Jonathan Stickel and David Sievers for their wonderful supervising at NREL. Jonathan, you are simply awesome mentor and so is Dave.

Many thanks to Prof. Yifu Ding, Prof. Daven Henze, and Dr. Jeffery Knutsen for taking the time to serve on my committee.

I am thankful to all the Separation Science and Technology group members. Thanks to John Mersch, Rachel Sobke and Margaret Schneider for everything. I would also like to thank all my NREL colleagues and mentors, most notably Jim Lischeske and Dr. Nathan Crawford.

Last but not the least, this research would not have been possible without support from numerous funding sources, and for this I thank Colorado Center for Biorefining and Biofuels (C2B2), Phillips66 and National Renewable and Energy Laboratory (NREL) for sponsoring my research.

Table of Contents

List of Tables

List of Figures

Chapter 1 Introduction

1.1 Introduction and background

Biofuels, such as those derived from algae are a possible renewable alternative to fossil fuels. Algae has a particular interest because the microorganisms have a faster growth rate, a shorter maturity rate, and a higher biomass content than other terrestrial crops used for biofuels, such as corn and soybeans.[1] Algae has far lower space requirements for growth than land-based plant production and several algal species can double their biomass in one day.[2] Also, they do not compete with food crops.[3] The biochemical limitations, as well as advantages, of using microalgae are well documented from experimental [4] and theoretical perspectives [5].

Lignocellulose, on the other hand, is the most abundant organic polymer in the world.[6] The potential of using cheaply available raw lignocellulosic biomass to convert to the fuel sources of interest such as ethanol, butanol, etc., is alluring. Nonetheless, there are still major process hurdles to be overcome. For the conversion of lignocellulosic biomass to the derivative fuels, cellulose and hemicellulose first must be hydrolyzed to their component sugars. Before it can be hydrolyzed, biomass must be pretreated to make it soft enough. The hydrolysis itself is slow and produces inhibitors, and this step combined with other separation steps ultimately makes the cost of production of biofuel from lignocellulosic biomass high.

For a process to be sustainable for longer duration, it has to be sustainable environmentally as well as economically. The environmental footprints left by the construction and operation of these processes should not have adverse environmental effects [7],[8]. Because of newly emerging ecological and environmental problems, future regulations aimed at curbing various emissions have begun in recent past [9],[10]. Thus the studies like life-cycle analysis

(LCA) along with traditional techno-economic analysis of many new and old processes are gaining ground.

Thus, our research work focuses primarily on two aspects: (i) techno-economic and life-cycle analysis of these biofuel processes and (ii) proposed solutions to major technical hurdles for these processes by the detailed studies of the processing steps using solid-liquid and liquid-liquid separation techniques using but not limited to membrane processes.

1.2 Algal Biofuels

We divided the study into two core groups: (i) Techno-economic and life cycle studies and (ii) extraction studies of lipids from the algae using low cost solvents.

1.2.1 Techno-economic and life cycle analysis

The feasibility of algal biofuel processes was studied in this work by performing techno-economic analysis and life-cycle analysis. Five algae-to-fuel scenarios that currently exist were studied in detail. Those processes were: (i) the classical open pond growth system using conventional solvent extraction to recover the lipid product; (ii) a closed, sunlight-supplied photobioreactor that avoids extraction by producing a biodiesel from in-situ transesterification; (iii) an unconventional, artificially-lighted photobioreactor that also uses conventional solvent extraction to recover the lipids, (iv) the classical open pond growth system that avoids extraction by producing biodiesel from in-situ transesterification and (v) a closed, sunlight-supplied photobioreactor that uses extraction.

These studies identified the major bottlenecks of these processes i.e. dewatering and lipid extraction.

1.2.2 Lipid extraction from wet algae

For the purpose of addressing the issue of the higher cost of dewatering of algal biomass and extraction of lipids from algae, diesel mixed with isopropanol was proposed as the novel solvent for extraction in this study. First and foremost, a detailed theoretical study of solubility parameters was done using "Hansen solubility parameter" analysis to predict the feasibility of different solvents in a solvent mixture. This study performed screening tests for extraction of lipids in harvesting condition and found the optimum extraction conditions and chemistry using hexane and diesel as primary solvents on the microalgae species *Chlorella vulgaris*. This study also focused on testing the viability of algae after the extraction with regrowth tests of lipid-extracted algae under different conditions. This question was motivated since the major nutrient for the algae growth, phosphorous, is a limited resource, and by keeping algae alive we can minimize the use of phosphorous. This study showed us that diesel can be used as the extracting solvent and algae can still regrow after the extraction with the application of an optimized amount of diesel and isopropanol.

1.3 Continuous saccharification of lignocellulosic biomass

In the last few years, researchers have broached the idea of incorporating membrane reactors into the enzymatic hydrolysis process in order reduce possible product feedback inhibition during the hydrolysis and provide greater utilization (including recovery/reuse) of the enzymes. The main goal of our study in this area is intended to design a functional continuous reactor for enzymatic hydrolysis of lignocellulosic biomass. For this matter, we divided our studies in four main parts:

1.3.1 Techno-economic studies of processes involving continuous saccharification

The economic feasibility of our proposed membrane-based continuous saccharification is studied primarily to determine how much enzyme cost can be lowered and how much overall cost of production can be lowered in comparison to the batch system.

1.3.2 Membranes and biomass screening studies for continuous saccharification

Membrane filtration tests were done to characterize how different membranes might, if at all, influence fouling caused by the cake build-up. In addition to that, biomass of interest at different insoluble fraction was characterized to assess whether significant differences in filtration cake resistance was measured.

1.3.3 Computation fluid dynamics (CFD) studies

When we first started these experiments, we learned that a hurdle materialized from clogging of the membrane and module structure. Because of the presence of particles, the slurry has complex rheological properties. Thus to better understand clogging aspects in detail, we performed computational fluid dynamics studies to understand the factors that could help minimize stagnant areas, mainly in the entrance region of the membrane module with varying tubes and header geometry. This study also helps us understand how the flow characteristics of the biomass change both while losing mass during filtration, and from speciation changes during extent of reaction. These rheological changes can dictate the clogging and ultimately, this would direct us to design a better membrane-reactor module geometry needed for the continuous enzymatic hydrolysis.

1.3.4 Continuous enzymatic hydrolysis experimental studies

After initial screening studies, a commercial tubular membrane (pilot) module was chosen with one tube of 0.5 inch ID and a foot length. A continuous enzymatic hydrolysis was done for over 100 h maintaining sugar concentration and fraction of insolubles constant in the bioreactor. In the future, multiple membrane modules and membrane modules with multiple tubes may be studied with higher solids loading in the bioreactor.

1.4 References

[1] R.E. Armenta, P. Mercer, Developments in oil extraction from microalgae, European Journal of Lipid Science and Technology, 113 (2011) 539-547.

[2] M. Odlare, E. Nehrenheim, V. Ribe, E. Thorin, M. Gavare, M. Grube, Cultivation of algae with indigenous species - Potentials for regional biofuel production, Applied Energy, 88 (2011) 3280-3285.

[3] A.F. Clarens, E.P. Resurreccion, M.A. White, L.M. Colosi, Environmental Life Cycle Comparison of Algae to Other Bioenergy Feedstocks, Environmental Science & Technology, 44 (2010) 1813-1819.

[4] Y.K. Lee, Microalgal mass culture systems and methods: Their limitation and potential, Journal of Applied Phycology, 13 (2001) 307-315.

[5] K.M. Weyer, D.R. Bush, A. Darzins, B. Willson, Theoretical Maximum Algal Oil Production, BioEnergy Research, (2009) 10.

[6] Y.H.P. Zhang, S.Y. Ding, J.R. Mielenz, J.B. Cui, R.T. Elander, M. Laser, M.E. Himmel, J.R. McMillan, L.R. Lynd, Fractionating recalcitrant lignocellulose at modest reaction conditions, Biotechnology and Bioengineering, 97 (2007) 214-223.

[7] K. Soratana, A.E. Landis, Evaluating industrial symbiosis and algae cultivation from a life cycle perspective, Bioresource Technology, 102 (2011) 6892-6901.

[8] B. Steubing, R. Zah, C. Ludwig, Life cycle assessment of SNG from wood for heating, electricity, and transportation, Biomass Bioenerg, 35 (2011) 2950-2960.

[9] T.M. Komarek, F. Lupi, M.D. Kaplowitz, Valuing energy policy attributes for environmental management: Choice experiment evidence from a research institution, Energ Policy, 39 (2011) 5105-5115.

[10] E.P. Johnson, Air-source heat pump carbon footprints: HFC impacts and comparison to other heat sources, Energ Policy, 39 (2011) 1369-1381.

Chapter 2 Technoeconomic analysis of five microalgae to biofuel processes with varying complexities

(J. Renewable Sustainable Energy **7**, 043136 (2015))

Abstract

The economics surrounding five algae-to-fuels process scenarios were examined. The different processes modeled were as follows; an open pond producing either triacylglycerides (TAG) or free fatty acid methyl ester (FAME), a solar-lit photobioreactor producing either FAME or free fatty acids (FFA), and a light emitting diode irradiated (LED-lighted) photobioreactor producing TAG. These processes were chosen to represent both classical and esoteric approaches presented in the open literature. Viable (or suggested) processing techniques to liberate and purify (and convert) the microalgal triacylglycerides were then modeled to accompany each growth option. The investment and cost per kg of fuel or fuel precursor for each process was determined. The open pond produced TAG at ~$7.50/kg, while the process using the LED-lit photobioreactor produced TAG at ~$33/kg. The scenario containing the solar-lit photobioreactor produced FAME at ~$25/kg, while the open pond produced FAME at ~$4/kg. The scenario containing the solar-lit photobioreactor produced FFA at ~$29/kg. The open pond scenarios appear to be closest to the $1/kg price point at this time, and thus are the most viable economic options. Future technological advancements that reduce the cost of bioreactor vessels, LED lighting, and solvent recovery, may reduce the oil production costs of these scenarios to a more attractive level.

2.1 Introduction

Population outburst together with increased motorization has led to an overwhelming increase in the demand for fuel [1]. The potential of algae as a renewable, carbon neutral, and domestic source for biofuel production has generated significant commercial interest in recent years [2]. The idea of producing fuel from algae is not a novel concept, with the DOE's Aquatic Species Program performing pioneering research on algal biochemistry and mass production methods from 1978 to 1996 [3]. Ultimately the program was discontinued in 1996 because of the low price (~$25/barrel) for oil at the time. As oil prices have increased since 2000 (now >$90/barrel), sustainable energy alternatives, including algal biomass-based fuels, once again have become popular research and commercial endeavors. Microalgae have the ability to mitigate CO_2 emission and produce oil with a high productivity, thereby having the potential for applications in producing the third-generation of biofuels [4]. Currently there are scores of private companies actively attempting to commercialize fuel derived from microalgae—none are fully operational at this point.

In its recent roadmap report [2], the Department of Energy has cited the need for robust modeling efforts to advance the commercialization efforts of microalgae based biofuel. Herein, we report an economic breakdown of multiple alga processing scenarios to help elucidate their techno-economic feasibility. The manufacturing cost (per kg of fuel or fuel precursor) was compared, with a cost breakdown for the contributions of equipment, raw materials, and utilities to the overall production cost. These metrics were used to compare the different processes and highlight the probable "leverage points," that is, the costliest parts of the process or areas where technological advancement could most influence the future production cost.

A techno-economic model with the capability of incorporating existing published technologies, and potential future innovation, has been created—titled SAFEER (Sustainable algae-to-fuel: environmental and economic realities). The purpose of the model is to examine different processes to produce fuels from alga with a common design framework, using processing techniques from both specific companies' public information and possible novel scenarios, and to compare the economic and environmental impacts of the processes using established correlations and databases. (This paper only reports the economic results.) The results from these simulations facilitates comparison between different production scenarios and determining potential leverage points.

2.2 Background

The biochemical limitations, as well as advantages, of using microalgae are well documented from experimental [5] and theoretical perspectives [6]. A comparison of the productivities of microalgae and other oil-based crops has been tabulated elsewhere [7] (and is in the supplemental information) and suggest a 10 to 100-fold greater oil yield than crops such as corn, soy, and oil palm.

Indigenous species of microalgae with high lipid yields are especially valuable in the biofuel industry [8]. The highest metric listed for microalgae (~137,000 $L \cdot ha^{-1} \cdot y^{-1}$) is based on cultivation in an enclosed photobioreactor, while growth in an open pond is only observed to reach ~53,000 $L \cdot ha^{-1} y^{-1}$. In practice, the actual observed maximum oil production of a species of algae with 70% oil content is less than the theoretical maximum for that species at 50% oil content, which easily illustrates the difference between real processes and simple stoichiometric analysis.

Despite the relative abundance of experimental data and calculations on the potential productivity of microalgae, there are relatively few projections regarding the economic viability of algal biomass processes for producing fuels and/or fuel precursors. [9] and [10] found out that the process of algal cultivation could be improved for the efficient yield of algal lipids through the screening and improvement of algal strains. [11] examined the viability of currently available cultivation processes and found that they have questionable viability from both economic and positive energy return perspectives. [12] examined the selling price of microalgal biomass and biodiesel, and determined that a selling price between $700 and $900 per Mg of algal lipid is required in order for the process to be profitable. [7] estimated the cost of growing 100 Mg of microalga in photobioreactors and raceway ponds to be $2.95 and $3.80 per kg, but did not examine the costs required for liberating or upgrading the algal oils to a useable fuel. Another study [13], estimated the biomass production cost at $34 per kg, while [14] estimated costs between $8 and $70 per kg. The differences among various economic estimates can reflect both modeling assumptions, as well as, production variations.

Several sources indicate that a realistic production cost, for the growth step only, is between $10 and $80 per gal of algal oil grown [15], with estimates as low as $1.4 per gal [16], [17]. Notably, [18] examined the production cost of microalgal biomass and crude algal oil – from growth vessel to pure product – using various harvesting methods; flocculation, centrifugal recovery, and filtration. Aside from Grima's analysis, there are very few complete process economic estimates available in the literature. Thus, it is useful to provide detailed modeling efforts for a variety of processes using a single, and consistent modeling framework.

The production cost of entire algae-to-biofuels processes was determined in this work, with an emphasis on capturing the costs associated with liberating and upgrading algal oils after

growth. Several novel growth and processing unit operations were modeled as well, reflecting some of the paths to commercialization currently being discussed. Coupling the economic figures from the models with the previously known production thresholds produced a clearer picture of microalgae's feasibility as a photosynthetic platform for biofuel production. The processes were modeled, using data from patents, patent applications, peer reviewed publications, and company presentations (details are in the supplemental information). Five distinct cases were done that included possible process/product variations.

2.3 Methods

2.3.1 Processes studied

For the purpose of this study we created estimates for five very different process approaches. They are: i) the classical open pond growth system using conventional solvent extraction to recover the lipid product; ii) a closed, sunlight-supplied photobioreactor that avoids extraction by producing a biodiesel from in-situ transesterification; iii) an unconventional, artificially lighted photobioreactor that also uses conventional solvent extraction to recover the lipids, iv) the classical open pond growth system that avoids extraction by producing biodiesel from in-situ transesterification and v) a closed, sunlight supplied photobioreactor that uses extraction. Table 2-1 lists the main unit operations in high-level categories for each of these processes, and the following sections contain more general descriptions of them. Process flow diagrams for each, indicating the main unit operation steps, are in Figure 1 (a - e). Detailed process assumptions and the data sources are in the supplemental material.

Table 2-1- Algae processing techniques. The methods utilized in each process are listed.

category	functional purpose	unit operations – solar-lit photobioreactor producing FAME	unit operations – LED-lit photobioreactor	unit operations – open pond producing TAG	unit operations – open pond producing FAME	unit operations – solar-lit photobioreactor producing FFA
inoculation	creating sufficient cell density quickly for start-up and recovery after harvesting or upsets	small-scale closed photobioreactors, usually batch reactors with high levels of process controls	small-scale closed photobioreactors, usually batch reactors with high levels of process controls	small-scale closed photobioreactors, usually batch reactors with high levels of process controls	small-scale closed photobioreactors, usually batch reactors with high levels of process controls	small-scale closed photobioreactors, usually batch reactors with high levels of process controls
algae growth	grow cell mass; induce and support lipid production	partially closed photobioreactor; water, nutrient and CO_2 supply subsystems, media filter	closed photobioreactor; artificial lighting, water, nutrient and CO_2 supply subsystems	open photobioreactor; nutrient and CO_2 supply subsystems	open photobioreactor; nutrient and CO_2 supply subsystems	partially closed photobioreactor; water, nutrient and CO_2 supply subsystems, media filter
algae harvesting	recovering algal solids for further processing and initial recycle of bulk water, salts, and nutrients	sedimentation, flotation, centrifugation, drying	clarification, flotation	flotation, centrifugation	sedimentation, flotation, centrifugation, drying	flotation, centrifugation
oil and "other biomass" recovery	fractionation of the harvested biomass into primary and secondary fuel precursors, by-products, and final recycle streams	in situ transesterification, decanting, distillation	"milking" or "live extraction", electromechanical oil release and skimming	hexane extraction	in-situ transesterification, decanting, flash separation	hexane extraction
oil and biomass-to-fuel	the conversion process to the final fuel(s) and/or energy carriers	in-situ transesterification to FAME (biodiesel)	anaerobic digestion of biomass	N/A	in-situ transesterification to FAME (biodiesel)	N/A

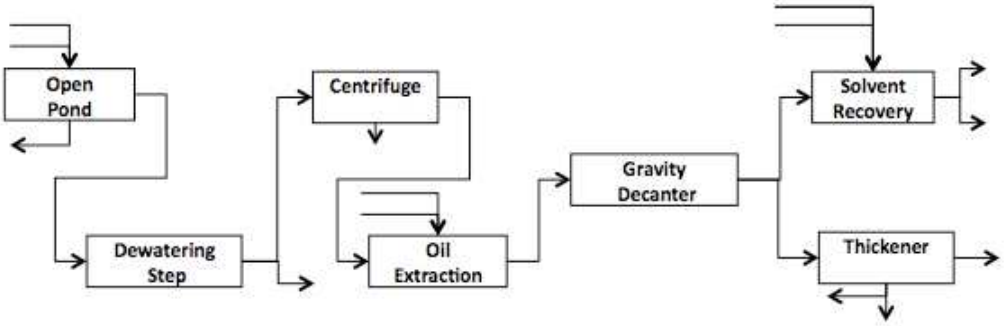
Open Pond
Centrifuge
Solvent Recovery
Gravity Decanter
Dewatering Step
Oil Extraction
Thickener

(a)

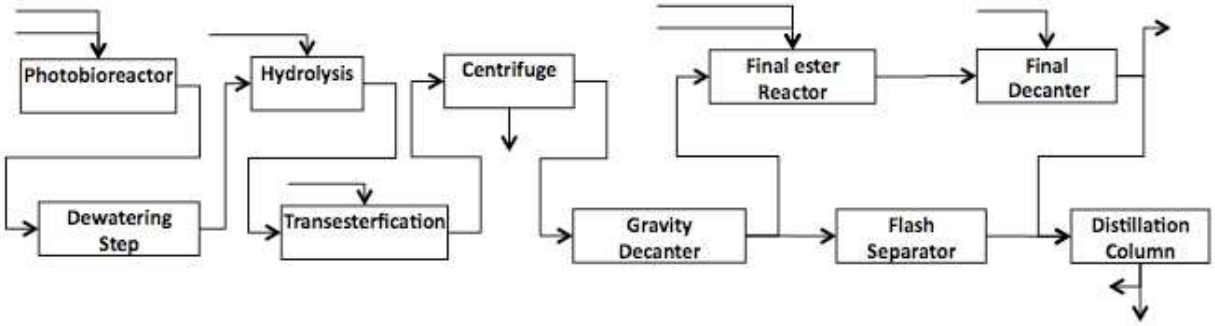
Photobioreactor
Hydrolysis
Centrifuge
Final ester Reactor
Final Decanter
Dewatering Step
Transesterfication
Gravity Decanter
Flash Separator
Distillation Column

(b)

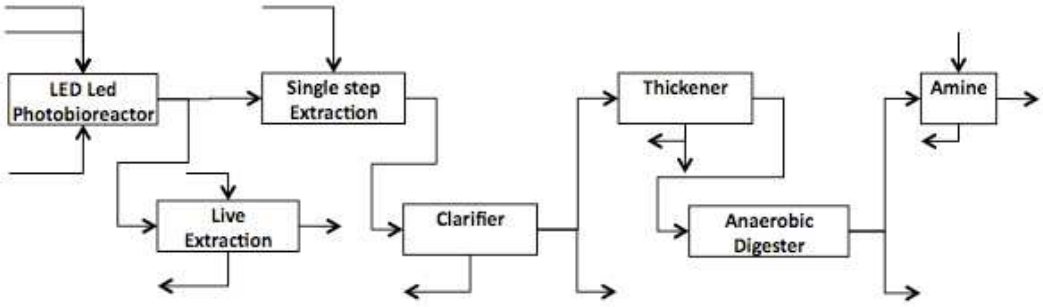
LED Led Photobioreactor
Single step Extraction
Thickener
Amine
Live Extraction
Clarifier
Anaerobic Digester

(c)

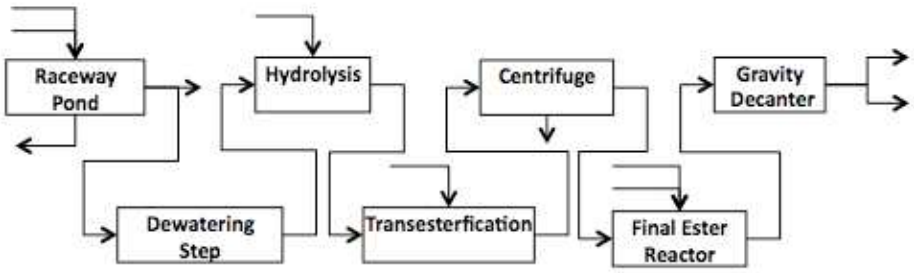

(d)

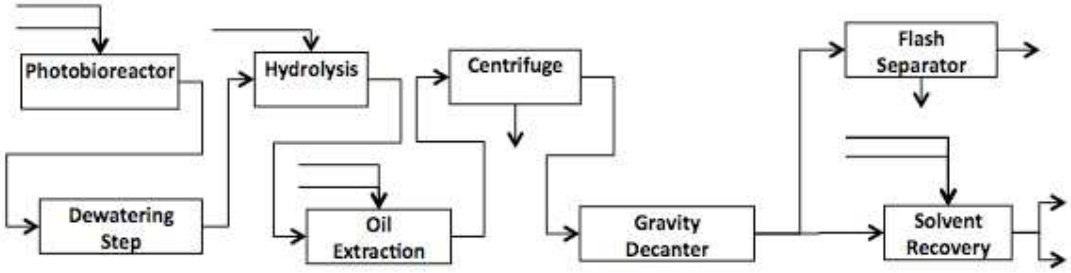

(e)

Figure 2.1-Process flow diagrams of the different processes studied: (a) open pond system producing TAG; (b) solar-lit photobioreactor producing FAME; (c) LED-lit photobioreactor; (d) open pond system producing FAME; and (e) solar-lit photobioreactor producing FFA.

2.3.1.1 Open pond producing TAG

Open pond growth systems producing *Spirulina* for nutritional and cosmetic purposes are currently in use. The specifics of a growth system were obtained from [19]. In this embodiment, microalga are grown in a pond with a surface area between 1 and 20 acres and an average depth of 6 to 15 inches. In our model, a gravity settler and centrifuge was used to dewater the microalgae, instead of the method described in the patent—contacting the microalgal slurry with hot flue gases or superheated steam to vaporize a portion of the water. The microalgal slurry is not completely dry after these unit operations; it still is only 5% cell matter (w/w). The partially

dewatered microalgae are extracted with hexane and ethanol to produce a three-phase solid, aqueous, and oil-rich mixture. The hexane must be recovered, using the industrially established procedure already common in soybean oil purification. The final three phase mixture is sent to a gravity settler, where the oil product is skimmed off the top layer. The cost of the growth ponds are estimated based on the report by Benemann and Oswald, with costs of site preparation, levee wall building, etc. calculated as $/ha of growth area [20].

2.3.1.2 Solar-lit photobioreactor

The growth system envisioned is a simple photobioreactor designed to grow microalgae in large suspended plastic bags housed within a concrete water basin [21]. The low density polyethylene (LDPE) bags float in a large water basin, which is engineered to provide a consistent favorable temperature for growth and to provide a barrier from contamination from wild algae strains or other microorganisms. Nutrients and carbon dioxide are pumped into the growth system, while microalgae are removed at a rate equal to the rate of new growth. The growth medium is continuously being filtered to reclaim any excess nutrients and disinfect the solution before being recycled to the growth vessel. The vessel is designed in a modular fashion, such that the areal footprint per vessel is constant – multiple modules are used to increase the overall production area.

The alga removed from the photobioreactor are further processed to isolate the algal lipids and produce biodiesel [22]. The algal slurry is first concentrated by removing a percentage of the water with a settling (or thermal drying) step. Acid hydrolysis then is used to lyse the alga and convert the cellular triacylglycerides into free fatty acids and glycerol. The free fatty acids are transesterified with methanol to produce fatty acid methyl esters (FAME), the main component of biodiesel. Separation of the aqueous, oil-rich, and solid phases is done in a three-

phase centrifuge, followed by gravity decanting and a "touch-up" transesterification reaction. Unreacted methanol is recovered using distillation.

2.3.1.3 Light emitting diode lighted photobioreactor

This "*unconventional"* photobioreactor foregoes using natural solar energy for an automated, tunable, light emitting diode (LED) lighting system within the reactor. This system, in theory, could be implemented anywhere – even in a warehouse or urban area – where natural sunlight is not abundant or consistent. The use of LEDs is to increase the area exposed to light within the reactor, allowing photosynthesis to occur more efficiently. [23]

An array of 4W LEDs, with a luminous efficacy of 60 lumens/W and spectral luminous efficiency of 0.7 yields a constant irradiance value of 286 $W \cdot m^{-2}$ at the surface of the light array. Additionally, the LED containing extensions are perforated and attached to a central stirrer shaft within the reactor, and serve to introduce nutrients and carbon dioxide to the cell culture [24]. The increased surface area in contact with the suspension makes the transport of nutrients proceed more efficiently than in standard cases where nutrients are bubbled into the reactor vessel. The design is modular, with each vessel having a motorized nutrient dispensing tube and LED array, and production scales linearly with the number of vessels in use . As described in [23], the vertical lighting design produces multiple growth planes within the reactor. This expands the apparent growth area of the vessel, increasing the productivity of the system while reducing the land use. Since multiple growth planes exist for photon transfer within the reactor, the projected skyward-facing surface area to volume ratio becomes moot, unlike photobioreactors using natural solar insolation.

Once the microalga have been grown, they are either lysed or milked using high voltage electromagnetic pulses of energy. The alga travels though waveguides, and based on the power

and duration of electrical stimulation the cell membranes either burst completely, or temporarily become porous, and allow intracellular oil to be released. This is similar to the process of electroporation [25]. Once the oil has been released, it floats to the top of a clarifying vessel, and is skimmed off as a product. Further settling of the algal biomass and water mixture allows separation into two distinct phases. The aqueous phase is recycled back to the growth vessel while the biomass is anaerobically digested to produce methane as a co-product.

2.3.1.4 Open pond producing FAME

This production scheme follows the scenario outlined by Lardon et al., (2009). The specifications of the open pond are same as the open pond producing TAG. The dewatering step dries the alga by removing 95% of water using a thermal drying process. Then the triglyceride is converted into FFA and glycerol in the presence of an acid catalyst. The solution is taken into a transesterification processing step where methanol (MeOH) is pressurized and combined with a stream containing the FFA, and sent to two reactor vessels in series. The transesterification reaction results in the formation of FAME. The resulting solution is then centrifuged and the solid is separated from the liquid stream. The liquid stream is again processed through a final ester reactor step where unreacted triglyceride is transesterified into FAME. The final solution is processed through a gravity decanter step and a pure stream of FAME is obtained.

2.3.1.5 Solar-lit photobioreactor producing FFA

This production scheme follows one of the two production scenarios proposed by [26]. Alga are grown in the solar-lit photobioreactor as described above. The solar-lit photobioreactor was used instead of an airlift tubular bioreactor to facilitate comparison with the other case. After the alga are grown, they are dewatered and hydrolyzed into FFA. The hydrolyzed FFA is extracted using the traditional hexane extraction method. [27]found that hexane is the better

solvent for extraction because it is not only less expensive, but also safer than another probable solvent toluene. After the extraction, the solids are separated from the solution by using centrifugation and two distinct liquid layers are separated using a gravity decanter. The oil-rich phase is processed using a solvent recovery step wherein hexane is recycled and a pure FFA stream is obtained. The water-rich phase is processed through a flash separator to recover solvent.

2.4 Modeling methodology

2.4.1 Process design and assumptions

In this study, the five process flow diagrams have been analyzed using our SAFEER modeling workbook. Several overarching assumptions serve as a common basis amongst all the cases. The SAFEER model is a series of coupled workbooks and worksheets linked by Visual Basic® coding and macros to determine economic expenses (and other figures-of-merit) required to produce a bio-based fuel from the microalgae feedstock. This is accomplished by breaking a proposed process scenario into multiple, linked unit operations. Each unit operation has a list of parameterized values that are used in the calculations that generate the material, energy, and capital flows for that step. These values were obtained in the literature for different unit operations within a design case. A full list of assumptions and citations can be found in the supplemental material.

Processes are constructed by assembling unit operations – like a simple process simulator – and an overall tabulation of the capital costs, operating costs, utility, and maintenance costs are calculated. Certain assumed values, dubbed user inputs, can be modified from case to case – allowing one to model a multitude of process scenarios with a great deal of flexibility. One can utilize values obtained from pilot scale experiments, or simply use a speculative best-case value

within a given case, and determine the sensitivity to a given parameter. This modeling approach allows one to model novel pieces of algae growth and processing equipment, and is not limited to equipment found within pre-existing commercial packages. Additionally, the ability of the model to run using only Microsoft Excel® enhances the ease of use and potential number of benefactors, since expensive process modeling software is not required.

For the purpose of this study, the baseline assumptions that are common for the different process cases are the composition of the algae (nominally *C. vulgaris*) that is grown, the total effective areal footprint of the growth system, and the yearly operating time of the proposed facility. These are tabulated in Table 2-2 and Table 2-3.

Table 2-2 - Solar characteristics.

PAR (annual mean)	226	$W \cdot m^{-2}$
E photon	0.2253	MJ/mol
Carbohydrate energy content	482.50	kJ/mol
Quantum requirement	8	photons
Growth area	500	ha
E solar	1.72	$W \cdot m^{-2}$
Yearly operating time	8000	h

The solar efficiency terms for with Alamosa, Colorado chosen as the location of the facility [6].

Table 2-3 - Algae composition.

Algae species	Chlorella vulgaris	
Biomass accumulation efficiency (respiration)	50%	
Cellular component	Overall % of biomass, molecular composition	HHV (MJ/kg)
Protein	30%	25.43
-C	4.43	
-H	7	
-O	1.44	
-N	1.16	

Carbohydrate	30%	15.90
-C	6	
-H	12	
-O	6	
Lipid	40%	47.26
-C	3	
-H	74	
-O	5	
E biomass	31.30	MJ/kg
Molecular formula	$C_{4.329}H_{35.3}O_{4.232}N_{0.348}$	

The molecular breakdown between protein, carbohydrates, and lipids comes from [28], while the energy of the biomass was estimated from [29].

For all the cases involving a solar-lit photobioreactor and open pond, the average annual PAR at the growth location, energy of a mole of photons, the number of photons required to produce a basic unit of energy— $CO_2 + H_2O + 8$ photons → $CH_2O + O_2$ —and the amount of energy used for cellular respiration are conserved between cases. The cellular respiration term represents a lumped biochemical efficiency value, and varies for the species of microalgae grown. The algal biomass is broken into classes of smaller biomolecules, proteins, carbohydrates, and lipids, comprising a percent of the overall dry biomass. Each cellular component is represented by a molecular formula detailing the C, H, O, and N content of the molecule. The amounts of phosphorous, potassium, magnesium, and sulfur are tabulated as an fraction of the total algal biomass [28].

The geometry and materials of the growth vessel determine the photon transmission efficiency, and the light source used also affects the photon utilization efficiency [6]. In the intermediate (solar-lit) photobioreactor system, the LDPE bags shield the alga from high light conditions, and ultimately increase the photon utilization efficiency of the system. An open pond is more exposed to potentially deleterious high light conditions, resulting in lower photon

utilization efficiency. The unconventional photobioreactor foregoes natural lighting in favor of LEDs and the tailored light source claims to drastically increase photon utilization. The photon energy transmission and utilizations for each case are listed in Table 2-4.

Table 2-4 - Algae growth reactor parameters.

Case	Photon transmission efficiency	Photon utilization efficiency	Areal productivity $kg \cdot m^{-2}\ h^{-1}$	Biomass production rate kg/h
Solar-lit photobioreactor	95%	50%	0.00165	8262
LED-lit photobioreactor	95%	90%	0.00376	244668
Open pond	95%	30%	0.00099	4957

Ultimately the transmission and utilization of photons determines the amount of solar energy available for biomass production. The respiration term accounts for how efficiently a given species of microalgae utilizes the incoming solar energy to grow and divide—more efficient microalgae species will have a lower respiration term. An empirically obtained higher heating value (HHV) per kg of the microalgae (in this case *C. vulgaris*) was calculated as 31.3 MJ/kg [30]. Dividing the amount of incident solar energy by the HHV of the biomass yields the areal productivity for a growth vessel. The higher the photon transmission and utilization efficiencies for a growth vessel, including the low cellular respiration parameter for the species of microalgae grown, the greater the areal productivity for that system. Since the gross areal footprint per reactor is the same for all five process scenarios, the processes' biomass production rate varies with these areal productivity values. The possible problems of contamination and inconsistent growth in the reactor vessels have not been addressed at this time, so the production rates presented are theoretical steady state, yearly-averaged values.

After the biomass is produced, the algal oils must be harvested, as described in the background section of this report. Flexible parameters account for the separation of components, conversion values, and temperature and pressure requirements. The amounts of raw materials and various utilities are specified for each unit operation as well. By-products are accounted for as credits, including the recycle of water and nutrients obtained from dewatering the microalga and the sale of the harvested cell matter as animal feed. For a detailed breakdown of the price of each raw material and credit value, see the supplemental material. A 15 y term at a 6% interest rate was used to calculate the yearly equipment cost based on the total depreciable capital investment.

2.4.2 Estimating equipment cost

Conducting an overall economic analysis for each of the processing scenarios requires an estimate of the purchased equipment cost, utility use, and raw material requirements for each unit operation. When standard process engineering equipment is required, cost and capacity estimates by [31] were used to calculate the capital equipment costs and the yearly inflation index (Chemical Engineering Plant Cost Index, aka CE index or CEPCI) was been applied to bring it to current year dollars. The cost of the open pond system was calculated by scaling values from [20]. The costs for novel pieces of processing equipment, like the unconventional LED-lit photobioreactor, was calculated by breaking the system into smaller parts with more easily estimable prices. This unconventional photobioreactor can be thought of a large closed vessel with an LDPE dispensing tube, LED arrays, motorized stirrer, and eductor for nutrient supply. Selling prices for these smaller component prices were estimated, along with installation factors, to produce an overall estimate for the price of the photobioreactor. Annual maintenance costs were calculated as a percent of the bare module cost of a piece of equipment. Replacement of

equipment was accounted for by specifying an equipment lifetime and using straight-line depreciation, assuming no equipment salvage value.

The annual yearly equipment costs, fixed costs, raw material costs, energy costs, and maintenance costs are tabulated for each process unit operation to yield an overall annual production cost. It should be noted that the production cost also includes first year startup costs, assumed as 10% of the total depreciable capital for the process. A complete list of the engineering assumptions used for each process can be found in the supplemental material for this chapter. The "assumptions" utilized were obtained from works in the literature, and represent reasonable values for separation factors, growth efficiencies, and processing conditions for an algae-to-fuel process.

2.5 Results and discussion

The breakdown of first year costs and costs of production for the first and second year for each of the five process scenarios are presented in Table 2-5. Relative comparisons of these data are presented in Figure 2.2. These economic model simulations assumed that CO_2 is available at no expense (no material, capital, or operating costs) to the biomass plant owner, so costs are very optimistic from that perspective. The equipment and cost summaries for each of the cases (at 500 ha production) are listed in tables in the supplemental material.

2.5.1 Open pond producing TAG

The investment for the open pond scenario is only a fraction of either the intermediate or unconventional photobioreactor processes. This is partially due to the fact that since the photon utilization efficiency is assumed to be a mere 30% for this process, the lower algal productivity decreases the size of the downstream processes. Only 4,957 kg/h of algal biomass (1983 kg/h of TAG) are produced, resulting in an overall productivity of 3,715 gal/acre/y (34,750 L/ha/y, only

about 9.8% of the theoretical maximum). Still, the amount of utility use is quite high in this process, and significantly increases the overall production cost.

Most of the utility use is associated with removing and recovering the solvent (hexane) that is used to extract the algal oils from the biomass. High-pressure steam is used to vaporize the solvent in a flash separator, evaporator, and stripping column. This energy use accounts for 63% of the total production cost per kg TAG manufactured. Ultimately, this value results from a (possibly) conservative overestimate for the amount of solvent required to fully extract the algal oil. The figure-of-merit for solvent use comes from a lab scale study by Ramirez [32], yet was adopted for the industrial scale model. If extraction experiments illustrated a difference in solvent requirements at larger scales, the overall use of high-pressure steam used to recover the solvent may be lowered. In addition, the amount of steam required for solvent recovery could be reduced if heat integration were practical for the process.

The equipment cost – especially the growth system – is not the dominant financial burden on this process scenario. The yearly equipment charge only accounts for 18% of the production cost, with only 3.7% of this attributable to the growth ponds. More than 90% of the equipment cost is used for dewatering the wet biomass harvested from the growth ponds prior to extraction.

2.5.2 Solar-lit photobioreactor producing FAME

For the solar-lit photobioreactor the cost is dominated by equipment and startup costs as illustrated in Figure 2.2. A total of 37,037 reactor basins, each with an area of 135 m^2, are required to generate the total growth area of 500 ha. Of the total equipment cost, 97.8% goes to purchasing and maintaining the photobioreactor basins. These equipment costs "roll-up" to ~79% of the overall production cost—the remaining processing equipment accounts for less than 1%. Steam and electricity also account for less than 1% of the production cost. Ultimately, the reactor

price will determine the viability of the overall process. Most of the reactor price goes to building the reactor basin and assembling the LDPE bags wherein the alga are grown. Streamlining and scaling this assembly for mass production scales *may* lead to reductions in the overall reactor price. 3,317 kg/h of FAME are produced in this case, equating to a production rate of 6,523 gal/acre/y (61,020 L/ha/y). The resulting FAME is "drop in" ready, meaning it can go directly into existing diesel engines without any further modification. This represents 17.3% of the theoretical maximum oil production for microalgae with 50% oil content, as calculated by [6].

2.5.3 LED-lit photobioreactor

This photobioreactor foregoes using natural lighting in favor of a tunable LED lighting system. This light source maintains optimal light conditions by minimizing high light exposure, such as is experienced outdoors during the middle of the day, thus allowing the photon transmission efficiency to increase from 30-50% to upwards of 90%. The average irradiance value in the lighting system is increased to 286 Wm^{-2} compared to the average annual value of 226 Wm^{-2} for natural light. An output of 97,867 $kg \cdot h^{-1}$ of algal triaclyglycerides (TAG) is produced, resulting in an apparent overall productivity of 183,363 gal/acre/y (1.71 million L/ha/y) [14,105 gal/acre/y/light-plane]. This represents 30% of the theoretical maximum algal oil production using direct sunlight if we consider just one light-plane of production. The productivity depends greatly on the assumption that the algae can use the input photonic energy with 90% efficiency. For example, if the photon utilization efficiency is only 50%, a lesser value of 3,305 $kg \cdot h^{-1}$ of algal triacylglycerides are produced per light-plane of production, and the overall productivity becomes 6,192 gal/acre/y per light-plane. The TAG oil must undergo further modification in order to be upgraded to a useable transportation fuel.

Table 2-5 - Net economic breakdown for all the cases at different growth acreages.

	Yearly equipment cost (M$)	Startup costs (M$)	Fixed costs (M$)	Raw materials costs (M$)	Credits (M$)	Energy (M$)	Maintenance costs (M$)	$/kg (1st year)	$/kg (2nd year)
50 ha Open pond (TAG)	1.53	1.49	4.50	11.8	27.0	7.42	1.69	10.2	9.3
500 ha Open pond (TAG)	14.1	13.7	4.50	118	270	74.2	16.1	7.5	6.6
5000 ha Open pond (TAG)	138	134	4.50	1185	2697	742	160	7.2	6.4
50 ha Solar-lit photobioreactor (FAME)	26.8	26.1	4.50	3.42	27.0	4.65	7.70	26.7	16.9
500 ha Solar-lit photobioreactor (FAME)	266	258	4.50	34.2	270	46.5	79.1	25.1	15.3
5000 ha Solar-lit photobioreactor (FAME)	2707	2629	4.50	342	2703	465	885	25.6	15.7
50 ha LED-lit photobioreactor	648	629	4.50	166	853	924	337	33.0	25.0
500 ha LED-lit photobioreactor	6467	6281	4.50	1662	8526	9313	3582	33.3	25.3
5000 ha LED-lit photobioreactor	64660	62799	4.50	16622	85256	101815	57137	37.1	29.1
50 ha Open pond (FAME)	1	1.41	4.50	2.22	17.0	1.90	1.60	6.8	5.9
500 ha Open pond (FAME)	13	12.7	4.50	22.2	170	19.0	15.6	4.1	3.0
5000 ha Open pond (FAME)	130	127	4.50	222	1701	190	156	3.8	3.0
50 ha Solar-lit photobioreactor (FFA)	26.5	25.7	4.50	16.7	35.9	11.5	7.66	31.7	21.5
500 ha Solar-lit photobioreactor (FFA)	262	254	4.50	167	359	115	78.2	29.9	19.9
5000 ha Solar-lit photobioreactor (FFA)	2667	2590	4.50	1667	3591	1155	876	30.5	20.3

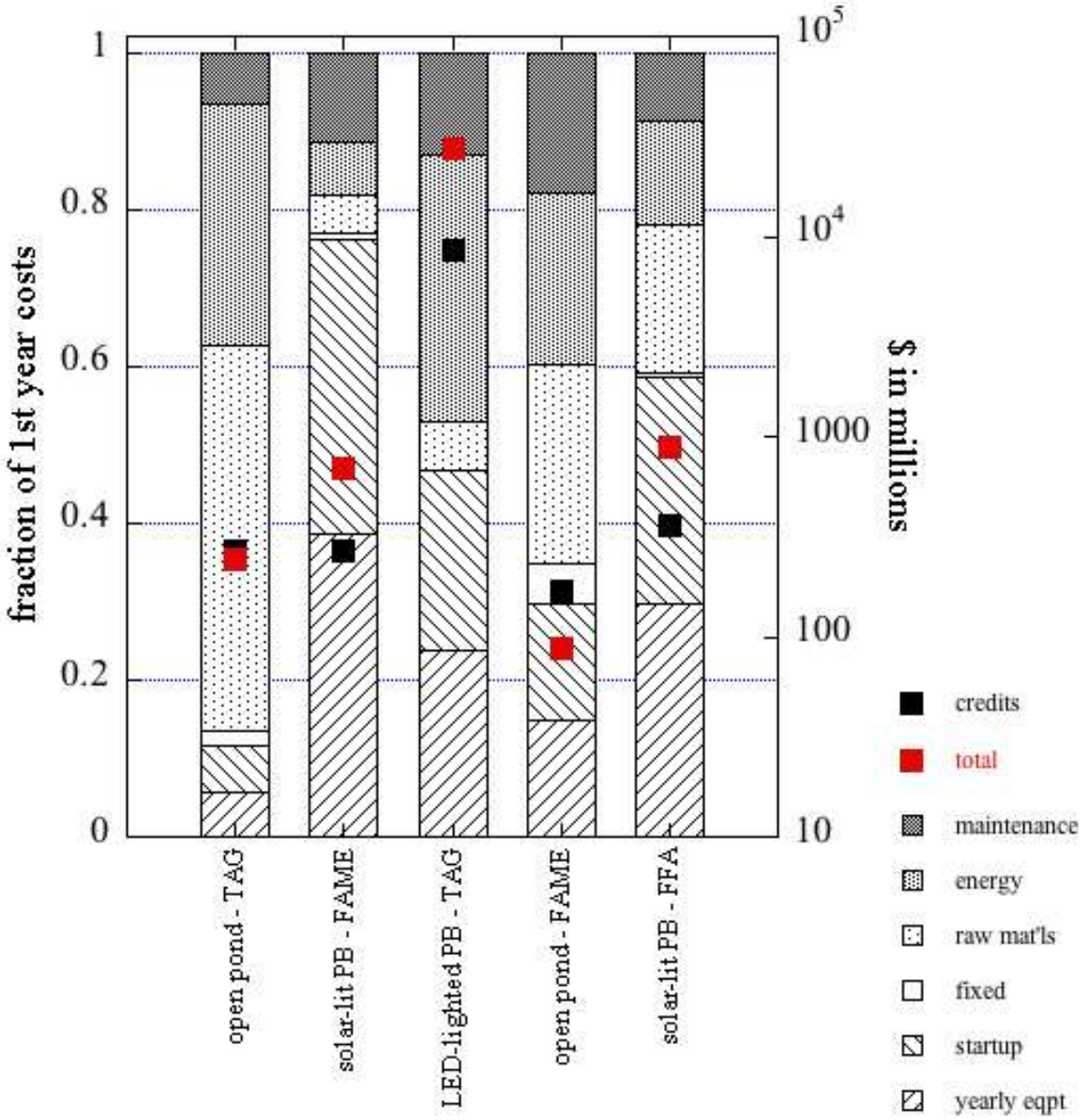

Figure 2.2 - Modeling summary. The fractional contributions (left hand axis) to the net 1st year equipment, maintenance, energy, raw materials, credits, startup, and fixed costs and the total 1st year costs and credits in $ millions (right hand log axis) for 500 ha facilities.

From an economics standpoint, the viability of this unconventional photobioreactor process is dependent upon the effectiveness of the multiple "growth planes" within the reactor. Increasing the number of growth planes – horizontal slices of the reactor receiving sufficient photonic energy to grow algae – decreases the number of reactors necessary to generate a

specified growth area. For example, a 2 m x 4 m photobioreactor with 10 cm LED arrays spaced 20 cm apart may have up to 13 growth planes in the reactor. The growth area of this vessel is thus effectively increased from 3.1 m^2 to 41 m^2; diminishing the number of reactors required by a proportionate amount.

The effect of the growth planes in the reactor is illustrated in the economic analysis of this process (see Figure 2.2 for the overall economic breakdown). If only one growth plane exists within the reactor, the basal area becomes the effective area, resulting in a production cost of ~$206/kg. However, if 13 growth planes exist in the reactor, the effective growth area and production rate per reactor is increased, reducing the production cost to ~$33/kg. The actual land use for the growth vessels becomes only 9.2% of the effective growth area, a significant reduction. At this point, the estimated production cost likely lies between $206 and $33/kg, with experimental photobioreactor productivity values needed to determine the actual number of growth planes within the reactor and the associated production cost.

The net utility costs of this unconventional process is hundreds of times greater than that for the solar-lit photobioreactor and open pond scenarios. If 13 planes per reactors are used, only 2% of the energy use goes towards the LED lighting system in the photobioreactor. The remaining 98% of electrical energy goes towards processing algal biomass to produce pure TAG. Although the required investment in utilities is significant, it is only a fraction of the process equipment costs. If all electrical energy use were eliminated, the cost of production would be reduced significantly. This represents about one half of the initial investment required for the photobioreactor vessels, comprising 25% of the production cost. Finally, 60% of the production cost goes into the gravity settling equipment used to separate the oil, water, biomass and solvent—mostly due to dewatering the algae and recovering the solvent.

2.5.4 Open pond producing FAME

Like the open pond producing TAG, the overall cost for growth is high and has similar production rates of algal biomass—4,957 kg/h of algal biomass (1,983 kg/hr of TAG) with 3,715 gal/acre/y (34,750 L/ha/y, 9.8% of the theoretical maximum). Since the traditional solvent extraction process was eliminated from this process, the processing cost is not as high. The energy cost comprises about 23% of the total production cost. Raw materials are ~27% of the total production cost making this production scenario the most inexpensive of all. FAME produced as the final product is 1991 kg/h (3,915 gal/acre/y or 36,627 L/ha/y). Figure 2.2 show the contributions to the net investment of yearly equipment, maintenance, energy, raw materials, credits, startup, and fixed costs used in an open pond producing FAME.

2.5.5 Solar-lit photobioreactor producing FFA

The overall cost for growth continues to be high since the production rate of algal biomass is modest at 8,262 kg/h (3,163 kg/h of FFA)—an overall productivity of 5,926 gal/acre/y (55,428 L/ha/y, ~15.6% of the theoretical maximum). Since a traditional solvent extraction process is incorporated in this process, the processing cost is higher, along with the high startup cost due to the expensive bioreactors. The energy cost comprises about 15.6% of total production cost. Raw materials make about 22% of total production cost making this production scenario an expensive one. Yearly equipment and startup comprises of 68% of the total production cost. Figure 2.2 provides further details on costs.

2.6 Comparison of process scenarios

Each process scales essentially linearly in terms of growth area, which leads to a corresponding linear increase in the overall production costs. There are few economies-of-scale at this time because the growth equipment is the dominant cost factor and are included with a

modular approach. For example, the maximum size of a pond is set as 10 ha, and a process with a growth area of 100 hectares would need 10 such ponds. This approach is meant to reasonably incorporate risk mitigation from ponds "crashing". The other growth systems have additional rationales for considering them as modular investments. The results for several growth areas are presented in Table 2-5.

Figure 2.3 presents the effect of photoconversion efficiency on the manufacturing cost of the specific product. Both types of photobioreactors display a geometric dependence on the photoconversion efficiency, while the open pond scenario is less affected by variations in this parameter. The manufacturing cost was calculated with PAR values of 160 Wm^{-2} and 310 Wm^{-2}, representing low and high light conditions, respectively. At low photoconversion efficiencies, the economic savings of operating at a higher PAR is substantial. At higher photoconversion efficiencies, this difference is diminished. The relatively flat sensitivity of the open pond scenario is because the reactor basin was not the major contributor to the production cost in the design.

Increasing the photoconversion efficiency leads to an increase in the overall algal oil production, but does not change the overall growth area or number of growth vessels required. The number of downstream processing units, however, does change with increased productivities. For each photobioreactor case, the increase in productivity does not substantially alter the overall equipment cost, since the reactor cost (which is dominant) is unchanged. But greater productivity from these reactors leads to a reduction in the cost per kg of the algal oil. In the open pond case, over 75% of the equipment cost is invested in creating the open pond. Since the equipment cost scales linearly with productivity in this case, the cost per kg of the algal oil is relatively unaffected by increased photoconversion efficiencies.

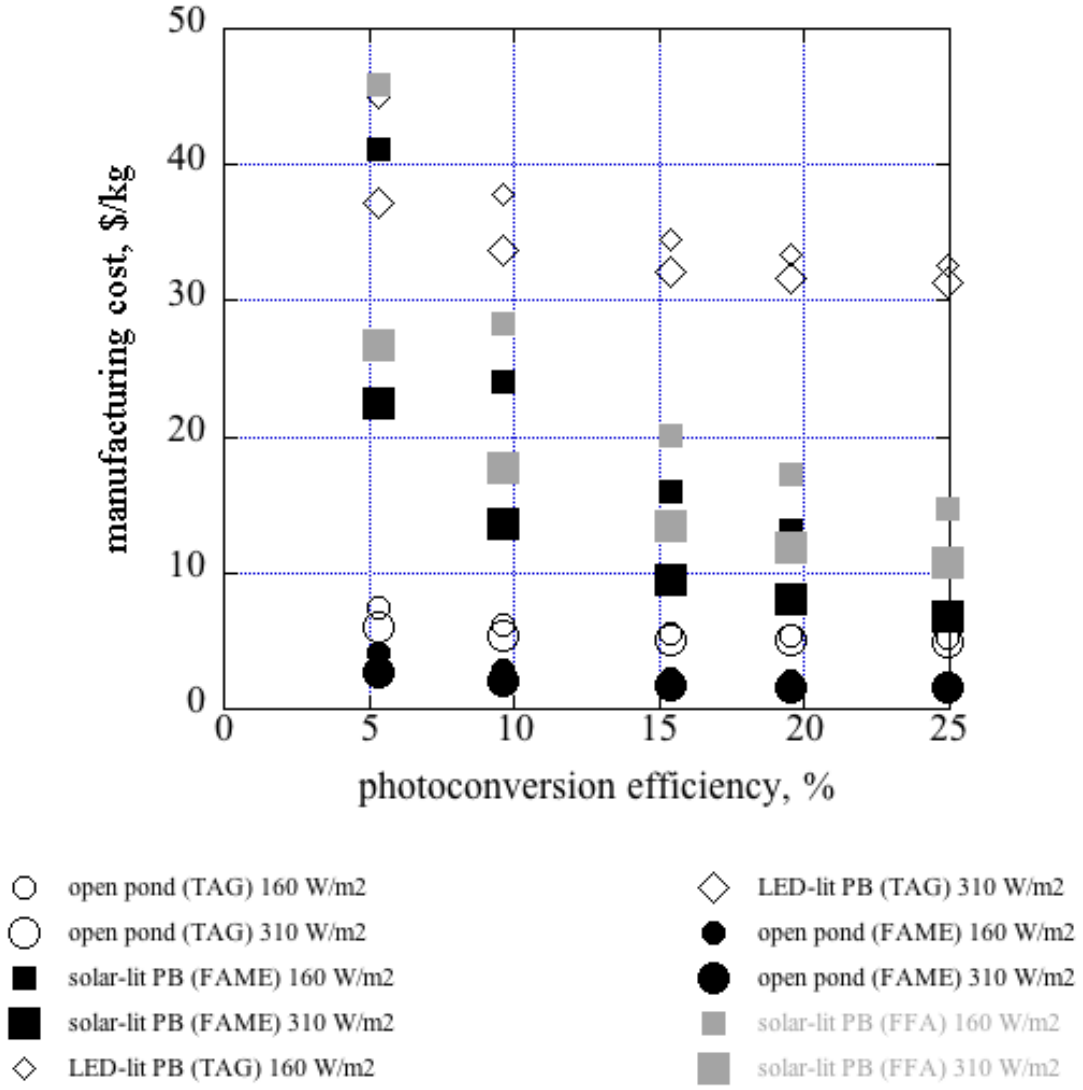

Figure 2.3 – Sensitivity analysis of product manufacturing cost to photoconversion efficiency.

2.7 Perspectives

There is significant interest in commercializing algae-derived biofuels. Nonetheless, there remains significant economic uncertainty surrounding many of the publicly proposed algae-to-biofuels processes. It was the goal of this work to estimate the production costs per unit of product obtained for several processes, with common underlying assumptions and cost estimation techniques constituting the basis of the simulation.

The most mature process, a classical open pond growth system, using large area shallow ponds, was shown to be the least expensive method for producing product at industrial scales. However, the use of solvents to extract algal oils and the required recovery of these solvents was found to be quite expensive, contributing ~30% of the ~$7.5/kg production cost for the open pond scenario. If heat integration is included in the process model, and the amount of energy required for solvent regeneration is diminished, a production cost of around $6/kg is a reasonable estimate for this scenario.

The solar-lit photobioreactor scenario, which uses in-situ tranesterfication to release the fuel value of the biomass, appears effective, from a relative financial standpoint, at liberating and upgrading algal oils to drop-in ready FAME, at a manufacturing cost of ~$25/kg. Experimentally verifying the actual effectiveness of in-situ transesterification will elucidate whether this process can be feasible or not. The major financial burden for this process lies in the novel growth basin cost; scaling this system in an economic fashion is crucial to its viability. However, the fact that the FAME produced need not be further refined to create a fuel adds to the potential commercial attractiveness of the process.

The LED-lighted growth system (and process) requires a significant supply of external energy to grow and process the algae. [23] claimed that this process can support very high algae growth rates, yet the energy intensive nature of the scenario results in a production cost of up to $206/kg oil, assuming only one growth plane in the reactor. The overall algal oil production is greatest for this photobioreactor, and the land requirement and cost may be greatly reduced if multiple vertical growth planes can be cost-effectively manufactured and maintained within the reactor. Within limits, each growth plane in the reactor decreases the production cost by the same factor; thus with 13 growth planes the production cost becomes $33/kg. The capital and utility

costs, however, reflect the large initial investment required for this unconventional process. At this time, the projected production costs seem more of a hurdle than the benefit of increased production. If the equipment cost, dominated by the price of the photobioreactor vessel, can be reduced below the current estimate, while maintaining productivity, the economic outlook of this process can improve.

The open pond system used for producing FFA, which is then converted to FAME, has the lowest production cost at $4/kg FAME. It eliminates the use of the solvent extraction process that demands large energy costs. Also, it has lower initial equipment and, concomitant, startup costs. So, further improvement of growth of algae within the open pond scenario can move closer to a desirable target of ~$1/kg production cost.

The solar-lit, photobioreactor system producing FFA is somewhat expensive because of the presence of several expensive equipment choices within one scenario. The solvent recovery and growth photobioreactors cost the most and are the major reasons behind the ~$30/kg production cost. If the cost of setting up of the photobioreactors decreases below the current estimates, then significant overall production cost savings can ensue. Alternative and efficient methods of solvent recovery are also indicated as technical lever points to lower the overall cost of production.

The implementation of genetic engineering techniques may lead to improvements in the photon utilization efficiency of microalgae. Coupling this with improvements in tunable light sources and photobioreactor optics can increase the overall photoconversion efficiency of a microalgae culture. This metric was shown to significantly affect the production cost of microalgae grown in photobioreactor vessels. Nonetheless, only the open pond growth system has been employed for industrial scale production of microalgae. The photobioreactor growth

vessels are still in the pilot stages and have not been demonstrated yet to scale effectively and economically.

In general, our model(s) has several speculative inputs, such as the actual cost of novel photobioreactors (as opposed to future, complete design-for-manufacturing estimates), the amount of solvent required to effectively extract oil from microalgae, the effectiveness of in-situ transesterification, and the incorporation of heat integration. A selling price of less than $1/kg of oil may be possible if many of these uncertainties and leverage points are addressed and are dramatically improved with further research, development, and manufacturing capability.

2.8 Conclusions

We have addressed scaleup and commercialization of algae-to-biofuels processes from a quantitative perspective. At this point, the production costs calculated are several orders of magnitude greater than the selling price of oil from seed crops. It has been shown that each process has multiple hurdles to overcome and price reductions to achieve before algae-based biofuels are economically competitive with traditional fossil oil or other oil crops. The open pond scenarios were closest to the $1/kg price point, and at this moment appear to be closest to commercialization. Bioreactor based growth methods were shown to currently be prohibitively expensive, but future technological advances may drastically improve the economic outlook for these scenarios.

2.9 Acknowledgments

The authors gratefully acknowledge the support and guidance provided by Dr. Geetha Kothandaraman of ConocoPhillips, Biofuels R&D through the Colorado Center for Biofuels and Biorefining Sponsored Research Program. We also acknowledge the VBA programming skills provided by Nisheeth Bhat and Jeff Harvey in developing the SAFEER modeling environment

and the assistance provided by Aaron Palumbo in developing databases on algal biomass-related process technologies.

2.10 References

[1] G.S. Anisha, R.P. John, K.M. Nampoothiri, A. Pandey, Micro and macroalgal biomass: A renewable source for bioethanol, Bioresource Technology, 102 (2011) 186-193.

[2] D. Fishman, R. Majumdar, J. Morello, R. Pate, J. Yang, National Algal Biofuels Technology Roadmap, in: U.S. DOE (Ed.), Office of Energy Efficiency and Renewable Energy, Biomass Proagram, 2010, pp. 1-114.

[3] J. Sheehan, T. Dunahay, J. Benemann, P. Roessler, A Look Back at the U.S. Department of Energy's Aquatic Species Program: Biodiesel from Algae; Close-Out Report, U.S. Department of Energy's Aquatic Species Program: Biodiesel from Algae, NREL, 1998, pp. 325 pages.

[4] J.S. Chang, C.Y. Chen, K.L. Yeh, R. Aisyah, D.J. Lee, Cultivation, photobioreactor design and harvesting of microalgae for biodiesel production: A critical review, Bioresource Technology, 102 (2011) 71-81.

[5] Y.K. Lee, Microalgal mass culture systems and methods: Their limitation and potential, Journal of Applied Phycology, 13 (2001) 307-315.

[6] K.M. Weyer, D.R. Bush, A. Darzins, B. Willson, Theoretical Maximum Algal Oil Production, BioEnergy Research, (2009) 10.

[7] Y. Chisti, Biodiesel from microalgae, Biotechnology Advances, 25 (2007) 294-306.

[8] F. Bux, T. Mutanda, D. Ramesh, S. Karthikeyan, S. Kumari, A. Anandraj, Bioprospecting for hyper-lipid producing microalgal strains for sustainable biofuel production, Bioresource Technology, 102 (2011) 57-70.

[9] P.S. Nigam, A. Singh, J.D. Murphy, Mechanism and challenges in commercialisation of algal biofuels, Bioresource Technology, 102 (2011) 26-34.

[10] P.S. Nigam, A. Singh, J.D. Murphy, Renewable fuels from algae: An answer to debatable land based fuels, Bioresource Technology, 102 (2011) 10-16.

[11] J.K. Pittman, A.P. Dean, O. Osundeko, The potential of sustainable algal biofuel production using wastewater resources, Bioresource Technology, 102 (2011) 17-25.

[12] P.J.L. Williams, L.M.L. Laurens, Microalgae as biodiesel & biomass feedstocks: Review & analysis of the biochemistry, energetics & economics, Energy & Environmental Science, 3 (2010) 554-590.

[13] Y. Shen, W. Yuan, Z.J. Pei, Q. Wu, E. Mao, MICROALGAE MASS PRODUCTION METHODS, Trans. ASABE, 52 (2009) 1275-1287.

[14] J.B. van Beilen, Why microalgal biofuels won't save the internal combustion machine, Biofuel Bioprod Bior, 4 (2010) 41-52.

[15] A. Darzins, The promises and challenges of algal derived biofuels, 2009.

[16] K.L. Kadam, Plant flue gas as a source of CO2 for microalgae cultivation. Economic impact of different process options, Energy Conversion and Management, 38 (1997) S505-S510.

[17] J.R. Benemann, Systems and economic analysis of microalgae ponds for conversion of CO2 to biomass. 4th Quarterly technical progress report, US/Japan meeting on coal energy research, University of California Berkley, Albuquerque, NM, 1994, pp. 9.

[18] E.M. Grima, E.H. Belarbi, F.G.A. Fernandez, A.R. Medina, Y. Chisti, Recovery of microalgal biomass and metabolites: process options and economics, Biotechnology Advances, 20 (2003) 491-515.

[19] G. Jensen, E.H. Reichl, Integrated microalgae production and electricity cogeneration in: U.S.P.a.T. Office (Ed.) United States Patent and Trademark Office, Cyanotech Corporation, 1997.

[20] J.R. Benemann, W.J. Oswald, Systems and economic analysis of microalgae ponds for conversion of CO to biomass. , in: U.S.D.o. Energy (Ed.) Final report, U.S. Department of Energy, 1996, pp. 214.

[21] B. Willson, Diffuse Light Extended Surface Area Water-Supported Photobioreactor in: U.S.P.a.T. Office (Ed.) United States Patent and Trademark Office, 2008.

[22] M.T.e.a. Machacek, Continuous Algal Biodiesel Production Facility, in: U.S.P.a.T. Office (Ed.) United States Patent and Trademark Officeusa, 2009.

[23] N. Eckelberry, T.R. Eckelberry, Algae Growth System for Oil Production, in: U.S.P.a.T. Office (Ed.) United States Patent and Trademark Office, 2009.

[24] N. Eckelberry, Apparatus for generating microbubbles while mixing an additive fluid with a mainstream liquid, 2001, pp. 9.

[25] J.C. Weaver, Y.A. Chizmadzhev, Theory of electroporation: A review, Bioelectrochem. Bioenerg., 41 (1996) 135-160.

[26] A.L. Stephenson, E. Kazamia, J.S. Dennis, C.J. Howe, S.A. Scott, A.G. Smith, Life-Cycle Assessment of Potential Algal Biodiesel Production in the United Kingdom: A Comparison of Raceways and Air-Lift Tubular Bioreactors, Energ Fuel, 24 (2010) 4062-4077.

[27] M.M. El-Halwagi, G. Pokoo-Aikins, A. Heath, R.A. Mentzer, M.S. Mannan, W.J. Rogers, A multi-criteria approach to screening alternatives for converting sewage sludge to biodiesel, Journal of Loss Prevention in the Process Industries, 23 (2010) 412-420.

[28] L. Lardon, A. Helias, B. Sialve, J.P. Stayer, O. Bernard, Life-Cycle Assessment of Biodiesel Production from Microalgae, Environmental Science & Technology, 43 (2009) 6475-6481.

[29] A.F. Clarens, E.P. Resurreccion, M.A. White, L.M. Colosi, Environmental Life Cycle Comparison of Algae to Other Bioenergy Feedstocks, Environmental Science & Technology, 44 (2010) 1813-1819.

[30] A.F. Clarens, E.P. Resurreccion, M.A. White, L.M. Colosi, Environmental Life Cycle Comparison of Algae to Other Bioenergy Feedstocks, Environmental Science & Technology.

[31] Seider, Product and Process Design Principles: Synthesis, Analysis, and Evaluation, 2nd Edition, Wiley2004.

[32] A.R. Fajardo, L.E. Cerdan, A.R. Medina, F.G.A. Fernandez, P.A.G. Moreno, E.M. Grima, Lipid extraction from the microalga Phaeodactylum tricornutum, European Journal of Lipid Science and Technology, 109 (2007) 120-126.

2.11 Supplementary information

2.11.1 Tables mentioned in the body of the chapter

Following tables illustrate some vital information mentioned into the body of the chapter:

Table 2-6 – Comparison of oil productivity from crops.

crop†	oil yield, L/ha/y
corn	172
soybean	446
canola	1,190
jatropha	1,892
coconut	2,689
oil palm	5,950
microalgae (70% oil content)	136,900 (theoretical)

†[7]

Table 2-7 – Equipment and cost summary of open pond case producing TAG on 500 ha.

unit operation	process equipment	quantity	total cost (in 1000's USD)
open pond	open ponds	50	34,500
	hollow fiber membranes	1	50,000
	inclined settler	1	0
	conveying pump	3	179
dewatering step	drying equipment	1	8,000
centrifuge	centrifuge	4	5,194
oil extraction	vessel	1	505
gravity decanter	decanter	1	308
solvent recovery	heat exchanger	1	94
thicker	flash vessel	1	44
	evaporator	1	29
	stripping column	1	14
	thickner	1	3,400

Table 2-8- Equipment and cost summary of solar-lit photobioreactor producing FAME on 500 ha.

unit operation	process equipment	quantity	total cost (in 1000's USD)
Photobioreactor	Solix bioreactor basin	37037	1,619,807
	compressor	1	2,473
	circulating pumps	5	1,090
	filtration membrane	1	32,965
dewatering step	drying equipment	1	8,000
hydrolysis	pump	1	42
	heat exchanger	3	352
	reactor vessel	2	279
transesterification (1)	pump	1	34
	reactor vessel	1	213
centrifuge	centrifuge	7	8,656
gravity decanter (1)	decanter	1	718
transesterification (2)	pump	1	40
	heat exchanger	1	116
	reactor vessel	1	35
gravity decanter (2)	decanter	1	230
flash separator	flash vessel	1	641
	heat exchanger	1	280
distillation column	columns	36	28,189

Table 2-9- Equipment and cost summary of unconventional LED-lit photobioreactor case on 500 ha.

unit operation	process equipment	quantity	total cost (in 1000's USD)
growth	LED-lit PB	119366	8,215,064
	compressor	1	4,946
	eductor	119366	477,465
live extraction	vessel	1882	526,650
	pulse generator	1	618
single step extraction	vessel	1711	247,798
	eductor	1711	10,374
clarifier vessel	clarifier vessel	2948	25,808,679
thickner	thickner	587	5,139,152
anaerobic digester	anaerobic digester	474	1,879,780
amine	vessel (type 1)	1	510
	vessel (type 2)	1	232
	pump (type 1)	1	117
	pump (type 2)	1	228

Table 2-10 – Equipment and cost summary of open pond case producing FAME on 500 ha

unit operation	process equipment	quantity	total cost (in 1000's USD)
open Pond	open ponds	50	34500
	hollow fiber membranes	1	50000
	inclined settler	1	0
	conveying pump	3	179
dewatering Step	drying equipment	1	8000
hydrolysis	pump	1	26
	heat exchanger	3	295
	reactor vessel	2	839
transesterification (1)	pump	1	23
	reactor vessel	1	59
centrifuge	centrifuge	1	989
transesterification (2)	pump	1	46
	heat exchanger	1	116
	reactor vessel	1	498
gravity decanter	decanter	1	216

Table 2-11 – Equipment and cost summary of solar lit photobioreactor case producing FFA on 500 ha.

unit operation	process equipment	quantity	total cost (in 1000's USD)
solar-lit photobioreactor	bioreactor basin	37037	1619807
	compressor	1	2473
	circulating pumps	5	1090
	filtration membrane	1	32965
dewatering step	drying equipment	4	8000
hydrolysis	pump	1	28
	heat exchanger	3	282
	reactor vessel	2	110
oil extraction	vessel	1	675
centrifuge	centrifuge	4	4575
gravity decanter	decanter	1	340
flash separator	flash vessel	1	145
	heat exchanger	1	280
solvent recovery	heat exchanger	1	96
	flash vessel	1	225
	evaporator	1	34
	stripping column	1	14

2.11.2 Assumptions for the simulation

Following tables illustrate assumptions for the simulation of five cases:

Table 2-12 – Scenario selector

assumption	value	units	source
purchase price index	609		(1)
operating time per year	8000	h	
PAR	100	W/m^2	(2)
Q	10%		
growth area	5000000	m^2	user input
functional unit of energy	317	GJ	(3)
algal composition - % protein	30%		user input
C	4.43	element comp	(4)
H	7	element comp	
O	1.44	element comp	
N	1.16	element comp	
algal composition - % carbohydrate	30%		user input
C	6	element comp	(4)
H	12	element comp	
O	6	element comp	
algal composition - % lipid	40%		
C	3	element comp	(4)
H	74	element comp	
O	5	element comp	
TG selling price	$9.30	kg	user input ~ $32/gal (5)
TG purchase price	$0	kg	
FFA selling price	$0.94	kg	user input
FFA purchase price	$0	kg	
methanol selling price	$0.5	kg	$1.5/gal – range $0.96-2/gal (6)
methanol purchase price	$(0.5)	kg	
water selling price	$0.0004	kg	(1)
water purchase price	$(0.0004)	kg	
H_2SO_4 selling price	$0.055	kg	$50/ton – range $25-100/ton (7)
H_2SO_4 purchase price	$(0.055)	kg	

assumption	value	units	source
glycerol selling price	$1.54	kg	$0.7/lb – range $0.7-1/lb (8)
glycerol purchase price	$0	kg	
cell matter selling price	$0.50	kg	user input
cell matter purchase price	$0	kg	not purchased
FAME selling price	$9.30	kg	user input ~ $32/gal (5)
FAME purchase price	$0	kg	not purchased
$Ca(NO_3)_2$ selling price	$0.33	kg	$300/ton – range $200-400/ton (9)
$Ca(NO_3)_2$ purchase price	$(0.33)	kg	
$CaH_6O_8P_2$ selling price	$0.88	kg	$418/ton – range $200-800/ton (9)
$CaH_6O_8P_2$ purchase price	$(0.88)	kg	
KCl selling price	$0.11	kg	$125/ton – range $105-125/ton (7)
KCl purchase price	$(0.11)	kg	
$Mg_3(PO_4)_2$ selling price	$0.32	kg	$0.145/lb – range $0.12-0.18/lb (6)
$Mg_3(PO_4)_2$ purchase price	$(0.32)	kg	
Na_2SO_4 purchase price	$(0.11)	kg	$110/tonne – range $110-125/tonne (7)
Na_2SO_4 selling price	$0.11	kg	
CO_2 purchase price	$(0.46)	kg	(10)
CO_2 selling price	$(0.10)	kg	user input – disposal price
CH_4 purchase price	$(0.15)	kg	$6/1000 ft^3 (11)
CH_4 selling price	$0.15	kg	
NH_3 purchase price	$(0.50)	kg	$500/tonne – range $385-770/tonne (12)
NH_3 selling price	$0.50	kg	
MEA purchase price	$(2.50)	kg	(13)
MEA selling price	$2.50	kg	

assumption	value	units	source
$C_6H_{12}O_6$ purchase price	$(0.56)	kg	(14)
$C_6H_{12}O_6$ selling price	$0.56	kg	
amino acid purchase price	$(0.58)	kg	(10)
amino acid selling price	$0.58	kg	
flue gas purchase price	$0	kg	not purchased
flue gas selling price	$(0.50)	kg	user input – disposal price
H_2 purchase price	$(4.00)	kg	(15)
H_2 selling price	$4.00	kg	
renewable diesel purchase price	$0	kg	not purchased
renewable diesel selling price	$2.86	kg	(16)
light naphtha purchase price	$0	kg	Not purchased
light naphtha selling price	$0.50	kg	$1.3/gal – range $1.21-1.64/gal (8)
EtOH purchase price	$(0.84)	kg	$2.5/gal – range $2.1-4/gal (12)
EtOH selling price	$0.84	kg	
hexane purchase price	$(0.48)	kg	$1.19/gal – range $1.15-1.19/gal (8)
hexane selling price	$0.48	kg	
adsorbent particle purchase price	$(1,800)	kg	(17)
adsorbent particle selling price	$1,800	kg	
catalyst purchase price	$(1.00)	kg	user input
catalyst selling price	$1.00	kg	user input
electricity purchase price	$(0.05)	kWh	(1)
electricity selling price	$0.05	kWh	(1)
LP Steam purchase price	$(1.81)	kg	(1)
LP Steam selling price	$1.81	kg	(1)
HP Steam purchase price	$(2.49)	kg	(1)
HP Steam selling price	$2.49	kg	(1)
LP steam production energy	2628380	J/kg	(18)
combustion efficiency source	90%		

assumption	value	units	source
fuel			
HP steam production energy	2628380	J/kg	
combustion efficiency source fuel	90%		
cooling water purchase price	$(0.05)	kg	(1)
cooling water selling price	$0.05	kg	(1)
annual interest rate	6%		user input
length of interest term	15	Yr	user input

Table 2-13 – Photobioreactor assumptions

assumption	value	units	source
kg P/kg algae	0.0099	kg/kg	(4)
kg K/kg algae	0.0082	kg/kg	
kg Mg/kg algae	0.0038	kg/kg	
kg S/kg algae	0.0022	kg/kg	
percent utilization of CO_2	10%		user input
conversion of CO_2 to biomass	100%		user input
mass fraction of algae	0.001	kg algae/kg H_2O	User input - 1 g/L – range 1-11g/L (19)
Solix bioreactor basin – installation factor	2		user input
compressor – installation factor	2		user input
circulating pumps – installation factor	4		user input
filtration membrane – installation factor	1.5		user input
Solix bioreactor basin – maintenance	1%	% of bare module cost	user input
compressor – maintenance	1%	% of bare module cost	user input
circulating pumps – maintenance	1%	% of bare module cost	user input
filtration membrane – maintenance	1%	% of bare module cost	user input
reactor chamber length	20	m	(19)
chamber/airtube thickness	0.0035	in	
air-tube height	0.26	m	
chamber height	0.91	m	
chamber width	0.3	m	
price of LDPE film	$(1.78)		$0.80/lb – range $0.80-0.96/lb (7)
number of tubes per basin	15		User input – company presentations
welding/installation factor	$300	per tube	user input

assumption	value	units	source
chamber lifetime	10	y	user input
basin material density	1000	kg/m^3	user input
basin length	20	m	(19)
basin width	6.75	m	
basin height	1	m	
basin wall thickness	0.125	m	
Basin material cost	$(0.02)	kg	user input
basin lifetime	30	y	user input
pump ΔP	14.07	psi	(19)
pump material factor (316SS)	2		(1)
pump head	200	ft	user input
pump lifetime	10	y	user input
percent of medium filtered per day	5%		user input
filter lifetime	3	y	user input
basin pump ΔP	14.07	psi	(19)
Basin water circulation time	24	h	user input
pump head	200	ft	user input
pump lifetime	10	y	user input
pH/temp/ionic species sensors	$2000		user input
pump lifetime	10	y	user input
compressor C_p/C_v	1.5		user input
R	8.314	J/molK	user input
T	300	K	user input
compression pressure	10	atm	user input
base cost	$(800,000)		user input
compressor lifetime	10	y	user input

Table 2-14 – Hydrolysis assumptions

assumption	value	units	source
H_2SO_4 pump ΔP	1	atm	(20)
HE tube inlet temp	27	°C	
HE tube outlet temp	100	°C	
HE shell inlet temp	202	°C	
HE shell outlet temp	28	°C	
Shell pressure	10	atm	
Steam requirement	11%	% of total mass flow	User input
H_2SO_4 requirement	0.44%	% of total mass flow	User input
Conversion of TG to FFA	99%		(20)
Conversion of carbs to sugars	99%		
Pump installation factor	4		User input
HE installation factor	3		User input
Reactor vessel installation factor	2		User input
Pump maintenance	1%	% of bare module cost	User input
HE maintenance	1%	% of bare module cost	User input
Reactor maintenance	1%	% of bare module cost	User input
Pump head	400	ft	User input
Pump material factor (316SS)	2		(1)
Pump lifetime	10	y	User input
Shell pressure	150	psi	(20)
HE lifetime	10	y	User input
Vessel material	Glass lined CS		User input
Vessel material density	0.284	lb/in^3	(1)
Operating temperature	100	°C	(20)
Operating pressure	2	atm	
Residence time	0.5	h	
Oversize factor	1.1		User input

Maximum allowable stress	13,750	psi	(1)
Weld efficiency	0.85		
H:D ratio	2		User input
Reactor vessel lifetime	10	y	User input

Table 2-15 – Transesterification assumptions

assumption	value	units	source
MeOH pump ΔP	1	atm	(20)
Conversion of FFA	0.77		
Pump installation factor	4		User input
Reactor vessel installation factor	2		User input
Pump maintenance	1%	% of bare module cost	User input
Reactor maintenance	1%	% of bare module cost	User input
Pump head	200	ft	User input
Pump material factor (316SS)	2		(1)
Pump lifetime	10	y	User input
Vessel material	Glass lined CS		User input
Vessel material density	0.284	lb/in^3	(1)
Operating temperature	100	°C	(20)
Operating pressure	2	atm	
Residence time	1	h	
Oversize factor	1.1		User input
Maximum allowable stress	13,750	psi	(1)
Weld efficiency	0.85		
H:D ratio	2		User input
Reactor vessel lifetime	10	y	User input

Table 2-16 – Centrifuge assumptions

assumption	value	units	source
% inlet TG to wet cake	0%		user input
% inlet FFA to wet cake	0%		
% inlet MeOH to wet cake	90%		
% inlet water to wet cake	90%		
% inlet H_2SO_4 to wet cake	90%		
% inlet glycerol to wet cake	90%		
% inlet cell matter to wet cake	100%		
% inlet FAME/diesel to wet cake	0%		
% inlet ionic species and sugar to wet cake	90%		
% inlet EtOH to wet cake	90%		
% inlet hexane/MEA to wet cake	0%		
% inlet gases to wet cake	0%		
% liquid TG to organic phase	100%		
% liquid FFA to organic phase	100%		
% liquid MeOH to organic phase	10%		
% liquid water to organic phase	10%		
% liquid H_2SO_4 to organic phase	10%		
% liquid glycerol to organic phase	10%		
% liquid cell matter to organic phase	0%		
% liquid FAME/diesel to organic phase	100%		
% liquid ionic species and sugar to organic phase	10%		
% liquid EtOH to organic phase	10%		

assumption	value	units	source
% liquid hexane/MEA to organic phase	100%		
% inlet gases to organic phase	0%		
centrifugal speed	5000	rpm	
centrifugal radius	0.5	m	
centrifuge L/D	3		
centrifuge installation factor	4		
centrifuge maintenance	5%		
cost per centrifuge	$(200,000)		
lifetime	10	yr	
k1	80	bar	(21)
k2	5.3	bar/atm	
hydraulic backdrive	281	in-lbf to bar	
I	0.5		
water viscosity	0.001002	$N \cdot s \cdot m^{-2}$	(22)

Table 2-17 – Gravity decanter assumptions

assumption	value	units	source
% TG in upper phase	0%		user input
% FFA in upper phase	0%		
% MeOH in upper phase	100%		
% water in upper phase	100%		
% H_2SO_4 in upper phase	100%		
% glycerol in upper phase	100%		
% cell matter in upper phase	100%		
% FAME/Diesel in upper phase	0%		
% Ionic species in upper phase	100%		
% EtOH in upper phase	100%		
% hexane/MEA in upper phase	0%		
% gases in upper phase	100%		
Decanter installation factor	4		
Decanter maintenance	5%		
Decanter residence time	2	h	(20)
Oversize	1.1		user input
L:D	5.56		user input
Vessel thickness	0.3125	in	(1)
Vessel material	316SS		(1)
Vessel density	0.284	lb/in^3	(1)
Vessel operating temperature	100	°C	(20)
Vessel operating pressure	2	atm	
Vessel lifetime	10	y	User input

Table 2-18-Final ester reactor assumptions

assumption	value	units	source
MeOH pump ΔP	1	atm	(20)
Conversion of FFA	0.99		
H_2SO_4 requirement	0.44%	% of total mass flow	User input
HE tube inlet temp	27	°C	(20)
HE tube outlet temp	100	°C	
HE shell inlet temp	150	°C	
HE shell outlet temp	30.1	°C	
Shell pressure	6.8	atm	
Steam for reboiler	8%	% of total mass flow	User input
Pump installation factor	4		User input
HE installation factor	3		User input
Reactor vessel installation factor	2		User input
Pump maintenance	1%	% of bare module cost	User input
HE maintenance	1%	% of bare module cost	User input
Reactor maintenance	1%	% of bare module cost	User input
Pump head	200	ft	User input
Pump material factor (316SS)	2		(1)
Pump lifetime	10	y	User input
Shell pressure	150	psi	(20)
HE lifetime	10	y	User input
Vessel material	Glass lined CS		User input
Vessel material density	0.284	lb/in^3	(1)
Operating temperature	100	°C	(20)
Operating pressure	2	atm	
Residence time	1	h	
Oversize factor	1.1		User input
Maximum allowable stress	13,750	psi	(1)
Weld efficiency	0.85		

assumption	value	units	source
H:D ratio	2		User input
Reactor vessel lifetime	10	y	User input

Table 2-19 – Final decanter assumptions

assumption	value	units	source
Water wash required	3%	% of total mass flow	User input
% TG in upper phase	0%		
% FFA in upper phase	0%		
% MeOH in upper phase	100%		
% water in upper phase	100%		
% H_2SO_4 in upper phase	100%		
% glycerol in upper phase	100%		
% cell matter in upper phase	100%		
% FAME/diesel in upper phase	0%		
% ionic species in upper phase	0%		
% EtOH in upper phase	0%		
% hexane/MEA in upper phase	0%		
% gases in upper phase	0%		
Decanter installation factor	4		
Decanter maintenance	5%		
Decanter residence time	2	h	(20)
Oversize	1.1		User input
L:D	6		User input
Vessel thickness	0.3125	in	(1)
Vessel material	316SS		(1)
Vessel density	0.284	lb/in^3	(1)
Vessel operating temperature	100	°C	(20)
Vessel operating pressure	2	atm	
Vessel lifetime	10	y	User input

Table 2-20 – Flash separator assumptions

assumption	value	units	source
HE tube inlet temp	27	°C	(20)
HE tube outlet temp	125	°C	
HE shell inlet temp	250	°C	
HE shell outlet temp	133.6	°C	
Steam for reboiler	0.0165	% of total mass flow	User input
Flash vessel installation factor	5		
Heat exchanger installation factor	3		
Flash vessel maintenance	5%		
Heat exchanger maintenance	1%		
Vessel density	0.284	lb/in^3	(1)
Vessel material factor (316SS)	2		(1)
Shell pressure	450	psi	(20)
HE lifetime	10	yr	User input

Table 2-21 – Distillation column assumptions

assumption	value	units	source
x_i TG	100%		User input
x_i FFA	100%		
x_i MeOH	99%		
x_i water	1%		
x_i H_2SO_4	100%		
x_i glycerol	100%		
x_i cell matter	100%		
x_i FAME/Diesel	100%		
x_i ionic species	100%		
x_i EtOH	100%		
x_i hexane/MEA	100%		
x_i gases	0%		
Steam for reboiler	6%	% of total mass flow	
CO_2 for solvent removal	8.5	w/w ratio of inlet mass flow	(23)
% hexane recovered (if used for solvent recovery)	99%		User input
% other components recovered (if used for solvent recovery)	1%		
Column installation factor	5		
Compressor installation factor	1		
Column maintenance	1%	% of bare module cost	
Compressor maintenance	1%	% of bare module cost	
Liquid surface tension	5	dyne/cm	
Csb			
Vessel thickness	0.3125	in	
Vessel material density	0.284	lb/in^3	
Vessel material	316SS		
Ftt	1		
Lifetime	10	yr	

Table 2-22 – LED-lit photobioreactor assumptions

assumption	value	units	source
kg P/kg algae	0.0099	kg/kg	(4)
kg K/kg algae	0.0082	kg/kg	
kg Mg/kg algae	0.0038	kg/kg	
kg S/kg algae	0.0022	kg/kg	
Percent utilization of CO_2	10%		User input
Conversion of CO_2 to biomass	100%		User input
Mass fraction of algae	0.001	kg algae/kg H2O	User input - 1 g/L – range 1-11g/L (19)
Vessel L:D	2		User input
Vessel diameter	6.2	m	
Vessel lifetime	20	yr	
Dispensing tube price	$(40)		
Installation factor	5		
Lifetime	30	yr	
Motor rpm	3	rpm	(26)
HP required	10	HP	
Motor lifetime	30	yr	User input
Paddle spacing	0.2	m	(26)
Paddle diameter	0.3	m	
Paddle material price	$(1.00)		User input
Paddle installation factor	10		
Paddle lifetime	30	yr	
Number of LEDs	50		(26)
Assembly factor	3		User input
Control system cost factor	3		
LED lifetime	5	yr	
Piping, and pressure regulation installation factor	1.5		
Compressor C_p/C_v	1.5		User input
R	8.314	J/molK	
T	300	K	
Compression pressure	10	atm	
Base cost	$(800,000)		

assumption	value	units	source
Compressor lifetime	10	yr	
Eductor price	$(1,000)	per unit	
Lifetime	50	yr	

Table 2-23 – Electroporation assumptions

assumption	value	units	source
Desired voltage across cells	1.1	V	(24)
EP Plate Separation	0.55	m	
Plate area	5.5	m^2	
Pulse time	0.000055 reversible 0.00011 lysis	s	
Capacitance of charging capacitor	0.11 reversible 0.22 lysis	F	
Algae radius	2.8e-6	m	(25) range 1-30 μm
Electrical conductivity of algae	5.26	S/m	User input (assume seawater)
No. time constants to charge capacitor	4		User input
Electrical duty time	0.01	% of time spent charging	User input

Table 2-24 – Live extraction assumptions

assumption	value	units	source
% of TG, FFA, FAME milked by electroporation	55%		User input
% non-solids milked	1%		User input
Extraction vessel installation factor	4		User input
Pulse generator installation factor	4		User input
Extraction vessel maintenance	5%	% of bare module cost	User input
Pulse generator maintenance	5%	% of bare module cost	User input
Residence time extraction vessel	1	h	(26)
Oversize factor	1.1	h	User input
Extraction vessel	30	y	User input
Pulse generator cost	$(100,000)		User input
Pulse generator lifetime	30	y	User input

Table 2-25 – Single step extraction assumptions

assumption	value	units	source
% of TG milked by electroporation	100%		User input
Extraction vessel installation factor	4		User input
Pulse generator installation factor	4		User input
Extraction vessel maintenance	5%	% of bare module cost	User input
Pulse generator maintenance	5%	% of bare module cost	User input
Residence time extraction vessel	1	h	(26)
Oversize factor	1.1	h	User input
Extraction vessel	30	y	User input
Eductor size	3	in	User input
Design factor	5		User input
Lifetime	30	y	User input

Table 2-26 – Clarifier assumptions

assumption	value	units	source
SF TG to oil phase	0%		User input
SF FFA to oil phase	0%		
SF MeOH to oil phase	0%		
SF water to oil phase	0%		
SF H_2SO_4 to oil phase	0%		
SF glycerol to oil phase	0%		
SF cell matter to oil phase	0%		
SF FAME/diesel to oil phase	0%		
SF ionic species/sugars to oil phase	0%		
SF EtOH to oil phase	0%		
SF hexane/MEA to oil phase	0%		
SF TG to aqueous phase	0%		
SF FFA to aqueous phase	0%		
SF MeOH to aqueous phase	0%		
SF water to aqueous phase	90%		
SF H_2SO_4 to aqueous phase	0%		
SF glycerol to aqueous phase	0%		
SF cell matter to aqueous phase	0%		
SF FAME/diesel to aqueous phase	0%		
SF ionic species/sugars to aqueous phase	90%		
SF EtOH to aqueous phase	0%		
SF hexane/MEA to aqueous phase	0%		
SF TG to solids phase	100%		
SF FFA to solids phase	100%		
SF MeOH to solids phase	100%		
SF water to solids phase	10%		
SF H_2SO_4 to solids phase	100%		
SF glycerol to solids phase	100%		
SF cell matter to solids phase	100%		
SF FAME/diesel to solids phase	100%		
SF ionic species/sugars to solids phase	10%		

SF EtOH to solids phase	100%		
SF hexane/MEA to solids phase	100%		
Vessel installation factor	4		
Vessel maintenance	5%		
Vessel diameter	100	m	
Area design correlation	8	m^2/ton/d	(27) wastewater primary sludge
Lifetime	30	y	User input

SF - separation factor

Table 2-27 – Thickener assumptions

assumption	value	units	source
SF TG to aqueous phase	0%		User input
SF FFA to aqueous phase	0%		
SF MeOH to aqueous phase	100%		
SF water to aqueous phase	100%		
SF H_2SO_4 to aqueous phase	100%		
SF glycerol to aqueous phase	100%		
SF cell matter to aqueous phase	0%		
SF FAMEdiesel to aqueous phase	0%		
SF ionic species/sugars to aqueous phase	100%		
SF EtOH to aqueous phase	0%		
SF hexane/MEA to aqueous phase	0%		
Vessel installation factor	4		
Vessel maintenance	5%		
Vessel diameter	100	m	
Area design correlation	8	m^2/ton/d	(27) Wastewater primary sludge
Lifetime	30	y	User input

SF = separation factor

Table 2-28 – Anaerobic digester assumptions

assumption	value	units	source
Methane production	40	mg CH_4/g VS	(28)
Ammonia production	40	mg NH_3/g VS	
Carbon dioxide	40	mg CO_2/g VS	
Retention time	240	h	
Hours of flow	12	h	User input
Clean in place, gas and biomass removal	12	h	
Installation factor	4		
Maintenance	5%	% of bare module cost	
Vessel oversize	1.5		
Cleaning and microbe removal cost	120%	% of bare module cost	
Lifetime	20	y	

VS = volatile solids

Table 2-29 – M.S. adosrber assumptions

assumption	value	units	source
Moles of CO_2/kg sorbent	6.7	mol/kg	(29) max = 25 mol/kg
% CO_2 captured	90%		
% CH_4 captured	0.0009%		
% NH_3 captured	0.0009%		
% of trace components captured	0%		
Sorbent packing density	700	kg/m^3	
Residence time	1	h	
Adsorption column pressure	20	atm	
Absorption vessel installation factor	4		
Regeneration vessel installation factor	4		
Absorption vessel maintenance	5%	% of bare module cost	
Regeneration vessel maintenance	5%	% of bare module cost	
Adsorption vessel residence time	0.1	h	
Adsorption vessel material factor	1		
Adsorption vessel oversize	1.5		
H:D ratio	2		
Adsorption vessel wall thickness	1	in	
Adsorption vessel material density	0.284	lb/in^3	(1)
Adsorption vessel lifetime	20	y	
Compressor C_p/C_v	1.5		User input
R	8.314	J/molK	
T	300	K	
Compression pressure	10	atm	
Base cost	$(1,000,000)		

assumption	value	units	source
Compressor lifetime	10	y	
Eductor price	$(1,000)	per unit	
Lifetime	20	y	

Table 2-30 – Open pond assumptions

assumption	value	units	source
kg P/kg algae	0.0099	kg/kg	(4)
kg K/kg algae	0.0082	kg/kg	
kg Mg/kg algae	0.0038	kg/kg	
kg S/kg algae	0.0022	kg/kg	
Percent utilization of CO_2	10%		User input
Mass fraction of algae	0.001	kg algae/kg H_2O	User input - 1 g/L range 1-11g/L (19, 30)
Pond surface area	100000	m^2	
Pond depth	0.3	m	(30)
Nutrient access	165%		User input
Energy for paddlewheel	165	W	(30)
Open pond installation factor	3		User input
Belt filter installation factor	4		
Open pond maintenance	5%	% of bare module cost	
Belt filter maintenance	5%	% of bare module cost	
Site preparation and leveling			(31)
Flattening			
Erosion control			
Levee wall building			
Lining of levees			
Paddlewheel			
Piping/CO_2 sparging			
Ancillary equipment			
Base size	10	ha	User input
Lifetime	50	y	User input
Number of ponds/dryer	10		User input
Cost per filter	$(350,000)		User input
Lifetime	10	y	User input

Table 2-31 – Oil extraction assumptions

assumption	value	units	source
Number of washes	2		(32)
Ethanol to biomass ratio	5	mL/g	
Wash time	11	h	
Number of washes	3		
Hexane wash required	20%	% of total volume	
Extraction vessel installation factor	3		User input
Extraction vessel maintenance	5%		
Operating pressure	2	atm	
Residence time	1	h	
Oversize factor	1.1		
Maximum allowable stress	13,750	psi	(1)
Weld efficiency	0.85		
H:D ratio	2		User input
Reactor vessel lifetime	10	y	User input

Table 2-32 – Solvent recovery assumptions

assumption	value	units	source
H_{vap} hexane	335.236	J/g	(27)
HE shell temp in	200	°C	(33)
HE shell temp out	28	°C	
% Hexane vaporized	80%		
% of other components vaporized	10%		
Cooling water requirement	500%	% on inlet flow	
HE installation factor	3		User input
Flash vessel installation factor	3		
Evaporator installation factor	4		
Stripping column installation factor	3		
HE maintenance	5%		
Flash vessel maintenance	5%		
Evaporator maintenance	5%		
Stripping column maintenance	5%		
HE shell pressure	150	psi	
HE lifetime	10	y	
Flash vessel material density	0.284	lb/in^3	(1)
Flash vessel lifetime	10	y	User input
Evaporator U	100	BTU/hr-ft^2-degF	(1)
Material factor	1		User input
Quantity	1		
Lifetime	10	y	
Number of trays in stripping column	2.375		
Plate spacing	36	in	
L:D	3		
Quantity	1		
Lifetime	10	y	

2.11.3 Supplementary information sources key

[1]Seider,W.D., Seader, J.D., Lewin, D.R. *Product and Process Design Principles: Synthesis, Analysis, and Evaluation*, 2nd Edition. 2004: J.W. Wiley & Sons.

[2]Dimitrov, K.; GreenFuel Technologies: *A Case Study for Industrial Photosynthetic Energy Capture* (www.nanostring.net/Algae/CaseStudy.pdf)
[3]Clarens, A.F., Resurreccion, E.P., White, M.A., Colosi, L.M., 2010. *Environmental Life Cycle Comparison of Algae to Other Bioenergy Feedstocks.* Environmental Science & Technology.
[4]Lardon, L., Helias, A., Sialve, B., Stayer, J.P., Bernard, O., 2009. Life-Cycle Assessment of Biodiesel Production from Microalgae. *Environmental Science & Technology*, 43, 6475-6481.
[5]Willson, B.; http://www.greentechmedia.com/articles/read/algae-biodiesel-its-33-a-gallon-5652/
[6]http://www.icis.com/StaticPages/k-o.htm#M
[7]http://www.icis.com/StaticPages/p-s.htm#S
[8]http://www.icis.com/StaticPages/f-j.htm#G
[9]http://www.ers.usda.gov/Data/FertilizerUse/
[10]Grima, E.M., Belarbi, E.H., Fernandez, F.G.A., Medina, A.R., Chisti, Y., 2003. *Recovery of microalgal biomass and metabolites: process options and economics.* Biotechnology Advances, 20, 491-515.
[11]http://www.eia.doe.gov/oil_gas/natural_gas/info_glance/natural_gas.html
[12]http://www.icis.com/StaticPages/a-e.htm#A
[13]http://www.diytrade.com/china/4/products/2431216/Monoethanolamine.html
[14]http://www.ers.usda.gov/Briefing/Sugar/Data.htm
[15]Doty, F. D.; A Realistic Look at Hydrogen Price Projections Doty Scientific, Inc. (www.dotyenergy.com/Markets/Hydrogen.htm)
[16]http://tonto.eia.doe.gov/oog/info/gdu/gasdiesel.asp
[17]http://www.aliexpress.com/wholesale/wholesale-adsorbent.html
[18]http://www1.eere.energy.gov/industry/bestpractices/pdfs/steam15_benchmark.pdf
[19]US Patent Application 20080160591, *Diffuse Light Extended Surface Area Water-Supported Photobioreactor*
[20]US Patent Application 2009108230, *Continuous algal biodiesel production facility*
Wallace W.F. Leung, *Torque requirement for high-solids centrifugal sludge dewatering*. Filtration and Separation, 1998, (35) 883-887.
[21]http://www.engineeringtoolbox.com/water-dynamic-kinematic-viscosity-d_596.html
[23]Eller, F.J., Taylor, S.L., Curren, M.S.S., 2004. *Use of liquid carbon dioxide to remove hexane from soybean oi*l. Journal of the American Oil Chemists Society, 81, 989-992.
[24]Weaver, J.C., Chizmadzhev, Y.A., 1996. *Theory of electroporation: A review.* Bioelectrochemistry and Bioenergetics, 41, 135-160.
[25]Ferrell, J., Sarisky-Reed, V., 2010. National Algal Biofuels Technology Roadmap. United States Department of Energy.
[26]US Patent Application 20090029445 – *Algae growth system for oil production*
[27]Green, Don W.; Perry, Robert H. (2008). Perry's Chemical Engineers' Handbook (8th Edition). McGraw-Hill. Online version available at: http://www.knovel.com/web/portal/browse/display?_EXT_KNOVEL_DISPLAY_bookid=2203&VerticalID=0

[28]Sialve, B., Bernet, N., Bernard, O., 2009. *Anaerobic digestion of microalgae as a necessary step to make microalgal biodiesel sustainable.* Biotechnology Advances, 27, 409-416.
[29]Siriwardane R.; *Adsorption and desorption of CO_2 on solid sorbents* (http://www.netl.doe.gov/publications/journals/vol1_no1.pdf)
[30]US Patent 5659977 - *Integrated microalgae production and electricity cogeneration*, Jensen
[31]Benemann, J.R., 1994. Systems and economic analysis of microalgae ponds for conversion of CO_2 to biomass. Trans. of US/Japan meeting on coal energy research. Albuquerque, NM, CONF 9409207--2 ed. pp. 9.
[32]Fajardo, A.R., Cerdan, L.E., Medina, A.R., Fernandez, F.G.A., Moreno, P.A.G., Grima, E.M., 2007. Lipid extraction from the microalga Phaeodactylum tricornutum. *European Journal of Lipid Science and Technology*, 109, 120-126.
[33]Brown, H.L., B.B. Hamel, and B.A. Hedeman, Energy Analysis of 108 Industrial Processes, Fairmont Press, Atlanta.

Chapter 3 Life-cycle analysis of five microalgae to biofuel processes with varying complexities

(Accepted, Journal of Renewable and Sustainable Energy)

Abstract

"Cradle-to-gate" life cycle analysis (LCA) surrounding five algae-to-fuel/fuel precursor scenarios were studied. The different processes modeled were: an open pond producing either triacylglycerides (TAG) or free fatty acid methyl ester (FAME); a solar-lit photobioreactor producing either FAME or free fatty acids (FFA); and a light emitting diode irradiated (LED-lit) photobioreactor-producing TAG. These processes were chosen from amongst the simplest to most sophisticated approaches available in literature. The scenarios of production with open ponds are close to being sustainable environmentally. On the other hand, the production scenarios with solar-lit and LED-lit photobioreactors are both far from being sustainable. The reason for this is the higher embedded and operating life-cycle impacts associated with the materials in the growth reactor (and some other equipment) in these two types of production facilities, as well as, the artificial photon source used in the latter. Many, difficult-to-achieve, improvements are required to make these processes less energy intensive. Algae strains with higher lipid productivity as well as changes in the number, the complexity, and energy expenditures in operation steps are always required to reduce overall life-cycle impacts when production of commodity fuels is the focus. An important perspective to keep in mind with algae-based processes is that there are currently no significant economies-of-scale with the environmental impacts for growth systems, since they are additive above a baseline production level.

3.1 Introduction

The continuous increase in atmospheric CO_2, and its association with global climate change[1, 2], has stimulated a search for new sources of alternative and sustainable fuels.[3, 4] Various renewable energy sources, including algae-based biofuels, have been explored and periodic production goals have been set in the past twenty years[5] only to slip by unmet. The U.S. passed the energy independence and security act (EISA) in 2007 that required a gradual increase in the production of renewable fuels to reach 36 billion gallons per year by 2022.[6] However, even in the year 2015, there are many economic and environmental prospects of biofuels that are yet to be addressed convincingly before such volumes can be realized, especially from generation 2 (non-corn ethanol) sources (~9.2% of 2014 US renewable fuels total)[7].

For example, the volume production of first-generation liquid biofuels has resulted in a series of societal concerns related to food prices, land usage, and carbon emissions.[6] Because priority should be given for the consumption of food crops as 'food', biofuel production from food crops has faced much criticism and is seen by many as undesirable.[8] Similarly, bioethanol production from sugarcane is considered to be a beneficial and cost-effective greenhouse gas (GHG) mitigation strategy from a 'sustainability' standpoint, but this is also controversial due to insufficient information on the total GHG balance of this system.[9]

Microalgae species as a feedstock for biofuels have gained considerable interest in the past decade. They can be produced in areas unsuitable for crops, and can potentially grow at a much faster rate.[10] Algae have higher energy yield per area of growth than many other terrestrial crops[11] and several algal species can have doubling times of even one day.[12] Microalgae is a prokaryotic or eukaryotic photosynthetic microorganism that can grow rapidly

and live in harsh conditions due to their unicellular or simple multicellular structure.[13] They produce lipids with high productivity[3] and potentially can serve as a viable fuel (such as, biodiesel) source[14] and, thus, have the ability to mitigate carbon dioxide emissions, A number of consortiums, and private/public investments in R&D, have and are considering algae as an effective platform to produce economical and environmentally-sustainable feedstock oils.[5], [15], [13] Despite the claims that microalgal biofuels are environment-friendly alternatives to conventional fuels, debates surrounding its ecological benefits and drawbacks still exist.[16-18] In fact, some studies deemed algal biofuel unsustainable in the long run because of its reliance on synthetic fertilizer production.[19]

With every new technology, it is important that its environmental impacts are very clearly understood before it is applied on a large scale.[20] For a process to be sustainable, it has to be sustainable environmentally as well as economically.[21-23] The environmental footprints embedded in the construction and operation of these processes must be considered and should be low.[24, 25] To avoid ecological problems, future regulations aimed at curbing various emissions are being critically assessed.[26-28]

Environmental impacts can be studied in detail with an analytical tool called life-cycle analysis (LCA). LCA is a methodology which quantifies the resource consumption and the environmental impacts of any product or service over its life cycle, from raw material acquisition through production, transportation, use and sometimes, the products' end of- life.[29] LCA study is essential to determine the sustainability of any products; including algae-to-fuel processes. LCA has four main steps: (1) goal and scope definition, (2) life cycle inventory analysis (LCI), (3) life cycle impact assessment (LCIA) and (4) improvement and interpretation.[24]

LCA gives the possibility to compare different production approaches, not only with respect to the overall life cycle impact, but also the individual unit operations' life cycle impact studies. These are useful to analyze a production scenario in order to target any lever points that exist.[30] For an algae-based production facility, the growth system operation appears to play a critical role,[31] as well as, the embedded infrastructure for the growth reactors and subsequent downstream processing.[32] However, results have varied, largely due to the lack of commercial-scale algae-to-fuel systems that could focus attention on a practical system design(s) with realistic operating parameters.[18] The outcomes of any analysis depend on the assumptions made to make the calculations and so with this study. To mitigate the some of these concerns we are performing a relative LCA case study wherein all scenarios are analyzed within the same modeling framework.

Thus, for this LCA study of algae-to-biofuel(s)/precursors, SAFEER (Sustainable algae-to-fuel: environmental and economic realities)[33], was modified to include an LCA section that comprises currently available database[34] information of life-cycle impacts of many different products. The purpose of this work is to present the LCA analysis for the production cases reported in a previous techno-economic study by our group.[33] The results from these facilitate comparison between the five different production scenarios; quantify their environmental sustainability; and relate to the previously reported economic metrics. It should be noted, that the processes create different products. This illustrates one of our purposes, which is to show that, independent of end products; a process' sustainability needs to (and can) be assessed versus other approaches leading to different points along the end-use spectrum.

3.2 Methods

3.2.1 Processes studied

The algae-to-biofuel processes discussed in this work have been previously described in detail in chapter 2.[33] The processes are: i) open pond growth producing tri-acylglycerides (TAG); ii) open pond growth producing fatty acid methyl esters (FAME); iii) solar-lit photobioreactor producing free fatty acids (FFA); iv) solar-lit photobioreactor producing FAME and v) light emitting diode (LED)-lit photobioreactor producing TAG. All the different assumptions and conditions for the simulation have been included in the Supplemental Information. These production schemes follow the scenarios outlined by Lardon et al.[35], Stephenson et al. [36] and Ekellebery et al.[37]. These studies; however, had several shortcomings in their LCA as mentioned by Xu, et al.,[38] thus, the current work has done a more detailed analysis to get a clearer picture of the processes' environmental sustainability.

3.3 Modeling methodology

3.3.1 Process design and assumptions

The major environmental metrics examined were the global warming potential (GWP) (equivalent kg CO_2), eutrophication potential (EP) (kg NO_3 equivalent), acidification potential (AP) (equivalent m^2 (un-protected ecosystem, UES), and energy from renewable and non-renewable sources (MJ). The data for each metric was obtained using GABI 4.3, a software window into the extensive NREL US LCI database.

Our simulation included the associated environmental burdens of the materials and manufacturing, either well known or forecasted, required to produce individual pieces of process equipment. For example, the materials required to produce a solar-lit photobioreactor basin are

polyethylene bags to house the algae, polyvinyl chloride (PVC) piping for nutrient supply, polycarbonate to produce the water basin, and an irrigation pump to circulate the water through the basin. The life cycle impacts of each material used is added and amortized over the life of that particular equipment. The amortized life cycle impacts of raw material feeds and utilities were also added to the equipment life cycle to get the complete analysis. The parameters and assumed values for simulation are tabulated in the Supplemental Information. The boundaries employed for each piece of process equipment were "cradle to gate", meaning that the associated environmental impact for the production, transport, and use of each part or material was considered, but not how efficiently it is used, its disposal, or the recycling of any of the materials at their end-of-service. The following Table 3-1 illustrates different equipment/process units and the raw materials for all the cases studied. All the assumptions are tabulated in the supplementary information in Tables 3-11 – 3-28.

Table 3-1 - Main process/equipment units and raw materials used for this study

equipment units		
1	solar-lit photobioreactor	Solix-type bioreactor that consists of a water filled reactor basin wherein polyurethane tubes are used to grow algae
2	LED-lit photobioreactor	A pressurized chamber that provides mixing and light to the algae slurry as well as serves as a dispensing tube for nutrients and CO2 fed to the reactor
3	open pond	A raceway pond growth system followed by a belt filter dryer
4	dewatering step	A unit that removes 95% of algal water
5	rotary dryer	A dryer that rotates and uses heat
6	pumps	
7	heat exchangers	
8	reactor vessels	A pressurized chamber for reactions with set conditions
9	centrifuges	
10	vessels	a. Large stainless steel vessels

		b. Small vessels
11	columns	Units that comprises of columns such as distillation columns.
12	compressors	A vessel that compresses CO_2
13	thickeners	A clarifier that separates two streams: solids and liquids
14	membranes	A membrane unit with tangential flow filtration
raw materials		
1	steam	a. Low pressure from natural gas
		b. Low pressure from coal
		c. High pressure from natural gas
		d. High pressure from coal
2	electricity	A fossil fuel source (modeled as coal) is combusted to produce electricity
3	methanol	
4	sulfuric acid	
5	nitrogen fertilizers	Compounds such as calcium nitrate
6	phosphorous fertilizers	Compounds such as magnesium phosphate and calcium phosphate
7	potassium chloride	
8	glycerin	
9	carbon dioxide	
10	ethanol	

In each case, the algal growth area, in hectares, served as the common basis. The base case was defined as 500 ha, the same growth area utilized for our earlier techno-economic analysis. The effect of the growth scale was modeled, with the life cycle impacts calculated for 50, 500, and 5000 ha production scenarios and compared with the accepted LCA metrics for conventional processes/products such as diesel and crude oil.

3.4 Results and discussions

In each case, the life cycle contributions are dominated by several similar factors – the growth basin, the carbon dioxide required to grow and sustain the microalgae, electricity use and

high-pressure steam use for separations. It must be noted that the environmental burdens of carbon dioxide production are calculated based on CO_2 available as a byproduct of ammonia production. Thus, the absolute value of this burden can be quite site-specific, and therefore variable. However, in all cases, the emissions due to the construction of equipment were less than the emissions due to raw materials and utility production. The following subsections describe the results of the five cases in detail.

3.4.1 Open pond producing TAG

The main component of this scenario is the open pond itself. Open ponds account for most of the area required for the overall process. In an open pond growth producing TAG, the open ponds accounts for most of the equipment-based emissions for this process; 98.7% of the greenhouse gases (GHG) equivalent. In this case, secondary pieces of equipment, like centrifuges and clarifying equipment, comprise a larger percentage of the operating-emissions sources. The following Table 3-2 summarizes the equipment and the raw materials life cycle impacts for this case.

Table 3-2 - Open pond growth producing TAG: equipment and raw materials' LCA summary

		Global warming potential ($\times 10^6$ kg CO_2 equivalent per year)	Aquatic eutrophication potential ($\times 10^3$ kg NO_3 equivalent per year)	Acidification potential ($\times 10^6$ m^2 UES equivalent per year)	Energy renewable and nonrenewable (net calorific value) ($\times 10^6$ MJ per year)
equipment	open ponds	4.73	3.58	0.312	0.027
	rotary dryer	0.0006	0	0.00003	0
	heat exchangers	0.013	0.009	0.001	0.055
	centrifuges	0.003	0.002	0.0003	0.013
	large vessels	0.033	0.022	0.003	0.136
	small vessels	0.0003	0.00002	0.000003	0.0001
	columns	0.013	0.009	0.001	0.055
	thickeners	0.0004	0	0.00002	0.0001
raw materials	calcium nitrite	19.4	8.01	3.33	0
	calcium phosphate	0.97	1510	0.802	0
	potassium chloride	0.12	0.11	0.117	0.989
	magnesium phosphate	0.4	0.277	0.252	2.52
	carbon dioxide	291	1020	17.5	2330
	ethanol	97.4	182	262	736
	electricity	170	137	183	1790
	HP steam	65.3	3.82	0.141	17.5

Most of the emissions associated with building the pond come from the production of the plastic liners used to line the bottom of the pond. If these liners were removed, and compacted clay used instead, the net GHG emissions would be reduced an order of magnitude, from 4.80×10^6 to 0.18×10^6 kg CO_2 equivalent per year. The eutrophication potential, acidification potential, and energy usage are also reduced by about an order of magnitude. Even with the environmentally-costly plastic liners in place, the raw material and utility contributions to the total emissions are still over an order-of-magnitude greater than the emissions embedded in the equipment. Carbon dioxide production accounts for 62.2% of the total GHG emissions, with the high-pressure steam used in solvent recovery accounting for 1.4% and electricity used for various purposes about 36.3%. Over 94.7% of the eutrophication potential comes from the

production of biomass and raw materials use, with the remaining 5.3% primarily resulting from the CO_2 production. Equipment contributes about 0.4% of total acidification potential whereas raw materials contribute 49.9%, and utilities contribute to 49.7%.

3.4.2 Open pond producing FAME

The open ponds account for 98.1% GHG equivalent, equipment-based embedded emissions, while the transesterification reactor vessels only account for 0.7%. Again, if compacted clay is used instead of plastic liners on the ponds, the net GHG emissions would be reduced from 4.82 to 0.18 $\times$ 10^6 kg CO_2 equivalent. Carbon dioxide production accounts for 63.2% of the total GHG emissions, with the high-pressure steam used in solvent recovery accounting for 0.3%, and electricity used for various purposes about 36.5%. 94.8% of the eutrophication potential comes from the production of biomass, with the remaining 5.2% primarily results from CO_2 production. Equipment contributes about 0.8% of total acidification potential whereas raw materials use contributes to 50.7% and utility use contributes to 48.5%. The increment in GHG of 0.4% versus the open pond growth producing TAG is due to the addition of the reactor vessels for transesterification.

Table 3-3 - Open pond growth producing FAME: equipment and raw materials' LCA summary.

		Global warming potential ($\times 10^6$ kg CO_2 equivalent per year)	Aquatic eutrophication potential ($\times 10^3$ kg NO_3 equivalent per year)	Acidification potential ($\times 10^6$ m^2 UES equivalent per year)	Energy renewable and non renewable (net calorific value) ($\times 10^6$ MJ per year)
equipment	open ponds	4.73	3.58	0.312	27.1
	pumps	0.0000004	0	0.00000002	0
	rotary dryer	0.0006	0	0.00003	0
	heat exchangers	0.053	0.036	0.005	0.218
	reactor vessels	0.035	0.023	0.003	0.142
	centrifuges	0.00077	0.0005	0.00007	0.003
raw materials	methanol	1.40	0.619	0.706	0
	sulfuric acid	0.188	0.142	0.007	0.966
	calcium nitrite	19.4	8.01	3.33	0
	calcium phosphate	0.97	1510	0.802	0
	potassium chloride	0.12	0.11	0.018	0.989
	magnesium phosphate	0.397	0.277	0.025	2.52
	carbon dioxide	291	1020	17.5	2340
	electricity	170	137	18.3	1790
	LP steam	1.20	0.704	25.9	3.22

3.4.3 Solar-lit photobioreactor producing FFA

The life cycle impacts embedded in the equipment for these process operations are dominated by the construction of the novel photobioreactors, while the other reactor vessels, pumps, and distillation columns have only a very minor contribution. Embedded within the equipment is 45.1% of the total emissions and 54.9% is from the raw materials feed. The photobioreactors account for over about 99.9% of the global warming potential embedded in equipment (45% of total emissions); 100% of the eutrophication potential from equipment (10.3 % of total emissions); more than 99% of acidification potential from equipment (31.3% of total emissions); and more than 99% of total net energy usage from equipment (28.6 % of total usage). The emissions associated with the construction of the polycarbonate basins (in which the

polyethylene bags are suspended) accounts for nearly this entire inventory, with the other materials in the photobioreactor assembly contributing less than 1% to the overall vessel lifecycle outputs. Producing the CO_2 accounts for 2.1% and generating electricity accounts for 94.3% of total raw material and utility GHG emissions. The production of fertilizers, salts, and other chemicals used in the process contribute less than 1% to the overall GHG emissions for the process.

Table 3-4 - Solar-lit photobioreactor producing FFA: equipment and raw materials' LCA summary for 500 ha

		Global warming potential ($\times 10^6$ kg CO_2 equivalent per y)	Aquatic eutrophication potential ($\times 10^3$ kg NO_3 equivalent per y)	Acidification potential ($\times 10^3$ m^2 UES equivalent per y)	Energy renewable and non renewable (net calorific value) ($\times 10^3$ MJ per year)
equipment	solar-lit photobioreactor basin	247	203	14500	1.23×10^5
	compressors	0.0002	0	0.01	0
	rotary dryer	0.0006	0	0.025	0
	heat exchangers	0.013	0.009	1.13	54.5
	centrifuges	0.005	0.004	0.457	22
	large vessels	0.033.	0.022	2.83	136
	small vessels	0.00003	0.00002	0.003	0.136
	columns	0.013	0.009	1.13	0.055
	thickeners	0.0004	0	0.016	0.105
	membranes	0.00006	0.00004	0.003	0.251
raw materials	calcium nitrite	19.6	8.09	3360	0
	calcium phosphate	0.98	1520	810	0
	potassium chloride	0.121	0.111	11.8	999
	magnesium phosphate	0.401	0.280	25.5	2540
	carbon dioxide	4.86	17	292	38900
	ethanol	16.2	303	436000	1230000
	electricity	284	228	305	2990000
	HP steam	10.9	6.40	235	29200

3.4.4 Solar-lit photobioreactor producing FAME

Again, the photobioreactors contribute almost the total embedded life cycle impacts due to equipment. Contrary to the previous scenario, only 4.1% of the total GHG emissions is embedded within the equipment and 95.9% is emitted by the raw materials and utilities. The photobioreactor accounts for over about 99.9% of the global warming potential due to equipment (4.1% of total emissions), and more than 99% eutrophication potential from equipment (1% of total emissions); ~99% of acidification potential from equipment (3.85% of total emissions); and ~99% of net energy use embedded in equipment (2.54% of total usage). The emissions associated with producing CO_2 and generating electricity account for about 95.3% and 4.6% of overall raw materials and utilities life cycle contribution.

Table 3-5 - Solar-lit photobioreactor producing FAME: equipment and raw materials' LCA summary.

		Global warming potential ($\times 10^6$ kg CO_2 equivalent per y)	Aquatic eutrophication potential ($\times 10^3$ kg NO_3 equivalent per y)	Acidification potential ($\times 10^3$ m^2 UES equivalent per y)	Energy renewable and non renewable (net calorific value) ($\times 10^6$ MJ per y)
equipment	solar-lit photobioreactor basin	247	204	14500	1230
	compressors	0.0004	0	0.019	0
	pumps	0.0000004	0	0.00002	0
	rotary dryer	0.0006	0	0.025	0
	heat exchangers	0.067	0.045	5.65	0.273
	reactor vessels	0.035	0.023	2.94	0.142
	centrifuges	0.005	0.004	0.457	0.221
	small vessels	0.00003	0.00002	0.003	0.0001
	columns	0.24	0.161	20.3	0.981
	membranes	0.06	0.00004	0.003	0.0003
raw materials	methanol	2.21	0.977	1120	0
	sulfuric acid	0.921	0.699	331	4.74
	calcium nitrite	18.6	7.67	3180	0
	calcium phosphate	0.928	1440	767	0
	potassium chloride	0.115	0.105	11.2	0.946
	magnesium phosphate	0.38	0.265	24.1	2.41
	carbon dioxide	5510	19300	331000	44200
	electricity	268	216	28900	2830
	LP steam	1.10	0.641	23.6	2.94
	HP steam	2.49	1.46	53.6	6.67

3.4.5 LED-lit photobioreactor

For this process also, the global warming potential embedded in equipment predominantly results from the construction of the unique photobioreactor vessel (38.1%) and its concomitant extraction vessels (61.2%). Thickeners and other equipment only have 0.7% of the embedded emissions. The production of high-density polyethylene for the photobioreactor vessel is an energy intensive process and the electricity required to produce this material is the predominant source of emissions—83.3% of the total GHG. Stainless steel used in the

production of extraction vessels and clarification skimmers are the significant GHG emission contributors among the other pieces of equipment. Electrical energy is used to illuminate the photobioreactor as well as to lyse and "milk" algae (liberating the intracellular fatty acids). Phosphorous and nitrogen fertilizer account for 55% of the aquatic eutrophication potential with the remainder resulting from electricity and CO_2 production (45%).

The construction of the intermediate bioreactors carries the largest environmental burden among all the equipment studied; 2.47×10^8 kg CO_2 equivalent per year, because of the swimming pool-like polycarbonate basin used in their construction. The open pond process, on the other hand, only produces between 4.73×10^6 kg CO_2 equivalent. The LED-lit photobioreactor claims to be the most productive[37] but it produces 9.44×10^7 kg CO_2 equivalent per year. The productivity comes with a concomitant increase in the raw material consumption use and other vessels required also accounts for larger life cycle impact. The electricity use for this process resulted in significant greenhouse emission. All GWP, EP, AP, net calorific values and total life cycle impacts of the production scenarios for all five cases (at 500 ha) have been shown in Figure 3.1 below. Refer to the supplementary information section in Tables 3-8 – 3-10 for the individual unit operations' accounting.

Table 3-6 - LED-lit photobioreactor producing TAG: equipment and raw materials' LCA summary

		Global warming potential ($\times 10^6$ kg CO_2 equivalent per year)	Aquatic eutrophication potential ($\times 10^3$ kg NO_3 equivalent per year)	Acidification potential ($\times 10^6$ m^2 UES equivalent per year)	Energy renewable and non renewable (net calorific value) ($\times 10^6$ MJ per year)
equipment	LED-lit photobioreactor basin	94.4	73.8	8.71	814
	compressors	0.0002	0	0.00001	0
	pumps	0.0000003	0	0.00000001	0
	large vessels	152	102	12.9	620
	thickeners	1.74	0	0.007	0.471
raw materials	calcium nitrite	5.81	240	99.5	0
	calcium phosphate	29	45100	24	0
	potassium chloride	3.59	3.28	0.349	29.6
	magnesium phosphate	11.9	8.29	0.754	75.3
	carbon dioxide	28800	101000	1730	230000
	electricity	144000	116000	15500	1520000

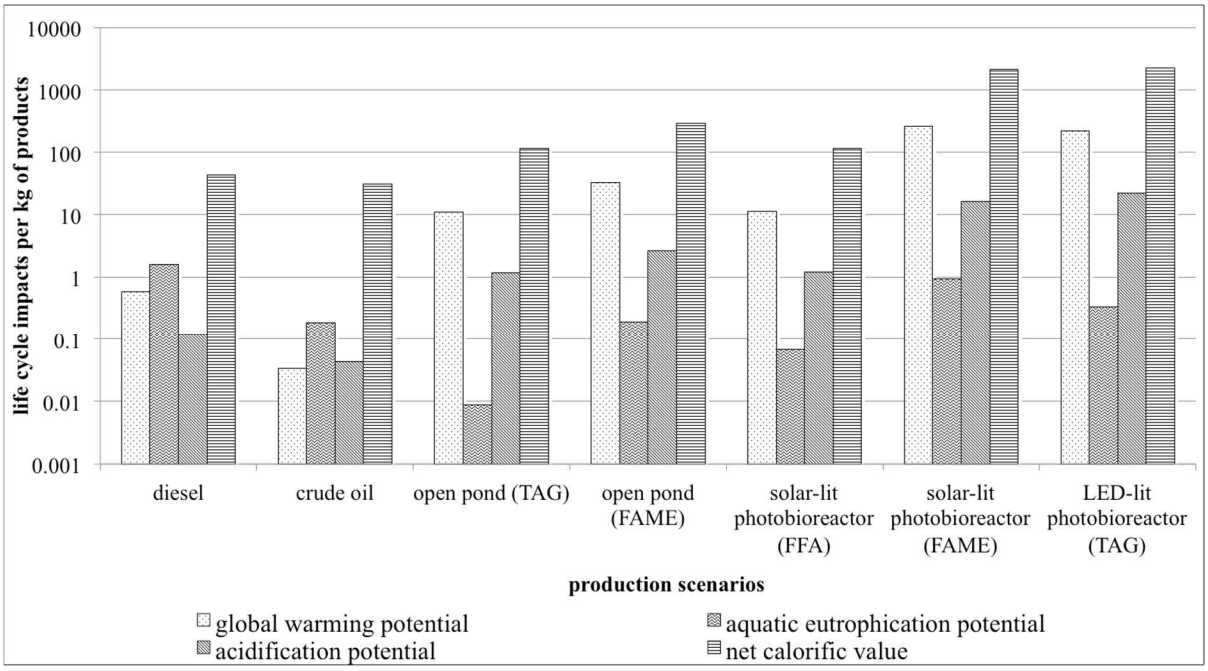

Figure 3.1: Global warming potential (kg CO_2 equivalent), eutrophication potential (kg NO_3 equivalent), acidification potential (m^2 UES), net calorific value (MJ) and total life cycle impacts of all five cases of production area of 500 ha.

3.5 Comparison of process scenario

The summary of the life-cycle impact equivalents per kg of product has been tabulated in Table 3-7. The life cycle impacts of the raw materials used and the equipment embedded life cycle impacts are combined for this calculation. The total life cycle impacts for a 500 ha facility (reflected in Figure 1) are tabulated in the Supplemental Information.

Open pond growth producing TAG has the lowest impact per kg of product. On the other hand, the LED-lit photobioreactor producing TAG has the highest cumulative life cycle impacts and in per kg of product basis for acidification potential and net calorific value whereas solar-lit photobioreactor producing FAME has highest life cycle impacts on global warming potential and aquatic eutrophication potential.

Table 3-7 – Summary of total life cycle analysis (raw materials and equipment combined) and comparison to each process scenario

production scenario	global warming potential, kg equivalent of CO_2/kg of product	aquatic eutrophication potential, kg equivalent of NO_3/kg of product	acidification potential, equivalent m^2 UES /kg of product	energy renewable and non renewable (net calorific value), equivalent MJ /kg of product
Open pond (TAG)	11.4	0.01	1.18	116
Open pond (FAME)	33.4	0.19	2.68	295
Solar-lit photobioreactor (FFA)	20.7	0.07	1.76	162
Solar-lit photobioreactor (FAME)	272	0.95	17	2170
LED-lit photobioreactor (TAG)	221	0.33	22.1	2233

Unsurprisingly, at this scale upon increasing the area of production, the life cycle impacts increase linearly. This is because the growth systems are additive and don't provide any economies-of-scale with respect to environmental impacts per unit of product. Thus, a 10x increment in production area (volume) produces 10x the amount of product and has 10x the environmental impacts. Overall life cycle impacts for the production scenarios with production areas of 50 ha, 500 ha and 5000 ha have been shown on Figure 3.4 (a-d) in the supplementary information section.

3.6 Perspective

The prospects for both economic and environmental sustainability for renewable fuels (and other products from biomass) at commercial scale are rightly being scrutinized. As alluded to in the Introduction, a major rationale for this particular study is to illustrate that, independent of end products, a process' sustainability can be assessed versus other approaches which lead to points along the same end-use spectrum. Certainly, depending upon the product, the environmental impacts would differ for a given processing scenario, as well as for different processes producing the same product. Nonetheless, with the granular results for the various unit operations, one can forecast what, if any, differences can be manifested by changing products. For example, TAG is at a lower level of conversion for the algal product (essentially it's the lipids), versus FFA or FAME, nonetheless, this doesn't improve the sustainability for the LED-lit photobioreactor process versus the two other growth reactor/processing approaches.

With algal-based biofuel processes, when we consider our previous economic analysis,[33] it appears that the cost of the production is directly related to the total life cycle emissions of these production scenarios. This suggests that the more sophisticated the production facility is (and thus incorporating more embedded life cycle impacts), the higher the chance of it

being both more costly and environmentally unsustainable. The open pond scenario, where the production facility consists of simple open ponds, uses less energy for the production. Although it has overall less productivity, the equipment life cycle and utility use is greatly reduced (versus the other scenarios), putting this process within the reach of being environmentally sustainable.

The solar-lit photobioreactors and LED-lit photobioreactors consume much energy for manufacturing the equipment. In addition, LED-lit photobioreactors consume energy to produce artificial light to grow the algae. These two processes have so much additional emissions, even before they start producing algae (in comparison to the open pond growth scenario) they would need to have significantly greater productivity than they either have or are likely to be able to achieve without economies-of-scale. This latter quality is difficult to envision due to the growth kinetics being more controlled by interfacial surface (to capture photon flux) than by volume.

Not only the algae growth scenario, but also the processing steps following the growth also contribute to the increase in environmental impacts. For example, the downstream processing that produces FAME has higher environmental impacts than producing TAG (or FFA), due to an increase in the number of unit operations. Therefore, if a take-off for TAG versus FFA versus FAME, as a useful precursor exists, it will obviously lower the overall environmental impact, no matter what the growth system is used.

When these production scenarios are compared to conventional diesel and crude oil production, they have very high life cycle impacts per kg of products. Conventional processes for diesel and crude oil have advantage over these algae production scenarios because of the higher energy density, higher concentration of products in the beginning and (for crude oil) not having to go through the production step as they are extracted directly from the ground or have highly,

energy-integrated downstream processing. Figure 3.2 illustrates the summary comparison of the algae-based products with their fossil fuel derived counterparts.

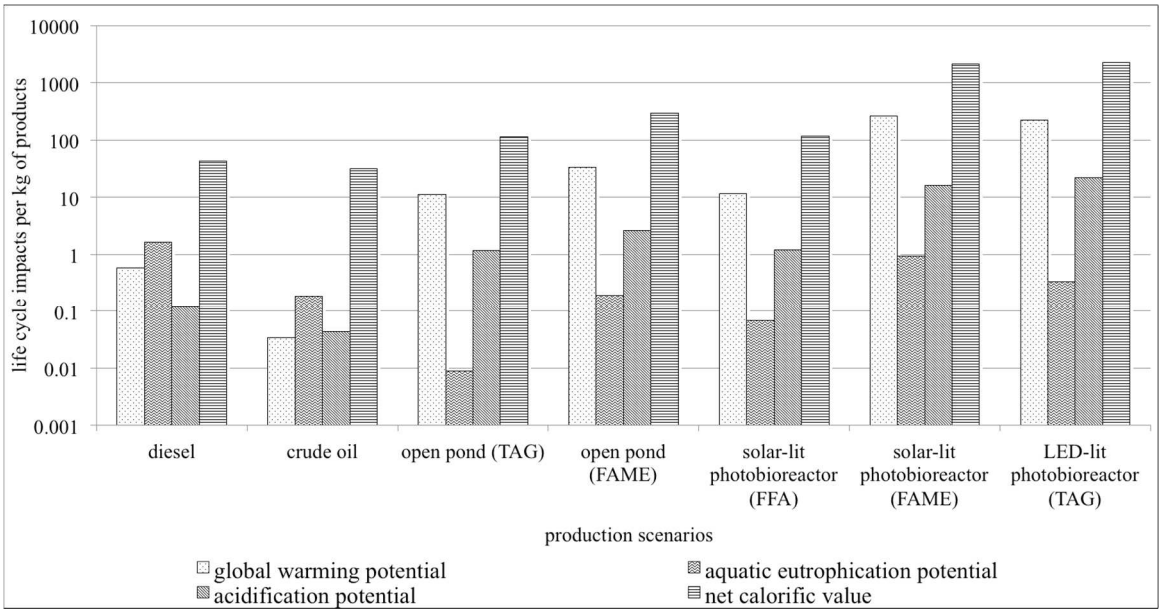

Figure 3.2 - LCA summary of all the production scenarios (in log scale) for a production facility of 500 ha.

The commercial production of algal biofuels/precursors still remains a challenge. Although the open pond growth scenario seems favorable, the challenges of growing algae efficiently without any contamination and efficiently providing the nutrients to the algae are still there.[39] Construction of open ponds with liners has significant life cycle impacts for materials, but without liners water losses can be too large. Improvements in the economic and environmental costs for downstream processes, such as dewatering[40] and solvent recovery[41], are consistently being sought, as well as, methods to utilize more of the algal biomass.[42], [43] Nutrient consumption (as well as, other environmentally and economically costly operations) may be mitigated by successful implementation of "no-kill" harvesting of algal products. For example, using cells that secrete extracellular fuel precursors into the medium and then continuously separating it from the medium (otherwise known as “milking”) is an attractive

possibility.[44-46] This approach could lower process energy, since cell dewatering, disruption, and drying are bypassed, and decrease fertilizer inputs, since cells are kept alive for continuous production.

3.7 Conclusions

Life cycle analysis of five algae-to-fuel production scenarios was done. At present none of them have lower life cycle impacts than their fossil fuel counterparts. Open pond growth is the most attractive form of production since it consumes less energy while growing and the environmental impacts for manufacturing the equipment are relatively lower than photobioreactors. However, it covers much land for such a low productivity that it is also unsustainable at this point. Photobioreactors have high producity, but the life cycle impacts of the scenarios including solar-lit photobioreactors and LED-lit photobioreactors are too high because of the equipment with higher life cycle impacts and higher net calorific value. Incremental improvements can certainly be made, especially in equipment manufacturing and processing of the algae. Examples of such improvements are use of compacted clay instead of plastic liners as open pond bases and possibly recycled materials in photobioreactors. Approaches with lower parasitic-energy consumption to achieve greater environmental and cost economies-of-scale in growth systems need to be explored and developed.

3.8 Acknowledgments

The authors gratefully acknowledge ConocoPhillips, Biofuels R&D through the Colorado Center for Biofuels and Biorefining Sponsored Research Program. We also acknowledge the initial studies and model building done by Luke Amer and Nisheet Bhat.

3.9 References

[1] W.S. Broecker, Climatic Change - Are We on Brink of a Pronounced Global Warming, Science, 189 (1975) 460-463.

[2] S. Lewandowsky, G.E. Gignac, S. Vaughan, The pivotal role of perceived scientific consensus in acceptance of science, Nat. Clim. Chang., 3 (2013) 399-404.

[3] J.S. Chang, C.Y. Chen, K.L. Yeh, R. Aisyah, D.J. Lee, Cultivation, photobioreactor design and harvesting of microalgae for biodiesel production: A critical review, Bioresource Technology, 102 (2011) 71-81.

[4] M.L. Ghirardi, O. Jorquera, A. Kiperstok, E.A. Sales, M. Embirucu, Comparative energy life-cycle analyses of microalgal biomass production in open ponds and photobioreactors, Bioresource Technology, 101 (2010) 1406-1413.

[5] D. Fishman, R. Majumdar, J. Morello, R. Pate, J. Yang, National Algal Biofuels Technology Roadmap, in: U.S. DOE (Ed.), Office of Energy Efficiency and Renewable Energy, Biomass Proagram, 2010, pp. 1-114.

[6] Y.S. Chen, J. Yang, M. Xu, X.Z. Zhang, Q. Hu, M. Sommerfeld, Life-cycle analysis on biodiesel production from microalgae: Water footprint and nutrients balance (vol 102, pg 159, 2011), Bioresource Technology, 102 (2011) 6633-6633.

[7] U.S.E.P. Agency, EPA Proposes 2014 Renewable Fuel Standards, 2015 Biomass-Based Diesel Volume, United States Environmental Protection Agency, Offie of Transportation and Air Quality, 2013, pp. 4.

[8] P.K. Campbell, T. Beer, D. Batten, Life cycle assessment of biodiesel production from microalgae in ponds, Bioresource Technology, 102 (2011) 50-56.

[9] K. Butterbach-Bahl, C.C. Lisboa, M. Mauder, R. Kiese, Bioethanol production from sugarcane and emissions of greenhouse gases - known and unknowns, Global Change Biology Bioenergy, 3 (2011) 277-292.

[10] Y. Chisti, Biodiesel from microalgae, Biotechnology Advances, 25 (2007) 294-306.

[11] A.F. Clarens, E.P. Resurreccion, M.A. White, L.M. Colosi, Environmental Life Cycle Comparison of Algae to Other Bioenergy Feedstocks, Environmental Science & Technology, 44 (2010) 1813-1819.

[12] M. Odlare, E. Nehrenheim, V. Ribe, E. Thorin, M. Gavare, M. Grube, Cultivation of algae with indigenous species - Potentials for regional biofuel production, Applied Energy, 88 (2011) 3280-3285.

[13] T.M. Mata, A.A. Martins, N.S. Caetano, Microalgae for biodiesel production and other applications: A review, Renewable & Sustainable Energy Reviews, 14 (2010) 217-232.

[14] S.O. Salley, H.Y. Tang, M. Chen, M.E.D. Garcia, N. Abunasser, K.Y.S. Ng, Culture of Microalgae Chlorella minutissima for Biodiesel Feedstock Production, Biotechnology and Bioengineering, 108 (2011) 2280-2287.

[15] P. Azadi, G. Brownbridge, S. Mosbach, A. Smallbone, A. Bhave, O. Inderwildi, M. Kraft, The carbon footprint and non-renewable energy demand of algae-derived biodiesel, Applied Energy, 113 (2014) 1632-1644.

[16] H.H. Khoo, P.N. Sharratt, P. Das, R.K. Balasubramanian, P.K. Naraharisetti, S. Shaik, Life cycle energy and CO(2) analysis of microalgae-to-biodiesel: Preliminary results and comparisons, Bioresour. Technol., 102 (2011) 5800-5807.

[17] K. Sander, G.S. Murthy, Life cycle analysis of algae biodiesel, International Journal of Life Cycle Assessment, 15 (2010) 704-714.

[18] M. Rickman, J. Pellegrino, J. Hock, S. Shaw, B. Freeman, Life-cycle and techno-economic analysis of utility-connected algae systems, Algal Res, 2 (2013) 59-65.

[19] P.H. Pfromm, V. Amanor-Boadu, R. Nelson, Sustainability of algae derived biodiesel: A mass balance approach, Bioresource Technology, 102 (2011) 1185-1193.

[20] D. Pant, A. Singh, G. Van Bogaert, Y.A. Gallego, L. Diels, K. Vanbroekhoven, An introduction to the life cycle assessment (LCA) of bioelectrochemical systems (BES) for sustainable energy and product generation: Relevance and key aspects, Renewable & Sustainable Energy Reviews, 15 (2011) 1305-1313.

[21] Y.L. Zhang, M.A. White, L.M. Colosi, Environmental and economic assessment of integrated systems for dairy manure treatment coupled with algae bioenergy production, Bioresource Technology, 130 (2013) 486-494.

[22] M. Debowski, M. Zielinski, A. Grala, M. Dudek, Algae biomass as an alternative substrate in biogas production technologies-Review, Renewable & Sustainable Energy Reviews, 27 (2013) 596-604.

[23] M.A. Meyer, A. Weiss, Life cycle costs for the optimized production of hydrogen and biogas from microalgae, Energy, 78 (2014) 84-93.

[24] K. Soratana, A.E. Landis, Evaluating industrial symbiosis and algae cultivation from a life cycle perspective, Bioresource Technology, 102 (2011) 6892-6901.

[25] B. Steubing, R. Zah, C. Ludwig, Life cycle assessment of SNG from wood for heating, electricity, and transportation, Biomass Bioenerg, 35 (2011) 2950-2960.

[26] T.M. Komarek, F. Lupi, M.D. Kaplowitz, Valuing energy policy attributes for environmental management: Choice experiment evidence from a research institution, Energ Policy, 39 (2011) 5105-5115.

[27] E.P. Johnson, Air-source heat pump carbon footprints: HFC impacts and comparison to other heat sources, Energ Policy, 39 (2011) 1369-1381.

[28] P. Collet, L. Lardon, A. Helias, S. Bricout, I. Lombaert-Valot, B. Perrier, O. Lepine, J.P. Steyer, O. Bernard, Biodiesel from microalgae - Life cycle assessment and recommendations for potential improvements, Renew Energ, 71 (2014) 525-533.

[29] S.I. Olsen, F.M. Christensen, M. Hauschild, F. Pedersen, H.F. Larsen, J. Torslov, Life cycle impact assessment and risk assessment of chemicals — a methodological comparison, Environmental Impact Assessment Review, 21 (2001) 385-404.

[30] F. Romagnoli, D. Blumberga, I. Pilicka, Life cycle assessment of biohydrogen production in photosynthetic processes, International Journal of Hydrogen Energy, 36 (2011) 7866-7871.

[31] L. Soh, M. Montazeri, B.Z. Haznedaroglu, C. Kelly, J. Peccia, M.J. Eckelman, J.B. Zimmerman, Evaluating microalgal integrated biorefinery schemes: Empirical controlled growth studies and life cycle assessment, Bioresource Technology, 151 (2014) 19-27.

[32] C.E. Canter, R. Davis, M. Urgun-Demirtas, E.D. Frank, Infrastructure associated emissions for renewable diesel production from microalgae, Algal Res, 5 (2014) 195-203.

[33] L. Amer, B. Adhikari, J. Pellegrino, Technoeconomic analysis of five microalgae-to-biofuels processes of varying complexity, Bioresour. Technol., 102 (2011) 9350-9359.

[34] N.R.E.L. (U.S.), U.S. LIFE CYCLE INVENTORY DATABASE ROADMAP, National Renewable Energy Laboratory, Golden, CO, 2009, pp. 12.

[35] L. Lardon, A. Helias, B. Sialve, J.P. Stayer, O. Bernard, Life-Cycle Assessment of Biodiesel Production from Microalgae, Environmental Science & Technology, 43 (2009) 6475-6481.

[36] A.L. Stephenson, E. Kazamia, J.S. Dennis, C.J. Howe, S.A. Scott, A.G. Smith, Life-Cycle Assessment of Potential Algal Biodiesel Production in the United Kingdom: A Comparison of Raceways and Air-Lift Tubular Bioreactors, Energ Fuel, 24 (2010) 4062-4077.

[37] N. Eckelberry, T.R. Eckelberry, Algae Growth System for Oil Production, in: U.S.P.a.T. Office (Ed.) United States Patent and Trademark OfficeUSA, 2009.

[38] L.X. Xu, D.W.F. Brilman, J.A.M. Withag, G. Brem, S. Kersten, Assessment of a dry and a wet route for the production of biofuels from microalgae: Energy balance analysis, Bioresource Technology, 102 (2011) 5113-5122.

[39] R. Putt, M. Singh, S. Chinnasamy, K.C. Das, An efficient system for carbonation of high-rate algae pond water to enhance CO(2) mass transfer, Bioresource Technology, 102 (2011) 3240-3245.

[40] N. Uduman, Y. Qi, M.K. danquah, G.M. Forde, A. Hoadley, Dewatering of microalgal cultures: A major bottleneck to algae-based fuels, Journal of Renewable and Sustainable Energy, 2 (2010) 15.

[41] C. Samori, D. Lopez Barreiro, R. Vet, L. Pezzolesi, D.W.F. Brilman, P. Galletti, E. Tagliavini, Effective lipid extraction from algae cultures using switchable solvents, Green Chemistry, 15 (2013) 353-356.

[42] R. Davis, C. Kinchi, J. Markham, E.C.D. Tan, L.M.L. Laurens, D. Sexton, D. Knorr, P. Schoen, J. Lukas, Process Design and Economics for the Conversion of Algal Biomass to Biofuels: Algal Biomass Fractionation to Lipid and Carbohydrate-Derived Fuel Products, NREL, Golden, CO, 2014.

[43] L.M.L. Laurens, N. Nagle, R. Davis, N. Sweeney, S. Van Wychen, A. Lowell, P.T. Pienkos, Acid-catalyzed algal biomass pretreatment for integrated lipid and carbohydrate-based biofuels production, Green Chemistry, 17 (2015) 1145-1158.

[44] M.A. Hejazi, R.H. Wijffels, Milking of microalgae, Trends Biotechnol., 22 (2004) 189-194.

[45] T.V. Ramachandra, D. Mahapatra, K. B, R. Gordon, Milking diatoms for sustainable energy: biochemical engineering versus gasoline-secreting diatom solar panels, Ind Eng Chem Res, 48 (2009) 8769-8788.

[46] F. Zhang, L.H. Cheng, X.H. Xu, L. Zhang, H.L. Chen, Screening of biocompatible organic solvents for enhancement of lipid milking from *Nannochloropsis*, Process Biochem., 46 (2011) 1934-1941.

3.10 Supplementary information

3.10.1 Tables

3.10.1.1 Simulation details and assumptions

Table 3-8 – Solar-lit photobioreactor

	EDIP 2003, Net acidification potential [m^2 UES]	EDIP 2003, Net aquatic eutrophication [kg NO_3-equiv.]	EDIP 2003, Net global warming [kg CO_2-equiv./year]	EDIP 2003, Net energy renewable and non renewable (net calorific value) [MJ]
GLO: Irrigation pump PE	2.97	0.15	15.9	0.00
RNA: Polyvinyl chloride resin, at plant USLCI/PE	4.19	0.01	17.9	0.00
US: Diesel at refinery PE (1)	0.03	0.00	0.40	1.61
US: Diesel at refinery PE (2)	0.01	0.00	0.11	0.46
US: Diesel at refinery PE (3)	0.01	0.00	0.11	0.46
US: Diesel at refinery PE (4)	6.00	0.08	76.9	310
US: Polycarbonate granulate (PC) PE	2918	40.8	49281	247338
US: Polyethylene film (PE-LD) PE	7.01	0.08	106	599
US: Polyvinyl chloride granulate (S-PVC) PE	1.77	0.02	29.3	150
US: Reactor basin assembly	0.00	0.00	0.00	0.00
US: Truck - Flatbed, platform, etc. / 4,000 lb payload - 3 / 2008 PE (1)	0.01	0.00	2.47	0.00
US: Truck - Flatbed, platform, etc. / 4,000 lb payload - 3 / 2008 PE (2)	0.00	0.00	0.71	0.00
US: Truck - Flatbed, platform, etc. / 4,000 lb	0.00	0.00	0.71	0.00

payload - 3 / 2008 PE (3)				
US: Truck - Flatbed, platform, etc. / 4,000 lb payload - 3 / 2008 PE (4)	1.86	0.08	476	0.00

Table 3-9 – LED-lit photobioreactor

Inventory	EDIP 2003, Net acidification potential [m^2 UES]	EDIP 2003, Net aquatic eutrophication [kg NO_3-equiv.]	EDIP 2003, Net global warming [kg CO_2-equiv./year]	EDIP 2003, Net energy renewable and non renewable (net calorific value) [MJ]
DE: Stainless steel sheet PE	0.11	0.00	1.30	5.31
RNA: High density polyethylene resin, at plant USLCI	0.17	0.01	1.34	0.00
US: Ethene (ethylene) PE	53.6	0.85	1137	3064
US: Gasoline (regular) at refinery PE (1)	0.00	0.00	0.07	0.22
US: Gasoline (regular) at refinery PE (2)	0.00	0.00	0.00	0.00
US: Liquefied petroleum gas, combusted in industrial boiler USLCI/PE	0.00	0.00	0.05	0.00

US: Natural gas, combusted in industrial boiler USLCI	0.35	0.02	47.6	0.00
US: Natural gas, processed, at plant USLCI/PE	8.29	0.00	10.4	0.00
US: Power grid mix PE (1)	10.1	0.08	98.0	999
US: Power grid mix PE (2)	474	3.66	4620	47099
US: Residual fuel oil, at refinery USLCI/PE	0.44	0.01	2.18	0.00
US: Residual fuel oil, combusted in industrial boiler USLCI	0.64	0.01	13.4	0.00
US: Transport, barge, average fuel mix USLCI/PE	0.00	0.00	0.00	0.00
US: Transport, combination truck, gasoline powered USLCI (1)	0.02	0.00	0.31	0.00
US: Transport, combination truck, gasoline powered USLCI (2)	0.00	0.00	0.00	0.00
US: Transport, train, diesel powered USLCI/PE (1)	0.00	0.00	0.01	0.00
US: Transport, train, diesel powered USLCI/PE (2)	0.00	0.00	0.00	0.00

Table 3-10 – Open pond

Inventory	EDIP 2003, Net acidification potential [m^2 UES]	EDIP 2003, Net aquatic eutrophication [kg NO_3-equiv.]	EDIP 2003, Net global warming [kg CO_2-equiv./year]	EDIP 2003, Net energy renewable and non renewable (net calorific value) [MJ]
DE: Stainless steel sheet PE	42.3	0.33	499	2044
GLO: Soil cultivation; ploughing (heavy, 160 kW) PE	81.5	4.08	1132	0.00
US: Diesel at refinery PE	14.3	0.20	183	740
US: Polyethylene film (PE-LD) PE	46666	532	708236	3990504

Table 3-11 – Dewatering step (rotary dryer) assumptions

Inventory	EDIP 2003, Acidification potential [m2 UES]	EDIP 2003, Aquatic eutrophication [kg NO3-Equiv.]	EDIP 2003, Global warming [kg CO2-Equiv.]	Energy renewable and non renewable (net calorific value) [MJ]
US: Iron and steel, production mix USLCI/PE	188	0.00	4395	0.00
US: Transport, train, diesel powered USLCI/PE	1.05	0.05	4.71	0.00

Table 3-12 – Pumps assumptions

Inventory	EDIP 2003, Net acidification potential [m^2 UES]	EDIP 2003, Net aquatic eutrophication [kg NO_3-equiv.]	EDIP 2003, Net global warming [kg CO_2-equiv./year]	EDIP 2003, Net energy renewable and non renewable (net calorific value) [MJ]

US: Iron and steel, production mix USLCI/PE	0.039	0.00	0.925	0.00
US: Pump materials at site	0.00	0.00	0.00	0.00
US: Transport, train, diesel powered USLCI/PE	0.01	0.00	0.02	0.00

Table 3-13 – Heat exchangers assumptions

Inventory	EDIP 2003, Net acidification potential [m^2 UES]	EDIP 2003, Net aquatic eutrophication [kg NO_3-equiv.]	EDIP 2003, Net global warming [kg CO_2-equiv./year]	EDIP 2003, Net energy renewable and non renewable (net calorific value) [MJ]
DE: Stainless steel sheet PE	8465	66.8	99880	408799
US: Stainless steel at site	0.00	0.00	0.00	0.00
US: Transport, train, diesel powered USLCI/PE	10.0	0.45	44.9	0.00

Table 3-14 – Reactor vessels assumptions

Inventory	EDIP 2003, Net acidification potential [m^2 UES]	EDIP 2003, Net aquatic eutrophication [kg NO_3-equiv.]	EDIP 2003, Net global warming [kg CO_2-equiv./year]	EDIP 2003, Net energy renewable and non renewable (net calorific value) [MJ]
DE: Stainless steel sheet PE	5502	43.4	64922	265720
US: Stainless steel at site	0.00	0.00	0.00	0.00

US: Transport, train, diesel powered USLCI/PE	6.50	0.29	29.2	0.00

Table 3-15 – Centrifuges assumptions

Inventory	EDIP 2003, Net acidification potential [m^2 UES]	EDIP 2003, Net aquatic eutrophication [kg NO_3-equiv.]	EDIP 2003, Net global warming [kg CO_2-equiv./year]	EDIP 2003, Net energy renewable and non renewable (net calorific value) [MJ]
DE: Stainless steel sheet PE	489	3.86	5773	23629
US: Stainless steel at site	0.00	0.00	0.00	0.00
US: Transport, train, diesel powered USLCI/PE	0.58	0.03	2.59	0.00

Table 3-16 – Large vessels assumptions

Inventory	EDIP 2003, Net acidification potential [m^2 UES]	EDIP 2003, Net aquatic eutrophication [kg NO_3-equiv.]	EDIP 2003, Net global warming [kg CO_2-equiv./year]	EDIP 2003, Net energy renewable and non renewable (net calorific value) [MJ]
DE: Stainless steel sheet PE	21163	167	249700	1021998
US: Stainless steel at site	0.00	0.00	0.00	0.00
US: Transport, train, diesel powered USLCI/PE	25.0	1.12	112	0.00

Table 3-17 – Small vessels assumptions

Inventory	EDIP 2003, Net acidification potential [m^2	EDIP 2003, Net aquatic eutrophication	EDIP 2003, Net global warming [kg	EDIP 2003, Net energy renewable and non renewable

	UES]	[kg NO_3-equiv.]	CO_2-equiv./year]	(net calorific value) [MJ]
DE: Stainless steel sheet PE	21.2	0.17	250	1022
US: Stainless steel at site	0.00	0.00	0.00	0.00
US: Transport, train, diesel powered USLCI/PE	0.03	0.00	0.11	0.00

Table 3-18 – Distillation column assumptions

Inventory	EDIP 2003, Net acidification potential [m^2 UES]	EDIP 2003, Net aquatic eutrophication [kg NO_3-equiv.]	EDIP 2003, Net global warming [kg CO_2-equiv./year]	EDIP 2003, Net energy renewable and non renewable (net calorific value) [MJ]
DE: Stainless steel sheet PE	4233	33.4	49940	204400
US: Stainless steel at site	0.00	0.00	0.00	0.00
US: Transport, train, diesel powered USLCI/PE	5.00	0.22	22.4	0.00

Table 3-19 – Membrane assumptions

Inventory	EDIP 2003, Net acidification potential [m^2 UES]	EDIP 2003, Net aquatic eutrophication [kg NO_3-equiv.]	EDIP 2003, Net global warming [kg CO_2-equiv./year]	EDIP 2003, Net energy renewable and non renewable (net calorific value) [MJ]
US: Polypropylene granulate (PP) PE	24.7	0.33	447	1884
US: Polypropylene	0.00	0.00	0.00	0.00

membrane				
US: Transport, train, diesel powered USLCI/PE	0.10	0.00	0.45	0.00

Table 3-20 – Thickener assumptions

Inventory	EDIP 2003, Net acidification potential [m^2 UES]	EDIP 2003, Net aquatic eutrophication [kg NO_3-equiv.]	EDIP 2003, Net global warming [kg CO_2-equiv./year]	EDIP 2003, Net energy renewable and non renewable (net calorific value) [MJ]
DE: Concrete C12/15 PE	14.7	0.51	520	731
GLO: Soil cultivation; ploughing (heavy, 160 kW) PE	6.40	0.32	88.9	0.00
US: Diesel at refinery PE	1.12	0.02	14.4	58.1
US: Iron and steel, production mix USLCI/PE	98.3	0.00	2302	0.00

Table 3-21 – Compressor assumptions

Inventory	EDIP 2003, Net acidification potential [m^2 UES]	EDIP 2003, Net aquatic eutrophication [kg NO_3-equiv.]	EDIP 2003, Net global warming [kg CO_2-equiv./year]	EDIP 2003, Net energy renewable and non renewable (net calorific value) [MJ]
US: Iron and steel, production mix USLCI/PE	70.8	0.00	1658	0.00
US: Steel at site	0.00	0.00	0.00	0.00
US: Transport, train, diesel powered USLCI/PE	0.90	0.04	4.04	0.00

Table 3-22 – Electricity assumptions

Inventory	EDIP 2003, Net acidification potential [m^2 UES]	EDIP 2003, Net aquatic eutrophication [kg NO_3-equiv.]	EDIP 2003, Net global warming [kg CO_2-equiv./year]	EDIP 2003, Net energy renewable and non renewable (net calorific value) [MJ]
GLO: Power from nuclear power plant PE	0.00	0.00	0.01	2.21
GLO: Power from wind power PE	0.00	0.00	0.00	0.00
US: Power from hard coal PE	0.07	0.00	0.57	3.92
US: Power from heavy fuel oil PE	0.00	0.00	0.03	0.22
US: Power from hydropower PE	0.00	0.00	0.00	0.06
US: Power from lignite PE	0.00	0.00	0.03	0.22
US: Power from natural gas PE	0.00	0.00	0.14	1.29

Table 3-23 – Steam (low pressure, natural gas) assumptions

Inventory	EDIP 2003, Net acidification potential [m^2 UES]	EDIP 2003, Net aquatic eutrophication [kg NO_3-equiv.]	EDIP 2003, Net global warming [kg CO_2-equiv./year]	EDIP 2003, Net energy renewable and non renewable (net calorific value) [MJ]
US: Steam from natural gas 89% PE	0.01	0.00	0.23	0.63
US: Superheated steam	0.00	0.00	0.00	0.00

Table 3-24 – Steam (low pressure, coal) assumptions

Inventory	EDIP 2003, Net acidification potential [m^2 UES]	EDIP 2003, Net aquatic eutrophication [kg NO_3-equiv.]	EDIP 2003, Net global warming [kg CO_2-equiv./year]	EDIP 2003, Net energy renewable and non renewable (net calorific value) [MJ]
US: Steam from hard coal 89%	0.04	0.00	0.30	0.37

PE				
US: Superheated steam	0.00	0.00	0.00	0.00

Table 3-25 – Steam (high pressure, natural gas) assumptions

Inventory	EDIP 2003, Net acidification potential [m^2 UES]	EDIP 2003, Net aquatic eutrophication [kg NO_3-equiv.]	EDIP 2003, Net global warming [kg CO_2-equiv./year]	EDIP 2003, Net energy renewable and non renewable (net calorific value) [MJ]
US: Steam from natural gas 89% PE	0.01	0.00	0.26	0.71
US: Superheated steam	0.00	0.00	0.00	0.00

Table 3-26 – Steam (high pressure, coal) assumptions

Inventory	EDIP 2003, Net acidification potential [m^2 UES]	EDIP 2003, Net aquatic eutrophication [kg NO_3-equiv.]	EDIP 2003, Net global warming [kg CO_2-equiv./year]	EDIP 2003, Net energy renewable and non renewable (net calorific value) [MJ]
US: Steam from hard coal 89% PE	0.04	0.00	0.34	0.41
US: Superheated steam	0.00	0.00	0.00	0.00

Table 3-27 – Raw chemicals assumptions

Inventory	EDIP 2003, Net acidification potential [m^2 UES]	EDIP 2003, Net aquatic eutrophication [kg NO_3-equiv.]	EDIP 2003, Net global warming [kg CO_2-equiv./year]	EDIP 2003, Net energy renewable and non renewable (net calorific value) [MJ]
RNA: Methanol, at plant USLCI/PE	0.29	0.00	0.58	0.00
US: Sulfuric acid aq. (96%) PE	0.10	0.00	0.28	1.44
US: Nitrogen fertilizer, production mix, at plant USLCI/PE	0.35	0.00	2.03	0.00
US: Phosphorous fertilizer, production mix, at plant USLCI/PE (Ave)	0.33	0.62	0.40	0.00
US: Potassium chloride (agrarian) PE	0.01	0.00	0.10	0.87
CA: Magnesium sulfate (agrarian) PE	0.02	0.00	0.28	1.79
RNA: Glycerin, at plant USLCI/PE	0.25	0.00	2.52	0.00

US: Carbon dioxide (by product ammonia) PE	0.07	0.00	1.09	8.71
US: Ethanol (96%) (Hydrogenation with nitric acid) PE	0.10	0.00	2.79	7.84

Table 3-28 – Equipment life-time assumption

Equipment	Life time (year)
Solar-lit photobioreactor basin	10
Open pond basins	10
LED-lit photobioreactor basins	10
Compressors	10
Pumps	10
Rotary dryer	10
Heat exchangers	10
Reactor vessels	10
Centrifuges	10
Large vessels	10
Small vessels	10
Columns	10
Thickeners	10
Membranes	10

3.10.2 Methodology example

Solar-lit photobioreactor, as designed by Solix, is a unit wherein microalgae are grown in what amounts to large polyethylene bags contained in a thermoset plastic basin. The basin is filled with water, allowing for temperature regulation of the contained algal slurry. Essentially, the entire reactor system can be thought of as a polycarbonate basin, polyethylene films made into bags, polyvinylchloride piping for CO_2 and nutrient supply. Additionally a pump, similar to an irrigation pump, circulates water through the external basin. Using GaBi 4.3, each of these materials of construction is tabulated, along with the required energy and transportation for each material. The assembly is simply considered to be the sum of each of the individual parts. The amount of each component required for the assembly is calculated using SAFEER. At this time, the additional energy and manpower required to assemble individual materials of construction into unique parts has not been accounted for.

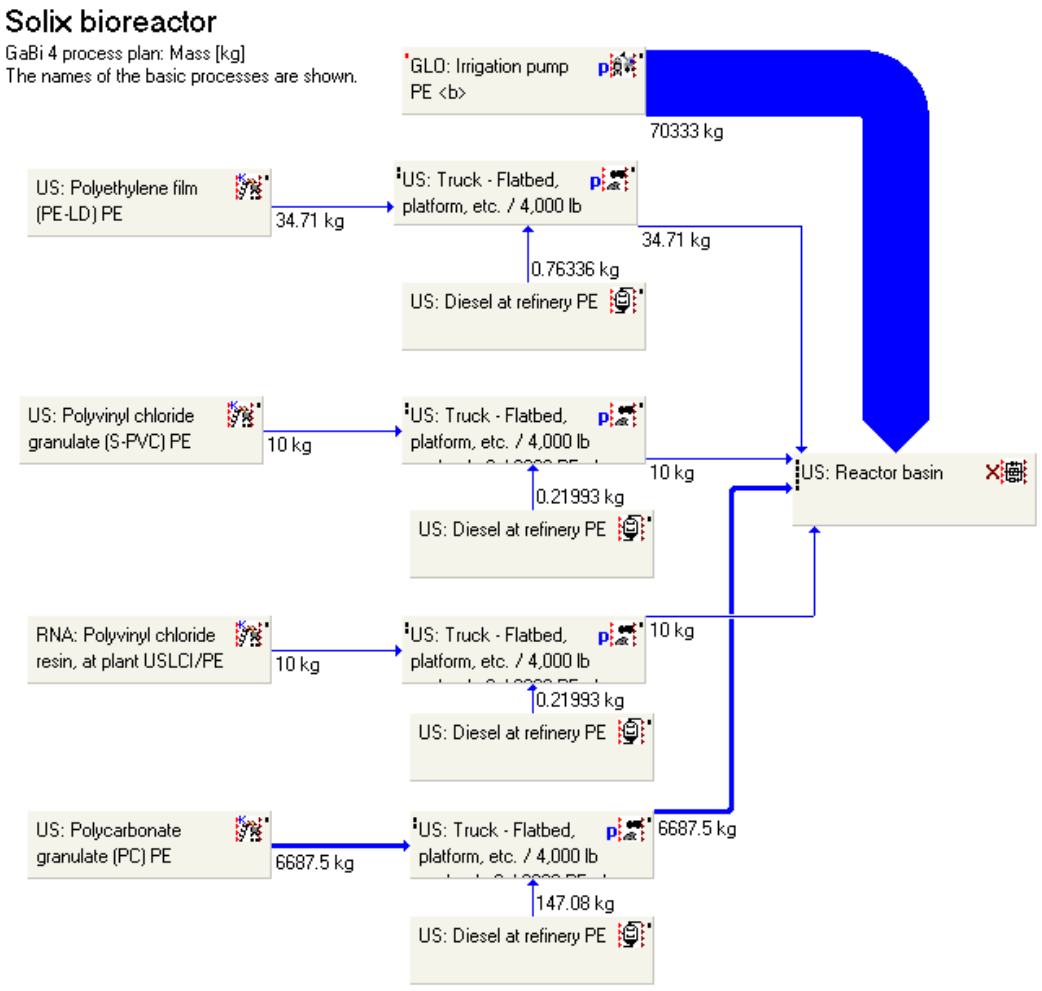

Figure 3.3 – Flow diagram showing the steps of determining life cycle impacts of solar-lit photobioreactor.

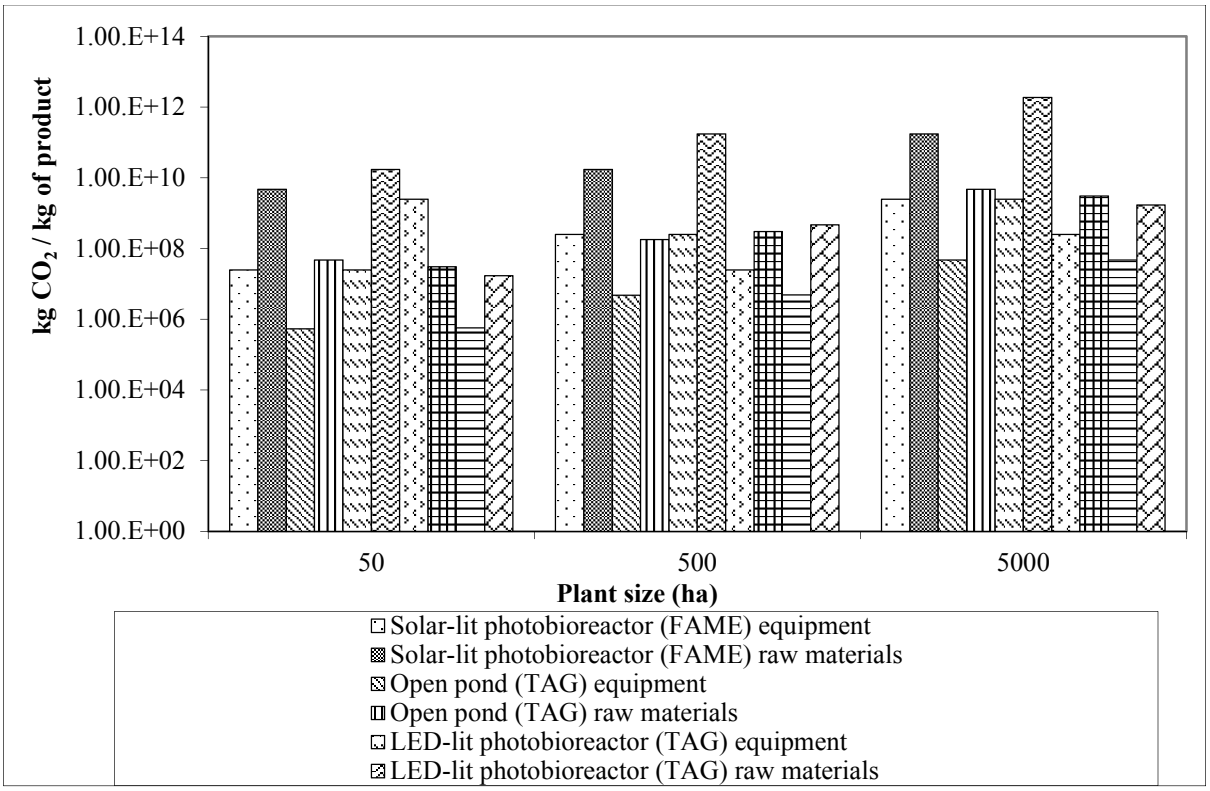
1.00.E+14
1.00.E+12
1.00.E+10
1.00.E+08
1.00.E+06
1.00.E+04
1.00.E+02
1.00.E+00
kg CO2 / kg of product
50
500
5000
Plant size (ha)
Solar-lit photobioreactor (FAME) equipment
Solar-lit photobioreactor (FAME) raw materials
Open pond (TAG) equipment
Open pond (TAG) raw materials
LED-lit photobioreactor (TAG) equipment
LED-lit photobioreactor (TAG) raw materials

(a)

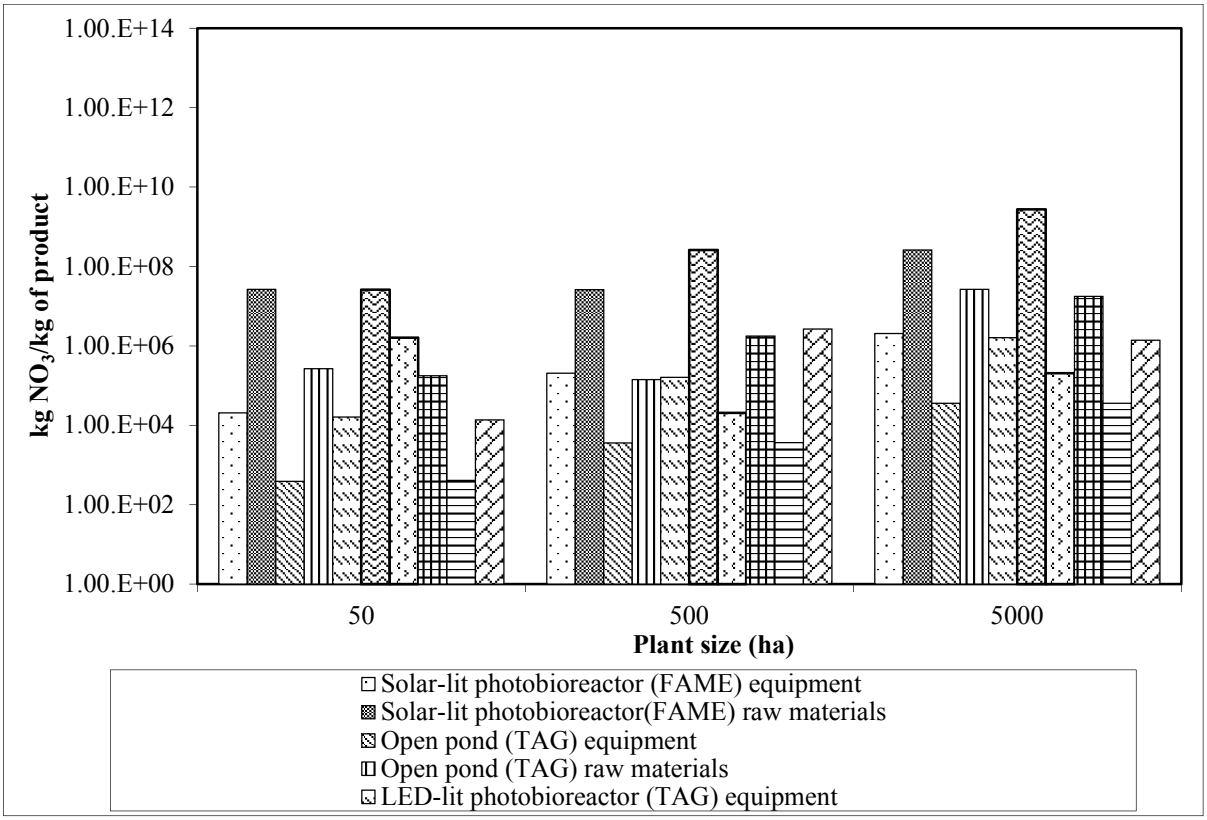
1.00.E+14
1.00.E+12
1.00.E+10
1.00.E+08
1.00.E+06
1.00.E+04
1.00.E+02
1.00.E+00
kg NO3/kg of product
50
500
5000
Plant size (ha)
Solar-lit photobioreactor (FAME) equipment
Solar-lit photobioreactor(FAME) raw materials
Open pond (TAG) equipment
Open pond (TAG) raw materials
LED-lit photobioreactor (TAG) equipment

(b)

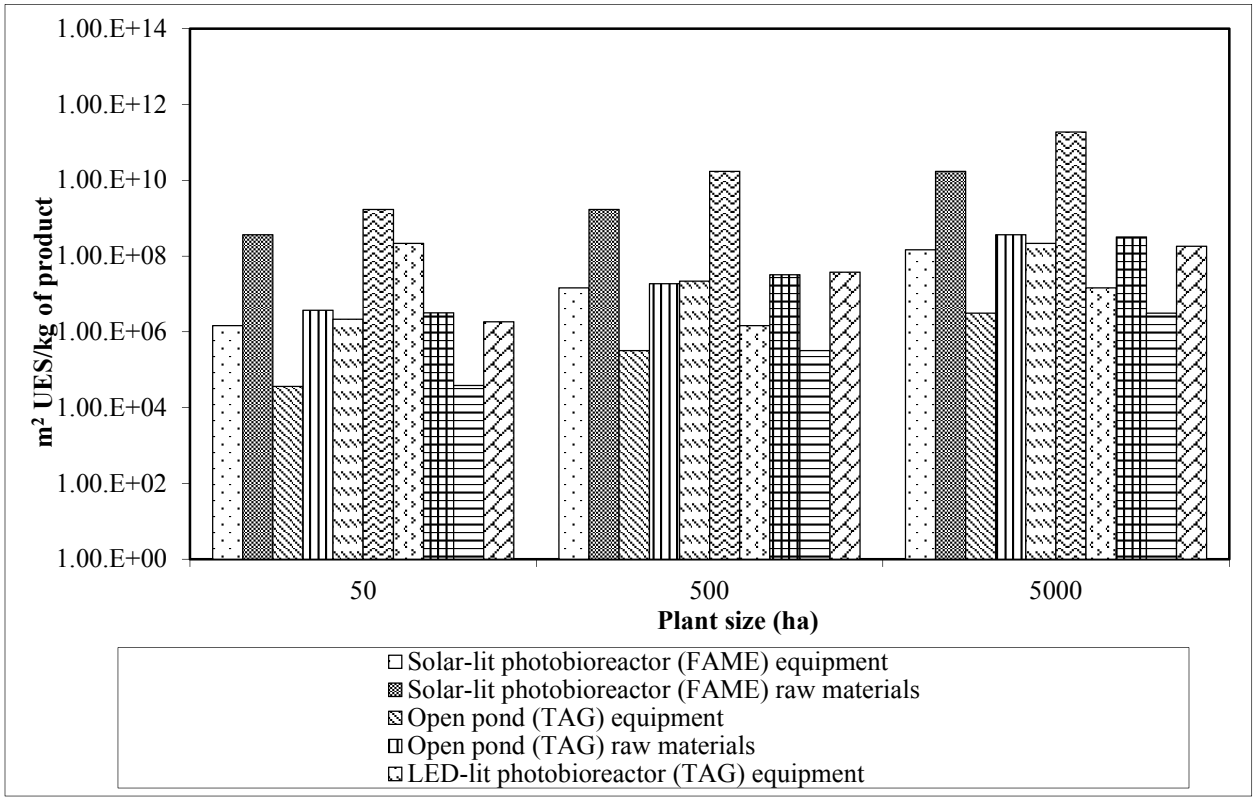
1.00.E+14
1.00.E+12
1.00.E+10
1.00.E+08
1.00.E+06
1.00.E+04
1.00.E+02
1.00.E+00
m2 UES/kg of product
50
500
5000
Plant size (ha)
Solar-lit photobioreactor (FAME) equipment
Solar-lit photobioreactor (FAME) raw materials
Open pond (TAG) equipment
Open pond (TAG) raw materials
LED-lit photobioreactor (TAG) equipment

(c)

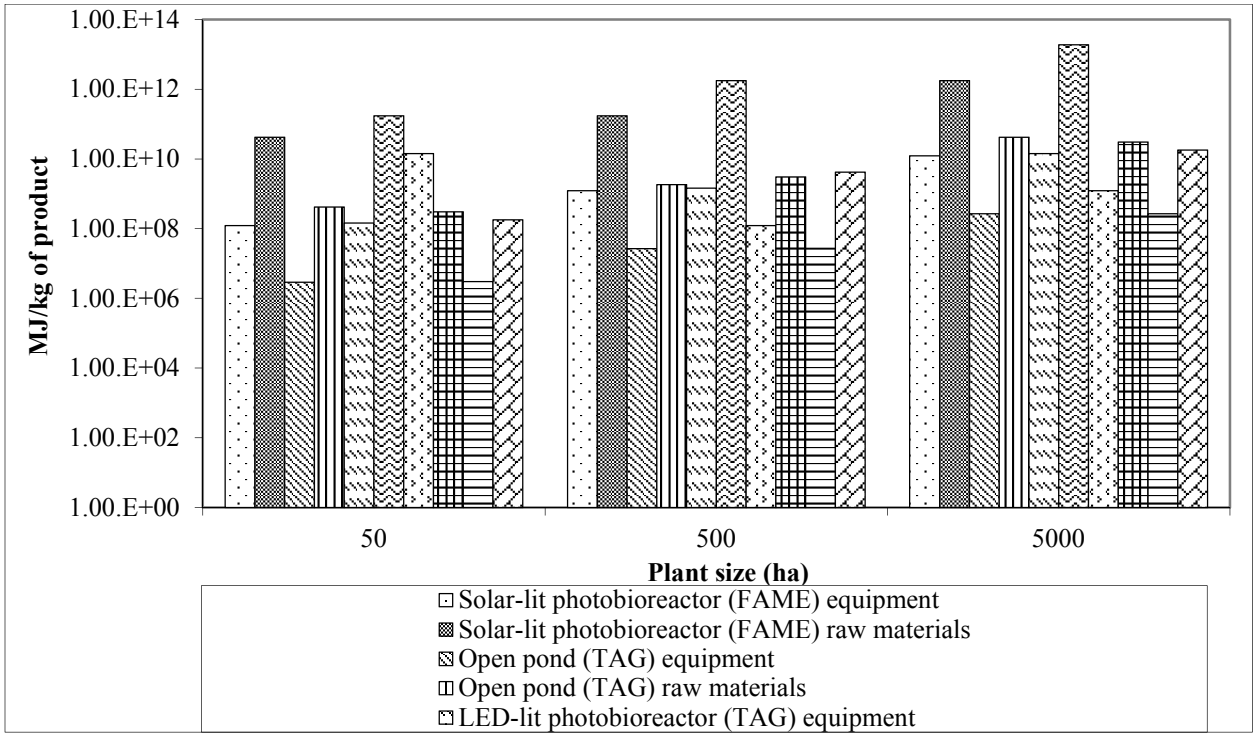
1.00.E+14
1.00.E+12
1.00.E+10
1.00.E+08
1.00.E+06
1.00.E+04
1.00.E+02
1.00.E+00
MJ/kg of product
50
500
5000
Plant size (ha)
Solar-lit photobioreactor (FAME) equipment
Solar-lit photobioreactor (FAME) raw materials
Open pond (TAG) equipment
Open pond (TAG) raw materials
LED-lit photobioreactor (TAG) equipment

(d)

Figure 3.4 – (a) Global warming potential (b) eutrophication potential, (c) acidification potential and (d) renewable and non-renewable energy sources of all five cases of different production area of 50, 500 and 5000 ha.

3.10.3 Supplemental information source key

[1]U.S. Life-Cycle Inventory Database v1.6.0., National Renewable Energy Laboratory,. 2008. (Accessed July 1, 2011 through GABI 4.3.)

[2]www. Solix.com (Accessed July 1, 2011)

[3]www.originoil.com (Accessed July 1, 2011)

[4]www.NREL.gov (Accessed July 1, 2011)

[5]Clarens, A.F., Resurreccion, E.P., White, M.A., Colosi, L.M., 2010. *Environmental Life Cycle Comparison of Algae to Other Bioenergy Feedstocks.* Environmental Science & Technology.

[6]Lardon, L., Helias, A., Sialve, B., Stayer, J.P., Bernard, O., 2009. Life-Cycle Assessment of Biodiesel Production from Microalgae. *Environmental Science & Technology*, 43, 6475-6481.

Chapter 4 Extraction of lipids from wet-algae using diesel and isopropanol in various proportions and testing the regrowth of *Chlorella vulgaris* towards sustainable biofuel production

Abstract

Lipid extraction is an important unit operation in biofuel and chemicals production from algae. A Hansen solubility parameter analysis indicated that mixed solvents diesel and isopropanol could be useful for extraction of lipids from wet-algae. An initial screening study was performed with this mixed-solvent system on freshly-harvested *Chlorella vulgaris* that had been concentrated to approximately 99.5% water, 0.4% organic (non-volatile) biomass, and 0.1% (all by mass) inorganic electrolytes. An experimental design was conducted where small volumes of wet algae and solvent mixture(s) were contacted at a constant temperature and mixing environment; three levels of wet algae to solvent mixture mass ratio and two different contact time levels. Lipids extracted using diesel and isopropanol were found to be comparable to lipids extracted using hexane and isopropanol at 6:4 by mass. The regrowth of algae after extraction were also studied and suggests the wet algal biomass, post-harvesting and after extraction, can be recycled to seed further culture growth.

4.1 Introduction

4.1.1 Motivation

The development and need for renewable and more cost "consistent" alternative fuels is very important in recent times[1]. Global warming (and its concomitant impacts) is also

attributed to excessive production of greenhouse gases from fossil fuel use, and other environmental concerns, with respect to water and air quality, are also associated with fossil fuel production and use[2] [3]. Hence, carbon-neutral, renewable liquid fuels are desired to eventually displace petroleum-derived transportation fuels that contribute to global warming[4].

Achieving economic, environmental, and production volume goals make the development of new alternative energy carriers a challenging endeavor. Many types of alternative sources of energies such as geothermal, wind, and solar energy have grown in share but do not alone provide a transportation fuel.. Biofuels, such as those derived from algae, are a possible renewable alternative to fossil transportation fuels, as well as, a source for chemical precursors[5].

More than 70% of Earth is covered with water, in which the most dominant group of living organisms is that of algae[6]. The history of microalgal utilization from natural populations is centuries old (Nostoc in Asia and Spirulina in Africa and Mexico), however, the purposeful cultivation of microalgae is only a few decades old[7]. Algae is of particular interest because the microorganisms have a faster growth rate, a shorter maturity rate, and a higher biomass content than other crops used for biofuels, such as corn and soybeans[8]. Algae can grow rapidly even in stressful conditions[9, 10]. Some strains of algae are confirmed to have high lipid content[11], for example, *Chlorella vulgaris* can have a high content of saturated fatty acids which can go as high as 55% of total biomass of algae[12]. Algae garnered applications in the food industry recently because different strains of algae are loaded with desirable fatty acids[13]. Algae can also be a very good protein and carbohydrate source[14]. Algae can be grown on non-arable land and has the potential for yields 50-100 times greater than biodiesel produced from soybeans. In addition, algal ponds can utilize waste CO_2 produced by fossil-fuel

power plants to reach maximal areal productivity[1]. These lipids can also be converted to fatty acid methyl ester or FAME, which is conventional biodiesel, by transesterification[15]. Many studies have confirmed the viability of microalgae for biofuel[15, 16].

Although algae is promising source of energy, there are still some major hurdles to overcome, including the harvesting energy, with respect to its development and commercialization. For example, algae grows differently in different parts of the world depending upon climatic condition and water supplies of those areas[17]. Despite long-standing interests, algae fuel is not yet fully commercialized and the 2014 National Renewable Energy Laboratory (NREL) estimation[18] for the cost of fuel production is ~$4.35/gal gasoline equivalent (in 2011 $) based on the baseline case scenario called algal lipid upgrading (ALU). Our own study[19] verified that growth and dewatering of algae, lipid extraction, lipid transesterification and solvent recovery processes are all energy intensive processes making the current cost of production of algae biofuel unsustainably high[20]. A study done in 2013 suggests that for the cost to decrease and be competitive to $3/gal, several processes have to be improved significantly, primarily the lipid extraction step. [21, 22] The costs[22] for dewatering/drying, extraction, and processing when using earlier process pathways have even less attractiveness for commercial scale production of biodiesel from algal biomass.

For the purpose of addressing the cost of extraction of lipids from algae, diesel is examined as a solvent (along with isopropanol), since its complete recovery from the lipid fraction targeted for fuel upgrading would be moot. This study performed screening tests for wet lipid extraction to find useful extraction conditions and chemistry using diesel as primary solvent with the microalgae species *Chlorella vulgaris*. This study also focused on testing the viability of algae to regrow after the extraction with regrowth tests of lipid-extracted algae.

4.1.2 Extractive processing

Depending upon particular circumstances, algae are grown in either closed system photobioreactors[11], [23], [24] or open raceway ponds[25]. After the cells have matured, algae are harvested for extraction (and other product recovery). The harvesting process can account for 20-30 % of the production cost[26]. Methods for harvesting include sedimentation, centrifugation, flotation, and filtration[27]. Once harvested, algae are often dried to reduce the water content if the extraction process requires dry biomass. Solar drying is the cheapest, but most time intensive method[28]. However, solar drying brings contaminants and degrades the lipids present in algae due to the long drying time[29]. Other drying technologies include drum drying, fluidized bed drying, freeze-drying, spray drying, and refractance window dehydration technology. While these technologies are efficient, they are also quite costly[30]. After the cells are dried, the lipids are extracted from the algae. Methods for extraction include presses, conventional solvent extraction, osmotic shock[31], microwave irradiation or ultrasonification[32], and supercritical carbon dioxide extraction[33]. It should be noted that all of the unit operations required are energy intensive and each process has to be optimized in order to make algae biofuel competitive in the market.

In the case of extraction, the method must also be acceptable in terms of toxicity, handling, safety, and cost. Many studies on viable lipid extraction technique were focused on expensive oils that can be extracted from algae, such as fish oil and oils for pharmaceutical uses[34] and, more recently, clever methods using "switchable" solvents have been presented[35]. Traditional solvent extraction is seen as the most viable option, thus far, because it uses familiar organic solvents such as hexane to capture the lipids from the algae cells in either the dry or wet phase. The solvent degrades the cell walls and dissolves the lipids into solution[8]. The extracted

oil is then separated from the solvent via distillation, and the solvent is recycled[36]. The most accepted, analytical (bench-scale) method for lipid extraction from microalgae is the Bligh and Dyer method[37]. The Bligh and Dyer method uses a mixture of chloroform and methanol for extraction. However, chloroform is a toxic and carcinogenic compound and is not a reasonable choice for a process producing a commodity product. To ameliorate this concern, Hara and Radin demonstrated a hexane-isopropyl alcohol extraction method[38]. Guckert et. al. reported that hexane-isopropyl alcohol is selective for neutral lipids but it demonstrated poorly recovered membrane lipids (glycol and polar lipids)[39, 40]. Some recent studies proposed solvent based extraction of lipids with higher yield, but they involve tedious and often expensive pretreatment from free nitrous acid (FNA)[41] and catalytic upgrading of the products after the extraction [42]. Some studied suggested to use switchable polar solvents so that the drying steps can be eliminated or reduced[43, 44], but the cost and toxicity of such solvents play an important role in the overall extraction economics[45]. All of these proposed methods are very laborious, time consuming and incur large energy cost on its own following the extraction for separation. A current study suggests to use a single step method for extraction but that neither addresses the use of toxic chemicals like chloroform nor suggests how to minimize the cost of subsequent separation[46]. There is no standard method till date for the extraction of lipids from algae[47].

As previously mentioned, dewatering has been an economic hurdle for the commercial scale production of algae based fuels[48]. An original suspension of algae, which contains less than 1 g/L of biomass solids, conventionally was felt to need dewatering to be able to extract the lipids. This increases energy consumption and process equipment requirements. Microalgal dewatering is a major challenge due to small particle size of algal cells (3-30 μm) and negligible density difference compared to water, which hinders cell aggregation and settling[49]. Processes

such as flocculation and filtration have been applied to dewater algae but these costs[39] are also impediments towards commercialization.

Underlying our wet extraction study is a mechanistic hypothesis (not investigated herein) that the extraction process with mixed solvents and water forms an emulsion, and collisions between an alga cell and an emulsion droplet(s) can lead to temporary fusion allowing extraction. However, if there is too little of the polar solvent components present, several things can happen, including insufficient number density/lifetime of emulsion droplets, and insufficient cell wall fusion. Thus, this research is simply an empirical proof-of-concept study.

Hexane is used as the baseline "good" solvent to see how much lipids can be extracted. Diesel is tested because theoretically, diesel is a good organic solvent and, since it is a fuel, it also can eliminate the necessity of solvent recovery/separation, which, in turn, further reduces the processing cost.

Additionally, we consider that if algae survive extraction and multiply, the economic and life cycle costs of biofuel production from algae would further diminish. For example, phosphorous, a rare element, is very essential for algae growth and keeping algae alive would minimize the use of phosphorous[50]. Thus, we also performed screening experiments to assess algae's regrowth viability after the extraction.

4.2 Materials and methods

A predictive modeling study of solvents was done using Hansen solubility parameter analysis. Hansen first proposed an extension of Hilderbrand solubility parameters in 1967 and since then, he has revised the parameters many times with new and more improved findings [51]. These parameters can be used to forecast the solubility of one compound/component with another compound or the combination (solution) of compounds. It has three parameters,

dispersion, hydrogen bond and polar, for each compound are valid simultaneously with those of all components having been regressed empirically from many experimental measurements[52], [53]. These solubility parameters are used to determine the solubility by forming a sphere of solubility in three-parameter space and measuring the distance of one sphere to the other. With no overlap, compounds are not considered miscible in each other.

The governing equations for the solubility tests are

$$Ra^2 = 4* (\delta_{d,i}- \delta_{d,j})^2+(\delta_{p,i}- \delta_{p,j})^2+(\delta_{h,i}- \delta_{h,j})^2$$

$$Ro^2 = 4* \delta_{d,i}^2+\delta_{p,i}^2+\delta_{h,i}^2$$

where δ_d is dispersion parameter, δ_p is polarity parameter and δ_h is hydrogen bonding parameter. *Ra* is the solubility distance between two species *i* and *j* and *Ro* is the radius of solubility sphere of species *j* centered at a point ($2\delta_{d,i}$, $\delta_{p,i}$, $\delta_{h,i}$). If Ra is less than *Ro*, the species *j* is soluble in species *i*. If *Ra* is equal to *Ro* then two species are partially soluble and if *Ra* is larger than *Ro*, the species *j* is not soluble in *i*.

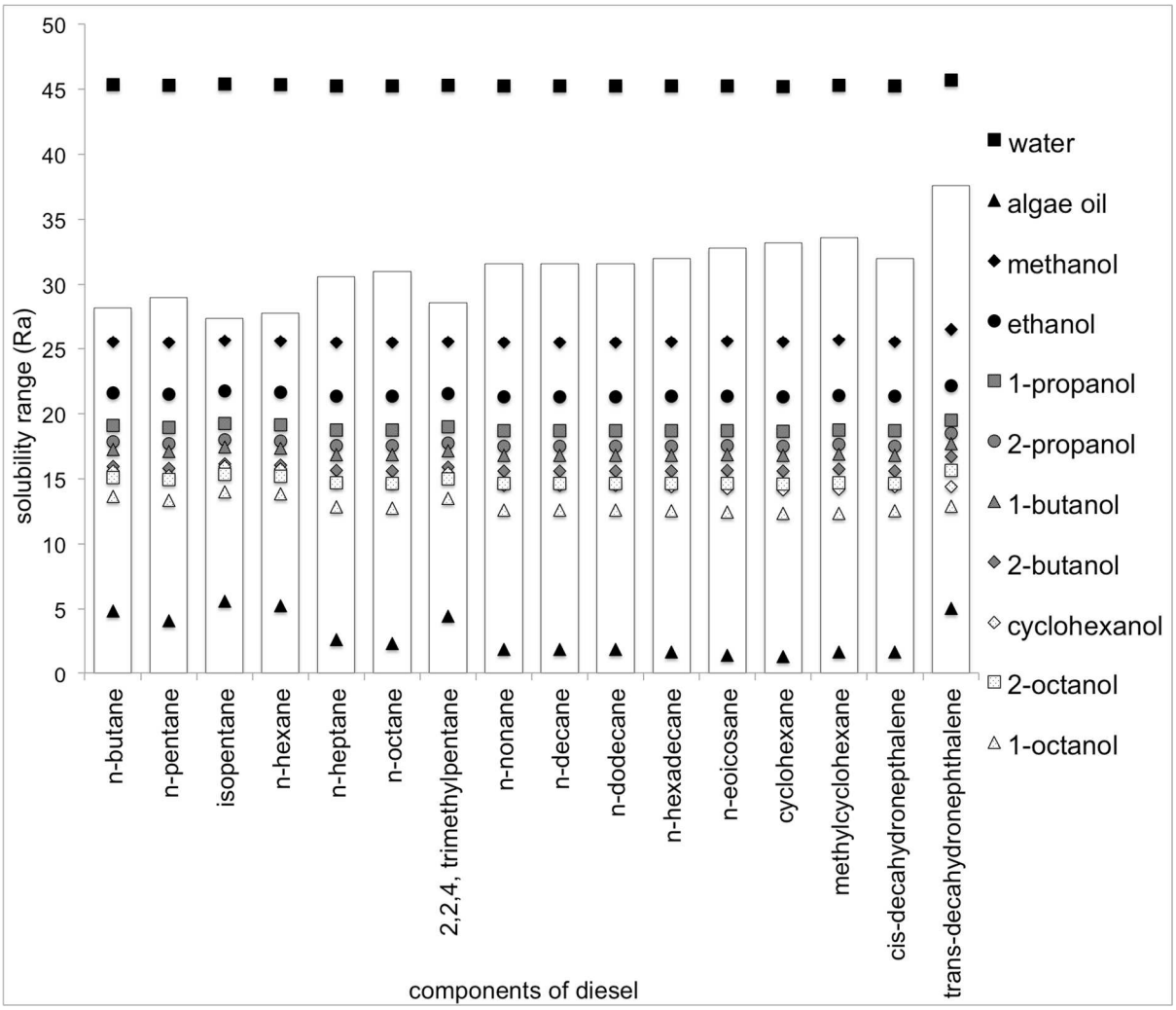

Figure 4.1 - Hansen solubility parameter plot of components of diesel, algae lipids, some lower alcohols and water.

Figure 1 illustrates the extent of solubility of majority of diesel components, few alcohols, water and algae lipids. For a particular component illustrated by the bar, if another component falls within the bar's range, those components are soluble with each other. If another component falls outside the bar, these two components are not soluble with each other. If another component is alongside the edge of the bar of one component, they are in partially solubility range. The plot illustrates that the components of diesel are capable of dissolving the algal lipids. As per the study of Guckert and White[40], an extra solvent was necessary to open up the lipid membrane of algae. In this study, a solvent that is less toxic; can dissolve both diesel and water;

and, in liquid-liquid separation process, should go to the aqueous phase, was needed. A few alcohols with lower molecular masses were chosen for initial theoretical screening for solubility of each alcohol with major diesel components and water. In addition, the toxicity of the alcohol used was also accounted for. As per the results, isopropanol seems to fulfill both criteria and is, thus, chosen for this study. For the comparison purpose, hexane and isopropanol as the base solvents were chosen, as proposed by Guckert and White[40].

Chlorella vulgaris (algae) with 0.4% dry mass, which had been settled but not dried, was used for lipid extraction. Previously, the algae were locally isolated from an agricultural washout, which contained high amounts of nitrogen and phosphorus from an incoming stream of manure. After purifying this particular microalgae, it was then scaled up to 50 gallons. The algae was then grown using MBBM (Modified Bold's Basal Medium) within an airlift photobioreactor at 23°C using 36, 5W LEDs at a pH of 7.0 with carbon dioxide as the source of carbon to stationary phase before removal. Figure 2 presents the thermogravimetric analysis of a representative wet alga aliquot. Water is the dominant mass loss until ~100°C. Afterwards, lower volatility components and some pyrolysis products are lost.

The extraction experiments used: (i) 60/40 (m/m) hexane/isopropanol, ii) 60/40 (m/m) diesel/isopropanol, iii) 80/20 (m/m) diesel/isopropanol), iv) 90/10 (m/m) diesel/isopropanol and v) diesel only. The solvent was mixed with the algae suspension at different mass ratios. The solvent mixture to algae mass ratios were 1:2, 1:1, and 2:1, each combined to a total volume of ~30 mL in a 125 mL Erlenmeyer flask. A magnetic stir bar (pill-shaped, 2.54 cm length, ~0.6 cm diameter) was placed in the flask, and the mixtures were covered to eliminate vapor loses and placed on magnetic stirrer plates at a constant shear rate of 10 rpm for either 30 min or 2 h. Afterwards, the mixture was placed in a 50 mL centrifuge tube. The samples were centrifuged at

45 N g-force for 10-15 min to create three phases: 1) organic-rich phase with lipids and 2) aqueous phase with isopropanol, and 3) aqueous phase with algae. The three layers were separated and the organic layer was derivitized to fatty acid methyl ester (FAME) for fatty acid analysis using 4% sulfuric acid by mass and methanol. FAME components were later analyzed using GC-FID in a capillary column of fused silica with a flame-ionization detector. This method was first proposed by Gardner et. al., and has since been modified by many researchers[54, 55].

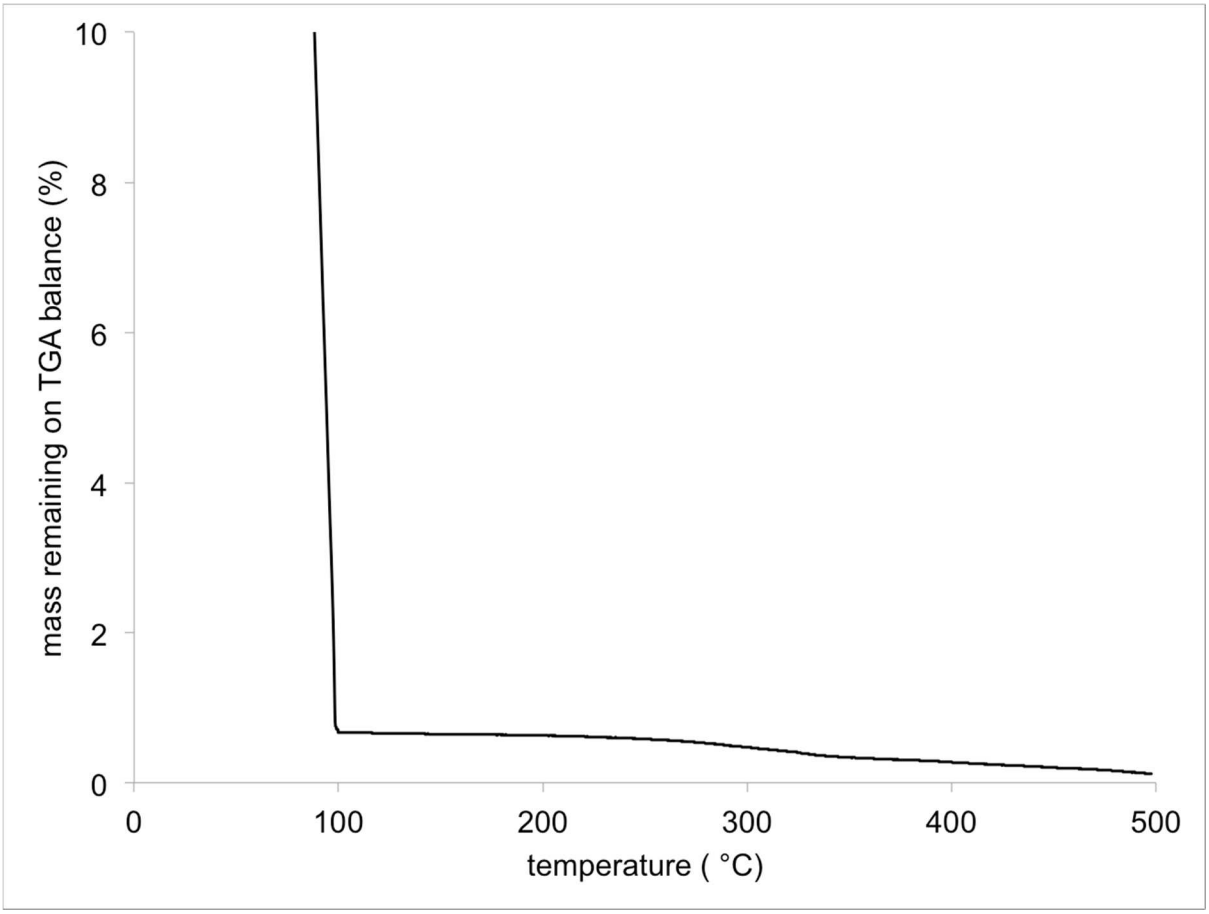

Figure 4.2 - TGA of mass change versus temperature in inert N_2 flow of the wet algae suspension used for extraction studies.

After the extraction, the recovered algae were taken to a simpler growth system to regrow. Only the samples extracted with 1:1 solvent to algae ratio were used in this regrowth study. The source of nitrogen was the algae media (Table 1) and the source of CO_2 was the

pressurized CO_2 tank. Small 50 mL test tubes were used. Four 13W fluorescent light bulbs were located at an equal distance and the algae suspension was constantly shaken with a shaker base. A temperature of 25°C was maintained and the algae was left to grow for 5 d. The optical density of algae before and after the regrowth tests was measured by the light attenuation of an aliquot sample from the algae suspension. Light attenuation was measured using a Turbiscan Classic spectrometer (Formulaction SA, L'Union, France). The idea is such that the portion of light of blocked or absorbed by a solution represents the algae cells (in our context) present in solution and that ultimately gives the cell density of algae per unit volume.

Table 4-1 - Algae media composition for the regrowth.

components	mM/L
NaCl	120.000
NH_4Cl	7.478
$CaCl_2.2H_2O$	0.340
$MgSO_4.7H_2O$	0.406
$K_2HPO_4.3H_2O$	0.609
KH_2PO_4	0.389
$Na_2EDTA.2H_2O$	0.134
$ZnSO_4.7H_2O$	0.077
H_3BO_3	0.184
$MnCl_2.4H_2O$	0.026
$FeSO_4.7H_2O$	0.018
$CoCl_2.6H_2O$	0.007
$CuSO_4.5H_2O$	0.005
$(NH_4)_6Mo_7O_{24}.H_2O$	0.008
Vitamin B1 (thiamine)	0.000
Vitamin B12 (cobalamin)	0.000
$NaHCO_3$	0.060

4.3 Results

4.3.1 Extraction of lipids

Several replicates of wet extractions were performed for each solvent "set" over separate days to randomize unmanaged, extraneous variables. Extraction results are reported as the lipids (g) with respect to the total dry biomass present in the wet suspension (100 g). Hexane/isopropanol (60/40 m/m) extracted the highest amount of lipids, 26.5 g lipids per 100 g of biomass in 2 h with 2:1 solvent to algae ratio (twice as much mixed solvent volume as algae volume). Not surprisingly, the higher solvent to algae ratio increases the nominal lipid extraction efficiency. Increases in extraction time also increased the amount of lipids extracted. Figure 3 summarizes the results of extraction using the hexane/isopropanol (60/40 m/m) mixed solvent and Table 2 is the analysis of the major lipids extracted.

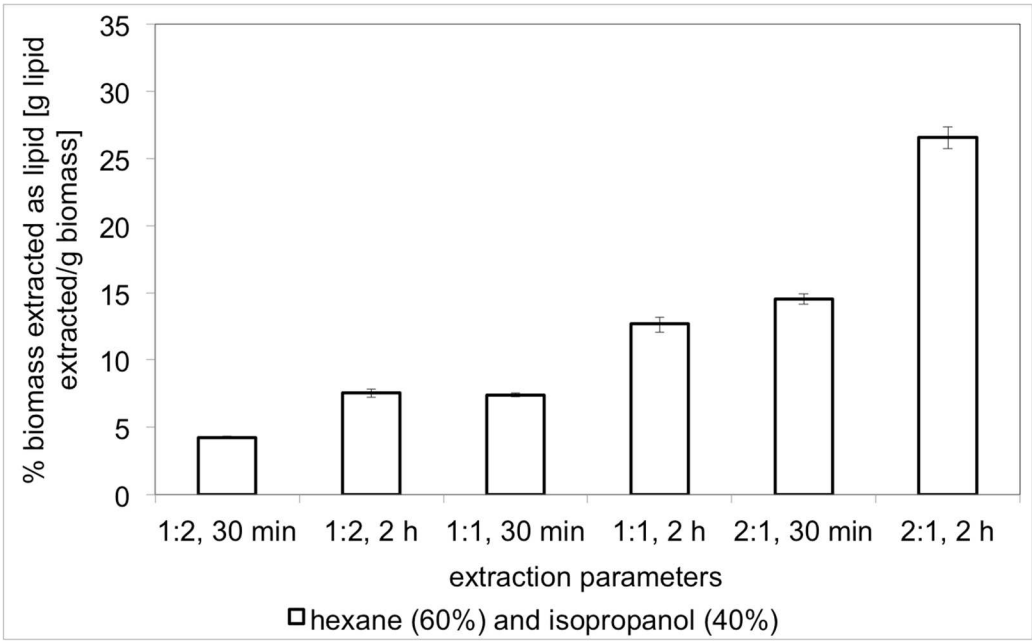

Figure 4.3 - Extraction results using hexane and isopropanol (60/40 m/m). The horizontal axis presents the nominal extraction conditions (at constant temperature and shear rate) as mass solvent: mass wet algae, contact time for extraction.

Table 4-2 - The compositional analysis of derivatized algae lipids as methyl ester components extracted with solvent hexane/isopropanol (60/40 m/m) for 2 h.

components	mass percentage
tetradecanoic acid, methyl ester	0.87
hexadecanoic acid, methyl ester	23.3
octadeconic acid, methyl ester	69.7
eicosanoic acid, methyl ester	3.14
docosanoic acid, methyl ester	1.75
tetracosanoic acid, methyl ester	0.62
others + impurities	0.59

When hexane was replaced by diesel, the highest extraction was seen when diesel/isopropanol (60/40 w/w) was used. With all the solvents, the lipid extraction increased with the increment of solvent to algae ratio, but not necessarily the time. There was also a great deal more variance among replicates. The average maximum of 20.2 to 11.5 g lipids per 100 g of biomass was extracted with the various mixtures at 2:1 solvent to algae ratio over 2 h. However,

when diesel was used without isopropanol, it could not extract very much lipid at all. An average maximum of 3 g lipids per 100 g of biomass was extracted in 2 h. Figure 4 summarizes the extraction results using all the diesel-based solvent sets.

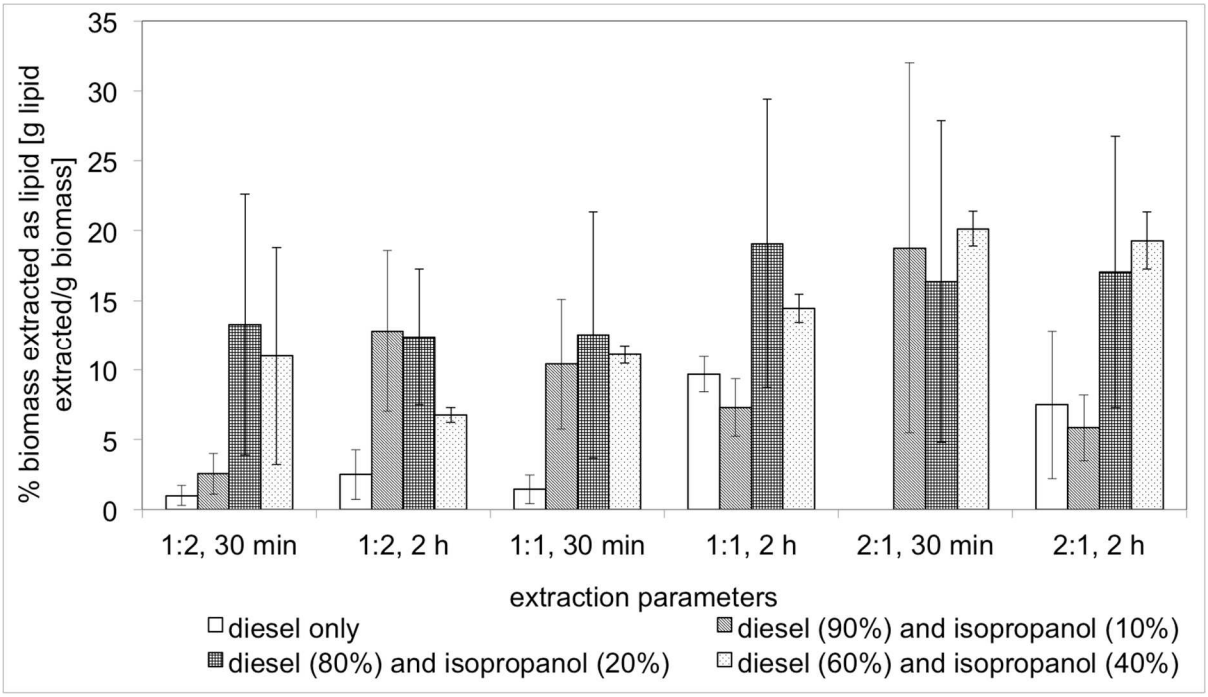

Figure 4.4 - Extraction results using solvents containing i) diesel only, ii) 90/10 (m/m) diesel/isopropanol and iii) 60/10 (m/m) diesel/isopropanol. The horizontal axis presents the nominal extraction conditions (at constant temperature and shear rate) as mass solvent mix: mass wet algae, and contact time for extraction.

4.3.2 Regrowth of algae after extraction

Chlorella vulgaris after the wet extraction could still regrow. Algae, whose lipids were extracted with 90-80% diesel and 10-20% isopropanol, were able to add 10 to 400% of their original amount in 5 d. whereas, both the control algae and wet extract which was only exposed to diesel in the extraction process, and whose lipids were therefore not extracted, added ~500% mass in 5d. Algae whose lipids were extracted with 60-100% isopropanol were able to add about 10-25% additional mass in 5 d. Illustrative growth results are shown in Figure 5.

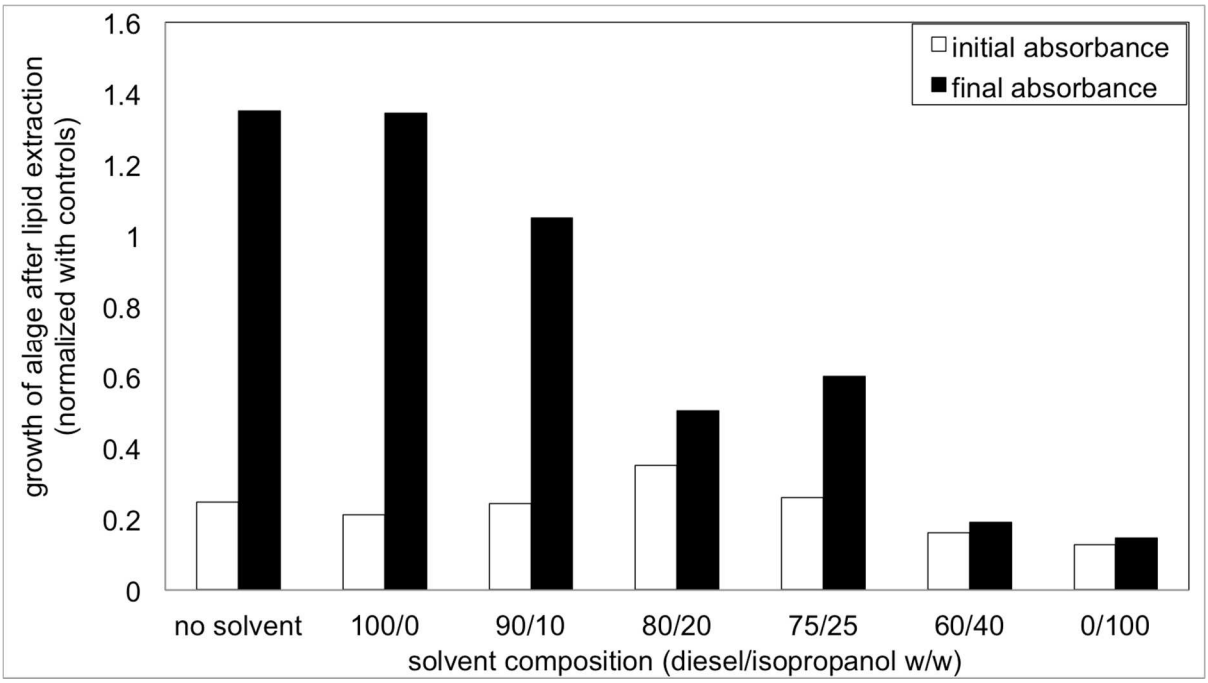

Figure 4.5 - The initial and final absorbance of algae grown after solvent extraction. The control is algae before the growth and before the addition of growth media.

4.4 Discussion/Perspective

Hansen solubility parameter analysis suggests that diesel components can solubilize algal lipids. Diesel cannot (by itself) create any favorable conditions to exude lipids from algae. An extra solvent is necessary with polar properties, which can open up the cell membrane of algae. Addition of isopropanol in diesel helps open membrane pores and sometimes, ruptures the cell membrane of algae[40].. The emulsions formed by isopropanol and diesel appears to disrupt our algae's cell membrane and dissolves the lipids. When phase separation takes places isopropanol separates with water and lipids separate with diesel.

The prospect of using diesel as a solvent for lipid extraction is attractive because diesel is easily accessible and relatively cheaper than hexane while being almost as effective. Hexane is very volatile (BP: ~80 °C) and larger amounts can be lost during the extraction. However, diesel is not as volatile (BP: ~310 °C) and has may experience less losses. Also, lipids extracted with

diesel can remain in diesel and can be either directly transesterified to FAME or upgraded via other routes to a viable fuel.

Within our experimental context, the extraction of lipids from live microalgae is a combination of chemical and biological processes. Many parameters, such as growth condition, temperature, algae dilution, and external environment at the time of extraction can affect the amount of lipids extracted. Hence, the difficulty to control all these variables is high and the extraction results are difficult to replicate. Nonetheless, the variability of the extraction yields with the diesel sets appear much more variable than what was obtained with the hexane/isopropanol system. This is illustrated by a 3-factor analysis of variance (ANOVA) (with interactions) to determine if some of the extraction conditions were significantly different from the others. Only the diesel (or isopropanol) content was somewhat significant at the 92% confidence level. Further two and three factor interaction analysis suggests that the extraction data shows no statistically significant trends. This variability in the extraction efficiency with diesel is possibly due to its chemically heterogeneous composition and further microscopic level scrutiny of this wet extraction is necessary to better understand the parametric sensitivity.

Chlorella vulgaris showed potential to regrow after the extraction as well. Diesel is found to not be harmful to algae regrowth. When isopropanol is not used, algae can regrow as if it interacted with no solvent. Similarly, the more the isopropanol, the lower would be the probability of regrowth. The regrowth we observed was possibly due to algae cells which had not experienced much, if any, extraction. The notable result is that the wet biomass, containing residual solvents, could seed further growth when put into an appropriate environment (medium, CO_2, and photons). Thus, this suggests the possibility of recycling extracted algae with new seed culture is a viable means of improving both the economic and life cycle costs.

4.5 Conclusions

A Hansen solubility parameter analysis suggests that the components of diesel are miscible with the neutral lipids from microalgae. Isopropanol, a relatively less toxic solvent and a compound with smaller molecular size, can be used as the alcohol to open up the pores to get algal lipids out of the algae. Thus, diesel/isopropanol mixtures can be used as a low cost solvent system in wet lipid extraction process. It can eliminate the need of a high level of dewatering; simplify (or eliminate) the solvent recovery step, since it can pass through into further fuel processing and distribution, and thus, it can reduce the cost of production of biofuels from algae. Algae can still regrow after the lipid extraction using diesel.

4.6 Acknowledgements

The authors gratefully acknowledge the seed grant provided by Colorado Center for Biofuels and Biorefining (C2B2), and Matthew Posewitz (Colorado School of Mines) and Nick Rancis (BioVantage) for providing algae and insights.

4.7 References

[1] B.J. Gallagher, The economics of producing biodiesel from algae, Renew Energ, 36 (2011) 158-162.

[2] E. Iakovou, A. Karagiannidis, D. Vlachos, A. Toka, A. Malamakis, Waste biomass-to-energy supply chain management: A critical synthesis, Waste Manage, 30 (2010) 1860-1870.

[3] Y.C. Shen, G.T.R. Lin, K.P. Li, B.J.C. Yuan, An assessment of exploiting renewable energy sources with concerns of policy and technology, Energ Policy, 38 (2010) 4604-4616.

[4] Y. Chisti, Biodiesel from microalgae beats bioethanol, Trends in Biotechnology, 26 (2008) 126-131.

[5] L.M.L. Laurens, N. Nagle, R. Davis, N. Sweeney, S. Van Wychen, A. Lowell, P.T. Pienkos, Acid-catalyzed algal biomass pretreatment for integrated lipid and carbohydrate-based biofuels production, Green Chemistry, 17 (2015) 1145-1158.

[6] V. Mimouni, L. Ulmann, V. Pasquet, M. Mathieu, L. Picot, G. Bougaran, J.P. Cadoret, A. Morant-Manceau, B. Schoefs, The Potential of Microalgae for the Production of Bioactive Molecules of Pharmaceutical Interest, Curr Pharm Biotechno, 13 (2012) 2733-2750.

[7] M. Olaizola, Commercial development of microalgal biotechnology: from the test tube to the marketplace, Biomol. Eng., 20 (2003) 459-466.

[8] R.E. Armenta, P. Mercer, Developments in oil extraction from microalgae, European Journal of Lipid Science and Technology, 113 (2011) 539-547.

[9] S. Gupta, S.C. Agrawal, Vegetative survival of some wall and soil blue-green algae under stress conditions, Folia Microbiol, 53 (2008) 343-350.

[10] S. Gupta, S.C. Agrawal, Survival of blue-green and green algae under stress conditions, Folia Microbiol, 51 (2006) 121-128.

[11] A. Demirbas, M.F. Demirbas, Importance of algae oil as a source of biodiesel, Energy Conversion and Management, 52 (2011) 163-170.

[12] N. Mallick, S. Mandal, A.K. Singh, M. Bishai, A. Dash, Green microalga Chlorella vulgaris as a potential feedstock for biodiesel, J. Chem. Technol. Biotechnol., 87 (2012) 137-145.

[13] B.N. Pietrowski, R. Tahergorabi, K.E. Matak, J.C. Tou, J. Jaczynski, Chemical properties of surimi seafood nutrified with omega-3 rich oils, Food Chem, 129 (2011) 912-919.

[14] G. Impellizzeri, S. Mangiafico, G. Oriente, M. Piattelli, S. Sciuto, E. Fattorusso, S. Magno, C. Santacroce, D. Sica, Constituents of Red Algae .1. Amino-Acids and Low-Molecular-Weight Carbohydrates of Some Marine Red Algae, Phytochemistry, 14 (1975) 1549-1557.

[15] Y. Chisti, Biodiesel from microalgae, Biotechnology Advances, 25 (2007) 294-306.

[16] M.H. Yanqun Li, Nan Wu, Christopher Q. Lan, Nathalie Dubois-Calero,, Biofuels from Microalgae, Biotechnology Progress, 24 (2008) 815-820.

[17] L.G. Speranza, A. Ingram, G.A. Leeke, Assessment of algae biodiesel viability based on the area requirement in the European Union, United States and Brazil, Renew Energ, 78 (2015) 406-417.

[18] R. Davis, C. Kinchi, J. Markham, E.C.D. Tan, L.M.L. Laurens, D. Sexton, D. Knorr, P. Schoen, J. Lukas, Process Design and Economics for the Conversion of Algal Biomass to Biofuels: Algal Biomass Fractionation to Lipid and Carbohydrate-Derived Fuel Products, NREL, Golden, CO, 2014.

[19] A. Sathish, R.C. Sims, Biodiesel from mixed culture algae via a wet lipid extraction procedure, Bioresource Technology, 118 (2012) 643-647.

[20] L. Amer, B. Adhikari, J. Pellegrino, Technoeconomic analysis of five microalgae-to-biofuels processes of varying complexity, Bioresour. Technol., 102 (2011) 9350-9359.

[21] R. Davis, M. Biddy, S. Jones, Algal Lipid Extraction and Upgrading to Hydrocarbons Technology Pathway National Renewable Energy Laboratory, Golden, CO, 2013.

[22] A. Sun, R. Davis, M. Starbuck, A. Ben-Amotz, R. Pate, P.T. Pienkos, Comparative cost analysis of algal oil production for biofuels, Energy, 36 (2011) 5169-5179.

[23] T. Holtermann, R. Madlener, Assessment of the technological development and economic potential of photobioreactors, Applied Energy, 88 (2011) 1906-1919.

[24] L. Xu, P.J. Weathers, X.R. Xiong, C.Z. Liu, Microalgal bioreactors: Challenges and opportunities, Eng Life Sci, 9 (2009) 178-189.

[25] J.S. Chang, C.Y. Chen, K.L. Yeh, R. Aisyah, D.J. Lee, Cultivation, photobioreactor design and harvesting of microalgae for biodiesel production: A critical review, Bioresource Technology, 102 (2011) 71-81.

[26] Y. Chisti, E.M. Grima, E.H. Belarbi, F.G.A. Fernandez, A.R. Medina, Recovery of microalgal biomass and metabolites: process options and economics, Biotechnology Advances, 20 (2003) 491-515.

[27] M.L. Jiang, Y.M. Gong, Biodiesel production with microalgae as feedstock: from strains to biodiesel, Biotechnol Lett, 33 (2011) 1269-1284.

[28] J. Prakash, B. Pushparaj, P. Carlozzi, G. Torzillo, E. Montaini, R. Materassi, Microalgal Biomass Drying by a Simple Solar Device, International Journal of Solar Energy, 18 (1996) 303-311.

[29] L. Lardon, A. Helias, B. Sialve, J.P. Stayer, O. Bernard, Life-Cycle Assessment of Biodiesel Production from Microalgae, Environmental Science & Technology, 43 (2009) 6475-6481.

[30] D.F. Ihrig, H.M. Heise, U. Brunert, M. Poschmann, R. Kuckuk, K. Stadtlander, Combination of biological processes and fuel cells to harvest solar energy, J. Fuel Cell Sci. Technol., 5 (2008) 5.

[31] G. Yoo, W.K. Park, C.W. Kim, Y.E. Choi, J.W. Yang, Direct lipid extraction from wet Chlamydomonas reinhardtii biomass using osmotic shock, Bioresource Technology, 123 (2012) 717-722.

[32] S. Balasubramanian, J.D. Allen, A. Kanitkar, D. Boldor, Oil extraction from Scenedesmus obliquus using a continuous microwave system - design, optimization, and quality characterization, Bioresource Technology, 102 (2011) 3396-3403.

[33] F. Sahena, I.S.M. Zaidul, S. Jinap, A.A. Karim, K.A. Abbas, N.A.N. Norulaini, A.K.M. Omar, Application of supercritical CO2 in lipid extraction - A review, J Food Eng, 95 (2009) 240-253.

[34] E.M. Grima, A.R. Medina, A.G. Gimenez, J.A.S. Perez, F.G. Camacho, J.L.G. Sanchez, Comparison between Extraction of Lipids and Fatty-Acids from Microalgal Biomass, Journal of the American Oil Chemists Society, 71 (1994) 955-959.

[35] C. Samori, D. Lopez Barreiro, R. Vet, L. Pezzolesi, D.W.F. Brilman, P. Galletti, E. Tagliavini, Effective lipid extraction from algae cultures using switchable solvents, Green Chemistry, 15 (2013) 353-356.

[36] J. Singh, S. Cu, Commercialization potential of microalgae for biofuels production, Renewable & Sustainable Energy Reviews, 14 (2010) 2596-2610.

[37] E.G. Bligh, W.J. Dyer, A Rapid Method of Total Lipid Extraction and Purification, Can J Biochem Phys, 37 (1959) 911-917.

[38] A. Hara, N.S. Radin, Lipid Extraction of Tissues with a Low-Toxicity Solvent, Anal Biochem, 90 (1978) 420-426.

[39] S. Salim, R. Bosma, M.H. Vermue, R.H. Wijffels, Harvesting of microalgae by bio-flocculation, Journal of Applied Phycology, 23 (2011) 849-855.

[40] J.B. Guckert, D.C. White, Evaluation of a Hexane Isopropanol Lipid Solvent System for Analysis of Bacterial Phospholipids and Application to Chloroform-Soluble Nuclepore (Polycarbonate) Membranes with Retained Bacteria, J Microbiol Meth, 8 (1988) 131-137.

[41] X. Bai, F.G. Naghdi, L. Ye, P. Lant, S. Pratt, Enhanced lipid extraction from algae using free nitrous acid pretreatment, Bioresource Technology, 159 (2014) 36-40.

[42] J.S. Kruger, E. Christensen, R.L. McCormick, P.T. Pienkos, Implications of pretreatment and lipid extraction conditions on catalytic upgrading of algae oils to hydrocarbon fuels, Abstr Pap Am Chem S, 248 (2014).

[43] C. Samori, D.L. Barreiro, R. Vet, L. Pezzolesi, D.W.F. Brilman, P. Galletti, E. Tagliavini, Effective lipid extraction from algae cultures using switchable solvents, Green Chem, 15 (2013) 353-356.

[44] C. Samori, C. Torri, G. Samori, D. Fabbri, P. Galletti, F. Guerrini, R. Pistocchi, E. Tagliavini, Extraction of hydrocarbons from microalga Botryococcus braunii with switchable solvents, Bioresource Technology, 101 (2010) 3274-3279.

[45] E.D. Frank, A. Elgowainy, J. Han, Z.C. Wang, Life cycle comparison of hydrothermal liquefaction and lipid extraction pathways to renewable diesel from algae, Mitig Adapt Strat Gl, 18 (2013) 137-158.

[46] M. Axelsson, F. Gentili, A Single-Step Method for Rapid Extraction of Total Lipids from Green Microalgae, Plos One, 9 (2014).

[47] Y. Li, F.G. Naghdi, S. Garg, T.C. Adarme-Vega, K.J. Thurecht, W.A. Ghafor, S. Tannock, P.M. Schenk, A comparative study: the impact of different lipid extraction methods on current microalgal lipid research, Microb Cell Fact, 13 (2014).

[48] N. Uduman, Y. Qi, M.K. danquah, G.M. Forde, A. Hoadley, Dewatering of microalgal cultures: A major bottleneck to algae-based fuels, Journal of Renewable and Sustainable Energy, 2 (2010) 15.

[49] R. Bhave, T. Kuritz, L. Powell, D. Adcock, Membrane-Based Energy Efficient Dewatering of Microalgae in Biofuels Production and Recovery of Value Added Co-Products, Environmental Science & Technology, 46 (2012) 5599-5606.

[50] V.H. Smith, The Nitrogen and Phosphorus Dependence of Algal Biomass in Lakes - an Empirical and Theoretical-Analysis, Limnol Oceanogr, 27 (1982) 1101-1112.

[51] C.M. Hansen, The three dimensional solubility parameter and solvent diffusion coefficient. Their importance in surface coating formalation, Danish Technical Press, Polyteknisk læreanstalt, Copenhagen, 1967, pp. 106 p.

[52] C.M. Hansen, Hansen solubility parameters : a user's handbook, 2nd ed., CRC Press, Boca Raton, 2007.

[53] Handbook of Solubility Parameters and Other Cohesion Parameters - Barton,Afm, Text Res J, 54 (1984) 138-138.

[54] G. Ahlgren, L. Merino, Lipid Analysis of Fresh-Water Microalgae - a Method Study, Arch. Hydrobiol., 121 (1991) 295-306.

[55] B.L. Brian, E.W. Gardner, Preparation of Bacterial Fatty Acid Methyl Esters for Rapid Characterization by Gas-Liquid Chromatography, Appl Microbiol, 15 (1967) 1499-&.

Chapter 5 Membrane-enabled continuous enzymatic saccharification

(Submitted, Bioresource Technology Journal)

Abstract

The current state-of-art for converting lignocellulosic biomass to fungible sugar is batch enzymatic hydrolysis of acid-pretreated biomass followed by other separation steps. Enzymatic hydrolysis is a significant cost for the process. We hypothesized that a continuous enzymatic hydrolysis (CEH) can be done using a membrane-based system to remove hydrolyzed sugars and minimize the feedback inhibition. This concept has been demonstrated using an un-optimized, commercial ultrafiltration membrane, in-line with a feed-and-bleed continuous-stirred-tank-reactor utilizing acid-pretreated corn stover with ~2.0 % insoluble solids. The conversion during an integrated, continuous run was ~96.3% of its theoretical maximum, and the glucose specific productivity increased by ~150%. We also studied membrane filtration resistance of hydrolysate using a combination of bench-scale characterization with microfiltration membranes and analysis of the membrane permeance during the integrated experiment. This study confirmed the small colloidal species should be excluded from entering the depth of the membrane to ensure efficacious cleaning. A simple techno-economic analysis identified operating targets needed to substantially reduce the cost of sugar production. It suggests that CEH with 5% total solids, and a more optimal membrane, which retains 99% of the enzymes, can potentially decrease the cost of sugar production by ~13%.

5.1 Introduction

Biofuels, such as those derived from lignocellulosic biomass, are possible renewable alternatives to fossil fuels [1]. Lignocellulose is the most abundant organic polymer in the world and it is present in the form of plant cell wall [2]. Large quantities of lignocellulosic biomass is locally available in many parts of the world in the form of annual and perennial dry energy grasses, forest woody feedstock, municipal solid waste and agricultural residues [3]. Lignocellulosic biomass is significantly cheaper than other biomass sources such as algae and sugarcane and is historically unused other than for soil enrichment. Thus, its potential as a relatively inexpensive feedstock for conversion to fuel sources of interest, such as, ethanol, butanol, or diesel, is significant [4].

The conversion of lignocellulosic biomass to fuels and chemicals is an area of active research in the last two decades. The conversion process has grown more efficient due to the availability of improved enzymes and more effective pretreatment and separation processes [5, 6]. However, lignocellulosic fuels and chemicals are not yet competitive with their fossil fuel counterparts —the benchmark of comparison for any alternative sources [7]. Several studies have pointed out that the processing costs, including that of the enzymatic hydrolysis, is still a major bottleneck to broad commercialization.

For the conversion of lignocellulosic biomass to the derivative sugars, cellulose and hemicellulose must be hydrolyzed. One hydrolysis process utilizes a high-temperature, dilute sulfuric acid pretreatment of biomass *followed by enzymatic hydrolysis at ~50 °C* [2, 8]. The sugars formed as the product during the hydrolysis inhibits the reaction and reduces efficiency, especially when a high concentration of sugars is achieved [9, 10]. To minimize this product inhibition, a continuous removal of sugars is necessary. However, because of the complex

rheology of lignocellulosic slurry [11], there are several technical difficulties to overcome to design and implement a continuous enzymatic hydrolysis (CEH) approach.

Solids/liquid separations appear integral to the path towards CEH. Along these lines, the National Renewable Energy Laboratory (NREL) previously evaluated [12-14] a pressure filter, vacuum belt filter, and a basket centrifuge at various conditions for performing batch-wise solids-liquid separations. This approach included a batch washing to recover/remove liquids and soluble species from the starting suspension, either post-enzymatic hydrolysis or as part of a "conditioning" step to remove inhibitory compounds prior to further reactions. This evaluation found that pressure filtration had potential advantages by removing the greatest amount of leachable species and providing a final cake with high solids content. They subsequently had tests performed with another vacuum filter design, and with a gravity settling system. Neither of these produced satisfactory results based on the criteria of high recovery of soluble sugars, and producing insoluble solids content $\geq$ 20%. Each of these earlier assessments (except the gravity settler) still seemed predicated on the notion of post-reaction, batch processing.

Additionally, in the last few years, researchers have broached the idea of incorporating a variety of membrane processes into the enzymatic hydrolysis in order to reduce possible product inhibition and provide greater utilization (including recovery/reuse) of the enzymes. Knutsen and Davis [15] showed that cellulase retention and sugar removal using an ultrafiltration (UF) membrane can increase the total conversion and efficiency of enzymatic hydrolysis. Not only that, the activity of enzyme can also be retained by recycling the slurry [16]. A seminal prior study by Andric et al. pointed out the conceptual hurdles for a membrane reactor to function in this processing milieu, not the least of which is that the system must operate at a significantly lower total insoluble solids content than economically reasonable [17]. For example, Ishola et al.

[18] reported pumping the slurry to a membrane module to remove hydrolyzed sugar, but they indicated that a system with 8% or more total solids is simply un-pumpable. Also, this study did not report how the membrane's permeance (pressure-normalized flux) changed with the volume filtered due to solids deposition on (or in) the membrane.

Other efforts to hydrolyze cellulose in a continuous manner have been documented but their total conversion was found to be lower than benchmark targets (~ 50 %), and they used cellulose instead of lignocellulosic biomass [19, 20]. In addition, a sequential batch and multiple-CSTR approaches have been proposed and tested on pilot scales [17]. Fed-batch and continuous modes for enzymatic hydrolysis in one reaction vessel, with retention of the undigested solid biomass, have been proposed in the literature [21]. A study with a fed-batch reactor was done by Zhang et. al. [22] in a stirred cell reactor but the volume was very small and the change in membrane permeance during the experiment was not mentioned, as is necessary to assess whether the system is a good proposition in the future. One earlier study [23] using a membrane process did not show how much difference a continuous system can make on the overall cost of production.

Additionally, the choice of a membrane is not completely obvious for this separation application. For example, highly porous membranes (with higher intrinsic productivity) are prone to greater internal fouling and pore blockage, whereas other nanoporous membranes can experience surface adsorptive fouling and osmotic pressure increases, all of which can correspond to an observed flux reduction [24]. Thus, the choice of a membrane must weight multiple objectives before identifying the best compromise.

Herein, we are considering a membrane-enabled CEH that may be both technically viable and economically feasible to lower the cost of fungible sugars' production. In this report, we

have characterized biomass; performed several preliminary membrane studies (to provide guidance for mass transfer expectations), which were followed by three CEH experiments using a membrane system in a lab-scale setting; and performed techno-economic calculations to concisely predict the cost of production of sugars using membrane-enabled CEH versus that from batch hydrolysis.

5.2 Methods

5.2.1 Theory

Since the enzymatic hydrolysis is a product-inhibited process[10, 25], the reaction rate and the conversion is going to be reduced when the product concentration in the reactor is high. The widely accepted empirical reaction-rate model for this is Michaelis-Menten product-competitive-inhibition model:

$$r = \frac{K_{cat} S E_0}{S + K_m (1 + \frac{P}{K_i})} \quad [1]$$

where r is the reaction rate at the certain time ($g \cdot L^{-1} \cdot s^{-1}$), K_{cat} is enzyme disassociation constant (s^{-1}), S is the substrate concentration (g/L) at that time, E_0 is the initial enzyme concentration (g/L), K_m is Michelis-Menten constant (g/L), P is product concentration at that time and K_i is product inhibition constant at that time (g/L). After obtaining best-fit parameters from a batch hydrolysis experiment, we used this kinetics expression to predict our CEH process outcomes and for techno-economic modeling.

5.2.2 Characterization of biomass

For this study, 1 L sample of acid-pretreated hydrolysate from corn-stover feedstock was provided by NREL. Total solids were determined by thermo-gravimetric analysis (TGA) using

an infrared drying balance. The fraction of insoluble solids (FIS) was determined by further measuring the soluble solids in the separated liquor and a mass-balance calculation. [26]. HPLC analysis provided structural and soluble carbohydrate analysis. [12, 13] In addition, to further elucidate the nature of possible "cake deposition" on membrane surfaces, centrifugation tests of this biomass were carried out with slurries of four different FIS loading using two centrifuges: EC CL30R (centrifuge 1) and Eppendorf 5810R (centrifuge 2). This data was reported as the acceleration applied.

5.2.3 Membrane filtration studies

A "screening" study of membrane filtration of the slurry was carried out to guide our choice of membranes for CEH studies. We started with bench scale testing of three commercially available, monolithic, microfiltration (MF) membranes. They were made of mixed cellulose esters (MCE), and were membranes for which we have significant physicochemical characterization data.[27] These membranes may not specifically be used in an industrial system since they are made primarily for small-scale bioseparation applications. But using them allows us to better understand what, if any, role the membrane's internal structure plays in the hydrolysate solid/liquid separation process. These membranes have high porosity and filter with both surface and depth sieving mechanisms. Their nominal rated pore sizes were 0.22, 0.65, and 1.2 μm—note, these are actually different than the measured smallest throat diameters. The following Table 5-1 below lists the measured properties of these membranes.

Table 5-1 – MF membrane properties used in initial studies.

membrane rating, µm	mean pore "throat" diameter, µm	thickness, µm	porosity (fractional)	pure water permeance ($x10^2$), $kg/s/m^2/kPa$	clean membrane resistance ($x\ 10^{-9}$) 1/m
1.2	2.31 (±0.068)	132	0.821	25.5	4.36
0.65	1.45 (±0.046)	124	0.790	20.7	5.37
0.22	0.28 (±0.002)	148	0.748	3.2	34.7

5.2.4 Continuous enzymatic hydrolysis (CEH)

The schematic of the experimental fixture for the CEH is shown in Figure 5.1 Based on the reasoning from our aforementioned screening studies, a commercially available membrane module, Koch M180, ultrafiltration (UF) retention was purchased from Koch Membrane Systems (Wilmington, MA, USA). The membrane module contains a 1 ft long membrane tube housed in a transparent polysulfone housing. The membrane module contained a single membrane tube with 13 mm inside diameter. The membrane material is polyvinylidene difluoride (PVDF) and the rated separation cutoff was 100 kg/mol (~10-14 nm Stokes diameter). The vendor-specified operating ranges are pH 2-12, temperatures up to 343 K and pressures up to 1 MPa.

A Seepex BCSB-05-12 (Bottrop, Germany) progressive cavity pump was used to recirculate the slurry from the reactor through the membrane module and back to the reactor. A Rosemount 8732 (Shakopee, MN, USA) magnetic flow meter measured recirculation loop flow rate. An automated Fisher V150 (Shakopee, MN, USA) backpressure control valve was used to automatically regulate the transmembrane pressure (TMP) to maintain a constant permeate mass flow rate out of the membrane module. Two separate Omega Engineering PX309 (Stamford, CT, USA) pressure transducers were used to measure the fluid pressure at the inlet and outlet of the module. Permeate, purge, and feed rates were calculated from container weights measured using

Ohaus Adventurer-Pro (Parsippany, NJ, USA) scales with RS-232 interfaces. The whole system was controlled using an Opto22 (Temecula, CA, USA) process automation controller and user interface.

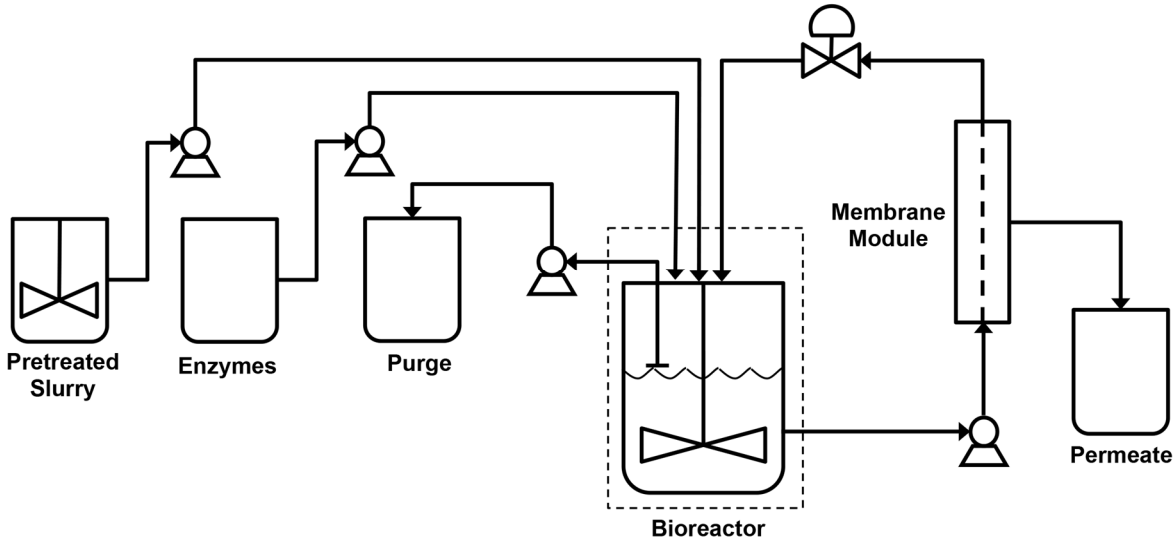

Figure 5.1. Schematic of membrane-enabled CEH system.

The hydrolysis reaction vessel was a New Brunswick Scientific (Edison, NJ, USA) BioFlo 3000 bioreactor that has controls for maintaining constant temperature and inlet feed rates of biomass, buffered water and enzymes. We maintained pH externally by providing feed and water with known buffered pH to the bioreactor. Feed slurry for the hydrolysis was prepared using pretreated corn-stover feedstock [28] and buffered water of pH 5 made up of citric acid and sodium citrate mixture. The feed slurry was fed to the bioreactor continuously using a peristaltic pump attached to the bioreactor. An impeller inside the feed vessel continuously mixed the feed slurry. A second metering peristaltic pump was used to continuously feed the buffered water and enzymes to the bioreactor from a separate vessel. A third peristaltic pump was used to take a purge stream out of the bioreactor to maintain a constant volume and prevent build-up of lignin. This pump was operated at full duty cycle and maintained the level in the bioreactor by placing

the suction tube at the desired level. Enzymes for this experiment were a proprietary mixture targeted for cellulosic materials (Cellic CTec2®, Novozymes).

The experimental methodology was such that the targets for total volume of the slurry in the bioreactor was set at either 3 or 4 L, the total solids from the pretreated feedstock was targeted at a steady concentration of 2.5% w/w, and the enzyme loading was targeted to be 20 mg/g of cellulose present in the bioreactor. After adding the enzymes to the feed slurry in the bioreactor, a batch hydrolysis reaction was run for 4 h at 20 mg enzyme loading per g of biomass without turning on the filtration. After 4 h, the membrane filtration was started. At the same time, the feeds of buffered water, enzyme and fresh slurry, as well as, the purge stream were started. The reaction reached steady state in terms of enzyme loading, sugar content, and total FIS after a few hours' time. Whenever the TMP across the membrane—required to maintain the constant permeate rate—reached a preset level (either 2 or 4 bar depending on the experiment), the system was operated in batch mode for a short interval (~30 min) to allow for offline cleaning of the membrane unit using 0.05 M NaOH.

5.2.5 Techno-economic analysis

Techno-economic modeling can help compare the economics of CEH versus batch process with similar annual productivities. For this study, a spreadsheet-based techno-economic model was developed. The inputs for the model are presented in the Supplemental Information.

The basis of this production scenario is: 418 x 10^6 kg of sugar/y. This number was chosen to compare the cost of production and cost of performing enzymatic hydrolysis as indicated by NREL 2012 Target model [29], which was $0.12/lb cost of production by 2012. Our model CEH process includes two continuous stirred tank reactors (CSTRs) in series and the sugar is

continuously removed from each reactor using UF membranes to lower the sugar concentration and increase conversion.

In this model, the two reactors were designed in such a way that 25% of the feed is withdrawn at the reactor's composition from the first one and then fed to the second one, and 75% of the total feed to each of them is permeated through the membrane. The first reactor had the enzyme loading of 20 mg/g cellulose, and it is doubled in the second. Also, it was assumed that the lignin and residual biomass are all fed to the turbogenarator to produce electricity, and that electricity was used to operate the power plant. It is also assumed that the excess heat from the generator was used to heat the water and produce steam that is sufficient for the power plant. The excess electricity was sold back to the grid. A distillation, dehydration and solids recovery unit produces pure sugar stream. The following block-flow-diagram (Figure 2) presents the production scenario considered for techno-economic analysis.

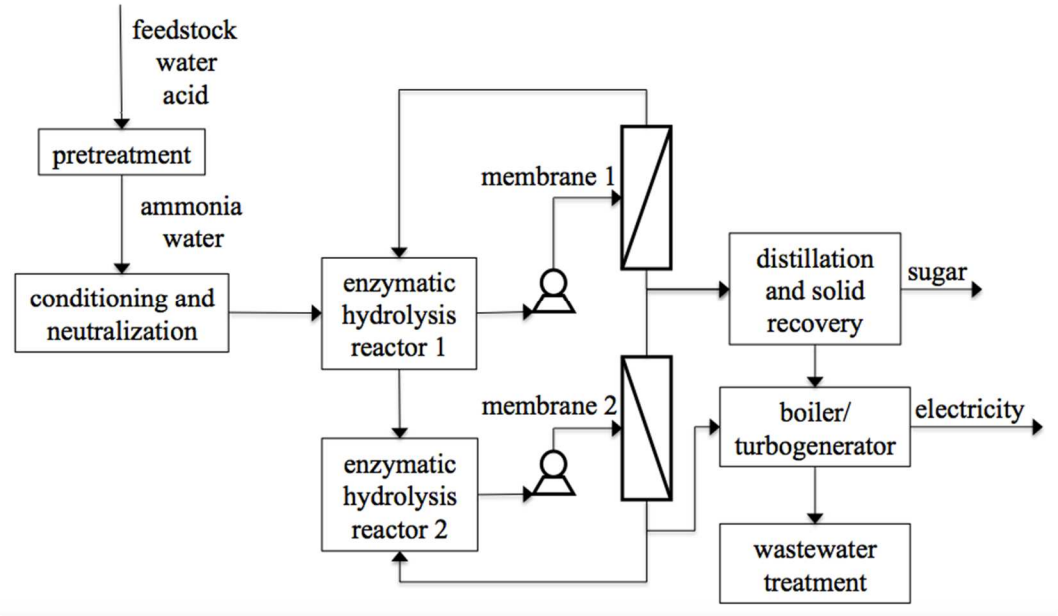

Figure 5.2. The techno-economic model of CEH sugar production.

5.3 Results and discussion

5.3.1 Biomass screening studies

5.3.1.1 Characterization results

The pretreated corn stover was acidic (pH 1.7) with a significant amount of soluble sugars, primarily xylose [30]. The hydrolysate had a conductivity of 9 mS/cm that indicates a significant amount of electrolytes (soluble ions). The following Table 5-2 provides the basic profile of the acid pre-treated, corn stover hydrolysate.

Table 5-2 - Analysis of bulk hydrolysate used in initial screening studies.

fraction (mass) total solids in slurry	0.301
fraction (mass) insoluble solids in slurry	.0.173
density of liquid phase	1.08 g/mL
soluble sugar concentration	139 g/mL
soluble other species	22 g/L
mass fraction of suspended solids as lignin	0.30
as ash	0.04
as polysaccahride	0.64
as other	0.02
pH	1.7
conductivity	9 mS/cm
% (mass) low volatility[1] solids	33
% (mass) mid volatility[2] solids	12
% (mass) non-volatile[3] solids	2

5.3.1.2 Centrifugation of hydrolysate

Centrifugation of hydrolysate was carried out with the slurries at FIS 1%, 2%, 5% and 10%, prepared by adding DI water to the bulk material. The total mass in each centrifuge tube

was 0.015 kg. The centrifugation tests were carried out for 3 different time intervals: 5, 10, and 20 min and four different accelerations, ×g, m/s^2: 44.7, 178.9, 715.6, and 1610 for centrifuge 1 and five different g's: 45, 180, 720, 1620, and 4500 for centrifuge 2. It should be noted that these studies are most relevant for the biomass slurry at very low conversion to sugar and the front end of the membrane filtration unit. During enzymatic hydrolysis, the particles become smaller and the magnitude of such a body force exerted on them versus Brownian diffusion will become less important.

The results from these tests are detailed in the supplementary information. For the slurry with 1% FIS, the sedimentation was quick and the pellets were very compact even with moderate force applied. Increased time and force for centrifugation did not increase the efficiency of sedimentation significantly for this slurry. When slurry with 2% FIS was used, the sedimentation rate slowed down. The sedimentation rate kept on slowing down further as the slurry's FIS increased. The overall sedimentation was not more efficient with increased time; however, the increased force made the sedimentation more effective because of the formation of more compact pellets. The rate of compaction was higher in the slurry with higher FIS than in the slurry with lower FIS at the same applied acceleration (particle aggregation/cooperativity is increased and, thus, so is the force). This study suggests that at the same membrane flux (velocity) but at different TMPs, the compaction of retained particles on the surface of the membrane will be greater at higher TMP. Thus, there is likely a local-optimum operating condition with respect to TMP, and the corresponding productivity, which balances capital versus operating costs.

5.3.1.3 Pressure driven filtration tests with acid-hydrolysate

Filtration tests were performed using the membranes listed in Table 5-1 with slurries comprised of 1%, 2% and 5% (by mass) of the hydrolysate in DI water. Dead-end (normal flow) filtration was carried out using 10, 20 and 50 psi (TMP) (supplied by N_2 blanket), in 500 mL stirred cells (Millipore). In all cases the starting volume of hydrolysate suspension was 350 mL. The membrane cross-sectional area was ~34 cm^2. The ambient pressure was P_{amb} ~ 83.6 kPa, but the gas pressures were measured as gauge pressure, and therefore can be considered the TMP.

The mass permeate flow over time was measured and the following simple Darcy's law was used to calculate the total filtration resistance R_{tot} (m^{-1}) as a function of mass collected.

$$J = \frac{\Delta V}{\Delta t A_{mem}} = \frac{\Delta P_{TM}}{\eta (R_m + R_c)} \qquad [2]$$

where ΔV is the volume of liquid permeated at time Δt, A_{mem} is membrane area, ΔP_{TM} is the TMP applied, η is viscosity, R_m is the resistance of a clean membrane (initially obtained with pure water) and R_c is then the fouling resistance including any deposited cake and any internal and/or surface pore plugging.

Since $R_{tot} = R_m + R_c$ and $\Delta V = \frac{\Delta w}{\rho}$ where R_{tot} is the total resistance of the membrane plus the cake (and any internal plugging), ρ is density, and Δw is the mass collected during the time interval Δt. Thus,

$$R_{tot} = \frac{\Delta t}{\Delta w} . \frac{\rho}{\eta} . \Delta P_{TM} . A_{mem} \qquad [3]$$

,

and

$$R_c = \frac{\Delta t}{\Delta w} . \frac{\rho}{\eta} . \Delta P_{TM} . A_{mem} - R_m \qquad [4]$$

.

The volume filtered per unit membrane area (V/A_{mem}) versus time (t) for each combination of membrane, ΔP_{TM}, and % solids is presented in the Supplemental Information. A linear fit of these data provides an intercept with the V/A_{mem} axis at t = 0 for all filtration cases that suggests that the permeance experienced an immediate decline but then remained steady afterward (in most cases) with no deposition build-up. The immediate decline in permeance implies that some MF pores were blocked with colloidal particles. The steady filtration after the initial, immediate decline suggests that the formation of the cake was minimal under the stirring conditions we used and, thus, its contribution to overall fouling was less. This is consistent with the critical flux paradigm [31] such that the lower permeance (flux) after the initial blockage was low enough to be balanced by the back mass transfer of particles due to stirring.

The intercepts of the linear fits were generally larger for the slurry with lower FIS and the membranes with larger nominal pore size. This suggests that the initial decline in permeance is directly proportional to the pore sizes, inversely proportional to the FIS (or the solids content) and independent of TMP. Figure 3 below provides an illustration of these data.

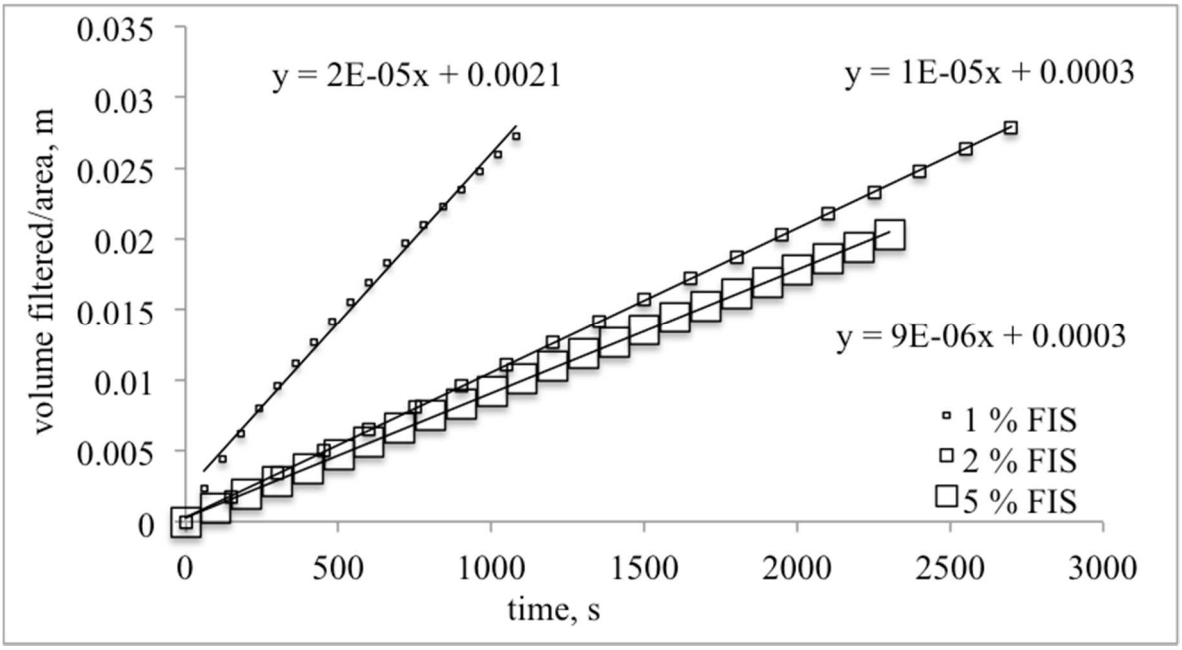

(a)

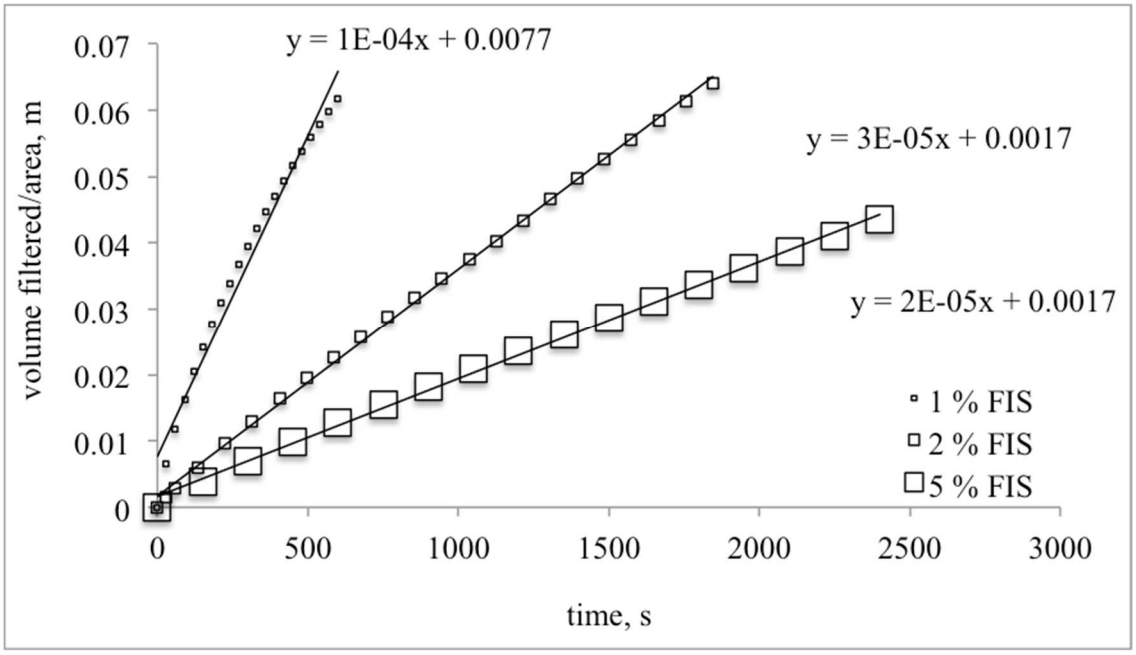

(b)

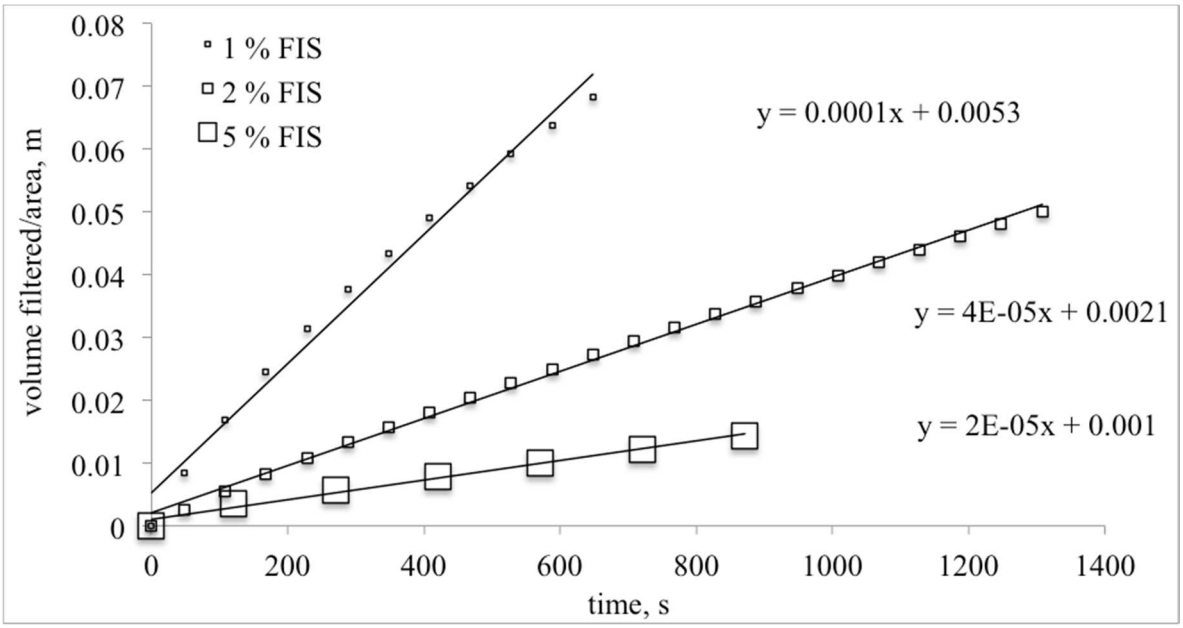

(c)

Figure 5.3. Filtration of diluted hydrolysate using the nominal (a) 0.22 µm (membrane 1), (b) 0.65 µm (membrane 2), and (c) 1.2 µm (membrane 3) MCE MF membranes at TMP = 10 psi. Linear fits are indicated.

A three-way analysis of variance (ANOVA) was done to determine the statistical significance of membrane choice (membrane 1, 2 or 3), TMP of operation (10, 20 or 50 psi) and the total solids present in the slurry (1, 2 or 5%) on the apparent fouling resistance (R_c in equation 4, m^{-1}) defined using the slope of the V/A_{mem} versus t data and the value of the intercept of the straight line fit—a measure of immediate depth filtration fouling. Higher the intercept, greater would be the initial blockage of the pores. The following Table 5-3 and Table 5-4 summarize the ANOVA results:

Table 5-3. Three-way ANOVA on membrane resistance (slope).

source	SS	df	mean square	F	Prob > F	$F_{crit,\ 0.05}$
membrane	1118926	2	559463	106.02	0	4.46
TMP	383698	2	191849	36.36	0.0001	4.46
% solids	606148	2	303074	57.43	0	4.46
membrane × TMP	49075	4	12269	2.33	0.1441	3.84
membrane × % solids	12949	4	3237	0.61	0.665	3.84
TMP × % solids	6106	4	1527	0.29	0.877	3.84
error	42215	8	5277			
total	2219117	26				

Table 5-4. Three-way ANOVA on immediate fouling metric (intercept).

source	SS	df	mean square	F	Prob>F	$F_{crit,\ 0.05}$
membrane	445.42	2	222.71	15.75	0.0017	4.46
TMP	39.56	2	19.781	1.4	0.3013	4.46
%solids	297.11	2	148.553	10.51	0.0058	4.46
membrane×TMP	20.3	4	5.075	0.36	0.8312	3.84
membrane×%solids	96.07	4	24.017	1.7	0.2426	3.84
TMP×%solids	264.7	4	66.175	4.68	0.0306	3.84
Error	113.12	8	14.141			
Total	1276.28	26				

The ANOVA analysis indicates that all three main variables affect the observed fouled membrane resistance at the 95% significance level, but only the membrane and the % solids influence that initial depth filtration blockage, as well as, the combination of TMP and % solids. As per the ANOVA, the choice of membrane will likely bring the most significant variance in terms of rate of fouling resistance per unit volume of permeate filtered during CEH. This is primarily because of the higher porosity of some membranes that can be irreversibly fouled and that can contribute to the unpredictably higher fouling resistance. For that reason, a relatively porous membrane that has a pore-size distribution slightly smaller than the sizes of particles in

the slurry is the most favorable membrane for these kinds of applications. If the direct irreversible blockage of pores can be mitigated, and the only factor for the decline in permeate rate is the cake formation on the top of the membrane, then it is more straightforward to clean and regain the original properties of the membrane. At the same time, the subsequent economics that is related to the passage of enzymes through the pores and the cost of the processes involving the recycling of those enzymes can also play a significant role if a very compact membrane is chosen. Thus, we chose a UF membrane module (Koch M180) for our subsequent experiments.

Similarly, a Hermia model [32] fit of these filtration data were done to understand if the membranes are following some particular trends of pore blockage. But, the nature of blockage was inconclusive from the model fit results. The reason could be the volume permeated was too low to provide sufficient resolution between mechanisms. These fitting results are also illustrated in the supplementary information section.

5.3.2 Continuous enzymatic hydrolysis (CEH)

5.3.2.1 Initial batch reaction

To obtain Michelis-Menten parameters for this acid-pretreated, corn stover hydrolysate, a batch hydrolysis was done with 10% FIS and 20 mg/g cellulose for 72 h. The following Michaelis-Menten parameters were obtained:

Table 5-5. Michaelis –Menten kinetic parameters.

parameter	value	units
K_{cat}	0.0035	s^{-1}
K_m	6.8	g/L
K_i	6	g/L

5.3.2.2 Membrane-enabled CEH

It should be noted that the tubular UF membrane's (previously described) clean resistance had already been compromised during initial system operational testing by performing uncontrolled filtration with the slurry. Afterward, the membrane was cleaned with 0.05M NaOH for 30 min in a sonication bath, and its permeance at that point represented the new baseline for the "clean membrane".

Subsequently, three separate experimental runs were performed using the protocol described in the Methods section. Each of these experiments have failings of various sorts, but provided stepwise validation of our overarching hypothesis, and guidance for our next generation studies. In the following, we are highlighting the significant information we gained from them.

Experiment I (performed for 28 h without a purge) established that the kinetic parameters, obtained in the batch measurements, provided reasonable forecasting for CEH reactions, as well as, providing initial metrics for the membrane's permeance and flux decline. The slurry was nominally 2.0% FIS and ~1.3% cellulose, both on a w/w basis with enzyme loading at 20 mg/g.

Figure 5.4 presents the comparison between forecast and measurement for the hydrolyzed biomass (conversion) and sugar concentration in the reactor. The sugar concentration reached about 12 g/L in 4 h and when the membrane permeation was turned on, the sugar concentration in the bioreactor remained more or less constant. The overall conversion was 288 g of biomass insolubles, versus 100 g that could be hydrolyzed in the same volume and residence time using a batch reactor.

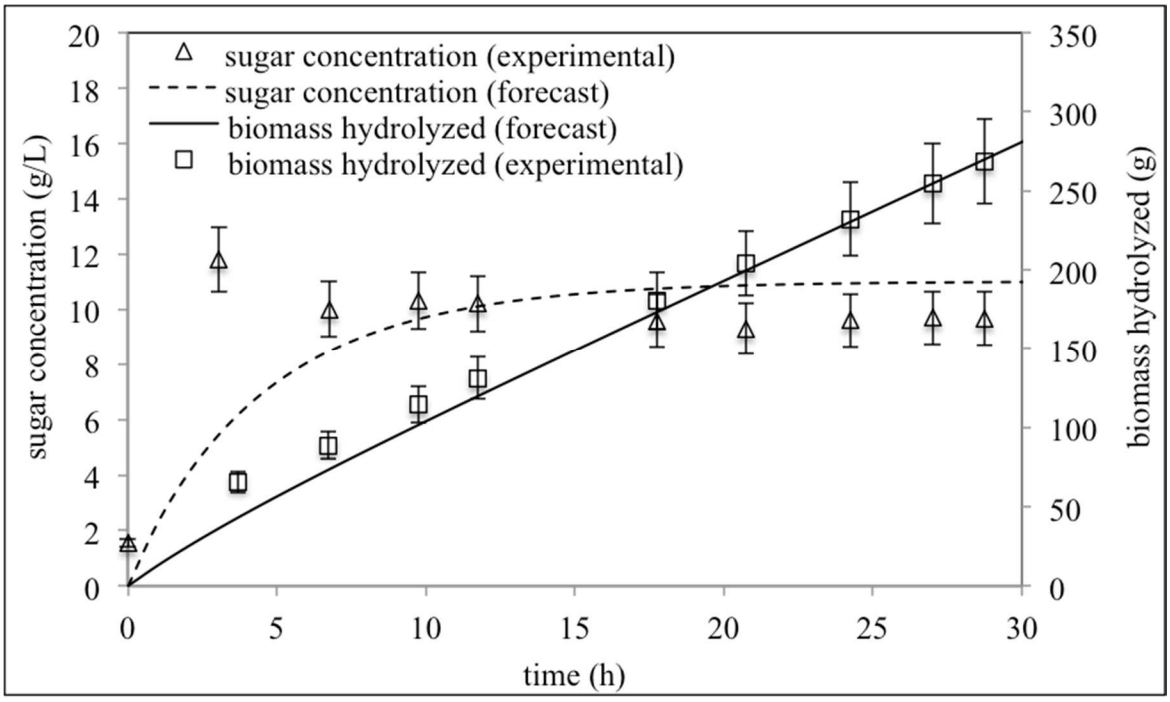

Figure 5.4. Membrane-enabled CEH results versus forecast for experiment I (initial run).

Figure 5.5 presents the membrane's permeance (TMP-normalized flux) during the course of this experiment. Since slurry flows tangentially across the surface of the membrane, a deposition cake may slowly build, as well as, smaller colloidal particles (enzyme proteins, lignin, polysaccharide oligomers) may enter the depth of the membrane and become immobilized. Both of these mechanisms can lead to decreased membrane productivity over time. At the beginning of the permeation, the overall permeance of the membrane was 72 $L \cdot m^{-2} \cdot h^{-1} \cdot bar^{-1}$ (LMH/bar). The permeance declined sharply to 52 LMH/bar until the total permeate collected was about ~ 5 kg and the permeance further declined to 33 LMH/bar until ~15 kg had been collected at the end of the experiment.

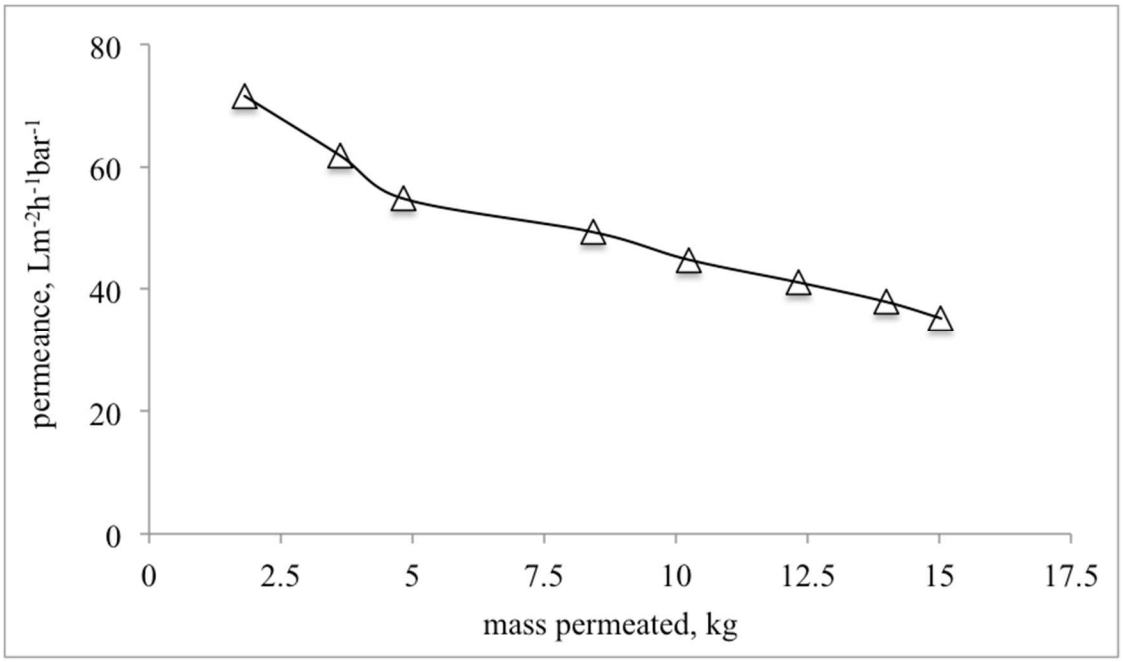

Figure 5.5. Membrane permeance versus total permeated during the initial experiment I.

Experiment II was for ~60 h and followed the same nominal protocol except that at 24 h the purge was started to remove lignin build-up. Membrane permeation rates were variable: 10 mL/min from 4-24 h, and 8 mL/min until the required TMP was 2 bar, at which point (28 h) approximately constant TMP was imposed.

Figure 5.6 presents the sugar concentration in the bioreactor along with model predictions. The sugar concentration decreased during 4 - 28 h of operation. This coincides with the time when the membrane permeation was the highest and enzymes were not fed to the system. After 28 h, the enzymes were again fed back to the reactor through the water stream and the sugar concentration went up immediately. However, from 28-60 h, the sugar concentration decreased below the forecast level by ~20%. This could be due to loss of enzymes through the membrane and also a decrease in the enzyme activity.

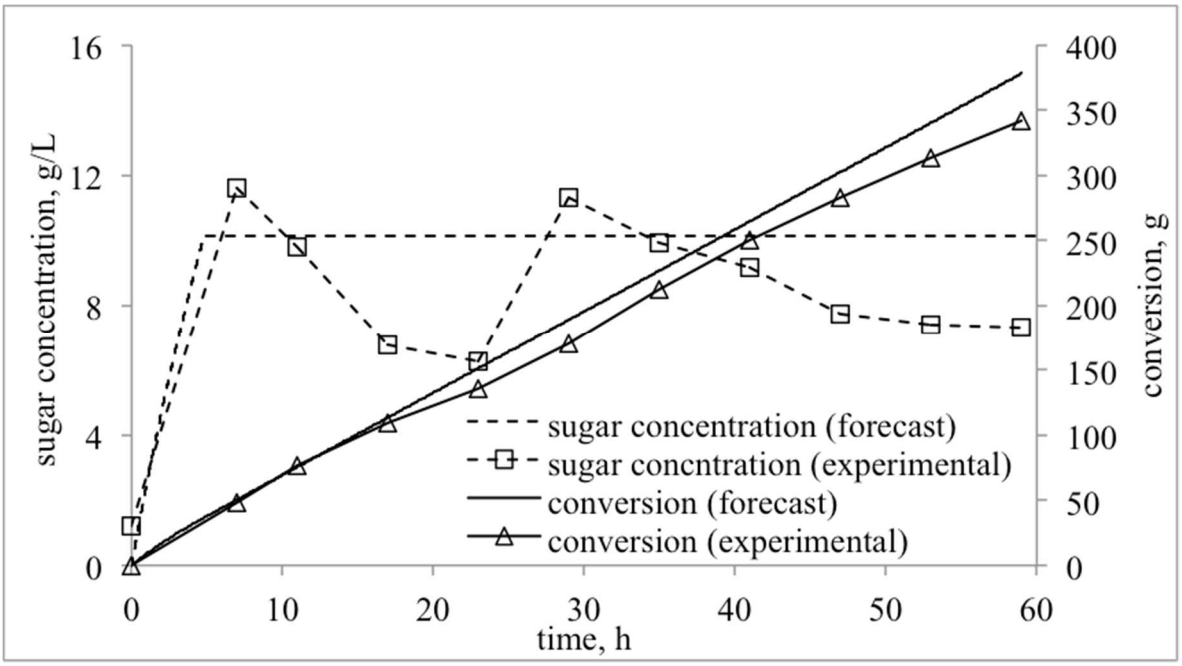

Figure 5.6. Membrane-enabled CEH results versus forecast for experiment II.

Figure 5.7 presents the running average membrane permeance over the course of the experiment. At the beginning of the filtration, the permeate flux was ~150 LMH/bar. The integrated average permeance declined steadily approximately tenfold to ~15-20 LMH/bar as the total permeate collected reached ~ 24 kg. This decline results from the deposition rate based on the material balance inherent in a filtration, as well as, any colloidal species captured in the depth of the membrane and changes in the intrinsic resistance of the deposited cake. The latter can be due to changes in porosity, pore structure, and size arising from changes in the types of particles being deposited.

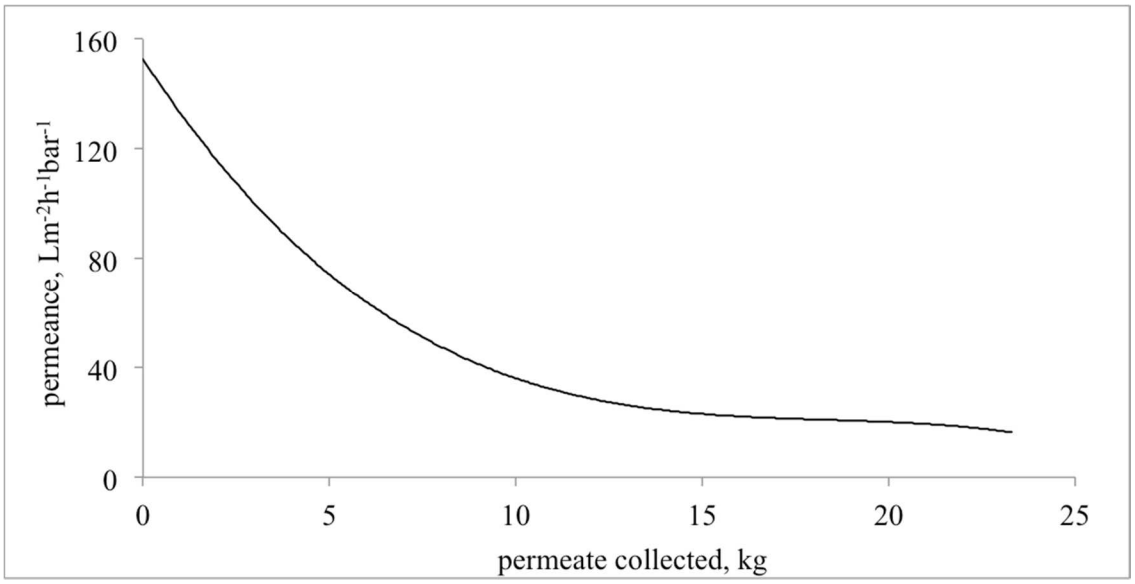

Figure 5.7. Membrane flux (running average) against total permeation for experiment II.

Figure 5.8 shows the sugar content and fraction insoluble solids (FIS) in the reactor during the course of the experiment III. The reactor volume was static at 3 L. When the filtration was started at 4 h, the permeation rate was 6 mL/min and the purge rate was 3 mL/min, which balanced the feed of fresh biomass slurry. Because the feed biomass was not washed, there was some amount of glucose and a significant amount of xylose already present along with other minor components in different proportions. The glucose content in the reactor increased rapidly in the beginning and reached a value of ~12 g/L in the first 4 h. When the continuous permeation, purge, and feed (biomass, enzyme, water, and buffer) started at 4 h, the sugar content started decreasing and the FIS increased steadily. The sugar concentration slowly declined up until the mechanical stoppage at 63 h. At that time, sugar content in the reactor was ~ 5 g/L. The sugar increased again to 8 g/L after addition of 4.5 mL of enzymes as make-up for the enzyme lost in the continuous purge and membrane permeation. Afterward, the sugar content steadily decreased and FIS increased up until the end of the experimental run.

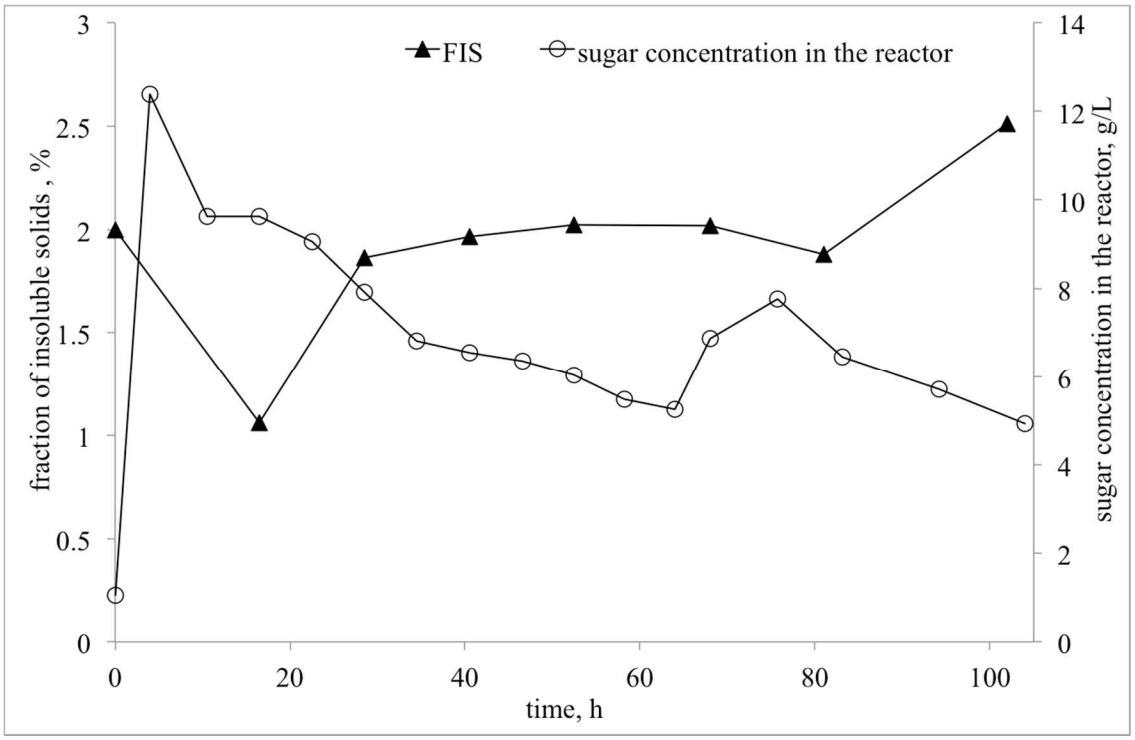

Figure 5.8. Membrane-enabled CEH results for experiment III.

As defined in Section 5.3.1.3, we have calculated the fouling (cake) resistance, R_c (see equation 4) and plotted that in Figure 5.9 for the four different phases of this experiment. During the initial period (up to ~60 h) the cake resistance, as expected, increases linearly until the total permeate was ~20 kg. At the end of that period, the slope was increasing substantially and the TMP required to maintain the desired flux exceeded our 2 bar threshold. The permeation was halted and the reaction was run in batch mode, while the membrane was flushed with DI water (the 4 h stoppage included an impromptu, cleaning setup time). Afterward, continuous feed, purge and permeation was restarted and regular membrane cleaning (by flushing) was performed every 6-10 h (then only taking 10 min). Because of the lack of chemical cleaning, there is a higher rate of fouled membrane resistance growth. This is possibly due to blockage of pore openings that require chemical cleaning (with 0.05M NaOH) to loosen up.

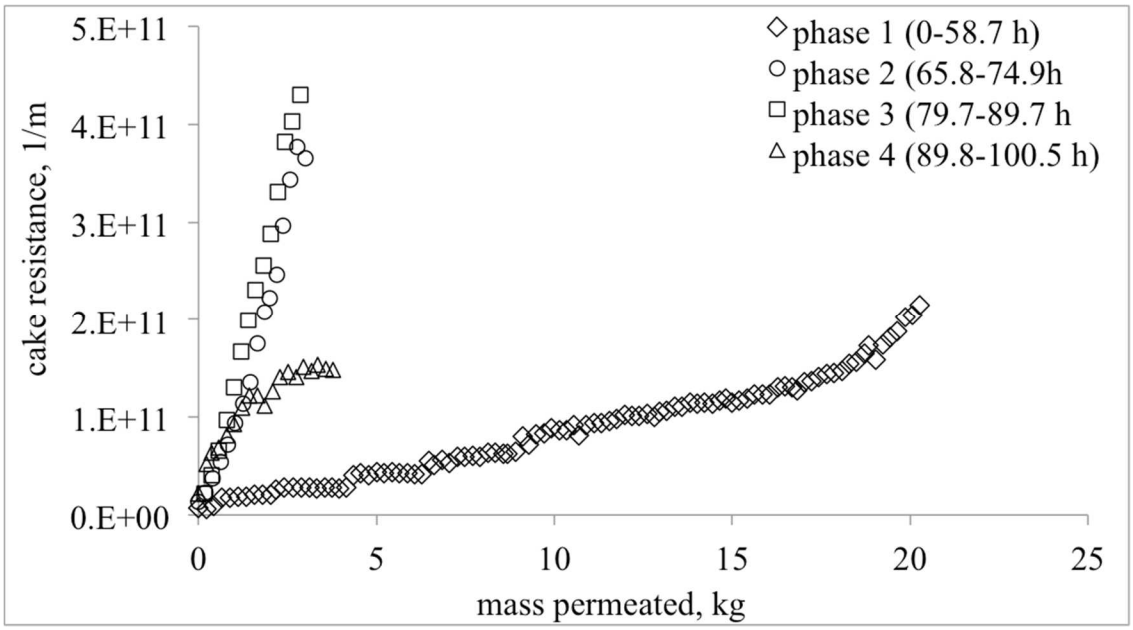

Figure 5.9. Membrane fouling (cake) resistance at different times during experiment III.

The fouling resistance (and by extension the dominant part of the overall membrane resistance) is on the order 0.5 - 4 x 10^{11} m^{-1} for the UF membrane filtering a nominal ~2.0% FIS slurry with approximately 64% conversion. By comparison to the results presented in Section 5.3.1.1, for microfiltration of acid-hydrolysate, the UF membrane has an order-of-magnitude lower resistance (4.6 ± 2.6 x 10^{12} m^{-1} for 2% solids) because it has minimal depth filtration. Thus, this experiment suggests that the choice of a UF membrane is the right choice for this application and that crossflow water flushing, done regularly, can be effective to control the fouling resistance.

5.3.2.3 Comparison of experiment III to the batch system

The amount of cellulose available for conversion altogether was 0.472 kg from the combined start-up and continuous feed slurry. The total cellulose hydrolyzed during the entire experiment was determined to be 0.305 kg, resulting in a total conversion yeild of 64.5%. Although this seems like a low yield compared to a batch process, the total theoretical yield for

this expeirment was 67% because of the continuous purge stream removing some unhydrolyzed solids from the system—this would be the feed to the 2nd CSTR in a full process. For comparison purposes, a hypothetical reactor is added in series to the first reactor and is fed by this purge stream. The only additional input to this stream is supplemental buffered water. The conservative assumption is that the conversion in this 2nd reactor is 50% (future experiments will determine the actual yield for this second reactor), thus a total of 387.1 g of cellulose is enzymatically hydrolyzed to sugars.

A comparison between this semi-hypothetical continuous system and the batch system with 10% total solids (from the earlier kinetics experiment, see Section 3.2.1) was made. The overall basis of this comparision is that the amount of cellulose converted is the same in both cases, i.e. 387.1 g. The duration of the batch and continuous hydrolysis was 4 days and the total yield in batch system was 95%. CEH only used 7.8 g of enzymes whereas the batch hydrolysis used 12.6 g of enzymes while both systems used 20 mg enzymes /g of cellulose . Because of having just two reactors in series, the overall yield in continuous hydrolysis was 82.5%. The overall volume of the reactors required in continuous hydrolysis was 4 L (3 + 1) compared to 10.8 L in the batch reactor. The final estimated productivity was 0.93 g/L/h glucose for the continuous system compared to 0.37 g/L/h glucose for the batch system. Thus, productivity is projected higher using the membrane-enabled CEH system over the batch system, and it also ultimately requires smaller equipment size for the same production of glucose. Also, less overall enzyme loading is needed to run the CEH system because enzymes are retained in the reactor while fresh biomass slurry is continuously added. These two factors are some of the main drivers of enzymatic hydrolysis cost, and the continuous hydrolysis system appears to offer benefits over

the standard batch process if the overall yield can be improved through reduction in the relative purge rate between staged continuous reactors. The following Table 5-6 summarizes the results.

Table 5-6. Comparison between continuous and batch systems.

	continuous	batch
cellulose converted, g	387.1	387.1
enzymes, g	7.8	12.6
mg enzymes/ g cellulose converted	20.1	32.5
yield, %	82.5	95.0
total process volume, L	4.0	10.8
productivity, g/L/h glucose	0.93	0.37

5.3.3 Techno-economic analysis

5.3.3.1 System with CEH

First of all, a continuous system was considered that had the same productivity as that of the batch system as described in the NREL target model.[29] The reactor design was based on 5% FIS (versus the 2.0% we have demonstrated herein). Also, the membrane used for the separation was a UF membrane that rejected 99% of the free enzymes (those that are not attached to substrate) versus the nominal 55% with the membrane used in our current experiments. At this time, the costs for concentrating the dilute sugar stream (membrane permeate) has been included in the distillation, dehydration, and solids recovery unit operations.

The results are presented in the following tables. Table 5-7 presents the summary of the membrane, pump and overall conversion.

Table 5-8 summarizes the capital costs projected for the different unit operations in the model. Table 5-9 is the summary of operating costs. The costs are also presented in terms of cost per kg of sugar produced.

Table 5-7. Summary of membrane, pump and overall conversion.

conversion (%)	93.7
total sugar production (millions kg/year)	421
membrane area required (m^2)	18,750
membrane cost ($/$m^2$)	50
membrane cost (MM $)	0.938
pump cost (MM $)	2.60
pump for membrane operation cost (MM $)	1.50
saccharification reactor cost (MM $)	2.16
saccharification reactor stirring cost (MM $)	0.717

Table 5-8. Summary of capital costs, expressed in $MM.

pretreatment	22.5
neutralization and conditioning	10.7
continuous saccharification	4.35
boiler/electricity generator	27.3
utilities	0.472
storage	0.226
wastewater	3.05
distillation and solids recovery	7.18
total installed equipment cost	75.8
total project cost (42% of TPI is added cost)	131

Table 5-9. Summary of operating cost indicating cost of production.

	MM $/year	$/kg sugar
feedstock	41.6	0.0990
enzyme	10.0	0.0238
sulfuric acid	1.14	0.0027
ammonia	10.3	0.0244
water	2.48	0.0059
waste disposal	1.17	0.0028
electricity	-11.6	-0.0276
fixed costs	6.53	0.0155
capital depreciation	6.53	0.0155
other costs (personnel, return on investment, taxation)	13.1	0.0310
total production cost	81.3	
cost of production ($/kg sugar)		0.1931

There is a significant improvement for the CEH system versus the batch system. Many factors influence this. Because enzymes are recycled, the cost of enzyme falls to $0.026/kg of sugar from $0.028/kg of sugar produced. Also, the total conversion also goes up to 93.7% from 87% in batch model. The reactor sizing decreases and this contributes to a decrement of capital cost for the reactor by about 47% (new cost $4.35 MM versus batch cost $8.1 MM). Similarly, the mixing cost of the reactor lowers because the slurry is less dense in CEH (5% insolubles feed and keeping 3% cellulose constant in the reactor at all times while the batch mode has 30% insolubles).

5.3.3.2 Electricity cost

The following pie chart (Figure 5.10) shows the usage of electricity. All the electricity is not used and, thus, some is sold back to the grid. The total electrical power produced is 44 MW.

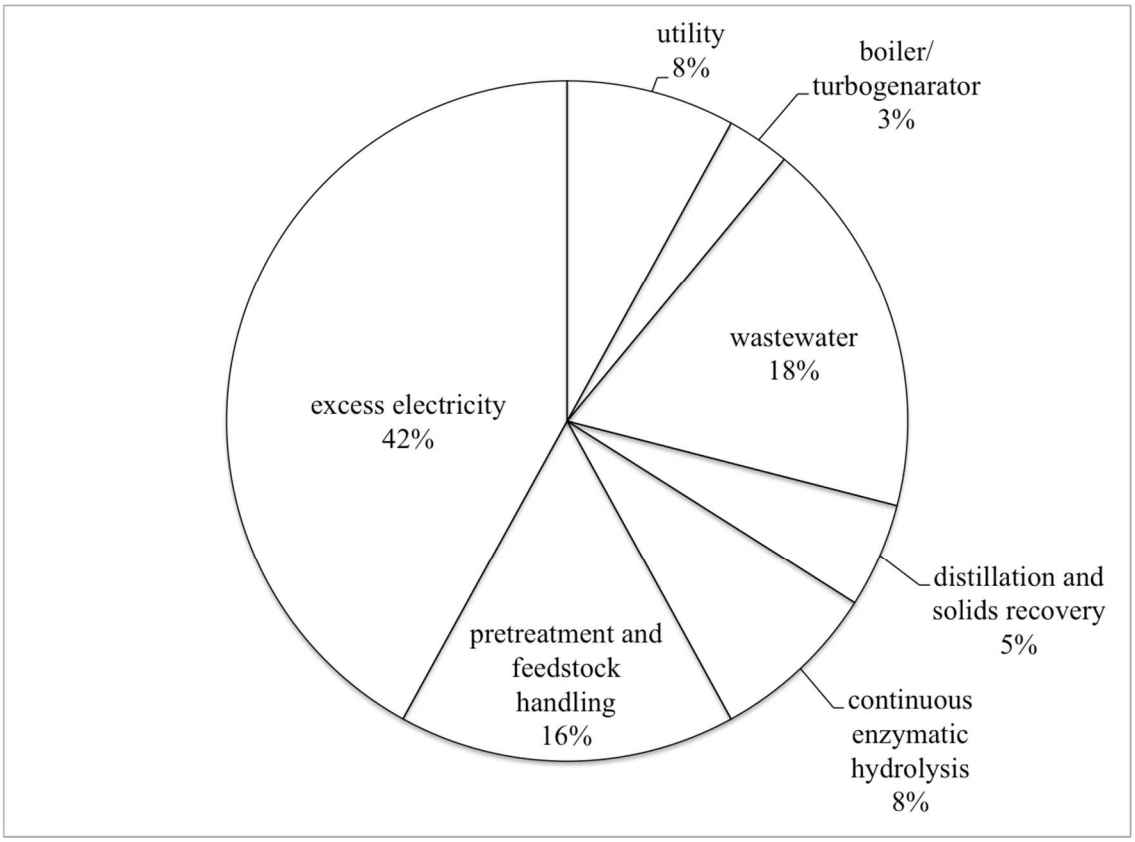

Figure 5.10. Electricity usage and production pie chart.

5.3.3.3 Comparison of different CEH systems

The costs associated for CEH with different process assumptions were also evaluated. The CEH capital cost decreases less significantly after 100 million kg/y (see Figure 5.11).

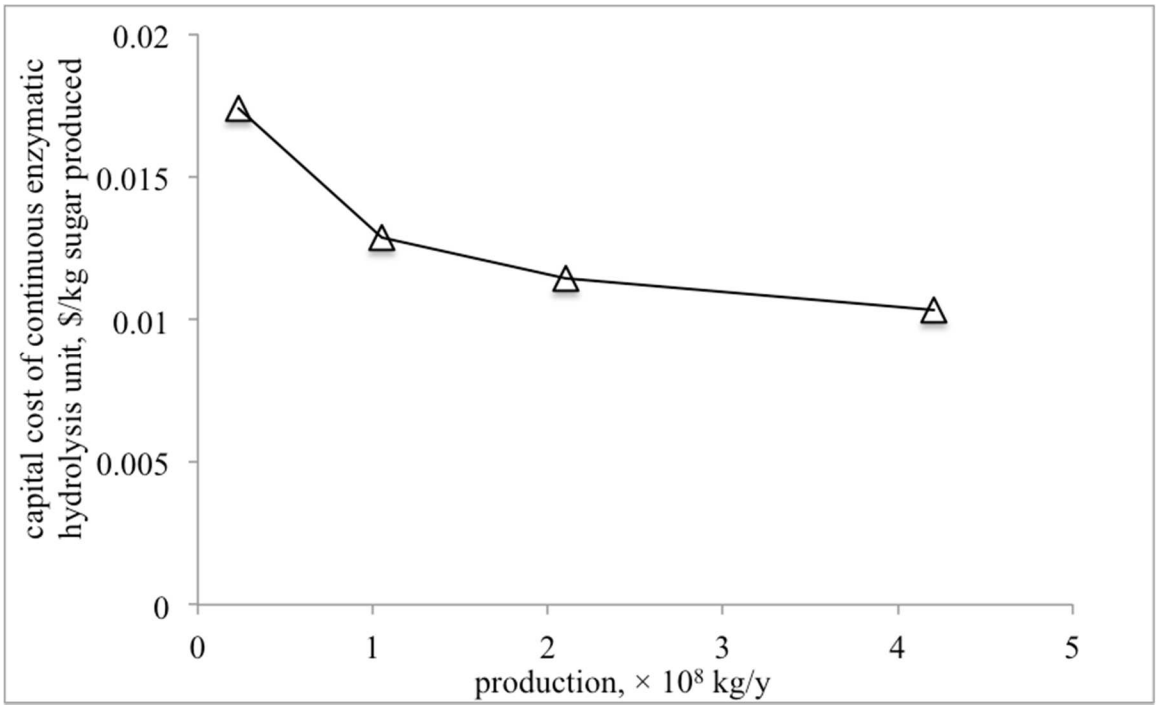

Figure 5.11. Evaluation of capital cost of CEH at different production volumes expressed in terms of $/kg sugar produced.

5.3.3.3.1 Cost of enzymes

Most of the time, enzymes cost is reported too low in the literature, while the actual cost of enzymes is much higher [33]. The cost of enzyme is one of the reasons for an economic advantage for the CEH process. We evaluated several production scenarios based on the type of membrane used and compared those to the batch process. Two different assumptions were used: (i) 80% of the enzymes bind with biomass and hence, 20% of the enzymes are free in the suspension and (ii) 90% of the enzymes bind with biomass and hence, 10% of the enzymes are free in the suspension. In addition, we considered variation in membrane rejection as being only applicable to the free enzyme (bound enzyme is always 100% retained). The scenarios considered were

i) batch process with 20% total solids

ii) CEH with same parameters as in the experiment III (~2.0% total solids, 10% assumed free enzymes in the reactor, and 47% membrane rejection for these)

iii) CEH (5% total solids, 10% assumed free enzymes in the reactor and 50% membrane rejection for enzymes) and

iv) CEH (5% total solids, 10% assumed free enzymes in the reactor and 99% membrane rejection for enzymes)

The summary of enzyme cost is illustrated in Figure 5.12 for the four cases.

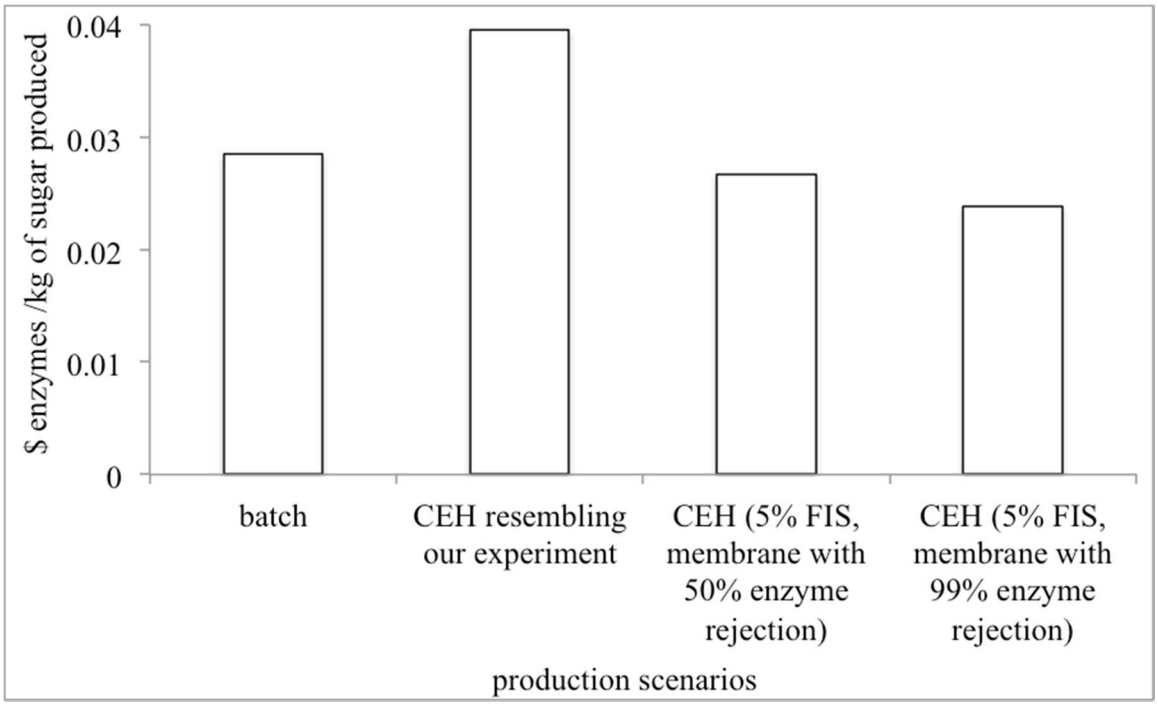

Figure 5.12. Summary of the cost of the enzyme at different production scenarios expressed in terms of $/kg of sugar produced.

The cost of enzymes for the batch process was determined as $0.028/kg of sugar. The cost of enzyme for the CEH system that has same operating conditions as our experiment III is $0.04/kg sugar produced. Other assumed cases (not included in Figure 5.12 and Figure 5.13) are: when the assumed free enzyme is doubled (to 20%) and 100% pass through the membrane altogether (20% free enzymes and 100% enzymes passage through the membrane), the overall

cost of enzymes goes up to $0.036/kg of sugar. When 10% of the enzymes can pass through the membrane (10% free enzymes and 100% enzymes passage through the membrane), the overall cost of enzymes becomes $0.03/kg of sugar. When going down to the scenario when 0.1% of the enzymes can pass through the membrane (10% free enzymes and 1% enzymes passage through the membrane), the overall cost of enzymes is $0.025/kg of sugar.

5.3.3.3.2 Overall cost of production

Full cost of production is the one of the primary metrics for process decisions. The different scenarios chosen for the enzyme cost study were also chosen for the overall cost of production comparison. Figure 13 summarizes these forecasts.

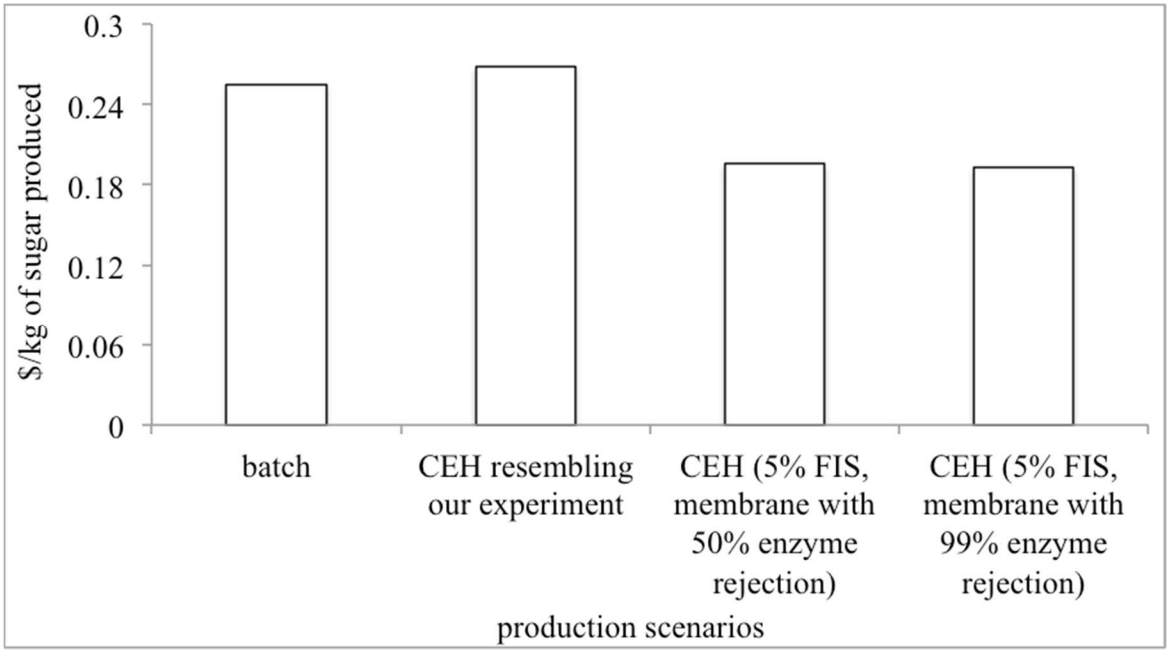

Figure 5.13. Summary of the cost of production at different production scenarios expressed in terms of $/kg of sugar produced.

The model predicted that the total cost of production is $0.1931/kg of sugar (see Table 7). This is ~26% less than the total projected cost of production targeted by NREL in 2012. The cost of production for the batch process was determined as $0.26/kg of sugar. The cost of production

for a CEH system exactly as our experiment III increases to $ 0.27/kg sugar. When 20% of the enzymes can pass through the membrane (20% free enzymes and 100% enzymes passage through the membrane), the overall production cost is $0.21/kg of sugar. When 10% of the enzymes can pass through the membrane (10% free enzymes and 100% enzymes passage through the membrane), the overall cost of production is $0.20/kg of sugar. When going down to the scenario when 0.1% of the enzymes can pass through the membrane (10% free enzymes and 1% enzymes passage through the membrane), the overall cost of production is $0.193/kg of sugar.

5.4 Conclusions

We demonstrated membrane-enabled CEH continuously for 100 h and showed that the system material balance can be reasonably predicted from simple kinetic parameters, reactor models, and membrane mass transfer calculations. Membrane-enabled CEH is challenging because a complex slurry with changing rheological and physicochemical properties are presented continuously to the separation process. The size distribution and number density of suspended, colloidal, and dissolved species vary somewhat with time and position along the membrane filtration. When this slurry moves through the membrane system, a "cake deposition" forms on the surface of the membrane, and reduces the effective permeance of the membrane. If this is too severe and difficult to clean, it can significantly affect the cost of the production due to requiring more membrane area to meet production goals. Our screening studies successfully led us to use UF versus MF membrane in order to avoid depth filtration occurring.

From the experiments presented, we found that the membrane permeance could be maintained sufficiently high by simple periodic flushing with water and regular chemical cleaning; similar to practices used in many membrane applications. We observed that the rate of

formation of cake resistance is higher in the later phases of experiments in comparison to the earlier ones. This can be rationalized by the hypothesizing that the particles are bigger earlier and those bigger particles form a cake with higher porosity and lower tortuosity, and hence, the permeance of the membrane module is not as low as the operating condition when the particles are much smaller later on.

The cost of production of sugar, using the membrane-enabled CEH results we've demonstrated thus far, won't be economically favorable in comparison to the traditional batch process and it will also consume more enzymes. This is because the membrane used in the laboratory could only reject 47% of the free enzymes and also, the total solids in the slurry is low (~2.5%). However, if the membrane remains the same and the total solids increase to 5%, the system becomes economically favorable versus the batch process. The overall cost can go even lower if we are able to optimize the system with a better membrane, higher solids, and production design.

5.5 Acknowledgements

The authors would like to acknowledge Nathan Crawford, Jim Lisheske, Daniel Schell, Jim McMillan and David Templeton from National Renewable Energy Laboratory. This work was conducted under Department of Energy funding (Contract No. DE-AC36-08-GO28308; Bioenergy Technologies Office) via NREL and University of Colorado agreement UGA-0-41026-56.

5.6 References

[1] N. Rahnama, H.L. Foo, N.A.A. Rahman, A. Ariff, U.K.M. Shah, Saccharification of rice straw by cellulase from a local Trichoderma harzianum SNRS3 for biobutanol production, Bmc Biotechnol, 14 (2014).

[2] Y.H.P. Zhang, S.Y. Ding, J.R. Mielenz, J.B. Cui, R.T. Elander, M. Laser, M.E. Himmel, J.R. McMillan, L.R. Lynd, Fractionating recalcitrant lignocellulose at modest reaction conditions, Biotechnology and Bioengineering, 97 (2007) 214-223.

[3] A. Limayem, S.C. Ricke, Lignocellulosic biomass for bioethanol production: Current perspectives, potential issues and future prospects, Prog. Energy Combust. Sci., 38 (2012) 449-467.

[4] A. Yousuf, Biodiesel from lignocellulosic biomass - Prospects and challenges, Waste Manage, 32 (2012) 2061-2067.

[5] P. Kumar, D.M. Barrett, M.J. Delwiche, P. Stroeve, Methods for Pretreatment of Lignocellulosic Biomass for Efficient Hydrolysis and Biofuel Production, Ind Eng Chem Res, 48 (2009) 3713-3729.

[6] Z.H. Zhang, B. Liu, Z.B. Zhao, Efficient acid-catalyzed hydrolysis of cellulose in organic electrolyte solutions, Polym Degrad Stabil, 97 (2012) 573-577.

[7] D. Klein-Marcuschamer, B.A. Simmons, H.W. Blanch, Techno-economic analysis of a lignocellulosic ethanol biorefinery with ionic liquid pre-treatment, Biofuel Bioprod Bior, 5 (2011) 562-569.

[8] C.M. Roche, C.J. Dibble, J.S. Knutsen, J.J. Stickel, M.W. Liberatore, Particle Concentration and Yield Stress of Biomass Slurries During Enzymatic Hydrolysis at High-Solids Loadings, Biotechnology and Bioengineering, 104 (2009) 290-300.

[9] Y.L. Miao, J.Y. Chen, X.J. Jiang, Z. Huang, Kinetic Studies on the Product Inhibition of Enzymatic Lignocellulose Hydrolysis, Applied Biochemistry and Biotechnology, 167 (2012) 358-366.

[10] P. Andric, A.S. Meyer, P.A. Jensen, K. Dam-Johansen, Effect and Modeling of Glucose Inhibition and In Situ Glucose Removal During Enzymatic Hydrolysis of Pretreated Wheat Straw, Applied Biochemistry and Biotechnology, 160 (2010) 280-297.

[11] J.B. Kristensen, C. Felby, H. Jorgensen, Yield-determining factors in high-solids enzymatic hydrolysis of lignocellulose, Biotechnol Biofuels, 2 (2009).

[12] A. Sluiter, J. Sluiter, Summative Mass Closure Laboratory Analytical Procedure (LAP) Review and Integration, National Renewable Energy Laboratory, Golden, CO., 2011, pp. 13.

[13] A. Sluiter, J. Sluiter, Summative Mass Closure Laboratory Analytical Procedure (LAP) Review and Integration : Pretreated Slurries, Golden, CO., 2011, pp. 12.

[14] O.o.E.E.a.R.E. United States Department of Energy, N.R.E.L. (NREL), Modeling tomorrow's biorefinery the NREL Biochemical Pilot Plant, U.S. Dept. of Energy, Energy Efficiency and Renewable Energy,, Washington, D.C., 2008, pp. 4 p.

[15] J.S. Knutsen, R.H. Davis, Cellulase retention and sugar removal by membrane ultrafiltration during lignocellulosic biomass hydrolysis, Applied Biochemistry and Biotechnology, 113 (2004) 585-599.

[16] N. Weiss, J. Borjesson, L.S. Pedersen, A.S. Meyer, Enzymatic lignocellulose hydrolysis: Improved cellulase productivity by insoluble solids recycling, Biotechnol Biofuels, 6 (2013).

[17] P. Andric, A.S. Meyer, P.A. Jensen, K. Dam-Johansen, Reactor design for minimizing product inhibition during enzymatic lignocellulose hydrolysis II. Quantification of inhibition and suitability of membrane reactors, Biotechnology Advances, 28 (2010) 407-425.

[18] M.M. Ishola, A. Jahandideh, B. Haidarian, T. Brandberg, M.J. Taherzadeh, Simultaneous saccharification, filtration and fermentation (SSFF): A novel method for bioethanol production from lignocellulosic biomass, Bioresource Technology, 133 (2013) 68-73.

[19] K. Belafi-Bako, A. Koutinas, N. Nemestothy, L. Gubicza, C. Webb, Continuous enzymatic cellulose hydrolysis in a tubular membrane bioreactor, Enzyme Microb Tech, 38 (2006) 155-161.

[20] Q. Gan, S.J. Allen, G. Taylor, Design and operation of an integrated membrane reactor for enzymatic cellulose hydrolysis, Biochem. Eng. J., 12 (2002) 223-229.

[21] R.N. Gurram, T.J. Menkhaus, Continuous Enzymatic Hydrolysis of Lignocellulosic Biomass with Simultaneous Detoxification and Enzyme Recovery, Appl. Biochem. Biotechnol., 173 (2014) 1319-1335.

[22] M.J. Zhang, R.X. Su, Q.A. Li, W. Qi, Z.M. He, Enzymatic saccharification of pretreated corn stover in a fed-batch membrane bioreactor, Bioenergy Research, 4 (2011) 134-140.

[23] J.S. Van Dyk, B.I. Pletschke, A review of lignocellulose bioconversion using enzymatic hydrolysis and synergistic cooperation between enzymes-Factors affecting enzymes, conversion and synergy, Biotechnology Advances, 30 (2012) 1458-1480.

[24] A. Gautam, T.J. Menkhaus, Performance evaluation and fouling analysis for reverse osmosis and nanofiltration membranes during processing of lignocellulosic biomass hydrolysate, Journal of Membrane Science, 451 (2014) 252-265.

[25] A. Cornish-Bowden, The origins of enzyme kinetics, Febs Lett, 587 (2013) 2725-2730.

[26] N.D. Weiss, J.J. Stickel, J.L. Wolfe, Q.A. Nguyen, A Simplified Method for the Measurement of Insoluble Solids in Pretreated Biomass Slurries, Applied Biochemistry and Biotechnology, 162 (2010) 975-987.

[27] S. Rajam, C.C. Ho, Graft coupling of PEO to mixed cellulose esters microfiltration membranes by UV irradiation, Journal of Membrane Science, 281 (2006) 211-218.

[28] J. Shekiro, E.M. Kuhn, N.J. Nagle, M.P. Tucker, R.T. Elander, D.J. Schell, Characterization of pilot-scale dilute acid pretreatment performance using deacetylated corn stover, Biotechnol Biofuels, 7 (2014).

[29] D. Humbird, National Renewable Energy Laboratory (U.S.), Harris Group Inc., Process design and economics for biochemical conversion of lignocellulosic biomass to ethanol dilute-acid pretreatment and enzymatic hydrolysis of corn stover, Nrel/Tp 5100-47764, National Renewable Energy Laboratory,, Golden, CO, 2011, pp. 1 online resource (ix, 136 p.).

[30] J. Zheng, L. Rehmann, Extrusion Pretreatment of Lignocellulosic Biomass: A Review, Int. J. Mol. Sci., 15 (2014) 18967-18984.

[31] P. Bacchin, P. Aimar, R. Field, Critical and sustainable fluxes: Theory, experiments and applications, J Membrane Sci, 281 (2006) 42-69.

[32] E.E. Chang, S.Y. Yang, C.P. Huang, C.H. Liang, P.C. Chiang, Assessing the fouling mechanisms of high-pressure nanofiltration membrane using the modified Hermia model and the resistance-in-series model, Separation and Purification Technology, 79 (2011) 329-336.

[33] D. Klein-Marcuschamer, P. Oleskowicz-Popiel, B.A. Simmons, H.W. Blanch, The challenge of enzyme cost in the production of lignocellulosic biofuels, Biotechnology and Bioengineering, 109 (2012) 1083-1087.

5.7 Supplementary information

5.7.1 Theory

The concept of continuous enzymatic hydrolysis using membrane is not just to continuously produce or remove sugar, but also to maintain a high biomass conversion by maintaining low sugar concentration in the reactor, as mentioned in the body of this chapter.

5.7.2 Experiments

5.7.2.1 Initial screening experiments

To be able to carry out a continuous enzymatic hydrolysis (CEH), several short experiments were carried out to find out the right membrane and right conditions for the experiments. Initially, an experimental set up was assembled with a ceramic membrane module with 85 membrane tubes with 1.05 mm in diameter and 1 foot length. The membrane had ultra-filtration capability with the nominal molecular weight cut off of 10 nm. A metering pump was assembled to pump the slurry. The system was good enough to run two short experiments of 12 h each but when trying to run the system for 36 h, all the tubes were clogged. These experiments

taught us that the choice and design of the membrane was very critical. The following is the picture of the clogged membrane module while trying to run those experiments:

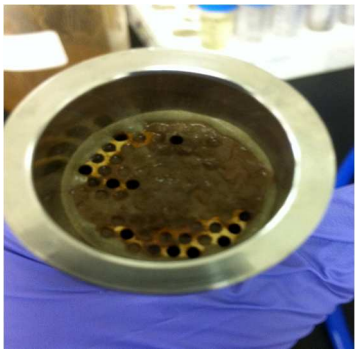

Figure 5.14. Clogged membrane module from earlier experiments

5.7.2.2 Rejection and permeance tests

Few enzyme and Polyethylene glycol (PEG) rejection tests were done using two membranes: i) Biomax30k Psf ultrafiltration membrane from Pall® Corp and ii) MW180 PVDF ultrafiltration membrane from Koch®, the same membrane material used in the CEH membrane module. The enzyme used is CTec2 from Novozymes®. Cellic Ctech2 is a mixture of (cellulases, β-glucosidases, and hemicellulose).[1] Hemicellulase has 95kDa molecular mass [2] and b-glucosidases have molecular mass of about 80 kDa.[3] Thus, the average molecular weight is ~70000 kDa. We prepared enzyme solution with 4.2 mL/L of enzyme that reflects to 1.0575 g/mL of protein. This is exactly the same amount of enzyme that we maintained in the bioreactor for our continuous enzymatic hydrolysis experiment. These tests provided some important information about the cleaning and rejection of the enzymes by the membranes and this information is very useful while doing the economics of these processes. The results are described in detail below:

i) Membrane permeation

Both Biomax30k and M180 membranes retained their permeability while going up and coming down in pressure. Clean M180 membrane had permeability of just above 3 L/m^2 /h/psi and clean Biomax30k had permeability of just above 2.5 L/m^2 /h/psi. After running all the samples of PEG and enzymes, both the membranes got dirty (fouled) and no cleaning technique was applied expect for rinsing with DI water after each sample run. The permeability decreased in both cases but the permeability of both membranes remained constant for decreasing and increasing pressure. Dirty M180 memmbrane had permeability of about 1.5 L/m^2 /h/psi and dirty Biomax30k had permeability of about 1 L/m^2 /h/psi. The results are summarized below:

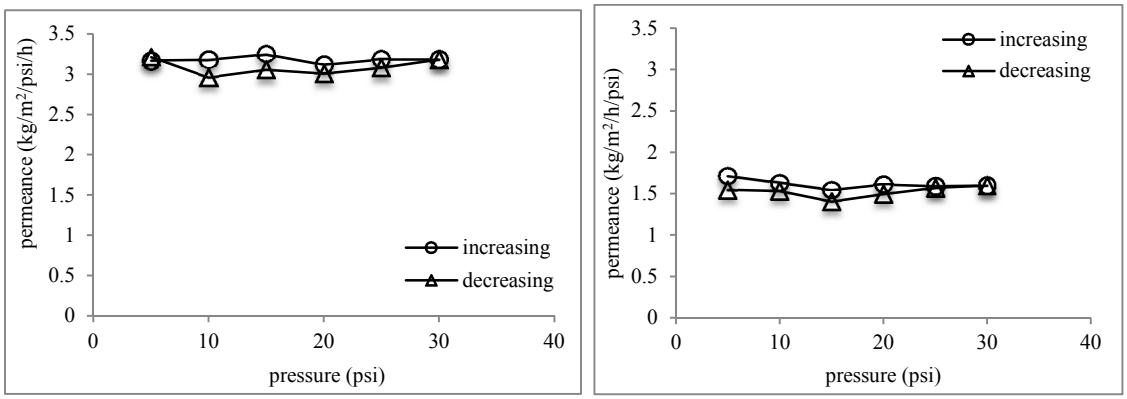

Figure 5.15 – (a) Clean M180 membrane DI water permeance and (b) dirty M180 DI water permeance. 'Increasing' line indicates TMP increasing from 5 to 30 psi and 'Decreasing' line indicates TMP decreasing from 30 to 5 psi.

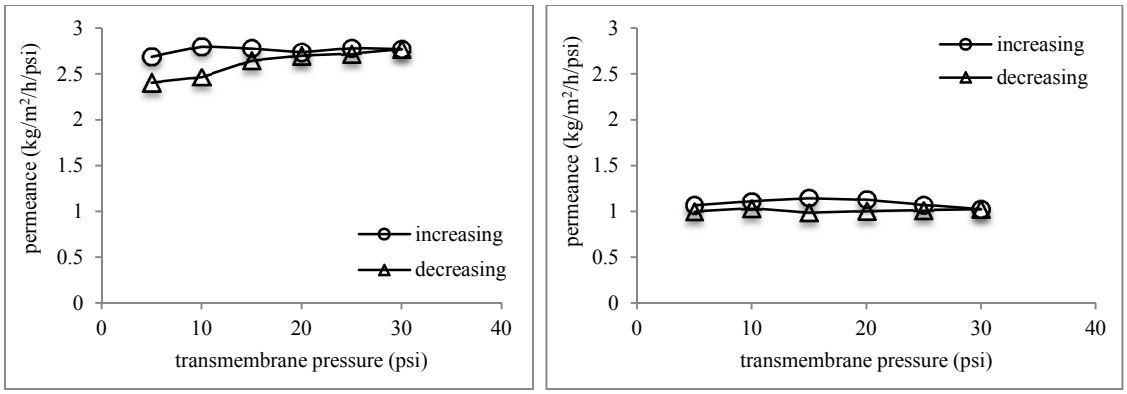

Figure 5.16 – (a) Clean Biomax30k membrane DI water permeance and (b) dirty Biomax30k DI water permeance. 'Increasing' line indicates TMP increasing from 5 to 30 psi and 'decreasing' line indicates TMP decreasing from 30 to 5 psi.

ii) PEG rejection

These filtration tests are done at low pressure (5 psi) with 200 mL solution of PEG solutions of various molecular weights from 400-100000 g/mol. Original samples were taken as 'initial feed sample' and permeation was started. First 5 mL of permeation was let to flow and the permeation sample was taken as 'initial permeation sample'. Then, after 25 mL of permeation, 'final permeation sample' was taken and from the remaining feed sample, 'final feed sample' was taken. After analyzing the results, the following rejection results are obtained.

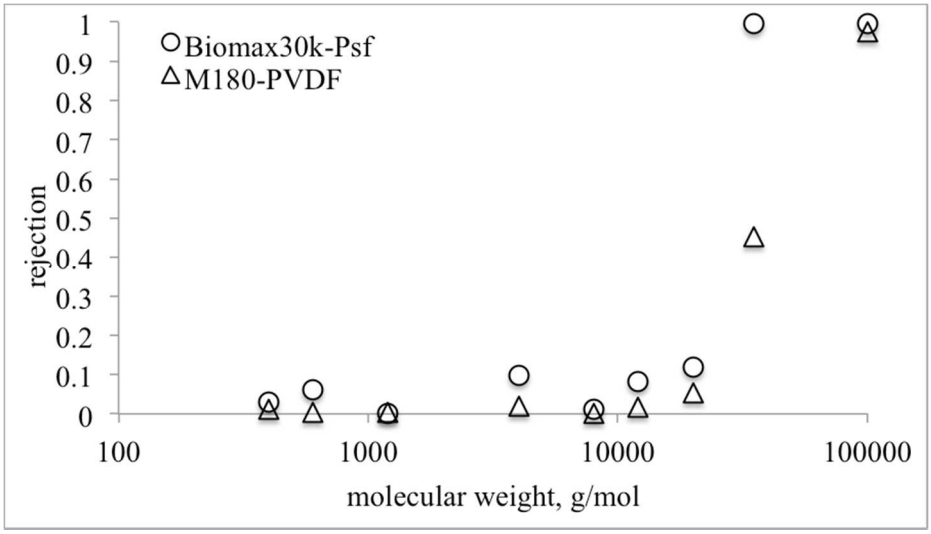

Figure 5.17 – Rejection observed by membranes Biomax30k and M-180

For Biomax30k membrane, the rejection of PEGs remained below 10% until the PEG molecular mass reached 35000 and at or above 35000, the rejection is above 99%. The red circles in the above graph represent Biomax30k membrane rejection. For M180 membrane, however, the rejection was almost non-existent until the molecular weight of PEGs reached 20000 g/mol. At 20000 g/mol, rejection was ~ 5%. At 35000 g/mol, rejection was about 50% and at 100000 g/mol, rejection was 99%. It tells that M180 PVDF membrane has MWCO of ~40000-50000 g/mol.

iii) Enzymes rejection

As per the literature, there is no particular molecular weight that we can potentially tell that these enzyme cocktails have. So, for the particular sample we tested, there were two main peaks on HPLC results from enzymes. Those two components had following rejections as tabulated in the table below. As per these results, we were actually loosing around 50% of the 'free (non-bounded)' enzymes in our experiment.

Table 5-10 – Enzyme rejection

	component 1	component 2
M180	0.53	0.56
Biomax30k	1.00	0.88

5.7.2.3 Centrifugation tests

Centrifugation of lignocellulosic biomass at different suspended solids (1%, 2%, 5% and 10%, all by mass) was done using IEC CL30R (centrifuge 1) and Ependorf 5810R (centrifuge 2) centrifuges. Centrifugation solutions were prepared by adding DI water on biomass provided by NREL. The centrifugation was carried out on 3 different times (5 min, 10 min and 20 min) and 4

different g forces (6.57 N, 26.3 N, 105.2 N and 236.7 N) for centrifuge 1 and five different g-forces (6.61 N, 26.5 N, 105.8 N, 238.1 N and 661.5) for centrifuge 2.

The results of the centrifugation are presented as the ratio of volume of centrifuged pellet to the volume of starting slurry (h_c/h_0). The assumption is all the soluble molecules (sugars and salt) are present on supernatant and all the suspended biomasses are present on precipitate or pellet. The following figures summarize the entire centrifugation.

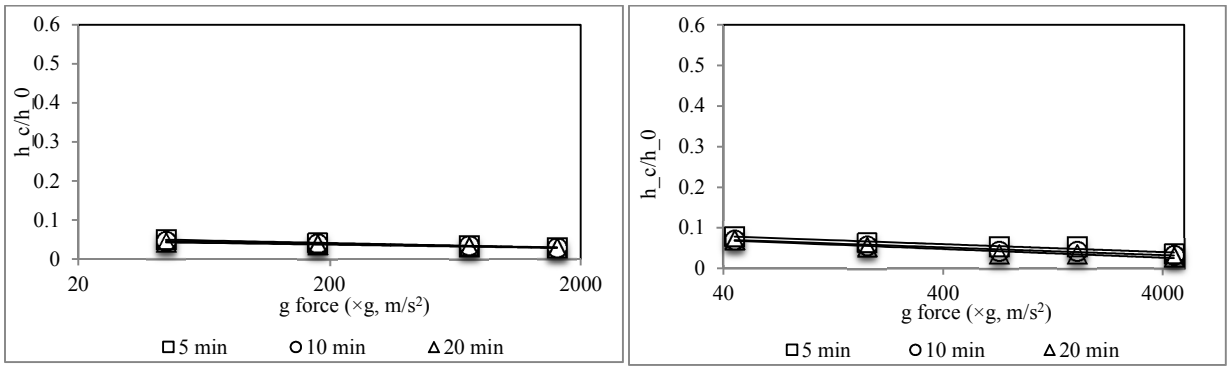

(a) (b)

Figure 5.18 – Centrifugation results of solutions with 1% fraction insoluble solids with (a) centrifuge 1 and (b) centrifuge 2. The straight lines represent logarithmic fits.

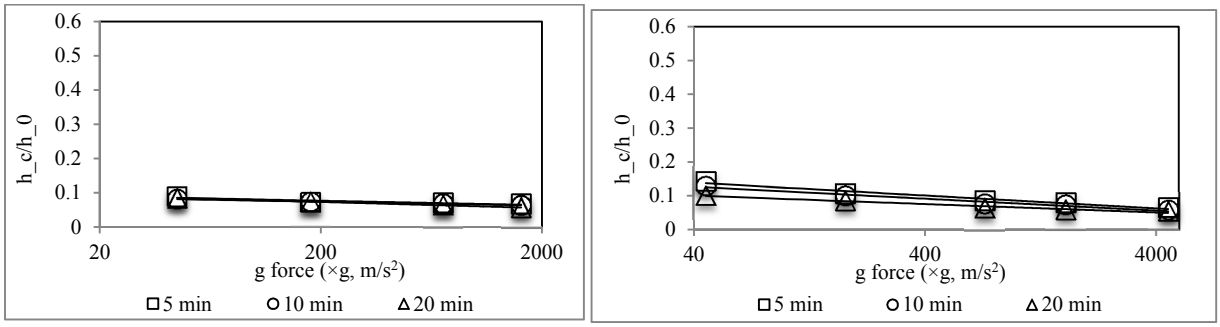

(a) (b)

Figure 5.19 – Centrifugation results of solutions with 2% fraction insoluble solids with (a) centrifuge 1 and (b) centrifuge 2. The straight lines represent logarithmic fits.

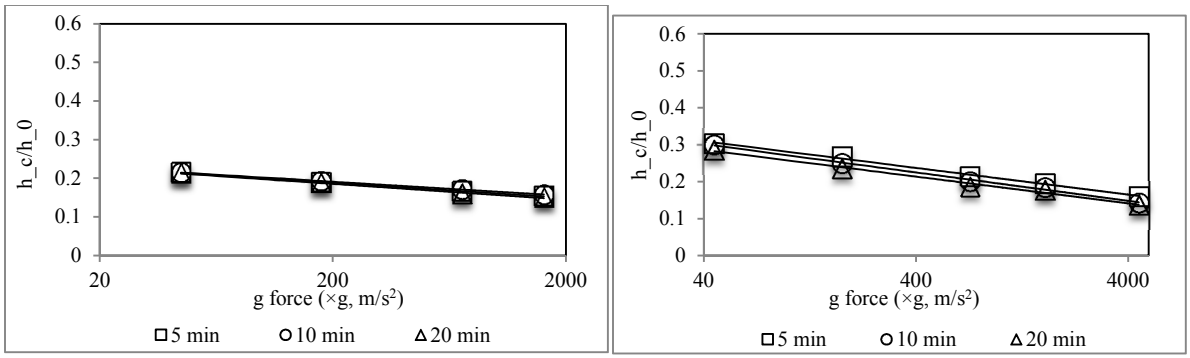

(a) (b)

Figure 5.20 – Centrifugation results of solutions with 5% fraction insoluble solids with (a) centrifuge 1 and (b) centrifuge 2. The straight lines represent logarithmic fits.

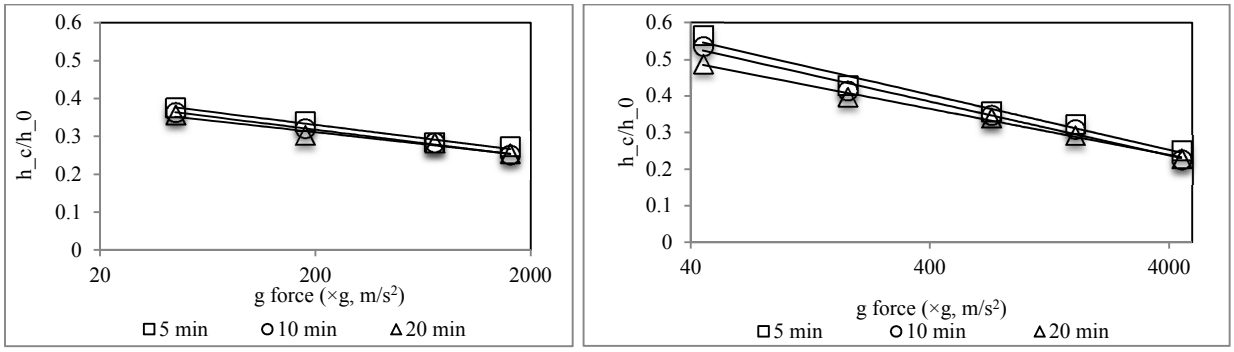

(a) (b)

Figure 5.21 – Centrifugation results of solutions with 10% fraction insoluble solids with (a) centrifuge 1 and (b) centrifuge 2. The straight lines represent logarithmic fits.

When 1% suspended solids are on the solution, the sedimentation is quick and the pellets are compact with moderate force applied. Increased time of centrifugation and and increased force won't significantly increase the sedimentation. When 2% fraction insoluble solids are on the solution, the sedimentation rate slows down and keeps on slowing down more up until 10 % FIS. The overall sedimentation doesn't become more efficient with time; however, the increasing force would make the sedimentation more effective by forming compact pellets. The rate of compaction with force is higher in the slurry with higher FIS than in the slurry with lower FIS.

5.7.3 Operation and modification of experimental set up

We had several problems with the Seepex recirculation pump. The high hardness NBR stator elastomer delivered with the pump was not compatible pumping water or dilute insoluble solids. A second stator using EPDM was able to pump water without damage, but the small slurry particles caused failure after only 60 hours operation. A softer version of the original NBR stator was used successfully for this experiment.

We had several problems with the Seepex recirculation pump. The high hardness NBR stator elastomer delivered with the pump was not compatible pumping water or dilute insoluble solids. A second stator using EPDM was able to pump water without damage, but the small slurry particles caused failure after only 60 hours operation. A softer version of the original NBR stator was used successfully for this experiment.

Because of the presence of a few bigger particles and viscous effect of the slurry, the original needle type backpressure regulator could not control backpressure when slurry was used. This valve was replaced with a notched ball control valve that was able to pass the larger slurry particles and improved performance. However, periodic pressure spikes still continued and the control system was programmed to twitch open the valve momentarily to clear blockages. This is likely caused by the scale-down of this system and we believe this problem would not be present at a larger scale.

We also had some early problems mixing the biomass feed and feeding it to the bioreactor vessel. The tubes were of small diameter (1.05 mm) and peristaltic pumps attached to the bioreactors are of fixed rpm. Biomass settled inside the tubes at times and twice in the earlier experiments the tubes got completely clogged and flow was obstructed. We changed the impeller, made the feeding vessel bigger and started suction of the biomass from the bottom of

the vessel. This solved the problem and this also helped us provide the feed with fixed FIS to the bioreactor all the time.

Once during the experiment, the transmembrane pressure was so high that it shut down the pump and hence the membrane separation. This made us consider a cleaning protocol of the membrane module while running the experiment. For that matter, just like in industrial application, we will be running two membrane modules in parallel so that we can clean once in 24 h by switching back and forth between the modules.

Another issue that we dealt with for this experimental run is enzymes: (i) binding of enzymes with biomass is incomplete and hence passage of enzymes with the permeate and (ii) inactivity of enzymes over time in the biomass and in the enzyme feed solution. We do not know the actual amount of enzyme that passes through the permeate side, and hence we are currently running some enzyme tests at University of Colorado laboratory. Results from these tests will inform future experiments so better sugar concentration and productivity stability is maintained.

When the input rate is 9 mL/min and the purge rate is 3 mL/min, the theoretical maximum yield in this CSTR is 66.7%. For this experiment involving only one reactor, the total yield was 64.5%. Additional CSTRs in series, fed by the upstream lignin purge stream would increase the overall theoretical yield ceiling. Additionally, if the purge rate is decreased relative to the feed rate, the theoretical yield will increase. However, this will affect other reactor parameters, most importantly FIS. Possible future testing will investigate elevated FIS to test system robustness.

This study suggests that the continuous system, even with total solids loading of 2.5% can compete with a batch system with total solids loading of 10% over the course of four days.

When optimizing the system with higher solids loading, such as 5% FIS, the better enzyme recovery and lower purge rate can achieve much better productivity.

5.7.4 Techno-economic analysis

Techno-economic analysis is based on i) batch production of sugar and ii) continuous production of sugar using continuous enzymatic hydrolysis. The graphical representation of the system is mentioned in Figure 5.2. The following table illustrates the major cost inputs of techno-economic analysis for CEH system.

Table 5-11 – Cost inputs

cost inputs		
heating efficiency (CSTR)	0.3	(unitless)
cellulase	3	$/kg
water	0.75	$/1000 gal
biomass	0.01	$/kg
electricity	87.6	$/MWh
operation hours	8760	h/yr
fraction of hours actually operated	0.833333333	(unitless)
interest rate	0.06	
term length	20	y
membrane	50	$/m2
pump (total isntallation)	2689	$/ unit of 2 gpm capacity
pump scaling factor	0.67	
efficiency of the pump	0.15	

5.7.5 Supplemental information source key

[1]M.J. Serapiglia, M.C. Humiston, H.W. Xu, D.A. Hogsett, R.M. de Orduna, A.J. Stipanovic, L.B. Smart, Enzymatic saccharification of shrub willow genotypes with differing biomass composition for biofuel production, Front Plant Sci, 4 (2013).

[2]A.M. Uhl, R.M. Daniel, The first description of an archaeal hemicellulase: the xylanase from Thermococcus zilligii strain AN1, Extremophiles, 3 (1999) 263-267.
[3]Glucosidase, Beta, Worthington Biochemical Corportaion, 730 Vassar Ave., Lakewood, NJ 08701.

Chapter 6 Membrane-enabled optimized continuous enzymatic saccharification

(Under preparation, Advances in Bioscience and Biotechnology)

Abstract

Batch enzymatic hydrolysis of lignocellulosic biomass to fungible sugars loses efficiency because the product sugars inhibit the reaction. We successfully designed and ran membrane-enabled, continuous enzymatic hydrolysis with biomass slurries of 2.5% and 5% fraction insoluble solids (FIS). The goal of continuously feeding the biomass, water and enzymes to the reactor and continuously removing the sugar and water in the membrane permeate, while continuously withdrawing lignin and unreacted cellulosics from the reactor were achieved. The figures-of-merit (permeance decline and membrane cleaning efficacy) for a crossflow, tubular membrane were studied. The membrane process metrics did not vary significantly when increasing FIS from 2.5% to 5%.

6.1 Introduction

Lignocellulosic biomass is a prominent renewable fuel source that has been investigated in the past three decades mainly due to the potential use of carbohydrates and lignin as sustainable sources of bioethanol or bioproducts precursors in a biorefinery concept. As opposed to synthetic chemicals and fossil fuels, these polymers are readily renewable, inexpensive, and environmentally benign. Interestingly, the systematic exploitation of this vast resource is still in its infancy, though periodically stimulated by rising fuel prices [1]. Lignocellulosic biomass is the most abundant organic polymer in the world and biomass, such as, switch grasses, and agricultural, domestic and municipal waste products, which would otherwise go unused [2], are

abundantly available as a local source in the many different parts of the world. Today, the total primary energy supply (TPES) gap between renewables and fossil fuels is too wide to close, and there is no readily deployable energy generation technology that can provide the necessary replacement base load to stabilize the intermittency of renewable energy generation [3]. Thus, conversion of abundant lignocellulosic biomass to a variety of fuels presents a possible option for improving energy security and reducing greenhouse emissions [4].

Lignocellulosic biomass is a complex biopolymer that is primarily composed of cellulose, hemicellulose, and lignin [5]. Lignocellulose can be hydrolytically broken down into simple sugars either enzymatically by a highly specialized enzyme mixture called cellulase at pH ~5 and temperature of ~50 °C or chemically by sulfuric or other strong acids [6]. The enzymatic hydrolysis process is one of the key steps in second-generation biofuel production [7] because it requires less energy and mild conditions, with fewer downstream fermentation inhibitor products being generated. In comparison to other methods of hydrolysis, enzymatic hydrolysis is less corrosive and the products formed are usually monomeric sugars such as glucose [8]. Enzymatic deconstruction of lignocellulose is complex because numerous structural features make it very recalcitrant. In addition to the complex network formed by cellulose, hemicellulose and lignin, some enzymes can be absorbed by condensed lignin that decrease the hydrolysis yield by non-specific linkages of these enzymes [9]. Not only that, the currently employed cellulolytic enzyme systems, that include the widely studied *Trichoderma reesei* enzymes, are significantly inhibited by the hydrolysis products cellobiose and glucose. This inhibition retards the overall conversion rate of lignocellulose-to-glucose [10, 11] .

It is shown in chapter 5 that a membrane-enabled, continuous enzymatic hydrolysis (CEH) can provide higher volumetric conversion and lower cost of production, if the overall

fraction insoluble solids in a reactor is maintained ≥ 5%. That study suggested that not only the overall cost of production went down, but the cost of enzymes and net energy cost went down. Our technoeconomic study found that the overall cost of production drops to $0.18 per kg of sugar from $0.24 kg of sugar from batch process.[12] The ezyme cost dropped from $0.03 per kg of product sugar to $0.26 per kg of product sugar. However the membrane-enabled CEH process has several unknown engineering problems that have to be answered before any idea of commercialization is raised [12]. Our earlier studies acknowledged that the increase in fraction insoluble solids (FIS) in lignocellulosic slurry makes the system more difficult to operate due to pump design requirements, and the potential for aggregation at stagnation points and inside the membrane. Thus, this study was directed towards measurement of the membrane filtration behavior with slurries of increasing FIS, as well as, the CEH figures-of-merit with the elevated FIS, and total solids in the reactor.

Several studies have tried using membrane for enzymatic hydrolysis but none of them were able to use membrane as a tool for CEH with continuous biomass flow and recycle.[10, 13] This is because the settling and high viscosity of the slurry makes it extremely difficult to make this work. In addition to that, the properties and behavior of slurries are not totally understood while it moves through the membrane module flow structure. It is not only the cake formation, but also the changing velocity profile for a non-Newtonian rheology slurry. For example, clogging in the inlet header of a multi-tube membrane module was observed during our initial exploratory studies. A photograph in the Supplemental Material shows how that membrane module became clogged. Stated simply, the feed header can act as a filter. This motivated us for further studies on flow of a biomass-like rheological fluid with various hypothetical header configurations. The notion is that flow stagnation points are the likeliest points where particle

aggregation will initiate clogging. We realized that to effectively understand the clogging, it is important to understand how the slurry behaves and moves inside the headers and membrane tubes with various geometrical arrangements, sizes, and composition-dependent rheological properties (i.e., solids content changing down the tube die to filtration). The Supplemental Material presents our initial results along this vein.

6.2 Methods

6.2.1 Continuous enzymatic hydrolysis

The integrated fed-purge-batch reactor and membrane system is presented in Figure 6.1 Two membrane modules of molecular weight cutoff (MWCO) of 100 kDa were obtained from Koch Membrane Systems (Wilmington, MA, USA). These membrane modules contained a single membrane tube with 0.5 inch inside diameter made up of polyvinylidene difluoride (PVDF). A progressive cavity pump Seepex BCSB-05-12 (Bottrop, Germany), a Rosemount 8732 (Shakopee, MN, USA) magnetic flow meter, an automated Fisher V150 (Shakopee, MN, USA) backpressure control valve, two separate Omega Engineering PX309 (Stamford, CT, USA) pressure transducers were all part of the experiment set up that was controlled by Opto22 (Temecula, CA, USA) process automation controller and user interface. Permeate, purge, and feed rates were calculated from container weights measured using Ohaus Adventurer-Pro (Parsippany, NJ, USA) scales with RS-232 interfaces. During the experiments, The hydrolysis reaction vessel was a New Brunswick Scientific (Edison, NJ, USA) BioFlo 3000 bioreactor that helped maintain constant temperature of 50 ºC. pH of 5 was maintained externally by adjusting pH on feed supply. Constant feed, supplemental water and enzymes were fed to the reactor. A constant purge stream out of the bioreactor to maintain a constant volume and prevent build-up of lignin was maintained along with the constant permeate rate, enzymes and water flow rate.

Enzymes for this experiment were a proprietary mixture targeted for cellulosic materials (Cellic CTec2®, Novozymes).

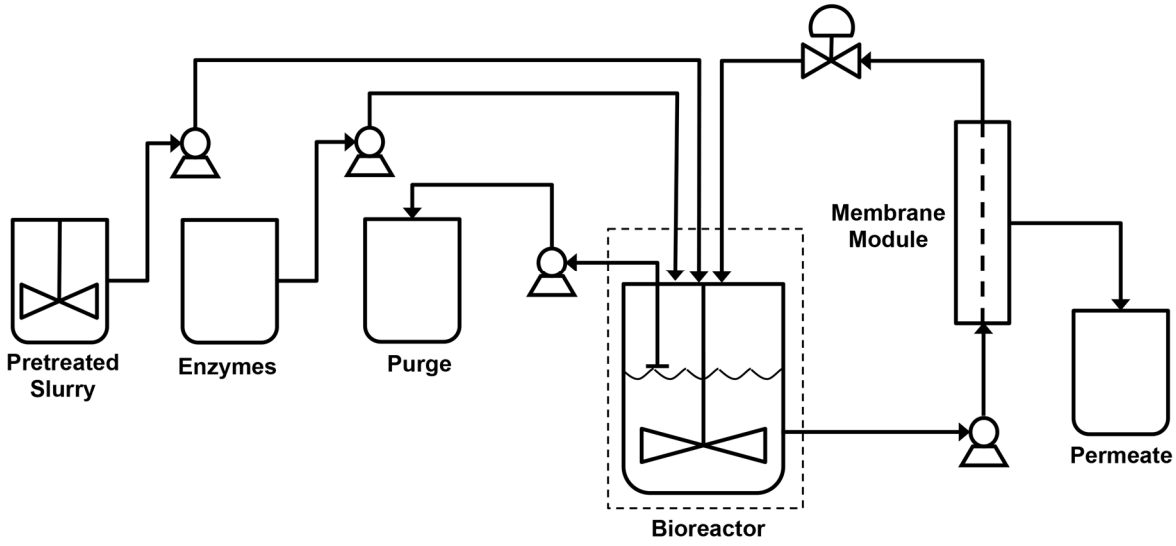

Figure 6.1- Experimental set up of the continuous enzymatic hydrolysis reactor system.

The experimental methodology was such that the total volume was always kept constant, as well as, the fraction insoluble solids (FIS) and the enzyme loading as at 20 mg/g cellulose. After adding the enzymes to the prepared slurry in the reactor, the reactor was run for a certain initial interval without turning on the permeation. After that, the permeation was turned on along with water, enzyme and slurry feeding to the reactor as well as a purge stream out of the reactor. The permeate rate was kept constant and the purge was kept constant as well. During the course of each experiment, membranes were switched after certain period of operation. After switching the membranes, the dirty membrane was cleaned thoroughly with 0.05 M NaOH solution for a certain time interval at constant transmembrane pressure of 8 psi and flowrate of 15 L/min. The pure water permeances of the membrane before and after the cleaning were collected.

A correct model is needed to predict any experimental results on acceptable range. In this study, we modeled the experiments that we were going to run using the kinetic parameters

obtained from the batch experiments and compared the results from the model as forecast with real experimental results.

We are presenting results from three conditions at which the experiments were run listed in Table 6-1. The FIS was increased in two increments from our earlier work up to 5% FIS and then the residence time in the reactor was doubled to expose the membrane-filtration to compositions mimicking greater conversions. As discussed in our earlier publication, we envision the membrane-enabled CEH to consist of (minimally) two CSTRs-in-series, each with an appropriately sized volume and reactor module. Thus, the experiment III brings compositions closer to the second reactor in the series.

Table 6-1 - The experimental parameters of three experiments

Experiment	FIS in the reactor (%)	Volume of the reactor (L)	Permeate rate (mL/min)	Purge rate (mL/min)
I	2.5	3	6	3
II	5	3	6	3
III	5	4.5	4.5	2.3

6.3 Results and discussion

6.3.1 Batch experiments to determine kinetic parameters

Two biomass feedstocks were used for these experiments: feedstock 1 and feedstock 2. These two feedstocks were prepared using the pretreated corn stover feedstocks at different times.[14] Feedstock 2 seemed slightly coarser than Feedstock 1. Total solids were determined by thermo-gravimetric analysis (TGA) using an infrared drying balance. The fraction of insoluble solids (FIS) was determined by further measuring the soluble solids in the separated

liquor and a mass-balance calculation [15]. The following table tabulates the major contents of feedstock:

Table 6-2 – Biomass feedstock characteristics

	feedstock 1	feedstock 2
fraction (mass) total solids in slurry	0.301	0.389
fraction (mass) insoluble solids in slurry	0.173	0.201
density of liquid phase, g/mL	1.08	1.08
soluble sugar concentration, g/mL	139	182
soluble other species, g/L	22	33
mass fraction of suspended solids as lignin	0.3	0.27
as ash	0.04	0.024
as polysaccharide	0.64	0.65
as other	0.02	0.05
pH	1.7	1.6

Enzymatic hydrolysis of lignocellulosic biomass is a product inhibitive process.[16] Depending upon the overall properties and content of the slurry, the kinetics they show during the hydrolysis might be different. It is now widely accepted that the enzymatic hydrolysis follows Michaelis-Menten kinetics of product inhibition.[10, 11] Thus, two get the kinetic parameters, two separate batch experiments for above 100 h were done. These Michaelis-Menten kinetic parameters were used to model the CEH experiments.

Table 6-3 – Michelis-Menten parameters of two biomass feedstocks

parameter	unit	biomass type 1	biomass type 2
Kcat	s^{-1}	0.0035	0.0032
Km	g/L	6.8	8.2
Ki	g/L	6	6.1

6.3.2 Continuous enzymatic hydrolysis

6.3.2.1 2.5% FIS

First two continuous enzymatic hydrolysis experiments were done using Feedstock 1 and the last experiment was done using Feedstock 2. During all three experiments, a batch mode was applied for the first 18 hours before they turned into continuous mode. All three CEH experiments were done using same slurry recirculation rate of 2 L/min.

6.3.2.1.1 Achieving the steady state in terms of sugar concentration and fraction insoluble solids

Figure 6.2 shows the sugar content and fraction insoluble solids (FIS) in the reactor during the entire course of the experiment. Because the feed biomass was not washed, there was some amount of glucose and a significant amount of xylose already present along with other minor soluble/insoluble components in different proportions. The glucose content in the reactor increased rapidly in the beginning and reached a value of ~12 g/L in the first 18 h of batch reaction. When the continuous permeation, purge, and feed (biomass, enzyme, water, and buffer) started at the end of the 18th h, the sugar content started decreasing and the FIS level started increasing steadily in the reactor. The sugar concentration slowly declined up until a mechanical interruption at around the 78th h, after which the system was restarted. The sugar concentration increased again after the addition of 2 mL of enzymes as make-up for the enzyme lost in the

continuous purge. After that, the sugar content remained constant up until the end of the experiment.

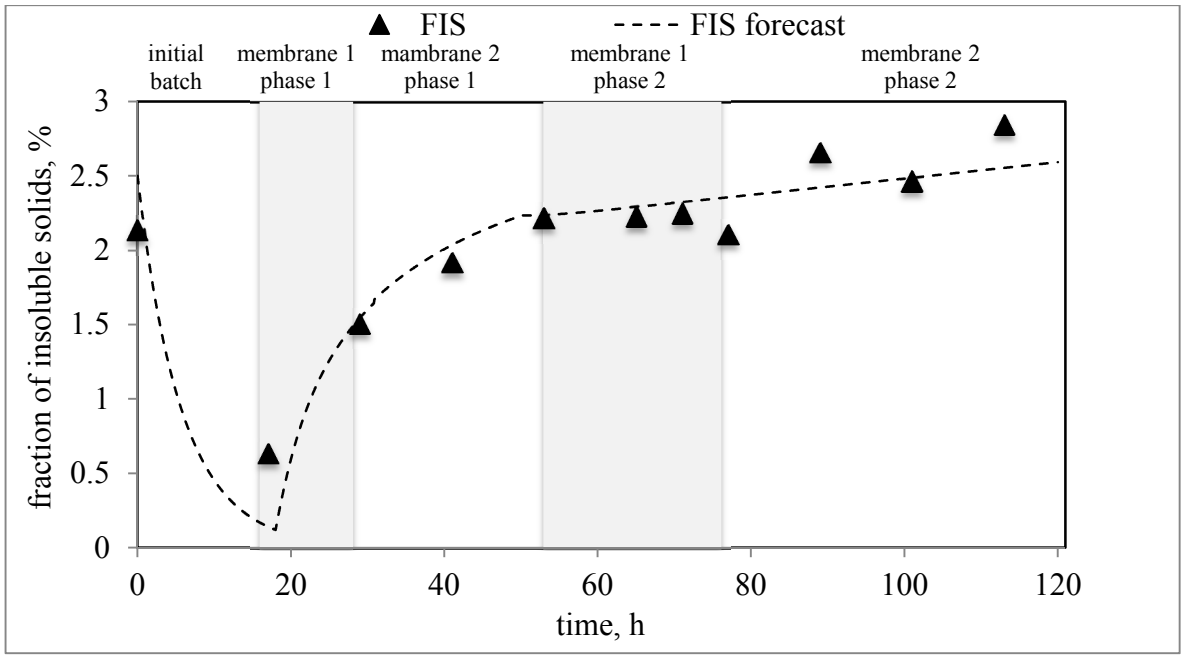

(a)

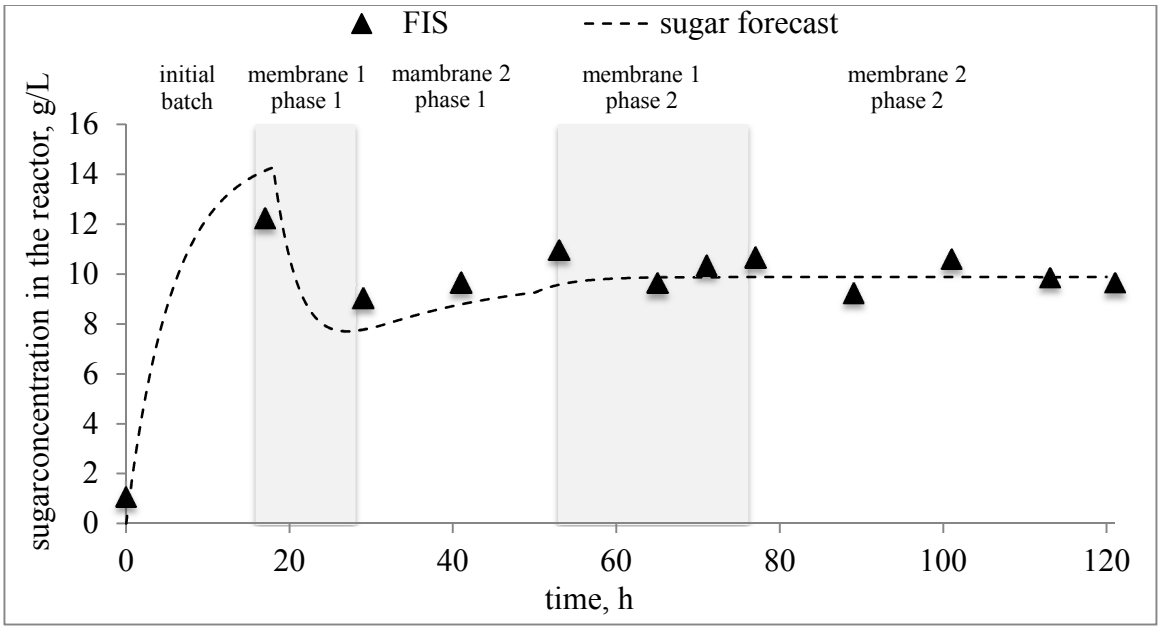

Figure 6.2. (a) FIS profile in the reactor and (b) the sugar concentration (forecast and experimental)

6.3.2.1.2 Particle size distribution (PSD)

The particle size distribution measurements, at different points of the experiment, were taken using laser diffraction and are presented in Figure 6.3. The particles sizes appeared larger (averaged 1 μm) before the batch phase. After the initial batch phase, the amount of the particles of 0.02 μm went up sharply while decreasing the size of average particles to 0.5 μm. Later the particle sizes for almost all the phases remained pretty constant at ~0.8 μm and the proportion of particles of around 0.02 μm remained higher than at the start of the batch. This suggests that hydrolysis was consistent both in the batch and continuous phases of the experiments and because of the hydrolysis, the bigger particles get smaller and a significant amount of lignin and other undigested biomass of ~0.02 μm were present in the bioreactor at all times.

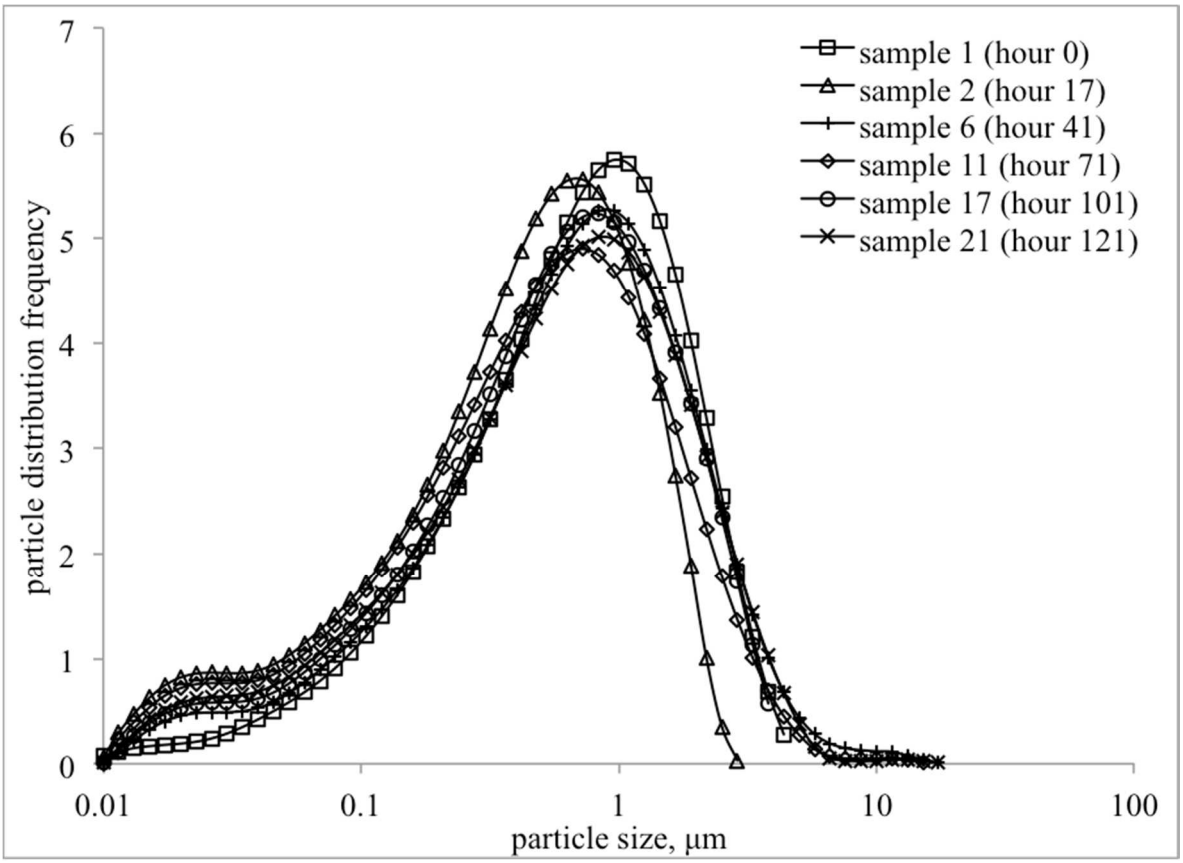

Figure 6.3. Particle size distribution of the particles in the reactor slurry at different point of the experiment.

6.3.2.1.3 Membrane cleaning

The membrane filtration was switched between two membrane modules called membrane 1 and membrane 2. The system was run with membrane 1 for 12 h; and then switched to membrane 2 for a 24 h period; and switched to the cleaned membrane 1 for 24 h; and then switched to the cleaned membrane 2 for the remainder of the experiment. After each period, the membranes were cleaned with a solution of 0.05 M sodium hydroxide (NaOH) at 8 psi transmembrane pressure. The initial permeances (transmembrane pressure-normalized flux, a measure of a membrane's productivity) were measured for each cycle and the permeances were measured after 10 min of cleaning. If the permeance was already within 90% of the initial (clean)

permeance, the cleaning was stopped. If this was not the case, then the cleaning was continued for further 10 min segments until attaining 90% or more of the initial permeance. The following figure illustrates the cleaning during experiment I.

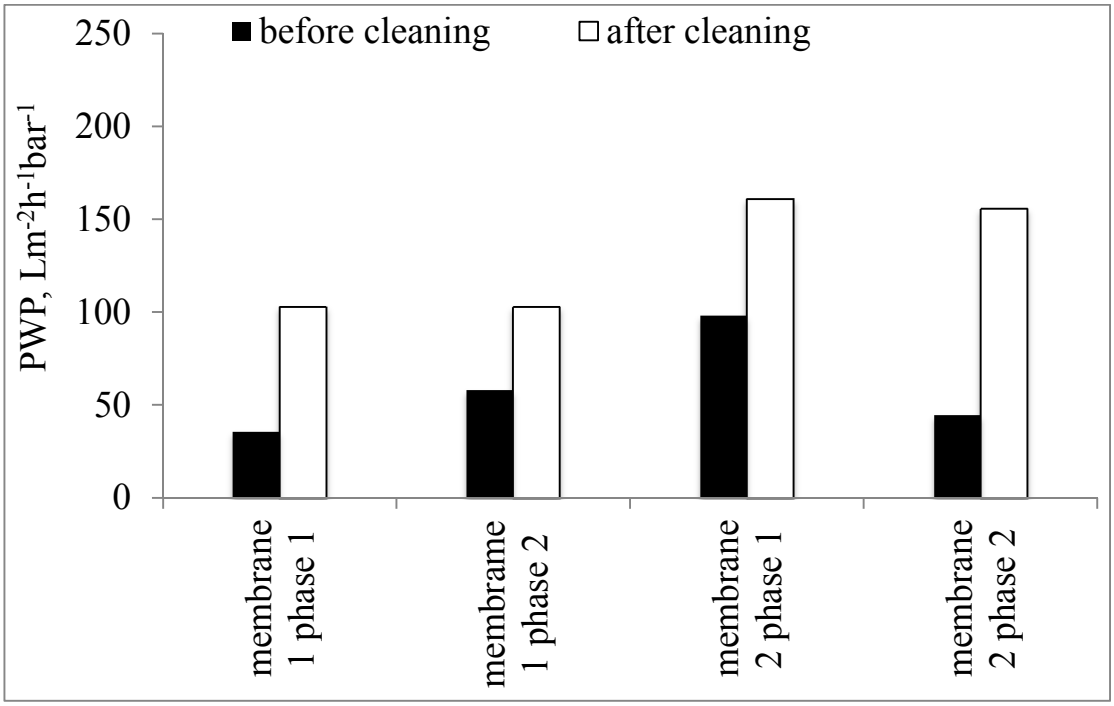

Figure 6.4 – Cleaning of the membrane module. Initial permeance of membrane 1 was 115 $Lm^{-2}h^{-1}bar^{-1}$ and membrane 2 was 175 $Lm^{-2}h^{-1}bar^{-1}$.

Membrane cleaning was very effective and could recover the initial permeances. However, membrane 2 experienced slower recovery on the phase 2. It happened probably because of the pore blockage by the smaller particles and that could lead membrane to potentially irreversible blockage. At the later phase of the experiment, overall particle size decreased in comparison to the feed slurry and the proportionate presence of smaller particles of range 0.01-0.02 μm was much higher. The longer the operation, the longer the time required for the cleaning. This suggests that the time of operation between cleaning cycles is important to minimize the cleaning cost.

6.3.2.1.4 Membrane fouling study

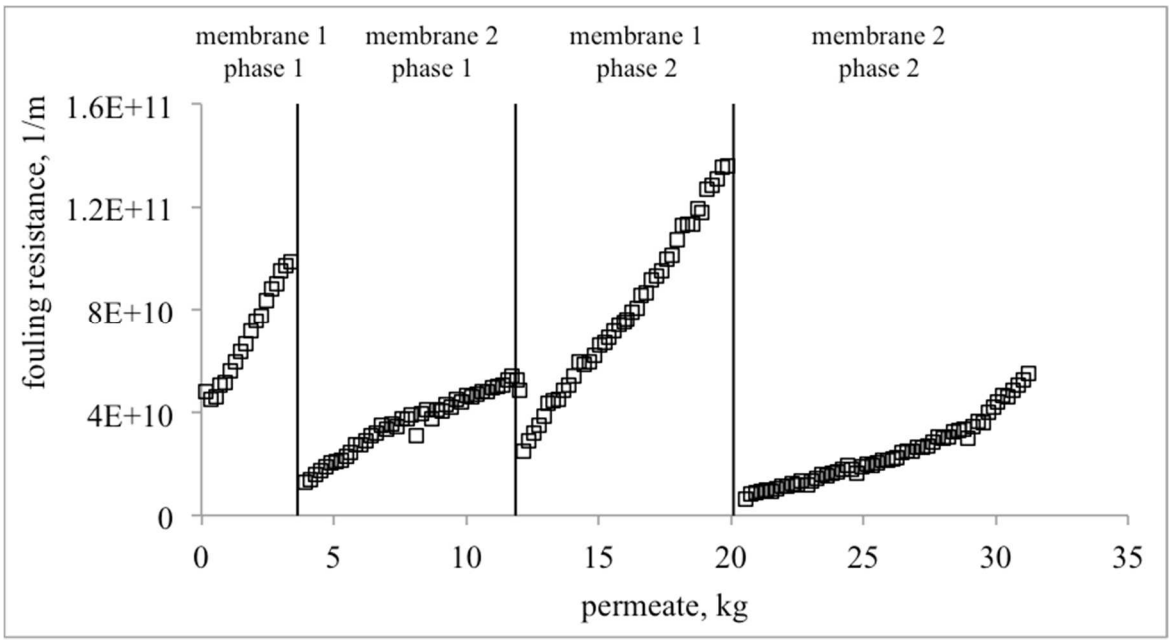

Figure 6.5 – Increasing filtration resistance observed with membranes 1 and 2 during the phases of the experiment. The resistance shown here is overall resistance minus pure membrane resistance.

While operating the membrane filtration in a condition that contains particles of different physico-chemical characteristics, the main obstacle for a continuous operation is understanding and forecasting the increase in filtration resistance (aka fouling), which must inevitably occur. Both insoluble and soluble solids influence the overall resistance of the membrane. Formation of cake layer and the osmotic potential of the slurry contribute the most. Also, because of the polydisperse nature of the slurry, some particles enter (and become lodged) in the internal pore structure. These can permanently form an irreversible blockage of the membrane pores.

The overall resistance observed was higher in the membrane 1 than in the membrane 2 and the early phases had higher cake resistance versus the latter ones. As seen in the particle size distribution results, the feed slurry and early phases were richer in bigger particles, while the middle and late phases were richer in smaller particles. The increment in the fouling resistance in

the later phase with membrane 2 could be because of the presence of higher amount of smaller particles that could form a denser deposition layer, as well as, be entering into the membrane pores to form irreversible blockages. The longer time taken for the cleaning also suggests that something more happened than just the cake build-up on the membrane surface. The cleaning time has been tabulated in the following table:

Table 6-4 – Time required for membrane cleaning during Experiment I

	time (min)
membrane 1 phase 1	10
membrane 2 phase 1	10
membrane 1 phase 2	10
membrane 2 phase 2	50

6.3.2.2 5% FIS

6.3.2.2.1 Achieving the steady state in terms of sugar concentration and fraction insoluble solids

This experiment was also done using feedstock 1. Figure 6.6 shows (a) the sugar content and (b) fraction insoluble solids (FIS) in the reactor during the course of the experiment. The glucose content in the reactor increased rapidly in the beginning and reached a value of ~25 g/L in first 18h. When the permeation, purge, biomass feed, enzyme, water and buffer started at the top of the 18th hour, the sugar content started decreasing and the FIS started increasing steadily. After that, the sugar content remained steady while FIS increased up until the end of the experiment.

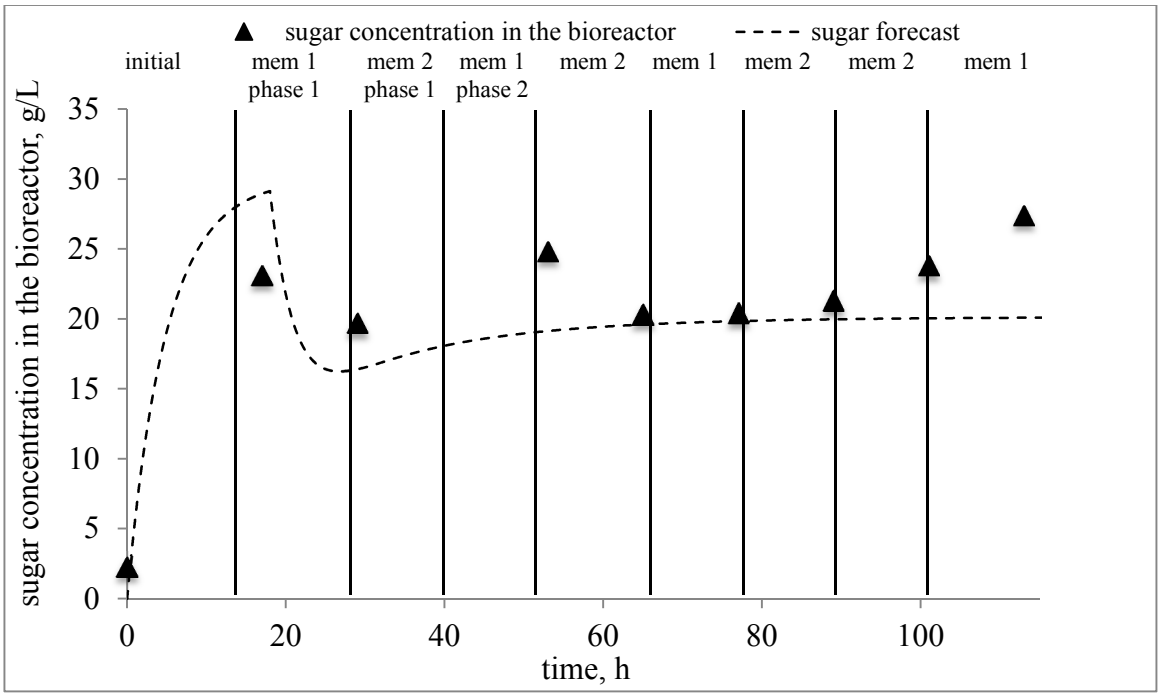

(a)

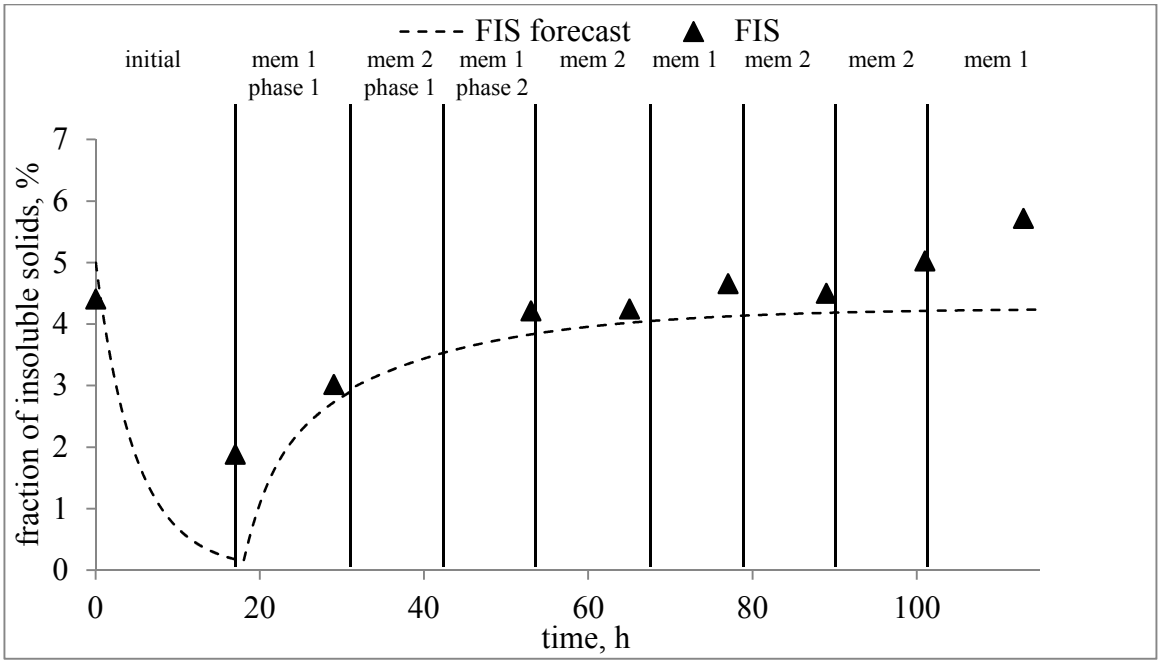

(b)

Figure 6.6 - (a)The sugar concentration (forecast and experimental) and (b)FIS profile in the reactor. The steady state FIS is 5% (mem refers to membrane).

6.3.2.2.2 Membrane cleaning

Again the membrane filtration was switched between two membrane modules: membrane 1 and 2. The system was run with membrane 1 for 12 h; then switched to membrane 2 for 12 h; then switched to the clean membrane 1 again; and this switching continued every 12 h until the end of the experiment. After each period, the membranes were cleaned with a solution of 0.05 M sodium hydroxide (NaOH) at 8 psi transmembrane pressure. The initial permeances were measured for each period and the permeances were measured after 30 min of cleaning. This cleaning turned out to be more effective because of the fixed run time and constant method of cleaning throughout the experiment. The following is the cleaning data.

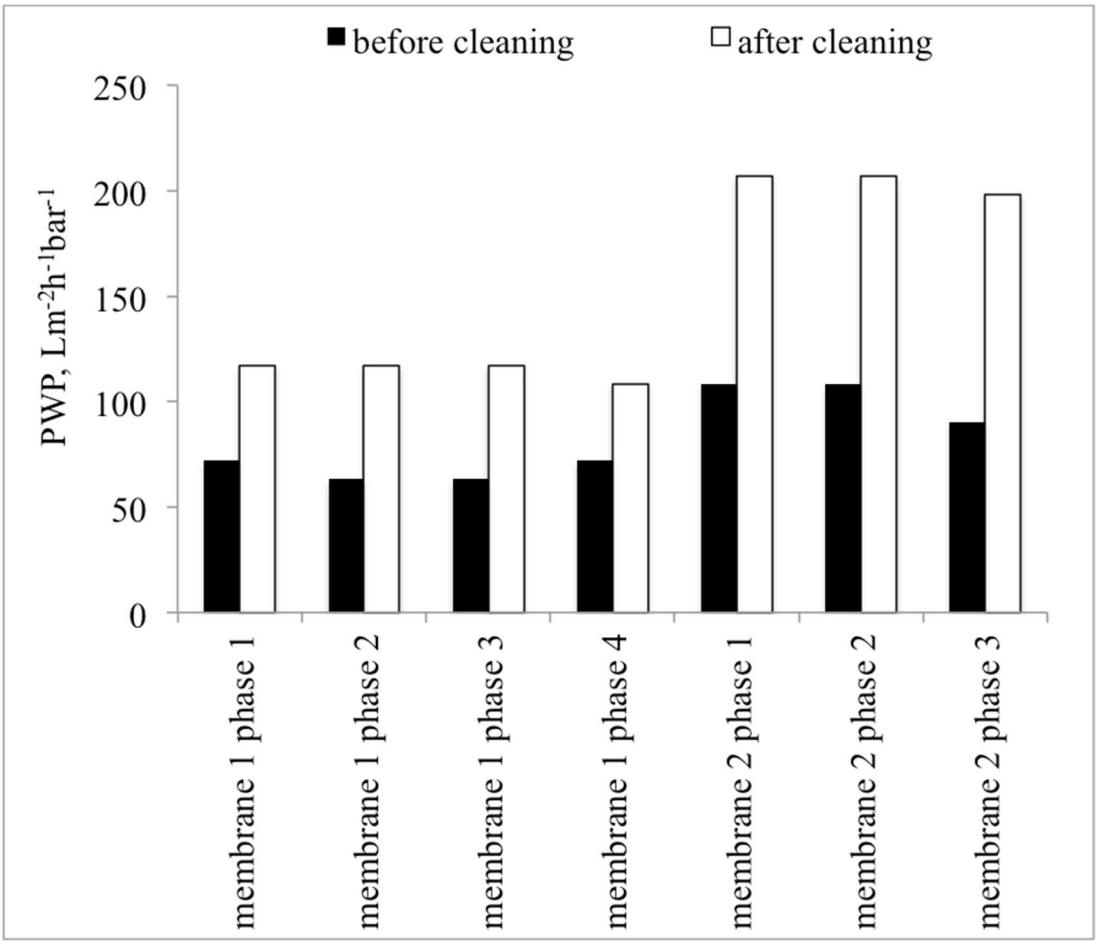

Figure 6.7 - Cleaning of the membrane module.

6.3.2.2.3 Membrane fouling study

Figure 6.8 below represents the overall fouling resistance of membranes 1 and 2 observed during the experiment.

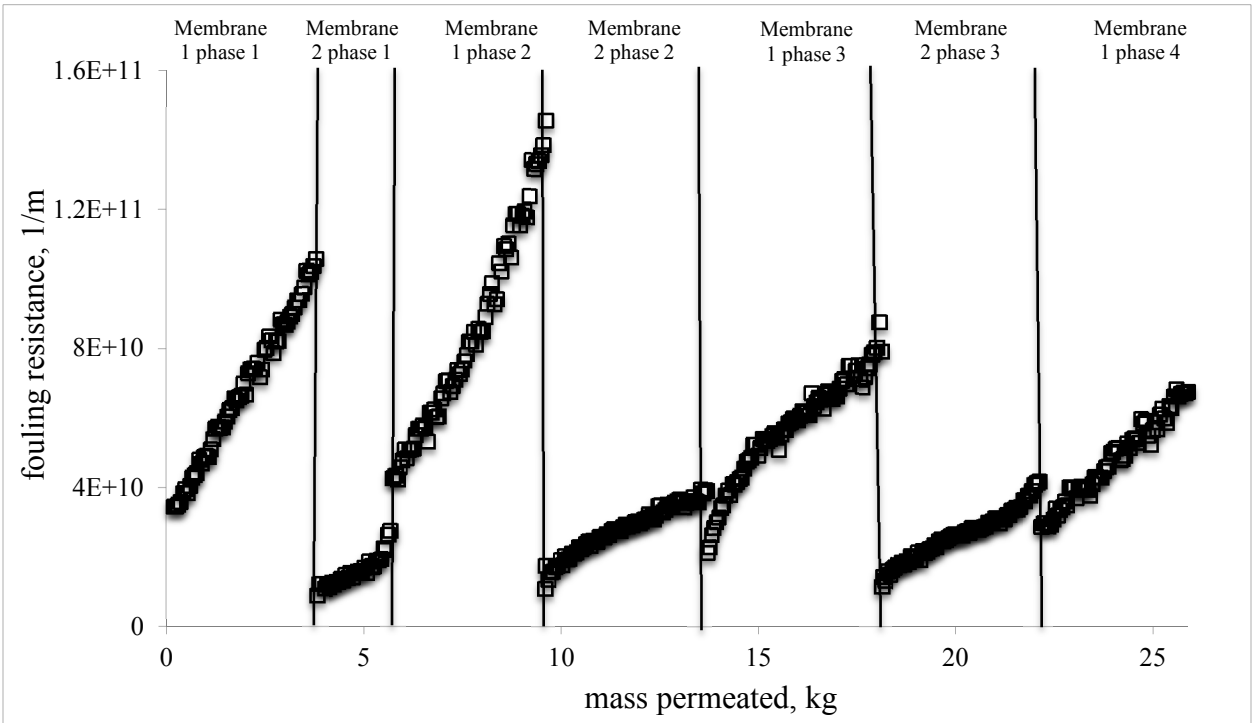

Figure 6.8 - Fouling resistance observed on membrane 1 and membrane 2 at different phases of the experiment. The resistance shown here is overall resistance minus pure membrane resistance.

6.3.2.3 5% FIS at doubled residence time

The double residence time in comparison to past two experiments was achieved by elevating the feed volume to 4.5 L and input biomass and water rate to 6.75 mL/min. The permeate rate of 4.5 mL/min and purge rate of 2.25 mL/min were maintained. The FIS was targeted to achieve at 5% at the steady state. Additionally, this experiment was performed with Feedstock 2 that had slightly different starting characteristics than Feedstock 1 in terms of total solids and sugar content in the starting slurry.

6.3.2.3.1 Achieving the steady state in terms of sugar concentration and fraction insoluble solids

The experiment was designed to achieve a steady state at later hours of the experiment (after 60th hour of experiment time). Because of the initial batch phase, the sugar concentration went up. When the permeation started, the sugar concentration went down sharply but after that, it slowly elevated to achieve the steady state after the 60th hour of the experiment. FIS, however, decreased due to the initial batch phase and then, slowly increased to gain close to steady state after 50th hour of the experiment.

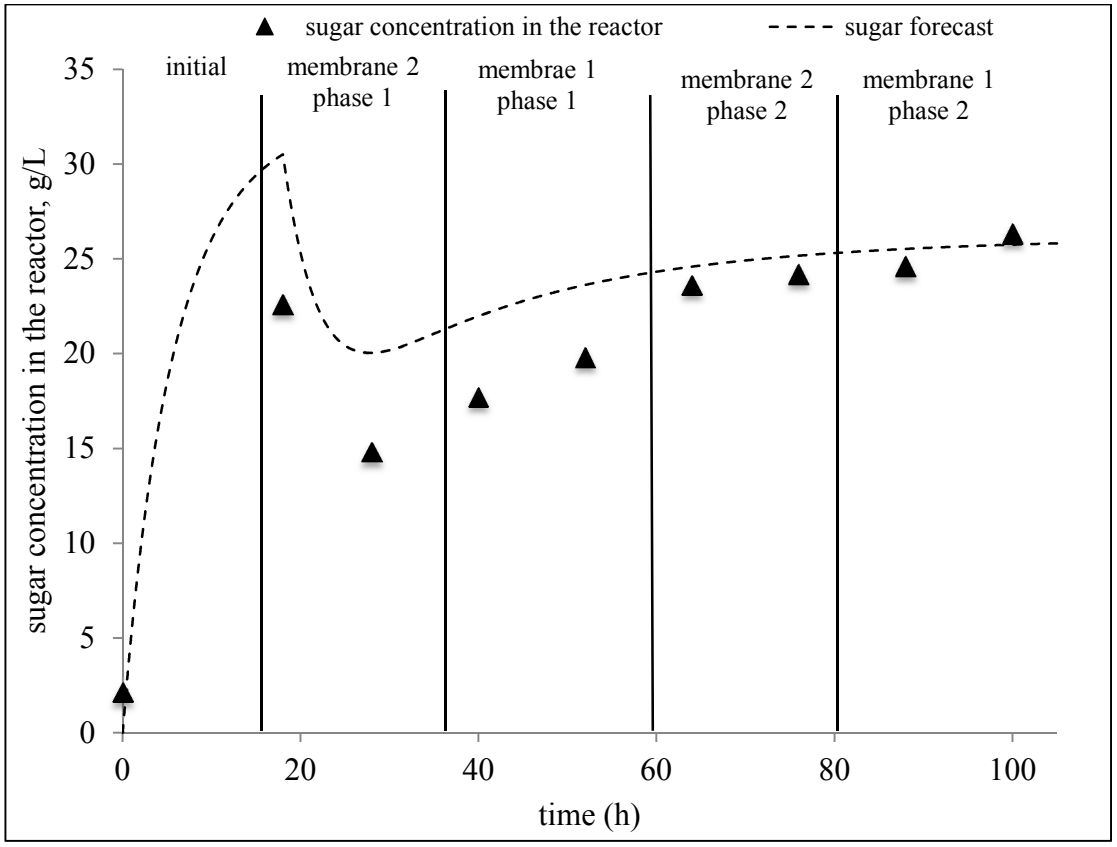

(a)

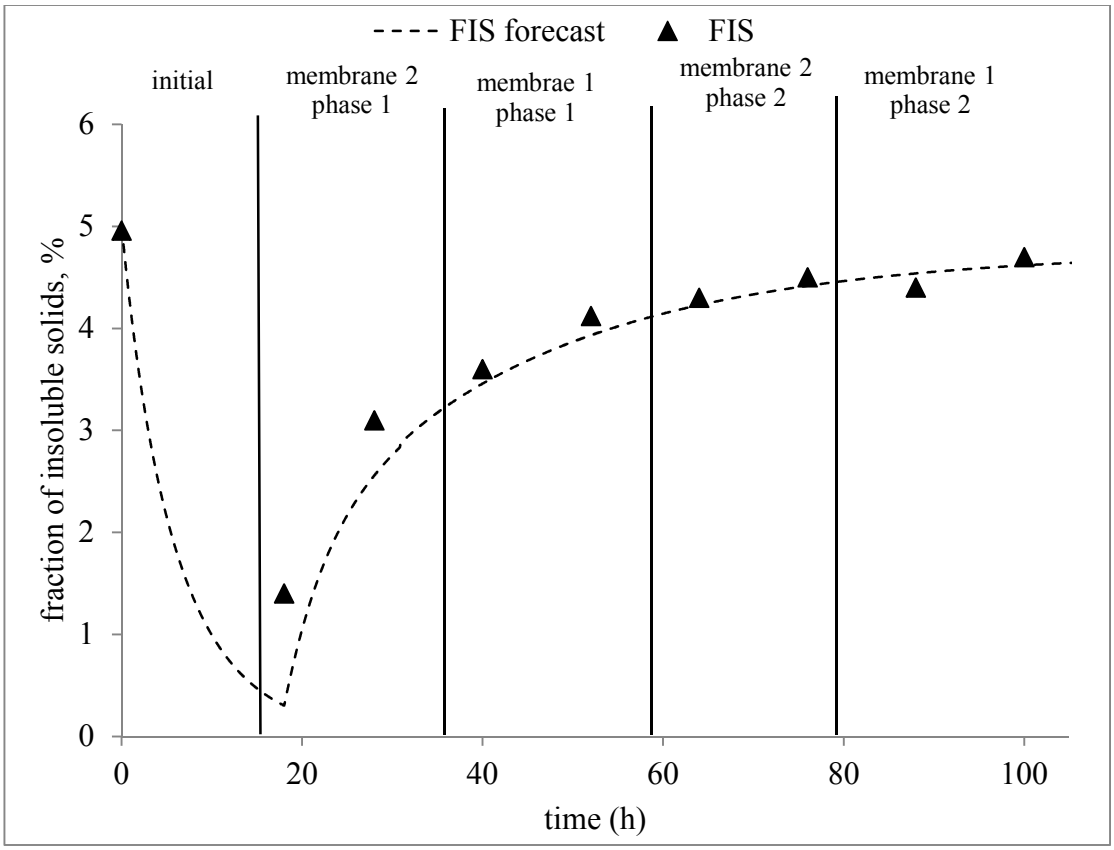

(b)

Figure 6.9. (a) The sugar concentration profile (forecast and experimental) and (b) FIS profile (forecast and experimental) in the reactor. The steady state FIS is 5%.

6.3.2.3.2 Membrane fouling resistance

Figure 6.10 below presents the overall fouling resistance observed during the experiment on membranes 1 and 2. The residence time was double than the previous experiments and that means, the biomass had double the time for the hydrolysis to take place. The feed rate was provided to the reactor in such a way that it was always trying to go higher in overall FIS in the reactor.

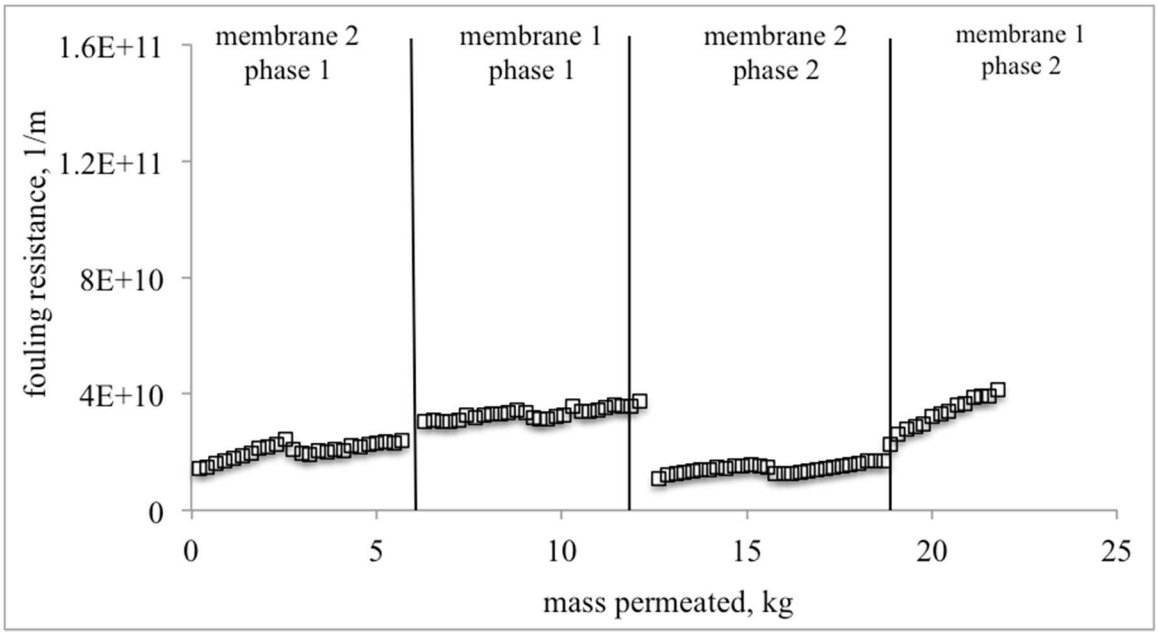

Figure 6.10 – Fouling resistance observed with membranes 1 and 2 during the different phases of the experiment. The resistance shown here is overall resistance minus pure membrane resistance.

The nature of fouling resistance seen here is lower and different than what it was observed during earlier two experiments. All the pores where irreversible blockage could happen might have happened in earlier two experiments. Because of longer residence time, the concentration of hydrophobic lignin particles and other rigid smaller particles dominated the nature of the slurry. As a result, membrane surface came in contact with lesser number of particles in comparison to the earlier experiments and lower membrane resistance was observed throughout the experiment for both the membrane modules.

6.3.2.3.3 Membrane Cleaning

We switched membrane modules once in 24 h time and that's when the membrane was cleaned with basic solution (0.05 M NaOH) for 30 min. It took approximately 5 minutes in switching from one membrane module to another. Membrane 1 and 2 behaved similarly the way

it did for the earlier two experiments and it proves that the membrane's properties can be regenerated if cleaned properly. The following Figure 6.11 illustrates the cleaning efficacy.

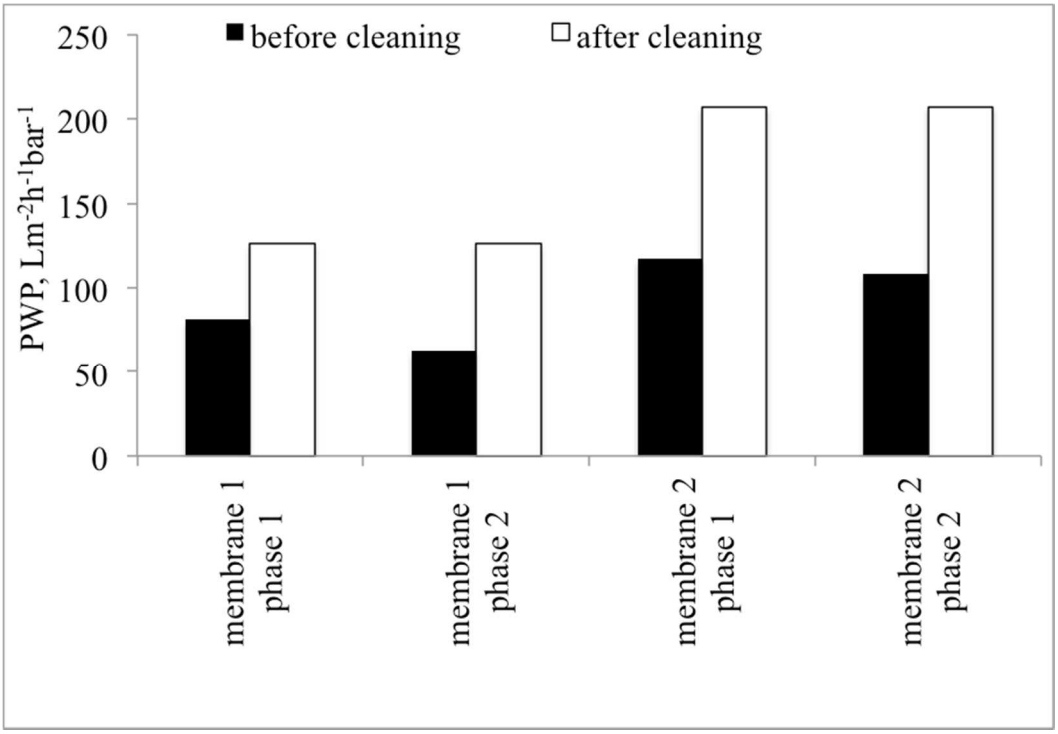

Figure 6.11 – Cleaning of the membrane module for experiment III.

6.4 Perspectives

Continuous enzymatic hydrolysis is advantageous over the current state of art batch hydrolysis because the overall cost of production for continuous enzymatic hydrolysis is lower than the batch hydrolysis. Our technoeconomic study found that the overall cost of production drops to $0.18 per kg of sugar from $0.24 kg of sugar from batch process.[12] It not only decreases the overall production cost, but also the enzyme cost. The primary reason for overall drop in cost of production and enzyme is due to lower energy cost, capital cost and recyclability of enzymes. A comparison between this continuous system and the batch system based on our earlier batch experiments is made in the following table. The overall basis of ths comparison is

the volume of the reactor being 3 L with the 2.5% and 5% FIS case. The duration of the batch hydrolysis is 4 d and the total conversion is 95%.

Table 6-5 – Comparison between a CEH and a batch system

basis	batch with biomass 1	batch with biomass 2	CEH (2.5% FIS)	CEH (5.0 % FIS)	CEH (5.0 % FIS) double residence time
enzymes, g	16.9	16.9	12	22.3	11.5
cellulose converted, g	520	498	410	869	536
mg enzymes/g cellulose converted	32.5	32.5	23	25.7	21.5
volume of the reactor, L	14.6	14.6	3	3	4.5
total whole slurry required, kg	4	4	4.6	9.58	4.65
productivity, g/L/h glucose	0.344	0.329	1.31	2.79	1.19

The system with 5% FIS has much higher productivity, 2.79 g/L/h glucose in comparison to the batch system and more than double than that of 2.5%. The system with double the residence time still has about 43% of the productivity although it was operated at the same enzyme loading and elevated total solids.

To better understand why the processes' experienced similar rates of fouling with the lower and higher % solids, we need to acknowledge that the level of shear stress at the membrane/slurry interface during the permeation significantly controls the fouling [17] [18]. Thus, we modeled the flow in the membrane tube for two hypothetical rheologies, which represented 2.5 and 5% solids (See Supplemental Material). These results are presented in Figure 6.12. Our modeling does not consider any change in composition due to permeation because of the low permeation rate of 6 mL/min in comparison to the slurry flow rate of 2 L/min inside the

tube. The velocity profile for both slurries is pretty similar. In addition to that, the shear stress profile for both slurries was similar with the exception of the middle of the tube. The membranes are on the edge of the tube and thus, at given flow rate, the shear rate experienced by the particles are same in both the cases. It implies that the increment in the slurry FIS won't necessarily increase the fouling due to the deposition of particles on the membrane surface if shear-induced diffusion is the dominant back mass transfer mechanism during filtration.

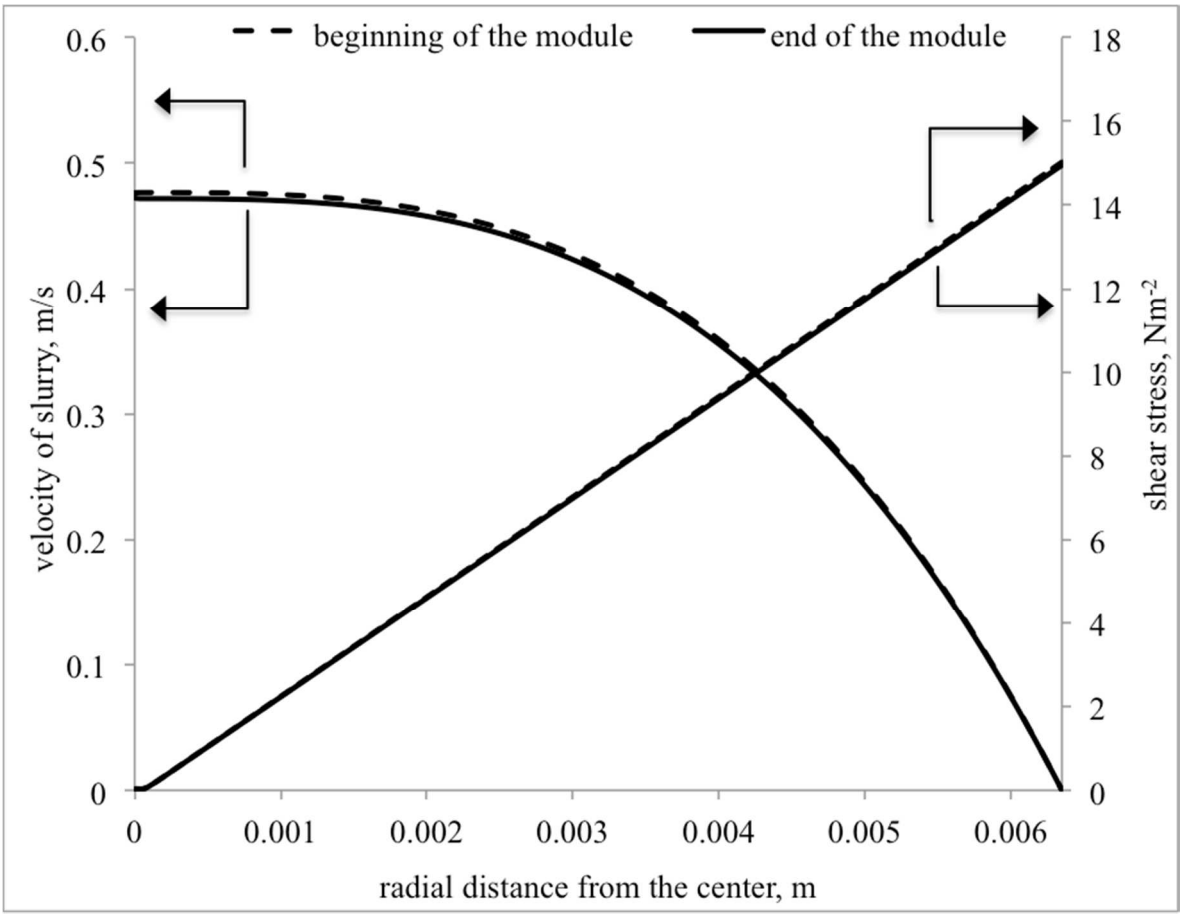

(a)

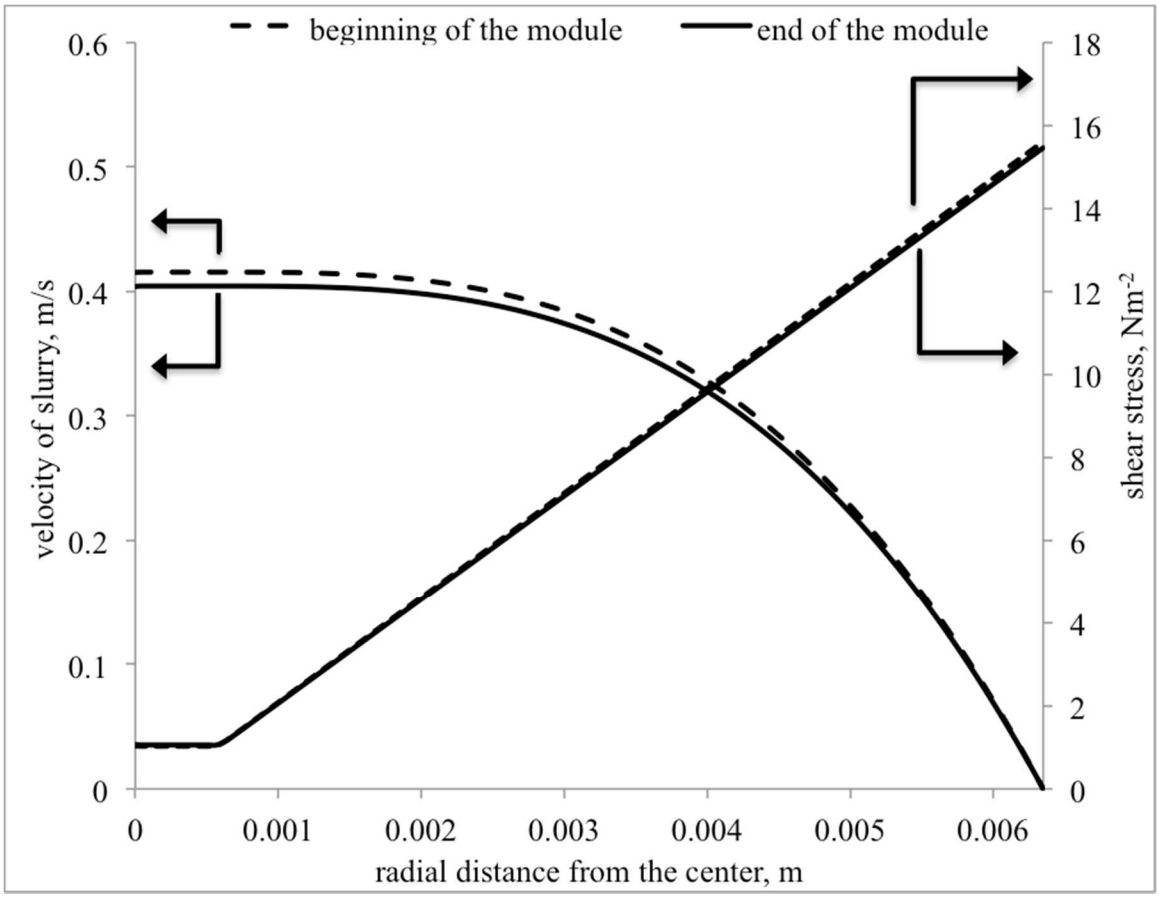

(b)

Figure 6.12 – The velocity profiles and shear stress profiles of a fully developed slurry flow in the beginning and end of a membrane tube (resembling the experiments). The slurry flow rate is 2 LPM and permeate rate is 6 mL/min of (a) 2.5% FIS and (b) 5% FIS.

Lignocellulosic biomass is a complex organic polymer consisting of both hydrophilic material (cellulose) and hydrophobic material (lignin). [19, 20] The PVDF membrane material present in Koch membrane module we used was hydrophilic in nature and thus, any component that is hydrophilic is easily attracted and attached to the surface of the membrane. When the bigger proper biomass particles are present in larger proportion in the reacting slurry, the tendency of attaching them on the membrane surface is higher than when the proportion of lignin and smaller particles are higher than the bigger particles. When the residence time is half, then the bigger particles dominate the slurry and when the residence time is double, smaller particles

and fully hydrophobic lignin dominate the slurry. This variation in slurry property caused the difference in fouling resistance between experiments with 5% FIS and 5% FIS with double the residence time.

6.5 Conclusions

Various aspects of continuous enzymatic hydrolysis were investigated in this study. The continuous enzymatic hydrolysis is superior method of enzymatic hydrolysis than the batch method because of overall lower cost of production and lower enzyme cost. Not only we were successful at running experiments lasting more than hundred hour continuously, we were able understand membrane performances at different slurry conditions created by different FIS in the feed of the slurry and different residence times of the experiments. The membranes used on these applications were able to regenerate their properties after basic cleaning with 0.5 M NaOH solution. Theoretical study suggested that change in FIS doesn't necessarily change the nature of cake formed and we also observed that the change in FIS from 2.5% to 5% did not alter the overall fouling resistance in both of the membrane modules. However, the overall physical properties of the slurry made huge difference in the nature of the cake formed on the membrane surface. When residence time was increased leaving all the parameters constant, the higher hydrolysis caused the biomass particles to get smaller and the slurry became more lignin rich than cellulose rich and became more hydrophobic. This nature translated in the decrement of overall fouling resistance at the time when residence time was doubled.

6.6 Acknowledgments

The authors would like to acknowledge Nathan Crawford, Jim Lisheske, Daniel Schell, Jim McMillan and David Templeton from National Renewable Energy Laboratory. This work was conducted under Department of Energy funding (Contract No. DE-AC36-08-GO28308;

Bioenergy Technologies Office) via NREL and University of Colorado agreement UGA-0-41026-56.

6.7 References

[1] L.A. Lucia, Lignocellulosic Biomass: A Potential Feedstock to Replace Petroleum, Bioresources, 3 (2008) 981-982.
[2] A.S.M. Hussin, S.R.A. Collins, Z. Merali, M.L. Parker, A. Elliston, N. Wellner, K.W. Waldron, Characterisation of lignocellulosic sugars from municipal solid waste residue, Biomass Bioenerg, 51 (2013) 17-25.
[3] M. Melikoglu, Shale gas: Analysis of its role in the global energy market, Renewable & Sustainable Energy Reviews, 37 (2014) 460-468.
[4] C.E. Wyman, Biomass ethanol: Technical progress, opportunities, and commercial challenges, Annu Rev Energ Env, 24 (1999) 189-226.
[5] H.V. Lee, S.B.A. Hamid, S.K. Zain, Conversion of Lignocellulosic Biomass to Nanocellulose: Structure and Chemical Process, Sci World J, (2014).
[6] Z.H. Zhang, B. Liu, Z.B. Zhao, Efficient acid-catalyzed hydrolysis of cellulose in organic electrolyte solutions, Polym Degrad Stabil, 97 (2012) 573-577.
[7] R.M. Prunescu, G. Sin, Dynamic modeling and validation of a lignocellulosic enzymatic hydrolysis process - A demonstration scale study, Bioresource Technology, 150 (2013) 393-403.
[8] Y. Sun, J.Y. Cheng, Hydrolysis of lignocellulosic materials for ethanol production: a review, Bioresource Technology, 83 (2002) 1-11.
[9] C.R. Poovaiah, M. Nageswara-Rao, J.R. Soneji, H.L. Baxter, C.N. Stewart, Altered lignin biosynthesis using biotechnology to improve lignocellulosic biofuel feedstocks, Plant Biotechnol. J., 12 (2014) 1163-1173.
[10] P. Andric, A.S. Meyer, P.A. Jensen, K. Dam-Johansen, Reactor design for minimizing product inhibition during enzymatic lignocellulose hydrolysis II. Quantification of inhibition and suitability of membrane reactors, Biotechnology Advances, 28 (2010) 407-425.
[11] P. Andric, A.S. Meyer, P.A. Jensen, K. Dam-Johansen, Effect and Modeling of Glucose Inhibition and In Situ Glucose Removal During Enzymatic Hydrolysis of Pretreated Wheat Straw, Applied Biochemistry and Biotechnology, 160 (2010) 280-297.
[12] B. Adhikari, D.A. Sievers, J.J. Stickel, J. Pellegrino, Membrane-enabled continuous enzymatic saccharification of lignocellulose, Biochem. Eng. J., 104 (2016) 300-313.
[13] R.N. Gurram, T.J. Menkhaus, Continuous Enzymatic Hydrolysis of Lignocellulosic Biomass with Simultaneous Detoxification and Enzyme Recovery, Applied Biochemistry and Biotechnology, 173 (2014) 1319-1335.
[14] J. Shekiro, E.M. Kuhn, N.J. Nagle, M.P. Tucker, R.T. Elander, D.J. Schell, Characterization of pilot-scale dilute acid pretreatment performance using deacetylated corn stover, Biotechnol Biofuels, 7 (2014).
[15] N.D. Weiss, J.J. Stickel, J.L. Wolfe, Q.A. Nguyen, A Simplified Method for the Measurement of Insoluble Solids in Pretreated Biomass Slurries, Applied Biochemistry and Biotechnology, 162 (2010) 975-987.
[16] S.T. Yang, M.R. Okos, A New Graphical-Method for Determining Parameters in Michaelis Menten-Type Kinetics for Enzymatic Lactose Hydrolysis, Biotechnology and Bioengineering, 34 (1989) 763-773.

[17] H.E. Wray, R.C. Andrews, P.R. Berube, Surface shear stress and membrane fouling when considering natural water matrices, Desalination, 330 (2013) 22-27.
[18] C.C.V. Chan, P.R. Berube, E.R. Hall, Relationship between types of surface shear stress profiles and membrane fouling, Water Res, 45 (2011) 6403-6416.
[19] M.M. Campbell, R.R. Sederoff, Variation in lignin content and composition - Mechanism of control and implications for the genetic improvement of plants, Plant Physiol, 110 (1996) 3-13.
[20] M.J. Selig, L.G. Thygesen, C. Felby, Correlating the ability of lignocellulosic polymers to constrain water with the potential to inhibit cellulose saccharification, Biotechnol Biofuels, 7 (2014).

6.8 Supplementary information

6.8.1 Computational fluid dynamics studies involving lignocellulosic biomass

6.8.1.1 Modeling and conceptualization

For the detailed understanding of slurry behavior inside the membrane module, computational fluid dynamics studies have been found very effective.[1-3] We have chosen OpenFOAM as our modeling tool. OpenFOAM is a freely available open source CFD software package developed by OpenCFD Ltd and ESI Group and distributed by the OpenFOAM Foundation. OpenFOAM has extensive range of features to solve anything from complex fluid flows involving chemical reactions, turbulence and heat transfer, to solid dynamics and electromagnetics.[4] It also includes the tools for meshing. For our work, two solvers are used: 'icoFoam' and 'nonNewtonianIcoFoam'. 'icoFoam' is a solver designed to solve for the system involving incompressible Newtonian fluids in laminar and transient regions and 'nonNewtonianIcoFoam' is a solver designed to solve for the system involving incompressible non-Newtonian fluids in laminar and transient regions as well.

6.8.1.2 Theory

The model calculates the shear stress as a function of shear rate using the following equation:

$$\tau(\gamma) = \tau_y + k\gamma^n \qquad \text{Equation (1)}$$

where τ_y is the shear stress at zero shear rate, also called yield stress, k is a constant parameter, γ is the effective shear rate and n is a dimensionless constant.[2,3,5-11] For a shear thinning fluid, e.g. a lignocellulosic biomass suspension flowing in a circular straight tube, the plugged-flow region (Rp) is defined by [12]

$$R_p = \frac{2\tau_y}{-\frac{dP}{dz}} \qquad \text{Equation (2)}$$

For the shear flow region (the region between r = R and r = Rp), the velocity profile of the fluid is given by

$$u(r) = -\frac{dz}{dP}2k\frac{(-\frac{1}{2}r\frac{dP}{dz} - \tau_y)^{\frac{1}{n}+1}}{\frac{1}{n}+1} + \frac{dz}{dP}2k\frac{(-\frac{1}{2}R\frac{dP}{dz} - \tau_y)^{\frac{1}{n}+1}}{\frac{1}{n}+1} \qquad \text{Equation (3)}$$

For the region between $r = Rp$ and $r = 0$, the velocity remains constant. Thus,

$$u(r) = -\frac{dz}{dP}2k\frac{(-\frac{1}{2}R_p\frac{dP}{dz} - \tau_y)^{\frac{1}{n}+1}}{\frac{1}{n}+1} + \frac{dz}{dP}2k\frac{(-\frac{1}{2}R\frac{dP}{dz} - \tau_y)^{\frac{1}{n}+1}}{\frac{1}{n}+1} \qquad \text{Equation (4)}$$

where

τ_y is yield stress and *k* is Herschel-Bulkley constant and n is a constant commonly called as fluid index parameter.

For laminar flow, Chilton and Stansby formulated an equation to calculate the pressure drop along a concentric tube with constant radius.[13] The equation requires an iterative solution to extract the pressure drop.

The equation is as follows:

$$\frac{\Delta P}{l} = \frac{4K}{d}\left(\frac{8v_{avg}}{d}\right)^n \left(\frac{3n+1}{4n}\right)^n \frac{1}{1-X}\left(\frac{1}{1-aX-cX^3-bX^2}\right)^n \qquad \text{Equation (5)}$$

where v_{avg} is the average velocity of fluid in the tube, *d* is the diameter of the tube, *K* is the Herschel-Bulkley constant, *l* is the length of the tube, *n* is the Herschel-Bulkley parameter with no units and $X = \frac{4l\tau_y}{d\Delta P}$, $a = \frac{1}{2n+1}$, $b = \frac{2n}{(2n+1)(n+1)}$ and $c = \frac{2n^2}{(2n+1)(n+1)}$.

The major input for CFD calculations is viscosity. Knowing shear stress from shear rate, the viscosity can be calculated from the Figure 6.13.[14] The data obtained deduced to following table that are the inputs to the *nonNewtonianIcoFoam* solver.

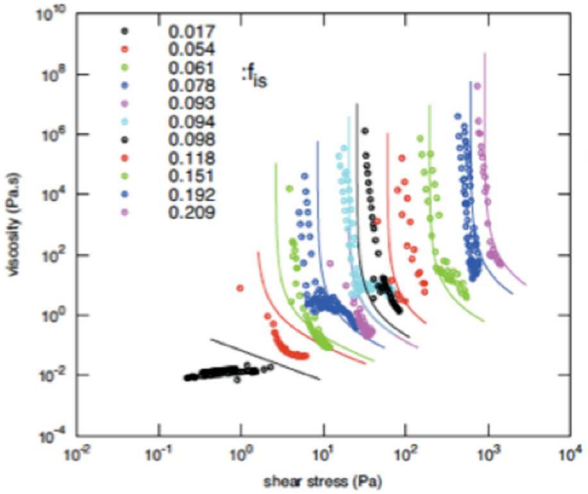

Figure 6.13 – Viscosity of slurry with different fractional (mass) insolubles (see legend) represented against shear stress [15]

The actual inputs turn out to be as follows with following units as mentioned in Figure 6.6:

Table 6-6: The actual input values for the simulation

FIS, %	$\tau(0)$ [m^2s^{-2}]	$\eta(0)$ [m^2s^{-1}]	k [m^2s^{-1}]	n [-]
5.4	0.001476	0.1	0.000833	0.5

6.8.1.3 Methods

The following is the step-by-step methodology to prepare and run a case with OpenFOAM.

6.8.1.3.1 Mesh generation

The partial differential equations that govern fluid flow and heat transfer are not usually amenable to analytical solutions, except for very simple cases. Therefore, in order to analyze fluid flows, flow domains are split into smaller subdomains (made up of geometric primitives like hexahedra and tetrahedra in 3D and quadrilaterals and triangles in 2D).[16] The governing equations are then discretized and solved inside each of these subdomains called meshes.

Meshes can be generated and sized in many different ways depending upon the geometric complexity and symmetry of the system that is being studied. For example, a tube can be meshed either in an axisymmetric way with a small angle of rotation or the whole system with or without defined meshing parameters. For this work, a separate meshing tool is used called 'gmsh'.

6.8.1.3.2 Boundary conditions

nonNewtonianIcoFoam solves for pressure and velocity. Depending upon the type of the system, the boundaries can be assigned values of velocity and pressure. Generally, the pressure of zero is assigned to one end and *OpenFOAM* calculates the pressure at each node, including the other end. For the velocity calculations, velocity profiles of known boundaries, inlet and outlet conditions should be assigned and *nonNewtonianIcoFoam* calculates the velocities in all remaining unknown nodes.

6.8.1.3.3 Patches

A patch is the group of grids whose flow variables are defined before the iterative solutions are obtained. All the different patches created during the mesh generation have to be defined properly and classify in which region they fall. The patches in the volume region can be left blank, but the patches on boundaries and entrance/exit regions must be defined and known by the solver.

6.8.1.3.4 Viscosity

The viscosity values of the slurries are defined on a separate input file called 'Transportproperties". The file specifies which viscosity law to use; i) Power law ii) Cross Power Law iii) BirdCarreau Law or iv) Herschel-Bulkley Law. User should identify the different constants associated with the viscosity laws for the system they are simulating.

6.8.1.3.5 Courant number

The Courant number reflects the portion of the cell that solute will transverse by advection in one time step:

$$C_r = \frac{v.\Delta t}{\Delta l} \qquad \text{(Equation 1)}$$

where *Cr* is called Courant number, *v* is the average linear velocity at that location, *Δl* is the dimension of the grid cell at each location and *Δt* is the maximum time step.[17] For the calculations to be stable, especially pressure, the Courant number has to be stable and less than 1.

6.8.2 Results

6.8.2.1 Validation of OpenFOAM calculations

6.8.2.1.1 Pressure validation of OpenFOAM calculations

Our validation experiment consisted of a system with 2.5% total solids at the steady state. The constant flow rate of 0.2632 m/s [2 L/min] was maintained in the module with 1-foot length and 13 mm inside diameter and two module heads on both sides with 1 inch inside diameter. Two pressure transducers continuously measured the pressures at the inlet and outlet of the membrane tube and their difference gave pressure drop across the two ends of the module. The following table illustrates the simulation results compared to the experimental results:

Table 6-7– Comparison between experimental and simulation results

hour of operation of the experiment	pressure transducer reading at the inlet of the module (bar)	pressure transducer reading at the outlet of the module (bar)	ΔP (bar)	*OpenFOAM* calculation (bar)	error (%)
16-17	0.6163	0.6101	0.0062	0.0080	22.1
24-25	0.8337	0.8264	0.0073	0.0080	8.1
36-37	1.1212	1.1138	0.0074	0.0080	7.9

6.8.2.1.2 Velocity validation of OpenFOAM results

The slurry with 5.4% insolubles exhibits more plug flow behavior. The slurry has to have higher yield stress (τ) to show such a behavior. For this validation, an average velocity of 0.1316 m/s was chosen based on an experimental target of 1 L/min. Slurry with 5.4% insolubles has a plug flow region up to a radius of ~ 0.0009 m at the middle section of the tube. The maximum velocity of ~0.2 m/s is found in this region of the tube. The velocity profiles obtained from the *OpenFOAM*, regardless of meshing, match closely with the analytical solution obtained using Herschel-Bulkley model. However, the higher the mesh density, the more closely the analytical solution matches with the result obtained from *OpenFOAM*. The following are summary of analytical solution and the *OpenFOAM* result:

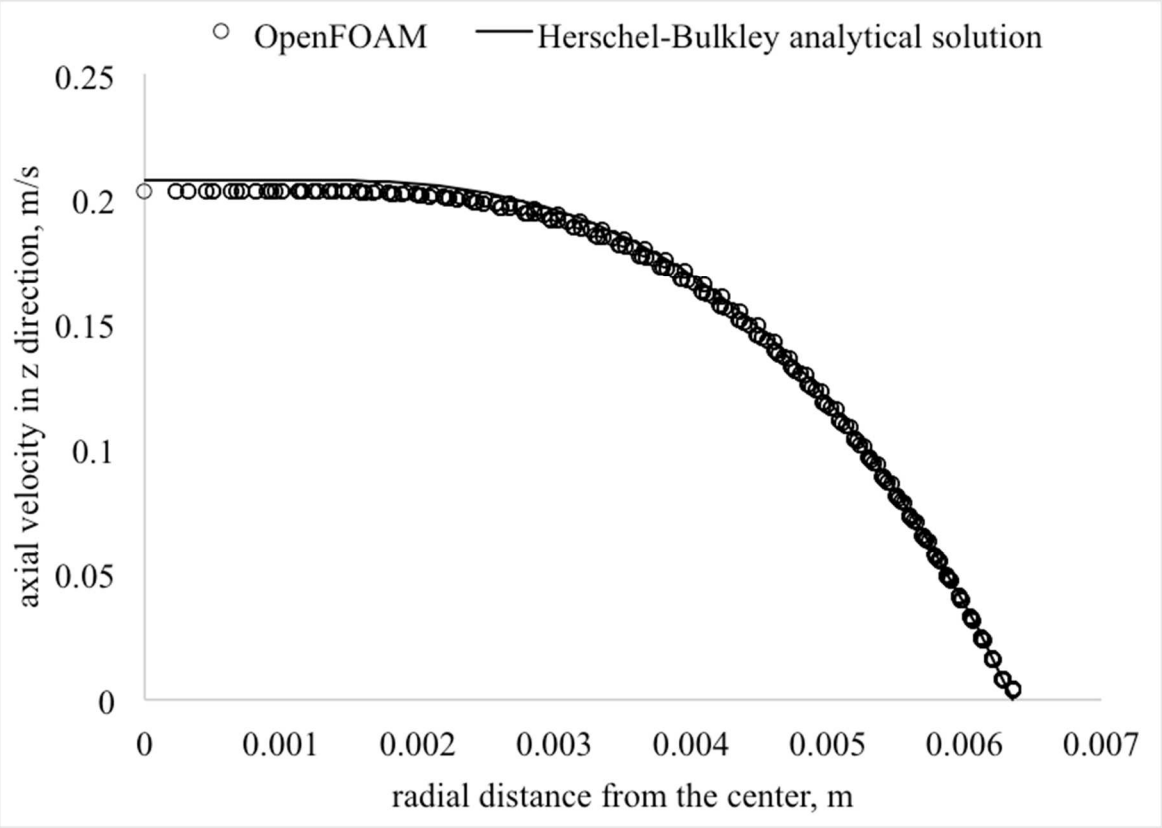

Figure 6.14 - The velocity profile of the slurry with 5.4% insolubles inside the tube from *OpenFOAM* calculation

6.8.2.2 Seven-tube vs six-tube module

For our experiments, we conducted experiments with one tube; however, it is not an optimized module. Thus, instead of one tube, we chose a module of six and seven impermeable tubes. In the case of seven tubes, the tubes are arranged in a hexagonal pattern with one central tube located in the axis of the hexagon and in the case of six tubes, all the tubes were arranged in the same hexagonal pattern without the central tube. Two heads (cavities) were attached to each end of tube. In addition to the spacing between the tubes, head cavity also includes a bordering edge that is equivalent to 1x the spacing between the tubes when the tube diameter is 6.5 mm. The following Figure 6.15 illustrates the module structure:

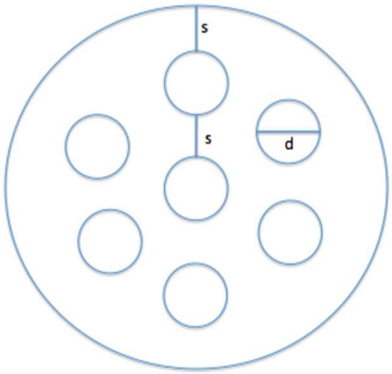

Figure 6.15 - Schematic showing the cross-section of the module with tubes. 's' represents the spacing between the tubes and 'd' represents the diameter of each tube.

Two scenarios with the tubes of varying diameters and spacings were chosen. For each case, a flow scenario involving the average velocity of the slurry with 5.4% insolubles of 0.1316 m/s that is equivalent to the flow rate of 1 L/min in a single tube of 13 mm inside diameter was created and simulated using the *OpenFOAM* with nonNewtonianIcoFoam solver. The scenarios are tabulated in Table 6-8 below.

Table 6-8 – Summary of diameter of tubes and spacing between the tubes for different cases

numbers of tubes	flow developing length, cm	tube ID (m)	spacing between the tubes, m	inlet velocity in the tube head, m/s	average velocity in each tube, m/s
7	2	0.00635	0.00635	0.0188	0.1315
6	2	0.00635	0.001	0.0161	0.1315

When the distribution of tubes in a module was different, the distribution of the fluid/slurry in the tubes was different. When the module had seven tubes and the header length is enough to form a fully developed flow, the innermost tube gets preference over the outermost tubes. However, for an axisymmetric distribution of the tubes, regardless of the geometry of the module, the flow is even in all the tubes, as shown in the case with six tubes. Both scenarios have the same pressure drop across the two ends of the module. The following Figure 6.16 has summarized the results of these scenarios.

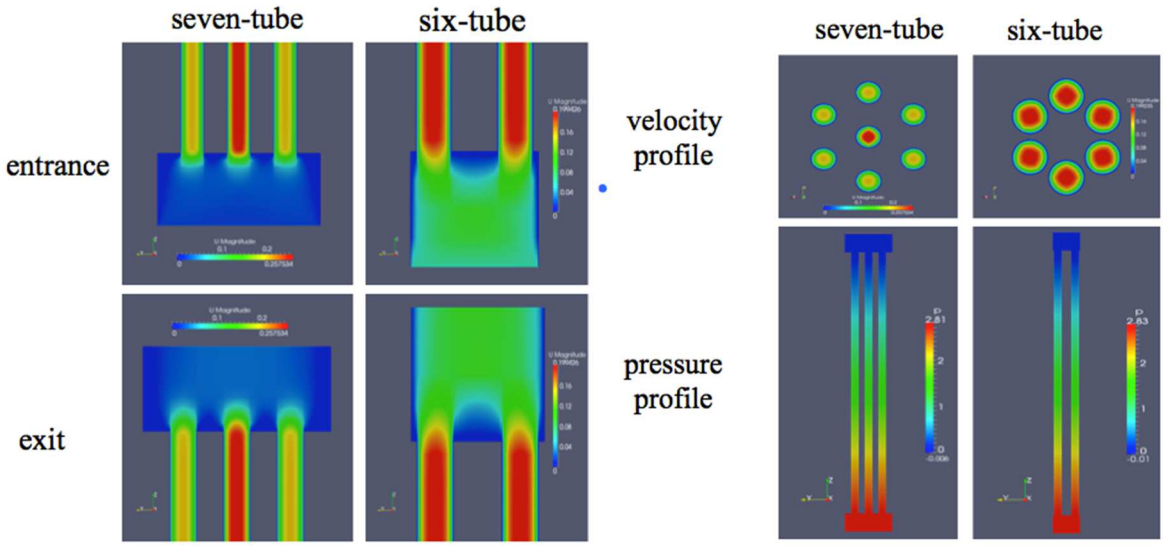

Figure 6.16 – Schematics showing (a) the velocity profile in the cross section of the module and pressure profile across the whole module and (b) velocity profiles of exit and entrance regions in both cases.

6.8.3 Continuous enzymatic hydrolysis

The successful completion of the entire experiment was shown by permeate rate and permeate collected overtime. The following subsections illustrate permeate rate and permeate collected.

6.8.3.1 2.5% FIS

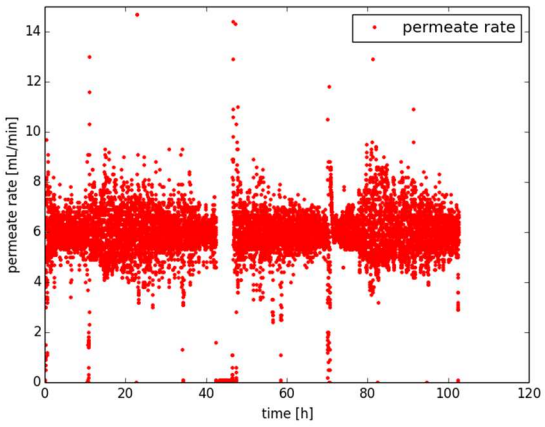

(a)

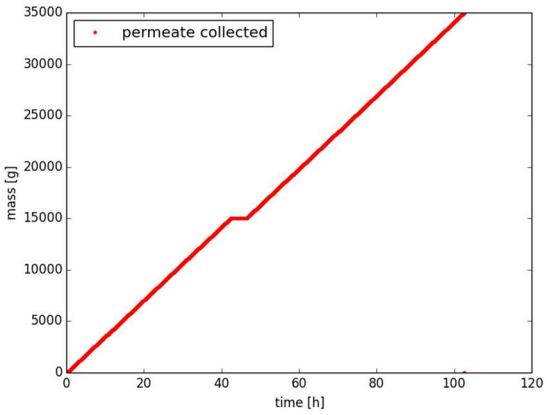

(b)

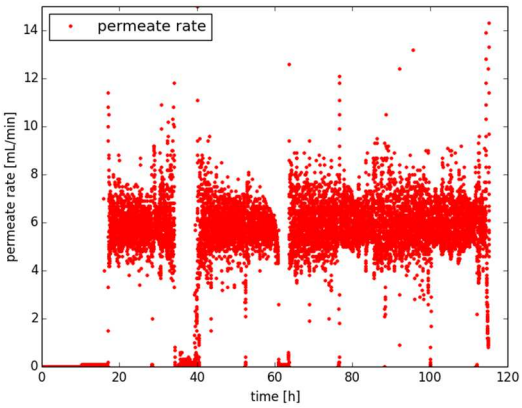

(a)

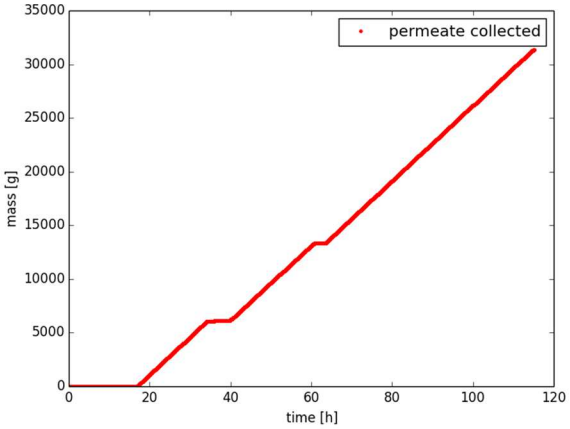

(b)

Figure 6.17 – (a) Permeate rate observed throughout the experiment and (b) permeation collected throughout the continuous run with 2.5% FIS

6.8.3.2 5% FIS

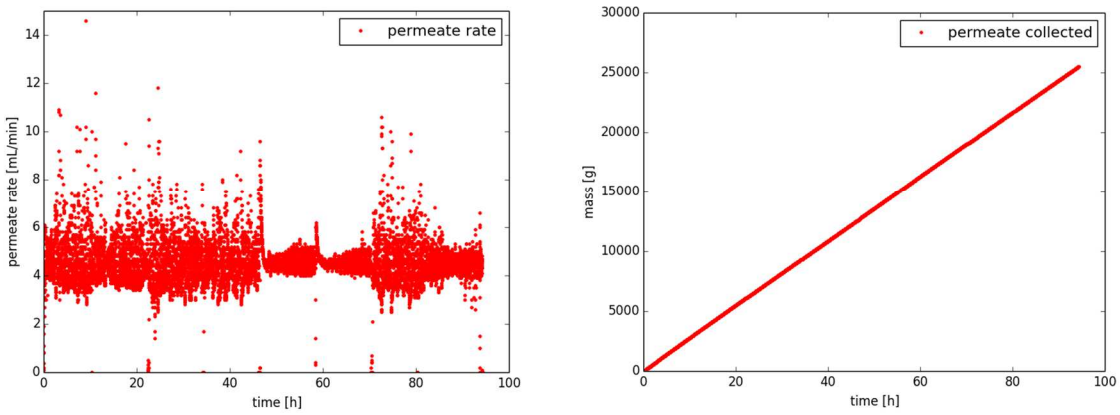

(a) (b)

Figure 6.18 – (a) Permeate rate observed throughout the experiment and (b) mass of permeate collected throughout the continuous run with 5% FIS

6.8.3.3 5% FIS with double residence time

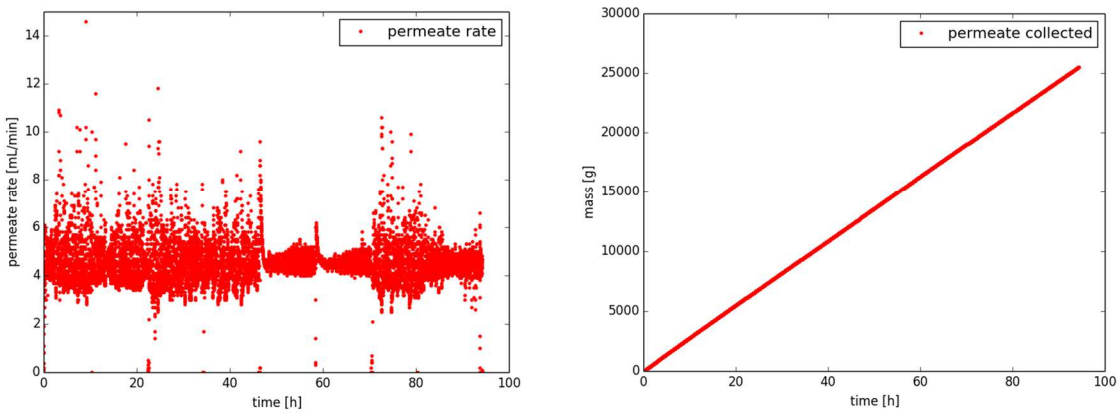

(a) (b)

Figure 6.19 – (a) Permeate rate observed throughout the experiment and (b) permeation collected throughout the continuous run with 2.5% FIS

6.8.4 Supplemental information reference keys

[1]M.S. Shah, J.B. Joshi, A.S. Kalsi, C.S.R. Prasad, D.S. Shukla, Analysis of flow through an orifice meter: CFD simulation, Chem Eng Sci, 71 (2012) 300-309.

[2]F. Habla, H. Marschall, O. Hinrichsen, L. Dietsche, H. Jasak, J.L. Favero, Numerical simulation of viscoelastic two-phase flows using openFOAM (R), Chem Eng Sci, 66 (2011) 5487-5496.

[3]D. Carvajal, D.L. Marchisio, S. Bensaid, D. Fino, Enzymatic Hydrolysis of Lignocellulosic Biomasses via CFD and Experiments, Industrial & Engineering Chemistry Research, 51 (2012) 7518-7525.

[4]A. Trusek-Holownia, Improvement of process productivity and product purity by the application of a membrane phase contactor in enzymatic conversions, Separation and Purification Technology, 41 (2005) 267-274.

[5]J.J. Stickel, R.L. Powell, Fluid mechanics and rheology of dense suspensions, Annu Rev Fluid Mech, 37 (2005) 129-149.

[6]F.X. Tanner, A.A. Al-Habahbeh, K.A. Feigl, S. Nahar, S.A.K. Jeelani, W.R. Case, E.J. Windhab, Numerical and Experimental Investigation of a Non-Newtonian Flow in a Collapsed Elastic Tube, Appl Rheol, 22 (2012) 328-335.

[7]C.M. Roche, C.J. Dibble, J.S. Knutsen, J.J. Stickel, M.W. Liberatore, Particle Concentration and Yield Stress of Biomass Slurries During Enzymatic Hydrolysis at High-Solids Loadings, Biotechnology and Bioengineering, 104 (2009) 290-300.

[8]C.T. Scott, J.R. Samaniuk, D.J. Klingenberg, Rheology and extrusion of high-solids biomass, Tappi J, 10 (2011) 47-53.

[9]J.J. Stickel, J.S. Knutsen, M.W. Liberatore, W. Luu, D.W. Bousfield, D.J. Klingenberg, C.T. Scott, T.W. Root, M.R. Ehrhardt, T.O. Monz, Rheology measurements of a biomass slurry: an inter-laboratory study, Rheol Acta, 48 (2009) 1005-1015.

[10]J.R. Samaniuk, J. Wang, T.W. Root, C.T. Scott, D.J. Klingenberg, Rheology of concentrated biomass, Korea-Aust Rheol J, 23 (2011) 237-245.

[11]J.S. Knutsen, M.W. Liberatore, Rheology of high-solids biomass slurries for biorefinery applications, J Rheol, 53 (2009) 877-892.

[12]T. Shu-tang, J. yI-an, ON THE LINKING UP BETWEEN BINGHAM FLUID AND PLUGGED FLOW, Appled Mathematics and Mechanics, 8 (1987) 6.

[13]R.A. Chilton, R. Stainsby, Pressure loss equations for laminar and turbulent non-Newtonian pipe flow, J Hydraul Eng-Asce, 124 (1998) 522-529.

[14]J. Stickel, Viscosity of different biomass fraction, National Renewable Energy Laboratory, 2013.

[15]J.J. Stickel, Viscoscity of lignocellulosic biomass slurry at various fraction insoluble solids (FIS) loading., Golden, CO., 2010.

[16]C. Geuzaine, J.-F. Remacle, Gmsh: a three-dimensional finite element mesh generator with built-in pre- and post-processing facilities, 2013.

[17]C. Schär, The Courant-Friedrichs-Levy (CFL) Stability Criterion ETH-Swiss Federal Institute of Technology, Zurich, 2013.

Chapter 7 Conclusions and recommendations

This dissertation has investigated the viability of algal biofuel both economically and environmentally by creating a techno-economic and life-cycle model with the capability of incorporating existing published technologies, and potential future innovation titled SAFEER (Sustainable algae-to-fuel: environmental and economic realities) and proposed a novel method of extraction of lipids from algae using diesel as the extraction solvent since dewatering and lipid extraction has been known as a bottleneck of for the commercialization of algal biofuels[1, 2]. In addition to that, this dissertation has investigated the various avenues of viability of membrane based continuous enzymatic hydrolysis of lignocellulosic biomass to produce sugar by conducting experiments with different fraction insoluble solids (FIS) in the bioreactor continuously and by removing sugar continuously from the hydrolysis reactor with the help of a membrane module. The design and operation of the rector system for the continuous enzymatic hydrolysis is a very difficult task because of the rheological complexities and high solid loading with uneven and polydisperse particle sizes of the biomass slurry [3-5]. The dissertation work started with a difficult task of studying biomass and membrane performances, designing membrane based reactor system with a and solving many new engineering challenges, unknown and unknowns, those come along while going forward on this task. The following conclusions have been made out of this work:

7.1 Conclusions

The main conclusions of this work are divided in the following sub sections are:

7.1.1 Algal biofuel techno-economic and life cycle analysis

We studied five algae to biofuel production scenarios. The scenarios include algae growth scenarios with open raceway ponds, photo-bioreactors and artificial light (LED-lit) photo-bioreactors. It also includes the processing scenarios of producing fatty acid methyl ester (FAME) or commonly called 'biodiesel', free fatty acids (FFA) and triacylglycerides (TAG). We have addressed scale up and commercialization of algae-to-biofuels processes from a quantitative perspective. Our study concluded that the production costs calculated are several orders of magnitude greater than the selling price of oil from seed crops as well as the current market price for fossil fuels. It has been shown that each process has multiple hurdles to overcome and price reductions to achieve before algae-based biofuels are economically competitive with traditional fossil oil or other oil crops. The open pond scenarios were closest to the $1/kg price point, and at this moment closest to commercialization. It has significantly lower algae production cost. Bioreactor based growth methods, both photo-bioreactors and LED-lit photobioreactors with quantum fracturing) were shown to very expensive, but future technological advances can potentially improve the economics these scenarios. These scenarios need improvements on all most all the unit operation steps to be economically competitive and viable.

For a production scenario to be viable, it has to be sustainable not just economically but also environmentally. Thus, life cycle analysis (LCA) of these scenarios were also studied using SAFEER. Not all of the scenarios are that compatible environmentally. Several unit operation wise improvements have to be made, specially in equipment manufacturing and processing the algae after the growth. Open pond scenario, just like economically, remains most environmentally sustainale form of production since it consumes so less energy while growing

and manufacturing the equipment for algae growth facilities. However, the land compustion is very high and the productivity is very low and it is hard to envision this process being commercial unless some significant improvements, primarily on the lipid content in algae are achieved. Photobioreactors have high producity, but the life-cycle impacts of the scenarios including solar-lit photobioractors and LED-lit photobioreactors are too high because of a huge number of equipment with higher life cycle impacts and higher net calorific value.

7.1.2 Lipid extraction from wet algae with diesel and isopropanol

Conventionally, lipids ate extracted from dry algae and solvents like hexane and isopropanol [6] and chloroform and methanol [7] are used to extract lipids. These methods are either every expensive or very toxic and on the top of that, bear very high processing cost. To tackle the problem of high extraction cost, we proposed diesel and isopropanol as an extracting solvent. Hansen solubility parameter analysis suggests that the components of diesel are miscible with the neutral lipids from microalgae. Isopropanol, a relatively less toxic solvent (in comparison to other available alcohols and solvents) and a compound with smaller molecular size, can be used as the alcohol to open up the pores to get algal lipids out of the algae. Diesel/isopropanol is a solvent mixture with cheaper cost of purchase and our study found that it is almost as effective as hexane/isopropanol. Use of diesel in wet lipid extraction process can eliminate the need of a high level of dewatering; simplify the solvent recovery step and thus, it can reduce the overall cost of production. We also examined the viability of algae regrowth after the extraction. We found that algae can still regrow after the lipid extraction-using diesel, but the growth number varies greatly with the extent of extraction. Diesel was found to be not harmful for algae regrowth.

7.1.3 Membrane based continuous enzymatic hydrolysis of lignocellulosic biomass

Biofuels, such as those derived from lignocellulosic biomass, are possible renewable alternatives to fossil fuels. Lignocellulose is the most abundant organic polymer in the world, which is present in the form of plant cell wall[8]. The current state-of-art of lignocellulosic biofuel, batch process is not yet competitive with fossil fuel sources because it is very slow and energy intensive. Thus, we proposed a membrane based continuous hydrolysis of lignocellulosic biomass by continuously removing sugar from the reactor.

For the conversion of lignocellulosic biomass to the derivative fuels, cellulose and hemicellulose first must be hydrolyzed to their component sugars. One of the hydrolysis processes studied utilizes a high-temperature, dilute sulfuric acid pretreatment of biomass *followed by enzymatic hydrolysis at ~50 °C*. To make a system with continuous hydrolysis, the system has to deal with several engineering problems starting with clogging of the tubes. Because of the impact biomass has over the system because of the total insolubles, it was quite hard for slurry to be pumped and made continuous with the desired pressure gradient. During few experiments we did, we changed the stator of the pump, backpressure regulator, method of mixing. Periodic pressure spikes are still something that came along during the experiments and better cleaning protocol is something that was developed over time. We were able to attain a reasonable steady state for longer run and this led us to do better design, such as use of parallel membranes to enhance cleaning during the experiment.

Experiments were successful, starting with 2% FIS. Subsequently, experiments with 2.5% FIS, 5% FIS and 5% FIS but doubled residence time were carried out successfully. To our interest, membrane system performed similarly all the times when constant recirculation flow rate was maintained in the membrane module. Cleaning was done once every 12 h with standard

acoustic solution of 0.05 M sodium hydroxide (NaOH) and that was the time when the membranes were switched. We also found that for a cross flow system, the rate of change of fouling resistance is much lower in comparison to other loose microfiltration membranes with higher porosity.

7.1.4 Designing membrane module

We studied the different geometries of 'probable membrane module' using *OpenFoam*. Our main goal was to understand the causes of clogging and come up with an optimize header with a system that has multiple membrane tube. We started with verifying the simulation results with analytical solution and experimental results. Then we compared a symmetric six tube system with an asymmetric seven tube system The uneven distribution of the flow in the tubes of a membrane module with seven tubes can potentially lead some tubes to be clogged. The system with six tubes, had even flow of slurry along all the tubes and that alone, minimizes the chances of clogging of some tubes over the others. It has also been found that on the membrane surface, regardless of FIS, the shear stress is same for the flow of slurry with constant volumetric flow rate and that suggests that the fouling resistance does not go up if we go up in FIS in a constant recirculation rate.

7.2 Recommendations

7.2.1 Algal biofuel

i) For algae to biofuel processes, dewatering and lipid extraction are the main bottleneck. So, diesel can potentially minimize the cost regarding the dewatering and extraction. For that to happen, motor vehicles should be able to use the mixture of fossil fuel and biodiesel together. These two things have different energy density and they burn differently inside

the engine producing different amount of energy. Hence, a special modification of engine and planning of policies are necessary for this to be commercialized.

ii) Genetic modifications enabling algae strains to have higher lipid content is necessary to minimize overall cost of production of algal biofuels.

iii) Use of Hansen solubility parameters is a great tool to understand about the solubility of diesel components with lipids. It helps to understand and implement other potential solvents if they come up for future use.

iv) Life-cycle analysis in parallel with the techno-economic analysis suggests the sustainability of overall algae to fuel scenarios. If a decision is made in context of one scenario while barring the other would prove costly. In the scenarios we studied, the cost of the production aligned with the LCA numbers, but not in all the potential scenarios we did not study. Thus, the answers we came up are good for these five cases only and separate case study has to be made for each process scenarios (that we didn't study) to come up with a definite answer.

7.2.2 Continuous enzymatic hydrolysis

i) The main cost associated with hydrolysis of lignocellulosic biomass is mixing cost, pumping cost, heating cost and enzyme cost. All of these have to be minimized before we could propose a continuous enzymatic hydrolysis system for commercial purpose. The mixing cost depended upon the volume of the reactor, the pumping cost depends upon the viscosity and flow rate of slurry, heating cost depends upon the volume and effective insulation of the system and enzyme cost depends upon the amount of enzyme that primarily is lost.

ii) The membrane module should be designed such a way that it can effectively handle the slurry with no clogging while maintaining higher surface area for a particular volume. If it can be achieved, the cleaning cost and membrane replacement cost can be minimized.

iii) Feeding of biomass to the reactor had been an issue in almost all the experiments we performed. It is something very critical. But an easy fix. The bigger the tubes of the feed side, the lesser would be the problems associated with it. A selective air and biomass feed can also be implemented to minimize the clogging of feed tubes.

iv) The purge rate of one reactor tells how much the theoretical maximum conversion for that reactor is. So, achieving lower purge rate would increase the conversion but at the same time, careful attention should be given to the total solids in the bioreactor that could dictate the overall performance of the system.

7.3 References

[1] L. Amer, B. Adhikari, J. Pellegrino, Technoeconomic analysis of five microalgae-to-biofuels processes of varying complexity, Bioresource Technology, 102 (2011) 9350-9359.

[2] L.G. Speranza, A. Ingram, G.A. Leeke, Assessment of algae biodiesel viability based on the area requirement in the European Union, United States and Brazil, Renew Energ, 78 (2015) 406-417.

[3] C.M. Roche, C.J. Dibble, J.S. Knutsen, J.J. Stickel, M.W. Liberatore, Particle Concentration and Yield Stress of Biomass Slurries During Enzymatic Hydrolysis at High-Solids Loadings, Biotechnology and Bioengineering, 104 (2009) 290-300.

[4] J.J. Stickel, R.L. Powell, Fluid mechanics and rheology of dense suspensions, Annu Rev Fluid Mech, 37 (2005) 129-149.

[5] P. Andric, A.S. Meyer, P.A. Jensen, K. Dam-Johansen, Reactor design for minimizing product inhibition during enzymatic lignocellulose hydrolysis II. Quantification of inhibition and suitability of membrane reactors, Biotechnology Advances, 28 (2010) 407-425.

[6] J.B. Guckert, D.C. White, Evaluation of a Hexane Isopropanol Lipid Solvent System for Analysis of Bacterial Phospholipids and Application to Chloroform-Soluble Nuclepore (Polycarbonate) Membranes with Retained Bacteria, J Microbiol Meth, 8 (1988) 131-137.

[7] E.G. Bligh, W.J. Dyer, A Rapid Method of Total Lipid Extraction and Purification, Can J Biochem Phys, 37 (1959) 911-917.

[8] Y.H.P. Zhang, S.Y. Ding, J.R. Mielenz, J.B. Cui, R.T. Elander, M. Laser, M.E. Himmel, J.R. McMillan, L.R. Lynd, Fractionating recalcitrant lignocellulose at modest reaction conditions, Biotechnology and Bioengineering, 97 (2007) 214-223.

Bibliography

[1] R.E. Armenta, P. Mercer, Developments in oil extraction from microalgae, European Journal of Lipid Science and Technology, 113 (2011) 539-547.
[2] M. Odlare, E. Nehrenheim, V. Ribe, E. Thorin, M. Gavare, M. Grube, Cultivation of algae with indigenous species - Potentials for regional biofuel production, Applied Energy, 88 (2011) 3280-3285.
[3] A.F. Clarens, E.P. Resurreccion, M.A. White, L.M. Colosi, Environmental life cycle comparison of algae to other bioenergy feedstocks, Environmental Science & Technology, 44 (2010) 1813-1819.
[4] Y.K. Lee, Microalgal mass culture systems and methods: Their limitation and potential, Journal of Applied Phycology, 13 (2001) 307-315.
[5] K.M. Weyer, D.R. Bush, A. Darzins, B. Willson, Theoretical Maximum Algal Oil Production, BioEnergy Research, (2009) 10.
[6] Y.H.P. Zhang, S.Y. Ding, J.R. Mielenz, J.B. Cui, R.T. Elander, M. Laser, M.E. Himmel, J.R. McMillan, L.R. Lynd, Fractionating recalcitrant lignocellulose at modest reaction conditions, Biotechnology and Bioengineering, 97 (2007) 214-223.
[7] K. Soratana, A.E. Landis, Evaluating industrial symbiosis and algae cultivation from a life cycle perspective, Bioresource Technology, 102 (2011) 6892-6901.
[8] B. Steubing, R. Zah, C. Ludwig, Life cycle assessment of SNG from wood for heating, electricity, and transportation, Biomass Bioenerg, 35 (2011) 2950-2960.
[9] T.M. Komarek, F. Lupi, M.D. Kaplowitz, Valuing energy policy attributes for environmental management: Choice experiment evidence from a research institution, Energ Policy, 39 (2011) 5105-5115.
[10] E.P. Johnson, Air-source heat pump carbon footprints: HFC impacts and comparison to other heat sources, Energ Policy, 39 (2011) 1369-1381.
[11] G.S. Anisha, R.P. John, K.M. Nampoothiri, A. Pandey, Micro and macroalgal biomass: A renewable source for bioethanol, Bioresource Technology, 102 (2011) 186-193.
[12] D. Fishman, R. Majumdar, J. Morello, R. Pate, J. Yang, National algal biofuels technology roadmap, in: U.S. DOE (Ed.), Office of Energy Efficiency and Renewable Energy, Biomass Proagram, 2010, pp. 1-114.
[13] J. Sheehan, T. Dunahay, J. Benemann, P. Roessler, A Look Back at the U.S. Department of Energy's Aquatic Species Program: Biodiesel from Algae; Close-Out Report, U.S. Department of Energy's Aquatic Species Program: Biodiesel from Algae, NREL, 1998, pp. 325 pages.
[14] J.S. Chang, C.Y. Chen, K.L. Yeh, R. Aisyah, D.J. Lee, Cultivation, photobioreactor design and harvesting of microalgae for biodiesel production: A critical review, Bioresource Technology, 102 (2011) 71-81.
[15] Y. Chisti, Biodiesel from microalgae, Biotechnology Advances, 25 (2007) 294-306.
[16] F. Bux, T. Mutanda, D. Ramesh, S. Karthikeyan, S. Kumari, A. Anandraj, Bioprospecting for hyper-lipid producing microalgal strains for sustainable biofuel production, Bioresource Technology, 102 (2011) 57-70.
[17] P.S. Nigam, A. Singh, J.D. Murphy, Mechanism and challenges in commercialisation of algal biofuels, Bioresource Technology, 102 (2011) 26-34.
[18] P.S. Nigam, A. Singh, J.D. Murphy, Renewable fuels from algae: An answer to debatable land based fuels, Bioresource Technology, 102 (2011) 10-16.

[19] J.K. Pittman, A.P. Dean, O. Osundeko, The potential of sustainable algal biofuel production using wastewater resources, Bioresource Technology, 102 (2011) 17-25.
[20] P.J.L. Williams, L.M.L. Laurens, Microalgae as biodiesel & biomass feedstocks: Review & analysis of the biochemistry, energetics & economics, Energy & Environmental Science, 3 (2010) 554-590.
[21] Y. Shen, W. Yuan, Z.J. Pei, Q. Wu, E. Mao, MICROALGAE MASS PRODUCTION METHODS, Trans. ASABE, 52 (2009) 1275-1287.
[22] J.B. van Beilen, Why microalgal biofuels won't save the internal combustion machine, Biofuel Bioprod Bior, 4 (2010) 41-52.
[23] A. Darzins, The promises and challenges of algal derived biofuels, 2009.
[24] K.L. Kadam, Plant flue gas as a source of CO2 for microalgae cultivation. Economic impact of different process options, Energy Conversion and Management, 38 (1997) S505-S510.
[25] J.R. Benemann, Systems and economic analysis of microalgae ponds for conversion of CO2 to biomass. 4th Quarterly technical progress report, US/Japan meeting on coal energy research, University of California Berkley, Albuquerque, NM, 1994, pp. 9.
[26] E.M. Grima, E.H. Belarbi, F.G.A. Fernandez, A.R. Medina, Y. Chisti, Recovery of microalgal biomass and metabolites: process options and economics, Biotechnology Advances, 20 (2003) 491-515.
[27] G. Jensen, E.H. Reichl, Integrated microalgae production and electricity cogeneration in: U.S.P.a.T. Office (Ed.) United States Patent and Trademark Office, Cyanotech Corporation, 1997.
[28] J.R. Benemann, W.J. Oswald, Systems and economic analysis of microalgae ponds for conversion of CO to biomass. , in: U.S.D.o. Energy (Ed.) Final report, U.S. Department of Energy, 1996, pp. 214.
[29] B. Willson, Diffuse Light Extended Surface Area Water-Supported Photobioreactor in: U.S.P.a.T. Office (Ed.) United States Patent and Trademark Office, 2008.
[30] M.T.e.a. Machacek, Continuous Algal Biodiesel Production Facility, in: U.S.P.a.T. Office (Ed.) United States Patent and Trademark Officeusa, 2009.
[31] N. Eckelberry, T.R. Eckelberry, Algae Growth System for Oil Production, in: U.S.P.a.T. Office (Ed.) United States Patent and Trademark Office, 2009.
[32] N. Eckelberry, Apparatus for generating microbubbles while mixing an additive fluid with a mainstream liquid, 2001, pp. 9.
[33] J.C. Weaver, Y.A. Chizmadzhev, Theory of electroporation: A review, Bioelectrochem. Bioenerg., 41 (1996) 135-160.
[34] A.L. Stephenson, E. Kazamia, J.S. Dennis, C.J. Howe, S.A. Scott, A.G. Smith, Life-cycle assessment of potential algal biodiesel production in the United Kingdom: a comparison of raceways and air-lift tubular bioreactors, Energ Fuel, 24 (2010) 4062-4077.
[35] M.M. El-Halwagi, G. Pokoo-Aikins, A. Heath, R.A. Mentzer, M.S. Mannan, W.J. Rogers, A multi-criteria approach to screening alternatives for converting sewage sludge to biodiesel, Journal of Loss Prevention in the Process Industries, 23 (2010) 412-420.
[36] L. Lardon, A. Helias, B. Sialve, J.P. Stayer, O. Bernard, Life-Cycle assessment of biodiesel production from microalgae, Environmental Science & Technology, 43 (2009) 6475-6481.
[37] A.F. Clarens, E.P. Resurreccion, M.A. White, L.M. Colosi, Environmental Life Cycle Comparison of Algae to Other Bioenergy Feedstocks, Environmental Science & Technology.
[38] Seider, Product and Process Design Principles: Synthesis, Analysis, and Evaluation, 2nd Edition, Wiley2004.

[39] A.R. Fajardo, L.E. Cerdan, A.R. Medina, F.G.A. Fernandez, P.A.G. Moreno, E.M. Grima, Lipid extraction from the microalga Phaeodactylum tricornutum, European Journal of Lipid Science and Technology, 109 (2007) 120-126.
[40] K. Dimitrov, GreenFuel Technologies: A Case Study for Industrial Photosynthetic Energy Capture, University of Queensland, Brisbane, 2007, pp. 30.
[41] E.M. Grima, A.R. Medina, A.G. Gimenez, J.A.S. Perez, F.G. Camacho, J.L.G. Sanchez, Comparison between Extraction of Lipids and Fatty-Acids from Microalgal Biomass, Journal of the American Oil Chemists Society, 71 (1994) 955-959.
[42] F.J. Eller, S.L. Taylor, M.S.S. Curren, Use of liquid carbon dioxide to remove hexane from soybean oil, Journal of the American Oil Chemists Society, 81 (2004) 989-992.
[43] B. Sialve, N. Bernet, O. Bernard, Anaerobic digestion of microalgae as a necessary step to make microalgal biodiesel sustainable, Biotechnology Advances, 27 (2009) 409-416.
[44] J.R. Benemann, W.J. Oswald, Systems and economic analysis of microalgae ponds for conversion of CO2 to biomass., Quarterly technical progress report, 1994, pp. 9.
[45] L.M. Brown, S. Sprague, Aquatic Species Project report, Aquatic Species, NREL, 1992, pp. 120 p.
[46] W.S. Broecker, Climatic change - are we on brink of a pronounced global warming?, Science, 189 (1975) 460-463.
[47] S. Lewandowsky, G.E. Gignac, S. Vaughan, The pivotal role of perceived scientific consensus in acceptance of science, Nat. Clim. Chang., 3 (2013) 399-404.
[48] M.L. Ghirardi, O. Jorquera, A. Kiperstok, E.A. Sales, M. Embirucu, Comparative energy life-cycle analyses of microalgal biomass production in open ponds and photobioreactors, Bioresource Technology, 101 (2010) 1406-1413.
[49] Y.S. Chen, J. Yang, M. Xu, X.Z. Zhang, Q. Hu, M. Sommerfeld, Life-cycle analysis on biodiesel production from microalgae: Water footprint and nutrients balance (vol 102, pg 159, 2011), Bioresource Technology, 102 (2011) 6633-6633.
[50] U.S.E.P. Agency, EPA Proposes 2014 Renewable Fuel Standards, 2015 Biomass-Based Diesel Volume, United States Environmental Protection Agency, Offie of Transportation and Air Quality, 2013, pp. 4.
[51] P.K. Campbell, T. Beer, D. Batten, Life cycle assessment of biodiesel production from microalgae in ponds, Bioresource Technology, 102 (2011) 50-56.
[52] K. Butterbach-Bahl, C.C. Lisboa, M. Mauder, R. Kiese, Bioethanol production from sugarcane and emissions of greenhouse gases - known and unknowns, Global Change Biology Bioenergy, 3 (2011) 277-292.
[53] T.M. Mata, A.A. Martins, N.S. Caetano, Microalgae for biodiesel production and other applications: a review, Renewable & Sustainable Energy Reviews, 14 (2010) 217-232.
[54] S.O. Salley, H.Y. Tang, M. Chen, M.E.D. Garcia, N. Abunasser, K.Y.S. Ng, Culture of Microalgae Chlorella minutissima for Biodiesel Feedstock Production, Biotechnology and Bioengineering, 108 (2011) 2280-2287.
[55] P. Azadi, G. Brownbridge, S. Mosbach, A. Smallbone, A. Bhave, O. Inderwildi, M. Kraft, The carbon footprint and non-renewable energy demand of algae-derived biodiesel, Applied Energy, 113 (2014) 1632-1644.
[56] H.H. Khoo, P.N. Sharratt, P. Das, R.K. Balasubramanian, P.K. Naraharisetti, S. Shaik, Life cycle energy and CO(2) analysis of microalgae-to-biodiesel: Preliminary results and comparisons, Bioresour. Technol., 102 (2011) 5800-5807.

[57] K. Sander, G.S. Murthy, Life cycle analysis of algae biodiesel, International Journal of Life Cycle Assessment, 15 (2010) 704-714.
[58] M. Rickman, J. Pellegrino, J. Hock, S. Shaw, B. Freeman, Life-cycle and techno-economic analysis of utility-connected algae systems, Algal Res, 2 (2013) 59-65.
[59] P.H. Pfromm, V. Amanor-Boadu, R. Nelson, Sustainability of algae derived biodiesel: A mass balance approach, Bioresource Technology, 102 (2011) 1185-1193.
[60] D. Pant, A. Singh, G. Van Bogaert, Y.A. Gallego, L. Diels, K. Vanbroekhoven, An introduction to the life cycle assessment (LCA) of bioelectrochemical systems (BES) for sustainable energy and product generation: Relevance and key aspects, Renewable & Sustainable Energy Reviews, 15 (2011) 1305-1313.
[61] Y.L. Zhang, M.A. White, L.M. Colosi, Environmental and economic assessment of integrated systems for dairy manure treatment coupled with algae bioenergy production, Bioresource Technology, 130 (2013) 486-494.
[62] M. Debowski, M. Zielinski, A. Grala, M. Dudek, Algae biomass as an alternative substrate in biogas production technologies-Review, Renewable & Sustainable Energy Reviews, 27 (2013) 596-604.
[63] M.A. Meyer, A. Weiss, Life cycle costs for the optimized production of hydrogen and biogas from microalgae, Energy, 78 (2014) 84-93.
[64] P. Collet, L. Lardon, A. Helias, S. Bricout, I. Lombaert-Valot, B. Perrier, O. Lepine, J.P. Steyer, O. Bernard, Biodiesel from microalgae - Life cycle assessment and recommendations for potential improvements, Renew Energ, 71 (2014) 525-533.
[65] S.I. Olsen, F.M. Christensen, M. Hauschild, F. Pedersen, H.F. Larsen, J. Torslov, Life cycle impact assessment and risk assessment of chemicals — a methodological comparison, Environmental Impact Assessment Review, 21 (2001) 385-404.
[66] F. Romagnoli, D. Blumberga, I. Pilicka, Life cycle assessment of biohydrogen production in photosynthetic processes, International Journal of Hydrogen Energy, 36 (2011) 7866-7871.
[67] L. Soh, M. Montazeri, B.Z. Haznedaroglu, C. Kelly, J. Peccia, M.J. Eckelman, J.B. Zimmerman, Evaluating microalgal integrated biorefinery schemes: Empirical controlled growth studies and life cycle assessment, Bioresource Technology, 151 (2014) 19-27.
[68] C.E. Canter, R. Davis, M. Urgun-Demirtas, E.D. Frank, Infrastructure associated emissions for renewable diesel production from microalgae, Algal Res, 5 (2014) 195-203.
[69] L. Amer, B. Adhikari, J. Pellegrino, Technoeconomic analysis of five microalgae-to-biofuels processes of varying complexity, Bioresour. Technol., 102 (2011) 9350-9359.
[70] N.R.E.L. (U.S.), U.S. LIFE CYCLE INVENTORY DATABASE ROADMAP, National Renewable Energy Laboratory, Golden, CO, 2009, pp. 12.
[71] N. Eckelberry, T.R. Eckelberry, Algae Growth System for Oil Production, in: U.S.P.a.T. Office (Ed.) United States Patent and Trademark OfficeUSA, 2009.
[72] L.X. Xu, D.W.F. Brilman, J.A.M. Withag, G. Brem, S. Kersten, Assessment of a dry and a wet route for the production of biofuels from microalgae: Energy balance analysis, Bioresource Technology, 102 (2011) 5113-5122.
[73] R. Putt, M. Singh, S. Chinnasamy, K.C. Das, An efficient system for carbonation of high-rate algae pond water to enhance CO(2) mass transfer, Bioresource Technology, 102 (2011) 3240-3245.
[74] N. Uduman, Y. Qi, M.K. danquah, G.M. Forde, A. Hoadley, Dewatering of microalgal cultures: A major bottleneck to algae-based fuels, Journal of Renewable and Sustainable Energy, 2 (2010) 15.

[75] C. Samori, D. Lopez Barreiro, R. Vet, L. Pezzolesi, D.W.F. Brilman, P. Galletti, E. Tagliavini, Effective lipid extraction from algae cultures using switchable solvents, Green Chemistry, 15 (2013) 353-356.
[76] R. Davis, C. Kinchi, J. Markham, E.C.D. Tan, L.M.L. Laurens, D. Sexton, D. Knorr, P. Schoen, J. Lukas, Process Design and Economics for the Conversion of Algal Biomass to Biofuels: Algal Biomass Fractionation to Lipid and Carbohydrate-Derived Fuel Products, NREL, Golden, CO, 2014.
[77] L.M.L. Laurens, N. Nagle, R. Davis, N. Sweeney, S. Van Wychen, A. Lowell, P.T. Pienkos, Acid-catalyzed algal biomass pretreatment for integrated lipid and carbohydrate-based biofuels production, Green Chemistry, 17 (2015) 1145-1158.
[78] M.A. Hejazi, R.H. Wijffels, Milking of microalgae, Trends Biotechnol., 22 (2004) 189-194.
[79] T.V. Ramachandra, D. Mahapatra, K. B, R. Gordon, Milking diatoms for sustainable energy: biochemical engineering versus gasoline-secreting diatom solar panels, Ind Eng Chem Res, 48 (2009) 8769-8788.
[80] F. Zhang, L.H. Cheng, X.H. Xu, L. Zhang, H.L. Chen, Screening of biocompatible organic solvents for enhancement of lipid milking from *Nannochloropsis*, Process Biochem., 46 (2011) 1934-1941.
[81] B.J. Gallagher, The economics of producing biodiesel from algae, Renew Energ, 36 (2011) 158-162.
[82] E. Iakovou, A. Karagiannidis, D. Vlachos, A. Toka, A. Malamakis, Waste biomass-to-energy supply chain management: A critical synthesis, Waste Manage, 30 (2010) 1860-1870.
[83] Y.C. Shen, G.T.R. Lin, K.P. Li, B.J.C. Yuan, An assessment of exploiting renewable energy sources with concerns of policy and technology, Energ Policy, 38 (2010) 4604-4616.
[84] Y. Chisti, Biodiesel from microalgae beats bioethanol, Trends in Biotechnology, 26 (2008) 126-131.
[85] V. Mimouni, L. Ulmann, V. Pasquet, M. Mathieu, L. Picot, G. Bougaran, J.P. Cadoret, A. Morant-Manceau, B. Schoefs, The Potential of Microalgae for the Production of Bioactive Molecules of Pharmaceutical Interest, Curr Pharm Biotechno, 13 (2012) 2733-2750.
[86] M. Olaizola, Commercial development of microalgal biotechnology: from the test tube to the marketplace, Biomol. Eng., 20 (2003) 459-466.
[87] S. Gupta, S.C. Agrawal, Vegetative survival of some wall and soil blue-green algae under stress conditions, Folia Microbiol, 53 (2008) 343-350.
[88] S. Gupta, S.C. Agrawal, Survival of blue-green and green algae under stress conditions, Folia Microbiol, 51 (2006) 121-128.
[89] A. Demirbas, M.F. Demirbas, Importance of algae oil as a source of biodiesel, Energy Conversion and Management, 52 (2011) 163-170.
[90] N. Mallick, S. Mandal, A.K. Singh, M. Bishai, A. Dash, Green microalga Chlorella vulgaris as a potential feedstock for biodiesel, J. Chem. Technol. Biotechnol., 87 (2012) 137-145.
[91] B.N. Pietrowski, R. Tahergorabi, K.E. Matak, J.C. Tou, J. Jaczynski, Chemical properties of surimi seafood nutrified with omega-3 rich oils, Food Chem, 129 (2011) 912-919.
[92] G. Impellizzeri, S. Mangiafico, G. Oriente, M. Piattelli, S. Sciuto, E. Fattorusso, S. Magno, C. Santacroce, D. Sica, Constituents of Red Algae .1. Amino-Acids and Low-Molecular-Weight Carbohydrates of Some Marine Red Algae, Phytochemistry, 14 (1975) 1549-1557.
[93] M.H. Yanqun Li, Nan Wu, Christopher Q. Lan, Nathalie Dubois-Calero,, Biofuels from Microalgae, Biotechnology Progress, 24 (2008) 815-820.

[94] L.G. Speranza, A. Ingram, G.A. Leeke, Assessment of algae biodiesel viability based on the area requirement in the European Union, United States and Brazil, Renew Energ, 78 (2015) 406-417.
[95] A. Sathish, R.C. Sims, Biodiesel from mixed culture algae via a wet lipid extraction procedure, Bioresource Technology, 118 (2012) 643-647.
[96] R. Davis, M. Biddy, S. Jones, Algal Lipid Extraction and Upgrading to Hydrocarbons Technology Pathway National Renewable Energy Laboratory, Golden, CO, 2013.
[97] A. Sun, R. Davis, M. Starbuck, A. Ben-Amotz, R. Pate, P.T. Pienkos, Comparative cost analysis of algal oil production for biofuels, Energy, 36 (2011) 5169-5179.
[98] T. Holtermann, R. Madlener, Assessment of the technological development and economic potential of photobioreactors, Applied Energy, 88 (2011) 1906-1919.
[99] L. Xu, P.J. Weathers, X.R. Xiong, C.Z. Liu, Microalgal bioreactors: Challenges and opportunities, Eng Life Sci, 9 (2009) 178-189.
[100] Y. Chisti, E.M. Grima, E.H. Belarbi, F.G.A. Fernandez, A.R. Medina, Recovery of microalgal biomass and metabolites: process options and economics, Biotechnology Advances, 20 (2003) 491-515.
[101] M.L. Jiang, Y.M. Gong, Biodiesel production with microalgae as feedstock: from strains to biodiesel, Biotechnol Lett, 33 (2011) 1269-1284.
[102] J. Prakash, B. Pushparaj, P. Carlozzi, G. Torzillo, E. Montaini, R. Materassi, Microalgal Biomass Drying by a Simple Solar Device, International Journal of Solar Energy, 18 (1996) 303-311.
[103] D.F. Ihrig, H.M. Heise, U. Brunert, M. Poschmann, R. Kuckuk, K. Stadtlander, Combination of biological processes and fuel cells to harvest solar energy, J. Fuel Cell Sci. Technol., 5 (2008) 5.
[104] G. Yoo, W.K. Park, C.W. Kim, Y.E. Choi, J.W. Yang, Direct lipid extraction from wet Chlamydomonas reinhardtii biomass using osmotic shock, Bioresource Technology, 123 (2012) 717-722.
[105] S. Balasubramanian, J.D. Allen, A. Kanitkar, D. Boldor, Oil extraction from Scenedesmus obliquus using a continuous microwave system - design, optimization, and quality characterization, Bioresource Technology, 102 (2011) 3396-3403.
[106] F. Sahena, I.S.M. Zaidul, S. Jinap, A.A. Karim, K.A. Abbas, N.A.N. Norulaini, A.K.M. Omar, Application of supercritical CO2 in lipid extraction - A review, J Food Eng, 95 (2009) 240-253.
[107] J. Singh, S. Cu, Commercialization potential of microalgae for biofuels production, Renewable & Sustainable Energy Reviews, 14 (2010) 2596-2610.
[108] E.G. Bligh, W.J. Dyer, A Rapid Method of Total Lipid Extraction and Purification, Can J Biochem Phys, 37 (1959) 911-917.
[109] A. Hara, N.S. Radin, Lipid Extraction of Tissues with a Low-Toxicity Solvent, Anal Biochem, 90 (1978) 420-426.
[110] S. Salim, R. Bosma, M.H. Vermue, R.H. Wijffels, Harvesting of microalgae by bio-flocculation, Journal of Applied Phycology, 23 (2011) 849-855.
[111] J.B. Guckert, D.C. White, Evaluation of a Hexane Isopropanol Lipid Solvent System for Analysis of Bacterial Phospholipids and Application to Chloroform-Soluble Nuclepore (Polycarbonate) Membranes with Retained Bacteria, J Microbiol Meth, 8 (1988) 131-137.
[112] X. Bai, F.G. Naghdi, L. Ye, P. Lant, S. Pratt, Enhanced lipid extraction from algae using free nitrous acid pretreatment, Bioresource Technology, 159 (2014) 36-40.

[113] J.S. Kruger, E. Christensen, R.L. McCormick, P.T. Pienkos, Implications of pretreatment and lipid extraction conditions on catalytic upgrading of algae oils to hydrocarbon fuels, Abstr Pap Am Chem S, 248 (2014).
[114] C. Samori, D.L. Barreiro, R. Vet, L. Pezzolesi, D.W.F. Brilman, P. Galletti, E. Tagliavini, Effective lipid extraction from algae cultures using switchable solvents, Green Chem, 15 (2013) 353-356.
[115] C. Samori, C. Torri, G. Samori, D. Fabbri, P. Galletti, F. Guerrini, R. Pistocchi, E. Tagliavini, Extraction of hydrocarbons from microalga Botryococcus braunii with switchable solvents, Bioresource Technology, 101 (2010) 3274-3279.
[116] E.D. Frank, A. Elgowainy, J. Han, Z.C. Wang, Life cycle comparison of hydrothermal liquefaction and lipid extraction pathways to renewable diesel from algae, Mitig Adapt Strat Gl, 18 (2013) 137-158.
[117] M. Axelsson, F. Gentili, A Single-Step Method for Rapid Extraction of Total Lipids from Green Microalgae, Plos One, 9 (2014).
[118] Y. Li, F.G. Naghdi, S. Garg, T.C. Adarme-Vega, K.J. Thurecht, W.A. Ghafor, S. Tannock, P.M. Schenk, A comparative study: the impact of different lipid extraction methods on current microalgal lipid research, Microb Cell Fact, 13 (2014).
[119] R. Bhave, T. Kuritz, L. Powell, D. Adcock, Membrane-Based Energy Efficient Dewatering of Microalgae in Biofuels Production and Recovery of Value Added Co-Products, Environmental Science & Technology, 46 (2012) 5599-5606.
[120] V.H. Smith, The Nitrogen and Phosphorus Dependence of Algal Biomass in Lakes - an Empirical and Theoretical-Analysis, Limnol Oceanogr, 27 (1982) 1101-1112.
[121] C.M. Hansen, The three dimensional solubility parameter and solvent diffusion coefficient. Their importance in surface coating formalation, Danish Technical Press, Polyteknisk læreanstalt, Copenhagen, 1967, pp. 106 p.
[122] C.M. Hansen, Hansen solubility parameters : a user's handbook, 2nd ed., CRC Press, Boca Raton, 2007.
[123] Handbook of Solubility Parameters and Other Cohesion Parameters - Barton,Afm, Text Res J, 54 (1984) 138-138.
[124] G. Ahlgren, L. Merino, Lipid Analysis of Fresh-Water Microalgae - a Method Study, Arch. Hydrobiol., 121 (1991) 295-306.
[125] B.L. Brian, E.W. Gardner, Preparation of Bacterial Fatty Acid Methyl Esters for Rapid Characterization by Gas-Liquid Chromatography, Appl Microbiol, 15 (1967) 1499-&.
[126] N. Rahnama, H.L. Foo, N.A.A. Rahman, A. Ariff, U.K.M. Shah, Saccharification of rice straw by cellulase from a local Trichoderma harzianum SNRS3 for biobutanol production, Bmc Biotechnol, 14 (2014).
[127] A. Limayem, S.C. Ricke, Lignocellulosic biomass for bioethanol production: Current perspectives, potential issues and future prospects, Prog. Energy Combust. Sci., 38 (2012) 449-467.
[128] A. Yousuf, Biodiesel from lignocellulosic biomass - Prospects and challenges, Waste Manage, 32 (2012) 2061-2067.
[129] P. Kumar, D.M. Barrett, M.J. Delwiche, P. Stroeve, Methods for Pretreatment of Lignocellulosic Biomass for Efficient Hydrolysis and Biofuel Production, Ind Eng Chem Res, 48 (2009) 3713-3729.
[130] Z.H. Zhang, B. Liu, Z.B. Zhao, Efficient acid-catalyzed hydrolysis of cellulose in organic electrolyte solutions, Polym Degrad Stabil, 97 (2012) 573-577.

[131] D. Klein-Marcuschamer, B.A. Simmons, H.W. Blanch, Techno-economic analysis of a lignocellulosic ethanol biorefinery with ionic liquid pre-treatment, Biofuel Bioprod Bior, 5 (2011) 562-569.
[132] C.M. Roche, C.J. Dibble, J.S. Knutsen, J.J. Stickel, M.W. Liberatore, Particle Concentration and Yield Stress of Biomass Slurries During Enzymatic Hydrolysis at High-Solids Loadings, Biotechnology and Bioengineering, 104 (2009) 290-300.
[133] Y.L. Miao, J.Y. Chen, X.J. Jiang, Z. Huang, Kinetic Studies on the Product Inhibition of Enzymatic Lignocellulose Hydrolysis, Applied Biochemistry and Biotechnology, 167 (2012) 358-366.
[134] P. Andric, A.S. Meyer, P.A. Jensen, K. Dam-Johansen, Effect and Modeling of Glucose Inhibition and In Situ Glucose Removal During Enzymatic Hydrolysis of Pretreated Wheat Straw, Applied Biochemistry and Biotechnology, 160 (2010) 280-297.
[135] J.B. Kristensen, C. Felby, H. Jorgensen, Yield-determining factors in high-solids enzymatic hydrolysis of lignocellulose, Biotechnol Biofuels, 2 (2009).
[136] A. Sluiter, J. Sluiter, Summative Mass Closure Laboratory Analytical Procedure (LAP) Review and Integration, National Renewable Energy Laboratory, Golden, CO., 2011, pp. 13.
[137] A. Sluiter, J. Sluiter, Summative Mass Closure Laboratory Analytical Procedure (LAP) Review and Integration : Pretreated Slurries, Golden, CO., 2011, pp. 12.
[138] O.o.E.E.a.R.E. United States Department of Energy, N.R.E.L. (NREL), Modeling tomorrow's biorefinery the NREL Biochemical Pilot Plant, U.S. Dept. of Energy, Energy Efficiency and Renewable Energy,, Washington, D.C., 2008, pp. 4 p.
[139] J.S. Knutsen, R.H. Davis, Cellulase retention and sugar removal by membrane ultrafiltration during lignocellulosic biomass hydrolysis, Applied Biochemistry and Biotechnology, 113 (2004) 585-599.
[140] N. Weiss, J. Borjesson, L.S. Pedersen, A.S. Meyer, Enzymatic lignocellulose hydrolysis: Improved cellulase productivity by insoluble solids recycling, Biotechnol Biofuels, 6 (2013).
[141] P. Andric, A.S. Meyer, P.A. Jensen, K. Dam-Johansen, Reactor design for minimizing product inhibition during enzymatic lignocellulose hydrolysis II. Quantification of inhibition and suitability of membrane reactors, Biotechnology Advances, 28 (2010) 407-425.
[142] M.M. Ishola, A. Jahandideh, B. Haidarian, T. Brandberg, M.J. Taherzadeh, Simultaneous saccharification, filtration and fermentation (SSFF): A novel method for bioethanol production from lignocellulosic biomass, Bioresource Technology, 133 (2013) 68-73.
[143] K. Belafi-Bako, A. Koutinas, N. Nemestothy, L. Gubicza, C. Webb, Continuous enzymatic cellulose hydrolysis in a tubular membrane bioreactor, Enzyme Microb Tech, 38 (2006) 155-161.
[144] Q. Gan, S.J. Allen, G. Taylor, Design and operation of an integrated membrane reactor for enzymatic cellulose hydrolysis, Biochem. Eng. J., 12 (2002) 223-229.
[145] R.N. Gurram, T.J. Menkhaus, Continuous Enzymatic Hydrolysis of Lignocellulosic Biomass with Simultaneous Detoxification and Enzyme Recovery, Applied Biochemistry and Biotechnology, 173 (2014) 1319-1335.
[146] M.J. Zhang, R.X. Su, Q.A. Li, W. Qi, Z.M. He, Enzymatic saccharification of pretreated corn stover in a fed-batch membrane bioreactor, Bioenergy Research, 4 (2011) 134-140.
[147] J.S. Van Dyk, B.I. Pletschke, A review of lignocellulose bioconversion using enzymatic hydrolysis and synergistic cooperation between enzymes-Factors affecting enzymes, conversion and synergy, Biotechnology Advances, 30 (2012) 1458-1480.

[148] A. Gautam, T.J. Menkhaus, Performance evaluation and fouling analysis for reverse osmosis and nanofiltration membranes during processing of lignocellulosic biomass hydrolysate, Journal of Membrane Science, 451 (2014) 252-265.
[149] A. Cornish-Bowden, The origins of enzyme kinetics, Febs Lett, 587 (2013) 2725-2730.
[150] N.D. Weiss, J.J. Stickel, J.L. Wolfe, Q.A. Nguyen, A Simplified Method for the Measurement of Insoluble Solids in Pretreated Biomass Slurries, Applied Biochemistry and Biotechnology, 162 (2010) 975-987.
[151] S. Rajam, C.C. Ho, Graft coupling of PEO to mixed cellulose esters microfiltration membranes by UV irradiation, Journal of Membrane Science, 281 (2006) 211-218.
[152] J. Shekiro, E.M. Kuhn, N.J. Nagle, M.P. Tucker, R.T. Elander, D.J. Schell, Characterization of pilot-scale dilute acid pretreatment performance using deacetylated corn stover, Biotechnol Biofuels, 7 (2014).
[153] D. Humbird, National Renewable Energy Laboratory (U.S.), Harris Group Inc., Process design and economics for biochemical conversion of lignocellulosic biomass to ethanol dilute-acid pretreatment and enzymatic hydrolysis of corn stover, Nrel/Tp 5100-47764, National Renewable Energy Laboratory,, Golden, CO, 2011, pp. 1 online resource (ix, 136 p.).
[154] J. Zheng, L. Rehmann, Extrusion Pretreatment of Lignocellulosic Biomass: A Review, Int. J. Mol. Sci., 15 (2014) 18967-18984.
[155] P. Bacchin, P. Aimar, R. Field, Critical and sustainable fluxes: Theory, experiments and applications, J Membrane Sci, 281 (2006) 42-69.
[156] E.E. Chang, S.Y. Yang, C.P. Huang, C.H. Liang, P.C. Chiang, Assessing the fouling mechanisms of high-pressure nanofiltration membrane using the modified Hermia model and the resistance-in-series model, Separation and Purification Technology, 79 (2011) 329-336.
[157] D. Klein-Marcuschamer, P. Oleskowicz-Popiel, B.A. Simmons, H.W. Blanch, The challenge of enzyme cost in the production of lignocellulosic biofuels, Biotechnology and Bioengineering, 109 (2012) 1083-1087.
[158] M.J. Serapiglia, M.C. Humiston, H.W. Xu, D.A. Hogsett, R.M. de Orduna, A.J. Stipanovic, L.B. Smart, Enzymatic saccharification of shrub willow genotypes with differing biomass composition for biofuel production, Front Plant Sci, 4 (2013).
[159] X.Z. Zhang, Q. Hu, M. Sommerfeld, E. Puruhito, Y.S. Chen, Harvesting algal biomass for biofuels using ultrafiltration membranes, Bioresource Technology, 101 (2010) 5297-5304.
[160] L.A. Lucia, Lignocellulosic Biomass: A Potential Feedstock to Replace Petroleum, Bioresources, 3 (2008) 981-982.
[161] A.S.M. Hussin, S.R.A. Collins, Z. Merali, M.L. Parker, A. Elliston, N. Wellner, K.W. Waldron, Characterisation of lignocellulosic sugars from municipal solid waste residue, Biomass Bioenerg, 51 (2013) 17-25.
[162] M. Melikoglu, Shale gas: Analysis of its role in the global energy market, Renewable & Sustainable Energy Reviews, 37 (2014) 460-468.
[163] C.E. Wyman, Biomass ethanol: Technical progress, opportunities, and commercial challenges, Annu Rev Energ Env, 24 (1999) 189-226.
[164] H.V. Lee, S.B.A. Hamid, S.K. Zain, Conversion of Lignocellulosic Biomass to Nanocellulose: Structure and Chemical Process, Sci World J, (2014).
[165] R.M. Prunescu, G. Sin, Dynamic modeling and validation of a lignocellulosic enzymatic hydrolysis process - A demonstration scale study, Bioresource Technology, 150 (2013) 393-403.
[166] Y. Sun, J.Y. Cheng, Hydrolysis of lignocellulosic materials for ethanol production: a review, Bioresource Technology, 83 (2002) 1-11.

[167] C.R. Poovaiah, M. Nageswara-Rao, J.R. Soneji, H.L. Baxter, C.N. Stewart, Altered lignin biosynthesis using biotechnology to improve lignocellulosic biofuel feedstocks, Plant Biotechnol. J., 12 (2014) 1163-1173.
[168] B. Adhikari, D.A. Sievers, J.J. Stickel, J. Pellegrino, Membrane-enabled continuous enzymatic saccharification of lignocellulose, Biochem. Eng. J., 104 (2016) 300-313.
[169] S.T. Yang, M.R. Okos, A New Graphical-Method for Determining Parameters in Michaelis Menten-Type Kinetics for Enzymatic Lactose Hydrolysis, Biotechnology and Bioengineering, 34 (1989) 763-773.
[170] H.E. Wray, R.C. Andrews, P.R. Berube, Surface shear stress and membrane fouling when considering natural water matrices, Desalination, 330 (2013) 22-27.
[171] C.C.V. Chan, P.R. Berube, E.R. Hall, Relationship between types of surface shear stress profiles and membrane fouling, Water Res, 45 (2011) 6403-6416.
[172] M.M. Campbell, R.R. Sederoff, Variation in lignin content and composition - Mechanism of control and implications for the genetic improvement of plants, Plant Physiol, 110 (1996) 3-13.
[173] M.J. Selig, L.G. Thygesen, C. Felby, Correlating the ability of lignocellulosic polymers to constrain water with the potential to inhibit cellulose saccharification, Biotechnol Biofuels, 7 (2014).
[174] M.S. Shah, J.B. Joshi, A.S. Kalsi, C.S.R. Prasad, D.S. Shukla, Analysis of flow through an orifice meter: CFD simulation, Chem Eng Sci, 71 (2012) 300-309.
[175] F. Habla, H. Marschall, O. Hinrichsen, L. Dietsche, H. Jasak, J.L. Favero, Numerical simulation of viscoelastic two-phase flows using openFOAM (R), Chem Eng Sci, 66 (2011) 5487-5496.
[176] D. Carvajal, D.L. Marchisio, S. Bensaid, D. Fino, Enzymatic Hydrolysis of Lignocellulosic Biomasses via CFD and Experiments, Industrial & Engineering Chemistry Research, 51 (2012) 7518-7525.
[177] A. Trusek-Holownia, Improvement of process productivity and product purity by the application of a membrane phase contactor in enzymatic conversions, Separation and Purification Technology, 41 (2005) 267-274.
[178] J.J. Stickel, R.L. Powell, Fluid mechanics and rheology of dense suspensions, Annu Rev Fluid Mech, 37 (2005) 129-149.
[179] F.X. Tanner, A.A. Al-Habahbeh, K.A. Feigl, S. Nahar, S.A.K. Jeelani, W.R. Case, E.J. Windhab, Numerical and Experimental Investigation of a Non-Newtonian Flow in a Collapsed Elastic Tube, Appl Rheol, 22 (2012) 328-335.
[180] C.T. Scott, J.R. Samaniuk, D.J. Klingenberg, Rheology and extrusion of high-solids biomass, Tappi J, 10 (2011) 47-53.
[181] J.J. Stickel, J.S. Knutsen, M.W. Liberatore, W. Luu, D.W. Bousfield, D.J. Klingenberg, C.T. Scott, T.W. Root, M.R. Ehrhardt, T.O. Monz, Rheology measurements of a biomass slurry: an inter-laboratory study, Rheol Acta, 48 (2009) 1005-1015.
[182] J.R. Samaniuk, J. Wang, T.W. Root, C.T. Scott, D.J. Klingenberg, Rheology of concentrated biomass, Korea-Aust Rheol J, 23 (2011) 237-245.
[183] J.S. Knutsen, M.W. Liberatore, Rheology of high-solids biomass slurries for biorefinery applications, J Rheol, 53 (2009) 877-892.
[184] T. Shu-tang, J. yI-an, ON THE LINKING UP BETWEEN BINGHAM FLUID AND PLUGGED FLOW, Appled Mathematics and Mechanics, 8 (1987) 6.

[185] R.A. Chilton, R. Stainsby, Pressure loss equations for laminar and turbulent non-Newtonian pipe flow, J Hydraul Eng-Asce, 124 (1998) 522-529.
[186] J. Stickel, Viscosity of different biomass fraction, National Renewable Energy Laboratory, 2013.
[187] J.J. Stickel, Viscoscity of lignocellulosic biomass slurry at various fraction insoluble solids (FIS) loading., Golden, CO., 2010.
[188] C. Geuzaine, J.-F. Remacle, Gmsh: a three-dimensional finite element mesh generator with built-in pre- and post-processing facilities, 2013
.
[189] C. Schär, The Courant-Friedrichs-Levy (CFL) Stability Criterion ETH-Swiss Federal Institute of Technology, Zurich, 2013.
[190] L. Amer, B. Adhikari, J. Pellegrino, Technoeconomic analysis of five microalgae-to-biofuels processes of varying complexity, Bioresource Technology, 102 (2011) 9350-9359.